

Gelled Non-Toxic Microemulsions

Von der Fakultät Chemie der Universität Stuttgart
zur Erlangung der Würde einer
Doktorin der Naturwissenschaften (Dr. rer. nat.)
genehmigte Abhandlung

Vorgelegt von

Ke Peng

aus Chongqing, China

Hauptberichterin: Prof. Dr. Cosima Stubenrauch

Mitberichter: Prof. Dr. Thomas Hellweg

Prüfungsvorsitz: Prof. Dr. Jens Brockmeyer

Tag der mündlichen Prüfung: 14.10.2021

Institut für Physikalische Chemie

der Universität Stuttgart

2021

Acknowledgements

First and foremost, I would like to thank my supervisor *Prof. Dr. Cosima Stubenrauch* for offering me the opportunity to start this PhD journey. It would not have been possible without her guidance and mentoring from the very beginning till the end. I have improved so much on my research skills, scientific writing, and presentation through this journey. I am also grateful for the opportunities to attend national and international conferences and build up the network.

Sincere thanks to *Prof. Dr. Thomas Hellweg* for being the second examiner for my thesis and *Prof. Dr. Jens Brockmeyer* for being the chair of the examination board.

Special thanks to *Prof. Dr. Thomas Sottmann* for being my second supervisor and the co-author of my publications. As the expert in microemulsions and scattering techniques, he provided so much guidance and helpful advice. I am also thankful for his help and explanations with SANS measurements.

I warmly thank *Dr. Natascha Schelero* for introducing me to the field of physical chemistry and the follow-up connections. I am also thankful to *Dr. María J. Vicent* for the intended collaboration; unfortunately, it did not come true due to COVID-19.

Furthermore, I would like to thank *Dr. Natalie Preisig* for surface tension and FFEM measurements. A big thank you goes to *Dr. Katja Steck* for her instructions on gelation, rheology, and DLS. Sincere thanks to *Kristina Schneider*, *Shih-Yu Tseng*, and *Karina Abitaev* for their help with SANS measurements. Further thanks go to *Dr. Sonja Dieterich* for her help and *Dr. Johanna Bruckner* for the SAXS measurement. Sincere thanks to *Birgit Feucht* for her help with the visual phase studies and *Diana Zauser* for all the help in labs and experiments. Warm thanks to *Dr. Herbert Dilger* and *Beate Holley* for dealing with all the administration issues. Further thanks go to *Gabriele Bräuning* and the *mechanical* and *electrical workshops* for their support in the laboratories.

Moreover, I thank all the *Stubenrauch* and the *Sottmann* group members for the shared time, scientific discussions, and hanging out. Special thanks to my office mates *Friederike Dehli* and *Tamara Schad*.

Finally, thank my family for giving me the freedom to pursue my life and for all supports. Thank *Douban* for the mental comfort, and I am grateful to find climbing as my new hobby alongside the PhD. Sincere thanks to my dear friends for their company, especially *Louise Burkart*, *Xiaoyue Chen*, and *June Li*. A special and heartfelt thank you to *Jiang*.

Abstract

Bicontinuous microemulsions gelled with a low molecular weight gelator (LMWG) have been found to be an orthogonally self-assembled system, *i.e.* the bicontinuous microstructure of the microemulsion and the fibrillar gel network form independently but simultaneously. Gelled non-toxic microemulsions have great potential to work as transdermal drug delivery systems because the non-toxic microemulsion provides optimum solubilization for drugs, while the gel network provides mechanical stability. In this work, we formulated gelled non-toxic bicontinuous microemulsions with an LMWG and investigated their formation via orthogonal self-assembly. Moreover, we provided a prototype for novel drug delivery systems.

To formulate non-toxic microemulsions, we started with the scouting system H₂O – *n*-octane – *n*-octyl- β -D-glucopyranoside (β -C₈G₁) – 1-octanol and replaced the oil and the co-surfactant with non-toxic components, namely isopropyl myristate (IPM) and 1,2-octanediol, respectively. Subsequently, the pure surfactant β -C₈G₁ was replaced by more efficient technical-grade sugar surfactants, including Plantacare 1200 UP (C₁₂G_{1.4}) and MEGA-12/14-HC (*n*-alkanoyl-*N*-methylglucamides with an average carbon chain length of 12–14). The new type of sugar surfactant, MEGA-12/14-HC, forms an ultra-efficient non-toxic microemulsion consisting of H₂O – IPM – MEGA-12/14-HC – 1,2-octanediol presumably due to the electrostatic stiffening effect. However, for more reproducible results, Plantacare 1200 UP was used for further investigations. Both hydrophobic and hydrophilic model drugs, namely lidocaine and diclofenac sodium salt, were solubilized in the non-toxic microemulsion consisting of H₂O – IPM – Plantacare 1200 UP – 1,2-octanediol. Moreover, phase studies were carried out at various oil-to-water ratios from $\phi = 0.2$ to $\phi = 0.8$. After the successful formulation of non-toxic microemulsions, the organogelator 1,3:2,4-dibenzylidene-D-sorbitol (DBS) was chosen for gelation since it does not affect the phase behavior of the non-toxic microemulsions. Rheological properties of the gelled non-toxic microemulsions were characterized by oscillatory shear rheometry. Furthermore, small-angle neutron scattering (SANS) evidenced that the gel network does not alter the microstructures of the bicontinuous microemulsion ($\phi = 0.5$), and freeze-fracture electron microscopy (FFEM) images showed the coexistence of microemulsions and a fibrillar gel network. We found that an oil-continuous phase must be present for the organogelator DBS to form a strong gel and that the orthogonality of the gelled microemulsions is given for $\phi \geq 0.35$.

Kurzzusammenfassung

Bikontinuierliche Mikroemulsionen, die mit einem niedermolekularen Gelator geliert sind, haben sich als orthogonal selbstorganisiertes System erwiesen, d. h. die bikontinuierliche Mikrostruktur der Mikroemulsion und das fibrilläre Gelnetzwerk bilden sich unabhängig, jedoch gleichzeitig. Gelierte, nicht-toxische Mikroemulsionen haben dabei ein großes Potenzial für die transdermale Wirkstoffabgabe, da diese Systeme eine optimale Solubilisierung der Wirkstoffe ermöglicht, wobei das Gelnetzwerk für mechanische Stabilität sorgt. In dieser Arbeit wurden gelierte, nicht-toxische, bikontinuierliche Mikroemulsionen mit einem niedermolekularen Gelator formuliert und ihre Bildung durch orthogonale Selbstorganisation untersucht. Außerdem wurde ein Prototyp für neuartige Wirkstoffabgabesystem entwickelt.

Um nicht-toxische Mikroemulsionen zu formulieren, wurde ausgehend von dem Scouting-System $\text{H}_2\text{O} - n\text{-Octan} - n\text{-Octyl-}\beta\text{-D-glucopyranosid} (\beta\text{-C}_8\text{G}_1) - 1\text{-Octanol}$ zunächst das Öl und das Co-Tensid durch die nicht-toxischen Komponenten Isopropylmyristat (IPM) bzw. 1,2-Octandiol ersetzt. Anschließend wurde das reine Tensid $\beta\text{-C}_8\text{G}_1$ durch die effizienteren technischen Zuckertenside ersetzt, nämlich Plantacare 1200 UP ($\text{C}_{12}\text{G}_{1,4}$) und MEGA-12/14-HC (*n*-Alkanoyl-*N*-Methylglucamide mit einer durchschnittlichen Kohlenstoffkettenlänge von 12–14). Das neuartige Zuckertensid MEGA-12/14-HC bildet dabei eine hocheffiziente, nicht-toxische Mikroemulsion bestehend aus $\text{H}_2\text{O} - \text{IPM} - \text{MEGA-12/14-HC} - 1,2\text{-Octandiol}$. Die außerordentliche Effizienz ist vermutlich auf den elektrostatischen Versteifungseffekt zurückzuführen. Um jedoch reproduzierbare Ergebnisse zu erzielen, wurde für weitere Untersuchungen Plantacare 1200 UP verwendet. Sowohl ein hydrophober als auch ein hydrophiler Modellwirkstoff, nämlich Lidocain und Diclofenac-Natriumsalz, wurden in der Mikroemulsion bestehend aus $\text{H}_2\text{O} - \text{IPM} - \text{Plantacare 1200 UP} - 1,2\text{-Octandiol}$ solubilisiert. Außerdem wurde das Phasenverhalten bei verschiedenen Öl-Wasser-Verhältnissen von $\phi = 0,2$ bis $\phi = 0,8$ untersucht. Nach der erfolgreichen Formulierung der nicht-toxischen Mikroemulsionen wurde der Organogelator 1,3:2,4-Dibenzyliden-D-Sorbit (DBS) zum Gelieren ausgewählt, da dieser das Phasenverhalten der Mikroemulsionen nicht beeinflusst. Die rheologischen Eigenschaften der gelierten Mikroemulsionen wurden durch oszillatorische Scherrheometrie charakterisiert. Darüber hinaus zeigte die Kleinwinkel-Neutronenstreuung (SANS), dass das Gelnetzwerk die Mikrostrukturen der bikontinuierlichen Mikroemulsion ($\phi = 0,5$) nicht verändert. Durch Gefrierbruch-Elektronenmikroskopiebilder (FFEM) konnte die Koexistenz von Mikroemulsionen und einem fibrillären Gelnetzwerk nachgewiesen werden. Wir fanden heraus, dass eine ölkontinuierliche Phase vorhanden sein muss, damit der Organogelator DBS ein starkes Gel bilden kann, und dass die Orthogonalität der gelierten Mikroemulsionen für $\phi \geq 0,35$ gegeben ist.

Publication List

- I. Gelled Non-Toxic Microemulsions: Phase Behavior & Rheology**
Ke Peng, Thomas Sottmann, and Cosima Stubenrauch
Soft Matter **2019**, *15* (41), 8361–8371.
- II. Formulation of Gelled Non-Toxic Bicontinuous Microemulsions Stabilized by Highly Efficient Alkanoyl Methylglucamides**
Ke Peng, Natalie Preisig, Thomas Sottmann, and Cosima Stubenrauch
Langmuir **2020**, *36* (42), 12692–12701.
- III. Gelled Non-Toxic Bicontinuous Microemulsions as Promising Transdermal Drug Carriers**
Ke Peng, Thomas Sottmann, Cosima Stubenrauch
Mol. Phys. **2021**, *119* (15–16), e1886363.
- IV. From Water-Rich to Oil-Rich Gelled Non-Toxic Microemulsions**
Ke Peng, Natalie Preisig, Thomas Sottmann, and Cosima Stubenrauch
Phys. Chem. Chem. Phys. **2021**, *23* (31), 16855–16867.

Contribution Report

- I.** Responsible for writing the manuscript and for all experimental work except small-angle neutron scattering measurements (done by Kristina Schneider, Shih-Yu Tseng, and Diana Zauser). The co-authors revised the manuscript.
- II.** Responsible for writing the manuscript and for most of the experimental work. The small-angle neutron scattering measurements were performed by Shih-Yu Tseng, Karina Abitaev, and Diana Zauser. Dr. Natalie Preisig carried out the freeze-fracture electron microscopy and surface tension measurements. The other co-authors revised the manuscript.
- III.** Responsible for writing the manuscript and for all experimental work. The co-authors revised the manuscript.
- IV.** Responsible for writing the manuscript and for all experimental work except freeze-fracture electron microscopy (done by Dr. Natalie Preisig). The co-authors revised the manuscript.

Contents

Nomenclature	vii
1 Introduction	1
1.1 Motivation.....	1
1.2 Task Description	5
2 Theoretical Background	8
2.1 Microemulsions.....	8
2.2 Molecular Gels.....	15
2.3 Rheology	20
3 Methods	32
3.1 Chemicals, Sample Preparation and Visual Phase Studies	32
3.2 Oscillatory Shear Rheometry	36
3.3 Small-Angle Neutron Scattering.....	37
3.4 Freeze-Fracture Electron Microscopy.....	40
3.5 Electrical Conductivity	41
4 Summary of Research	42
4.1 Gelled Non-Toxic Microemulsions: Phase Behavior & Rheology (Publication I).....	42
4.2 Formulation of Gelled Non-Toxic Bicontinuous Microemulsions Stabilized by Highly Efficient Alkanoyl Methylglucamides (Publication II).....	49
4.3 Gelled Non-Toxic Bicontinuous Microemulsions as Promising Transdermal Drug Carriers (Publication III).....	56
4.4 From Water-Rich to Oil-Rich Gelled Non-Toxic Microemulsions (Publication IV)....	60
5 Conclusion & Outlook	68
References	72

Nomenclature

Numerical

- 1 one-phase microemulsion
- $\underline{2}$ oil-in-water (o/w)-microemulsion (lower phase) coexisting with an excess oil phase (upper phase)
- $\overline{2}$ water-in-oil (w/o) microemulsion (upper phase) coexisting with an excess water phase (lower phase)
- 3 three-phase bicontinuous microemulsion coexisting with an excess water and an excess oil phase

Abbreviations

12-HOA/12-HSA	12-hydroxyoctadecanoic/hydroxystearic acid
1D	one-dimensional
3D	three-dimensional
β -C ₈ G ₁	<i>n</i> -octyl- β -D-glucopyranoside
AFM	atomic force microscopy
APG	alkyl polyglucoside
BisAm	<i>N,N'</i> -methylenebisacrylamide
C ₁₀ E ₄	tetraethylene glycol monodecyl ether
C _{<i>i</i>} E _{<i>j</i>}	<i>n</i> -alkyl polyglycol ether, <i>i</i> is the number of carbon atoms in the <i>n</i> -alkyl chain, <i>j</i> is the number of ethylene glycol units
C _{<i>n</i>} G _{<i>m</i>}	<i>n</i> -alkyl polyglucoside, <i>n</i> is the number of carbon atoms in the <i>n</i> -alkyl chain, <i>m</i> is the number of glucose units
<i>cgc</i>	critical gelation concentration
cp _{α}	the upper critical point of the binary system oil – nonionic surfactant
cp _{β}	the lower critical point of the binary system H ₂ O – nonionic surfactant
D ₂ O	deuterium oxide
DBC	<i>N,N'</i> -dibenzoyl-L-cystine
DBS	1,3:2,4-dibenzylidene-D-sorbitol
DBS–CONHNH ₂	1,3:2,4-dibenzylidene-D-sorbitol– <i>p,p'</i> -dihydrazide
DBS–COOH	1,3:2,4-dibenzylidene-D-sorbitol– <i>p,p'</i> -dicarboxylic acid
DLS	dynamic light scattering

Nomenclature

DSC	differential scanning calorimetry
H ₂ O	water
IPM	isopropyl myristate
FFEM	freeze-fracture electron microscopy
LMWG	low molecular weight gelator
LVE	linear viscoelastic
MEGA- <i>n</i>	<i>n</i> -alkanoyl- <i>N</i> -methylglucamide
<i>mgc</i>	minimum gelation concentration
NaCl	sodium chloride
NIPAm	<i>N</i> -isopropylacrylamide
NMR	nuclear magnetic resonance
o/w	oil-in-water
PIT	phase inversion temperature of the microemulsion
SANS	small-angle neutron scattering
SAXS	small-angle X-ray scattering
SEM	scanning electron microscopy
TEM	transmission electron microscopy
SLS	static light scattering
w/o	water-in-oil
\tilde{X}	the fishtail point on the phase diagram of a microemulsion where the 1-phase and 3-phase regions meet

Parameters

γ	(a) surfactant mass fraction; (b) shear strain (Equation (2.7))
$\dot{\gamma}$	shear rate (Equation (2.4) and (2.8))
$\tilde{\gamma}$	the minimal surfactant mass fraction needed to solubilize equal amounts of water and oil completely, also the composition coordinate of a microemulsion's fishtail point, which denotes the system's efficiency
γ_0	the lowest surfactant mass fraction where a microemulsion starts to form
γ_A	shear strain amplitude
γ_C	surfactant mass fraction (Equation (3.2))
$\tilde{\gamma}_C$	the lowest surfactant mass fraction needed to form a 1-phase microemulsion in the quaternary system H ₂ O – oil – C _{<i>n</i>} G _{<i>m</i>} surfactant – co-surfactant, also one coordinate

	of the fishtail point
γ_D	co-surfactant mass fraction (Equation (3.3))
$\tilde{\gamma}_D$	the lowest co-surfactant mass fraction needed to form a 1-phase microemulsion in the quaternary system $H_2O - oil - C_nG_m$ surfactant - co-surfactant, also one coordinate of the fishtail point
δ	(a) co-surfactant mass fraction in the surfactant mixture; (b) phase shift angle (Figure 2.15)
$\delta_{v,i}$	the volume fraction of co-surfactant in the interfacial surfactant monolayer
ε	salinity (Equation (3.4))
η	(a) shear viscosity (Equation (2.5)); (b) gelator concentration (Equation (3.5))
θ	scattering angle (Equation (3.6))
κ	electrical conductivity
λ	wavelength (Equation (3.6))
ξ_{TS}	correlation length of the bicontinuous microemulsion structure, a parameter in the Teubner-Strey model (Equation (3.8))
ρ	scattering length density
τ	shear stress (Equation (3.1))
τ_A	shear stress amplitude
φ	deflection angle (Equation (2.7))
ϕ	oil-to-water ratio (Equation (3.1))
ω	oscillation angular frequency
A	shear area (Equation (2.3))
c_1, c_2	the principal curvatures given by the two principal radii of curvature R_1 and R_2 of the surfactant monolayer (Equation (2.1) and (2.2))
$c_{gelator}$	gelator concentration
c_{sol}	gelator solubility in the solvent
d_{fibril}	diameter of gel fibers
d_{TS}	the periodicity of the oil and water domains, a parameter in the Teubner-Strey model (Equation (3.9))
F	shear force (Equation (3.1))
f_a	the amphiphilicity factor (Equation (3.10))
G	shear modulus (Equation (2.9))
G^*	complex shear modulus (Equation (2.17))

Nomenclature

G'	storage modulus (Equation (2.19))
G''	loss modulus (Equation (2.20))
H	the mean curvature of the interfacial surfactant monolayer (Equation (2.1))
H_0	the spontaneous curvature of the interfacial surfactant monolayer
$\Delta H_{\text{gel-sol}}$	the phase-change enthalpy of a molecular gel
K	the Gaussian curvature of the interfacial surfactant monolayer (Equation (2.2))
q	scattering vector (Equation (3.6))
s	deflection length (Equation (2.7))
t	time
$\tan \delta$	loss factor or damping factor (Equation (2.21))
T	temperature
\tilde{T}	the temperature coordinate of a C_iE_j -type microemulsion's fishtail point, which is also called the phase inversion temperature
T_l	the lowest temperature where the three-phase bicontinuous microemulsion exists
T_u	the highest temperature where the three-phase bicontinuous microemulsion exists
$T_{\text{sol-gel}}$	sol-gel transition temperature
v	shear velocity (Equation (2.4))
z	shear gap (Equation (2.4) and (2.7))

1 Introduction

1.1 Motivation

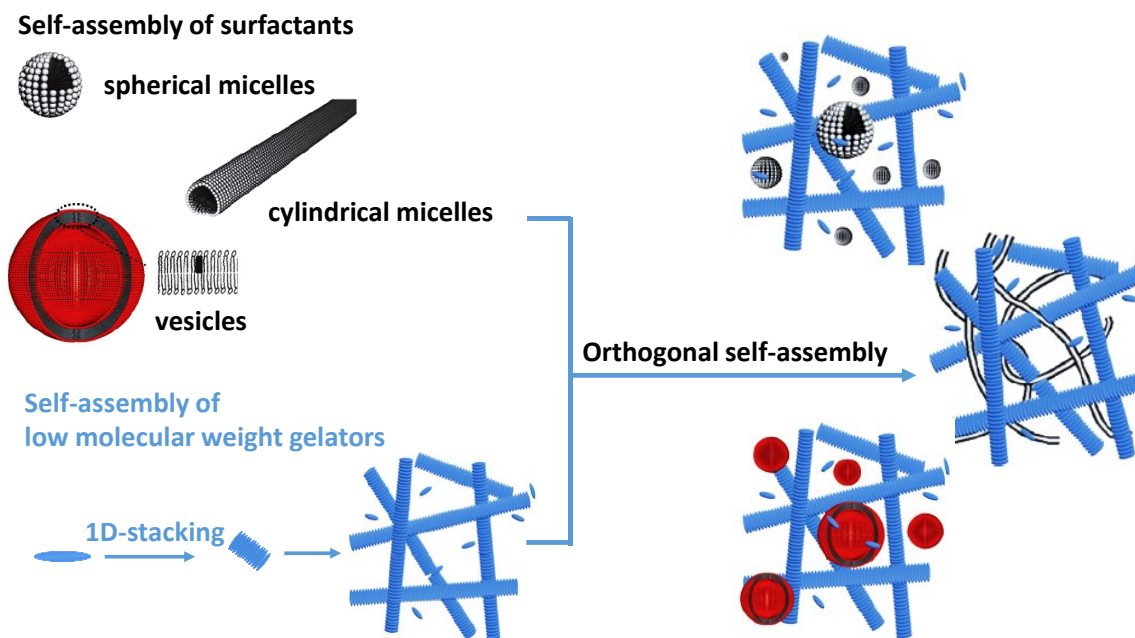


Figure 1.1: Schematic illustration of orthogonal self-assembly of surfactants and low molecular weight gelators (modified from [Bri09]).

Orthogonal self-assembly is the simultaneous but independent formation of two self-assembled structures. The concept was first proposed by Leibniz *et al.* for the simultaneous and independent formation of two self-assembled monolayers on the gold–aluminum oxide surface [Lai89]. In recent years, orthogonal self-assembly has been discovered in gelled complex fluids, which are promising for transdermal drug delivery, tissue healing, molecular electronics, or biomimetic cell membranes [Stu16]. According to the definition of Gelbert *et al.*, a complex fluid has a mesoscopic length scale which plays a key role in determining the properties of the system [Gel96]. Examples of complex fluids are micellar solutions, microemulsions, vesicles, and liquid crystals. Complex fluids form through the self-assembly of molecules. Molecular gels form through the self-assembly of low molecular weight gelators (LMWG) [Wei14]. If the two systems are combined and if the structures form simultaneously but independently, one speaks of orthogonal self-assembly. Examples of gelled complex fluids—which are not necessarily formed via orthogonal self-assembly—are gelled micelles [Hee03], gelled vesicles

[Bri08], gelled wormlike micelles [Bri09], gelled thermotropic liquid crystals [Kat01, Kat06, Kat07], gelled lyotropic liquid crystals [Koi17, Ste19, Ste19b, Ste19c, Ste20], and gelled liposomes [Bri09b, Boe16] (Figure 1.1).

Gelled Bicontinuous Microemulsions

One particularly interesting type of gelled complex fluid is a bicontinuous microemulsion gelled by an LMWG. Bicontinuous microemulsions contain two interweaving water and oil subdomains separated by an amphiphilic surfactant monolayer with domain sizes ranging from 5 to 100 nm [Str94]. The first gelled bicontinuous microemulsion was formulated by Tessendorf *et al.* with the ternary base system H₂O – *n*-dodecane – Lutensol AO5 (technical-grade nonionic *n*-alkyl polyglycol ether with an average molecular structure of C_{13/15}E₅) and the low molecular weight organogelator 12-hydroxyoctadecanoic acid (12-HOA) [Stu07, Stu08, Mag09, Tes09]. The aim was to use the “arrested” bicontinuous microstructure as a template for the synthesis of bicontinuous (sponge-like) nanoporous polymers. Therefore, the polymerizable aqueous phase contained the monomer *N*-isopropylacrylamide (NIPAm) and the cross-linker *N,N'*-methylenebisacrylamide (BisAm). Freeze-fracture electron microscopy (FFEM) images and small-angle neutron scattering (SANS) data of the non-polymerized systems suggested that the bicontinuous microstructure was not altered by the gel network. In other words, the gelled bicontinuous microemulsion was considered to be an orthogonal self-assembled system, where the bicontinuous microemulsion and the fibrillar gel network form simultaneously but independently.

Further investigations on gelled bicontinuous microemulsions were carried out by Laupheimer *et al.* with the model system H₂O – *n*-decane / 12-HOA – tetraethylene glycol monodecyl ether (C₁₀E₄) [Lau13, Lau13b, Lau14]. The characteristic properties and microstructures of the gelled bicontinuous microemulsion were compared with those of the two base systems, namely the non-gelled bicontinuous microemulsion H₂O – *n*-decane – C₁₀E₄ and the binary gel *n*-decane / 12-HOA. The phase boundaries of the non-gelled microemulsion were maintained

upon gelation but shifted to lower temperatures because 12-HOA is surface-active. The gelled microemulsion and the binary gel had similar rheological properties. The mere differences are that the gel network in the gelled microemulsion is slightly weaker than in the binary gel, and the sol–gel transition temperature of the gelled microemulsion is lower than that of the binary gel. These differences can be explained by the fact that (a) the surface-active 12-HOA molecules partly adsorb at the water–oil interface instead of forming gel fibers, (b) the change of the gel’s solvent from pure *n*-decane to a microemulsion leads to different gelator–solvent interaction and thus to slightly different rheological properties. Moreover, the coexistence of two self-assembled structures—the fibrillar gel network and the bicontinuous microstructure—was evidenced with the help of FFEM and SANS. Opposed to the assumption of Tessendorf that gel fibers only exist in the oil domain since 12-HOA is an organogelator, the gel fibers pass through the entire microemulsion, *i.e.* through both water and oil domains.

Non-Toxic Microemulsions

Non-toxic microemulsions are of great interest for drug delivery [Kre02, Heu08, Law12]. However, most of the microemulsions used in drug delivery are oil-in-water (o/w) type microemulsions, while bicontinuous microemulsions are hardly used [Cal17]. This is remarkable since bicontinuous microemulsions provide the optimum solubilizing capacity for drugs and facilitate the drug permeation through the skin barrier [Bo198, Bo199]. Several drug-containing bicontinuous microemulsions have been formulated up to now. (1) A dermal delivery system consisting of H₂O – isopropyl myristate (IPM) – polysorbates containing the local anesthetic lidocaine was characterized by NMR self-diffusion. However, the system was water-rich, and the surfactant mass fraction was as high as 30 wt.%, which means that a bicontinuous structure is not very likely [Car91]. (2) Froelich *et al.* presented bicontinuous microemulsions consisting of H₂O – oleic acid – polysorbates using ethanol and diethylene glycol monoethyl ether as co-surfactants [Fro17]. However, the total amount of surfactant and co-surfactant was as high as 70 wt.%, and only surface tension and electrical conductivity were measured, while no structural characterization was carried out. (3) In another bicontinuous

microemulsion, an alkyl ester was used as oil, sucrose esters as surfactant, and diethylene glycol monoethyl ether as co-surfactant [Bol98, Bol99]. The bicontinuous microstructure was evidenced by freeze-fracture electron microscopy (FFEM) and small-angle neutron scattering (SANS). However, the system was only studied on the oil-rich side, and the surfactant content was quite high (18 wt.% surfactant and 12 wt.% co-surfactant). Note that high surfactant contents are not preferred due to toxicity and economical considerations.

Kahlweit *et al.* made a series of attempts to formulate non-toxic microemulsions and carefully studied the phase behavior for the purpose of potential pharmaceutical applications. They started with the quaternary system $\text{H}_2\text{O} - n\text{-alkane} - \text{lecithin} - \text{alkanol}$ with equal weights of water and oil [Kah95a] and replaced the zwitterionic surfactant lecithin with nonionic alkyl polyglucosides (APGs, or glycosides) [Kah95b]. It turned out that APGs are efficient enough to form bicontinuous microemulsions, which was important progress because technical-grade APGs are less expensive than lecithin. Since the mineral *n*-alkanes are not biocompatible, Kahlweit *et al.* replaced *n*-alkanes with unsaturated fatty acid ethyl esters and replaced alkanols with alkane-1,2-diols, which are biocompatible yet surface-active enough to act as co-surfactant [Kah95c, Kah96]. Finally, due to its sensitivity to light and oxygen, the unsaturated fatty acid ethyl ester was replaced by the more stable saturated fatty acid ester isopropyl myristate (IPM). In this way, a non-toxic bicontinuous microemulsion consisting of $\text{H}_2\text{O} - \text{IPM} - \text{APG} - 1,2\text{-octanediol}$ was successfully formulated [Kah97].

Gelled Non-Toxic Microemulsions

Gelled non-toxic microemulsions are preferred to their non-gelled counterparts in transdermal drug delivery due to the mechanical stability, which provides an easy application and immobilizes drugs on the applied surface [Law12]. So far, most of the gelled microemulsions are polymer gels [Kan99, Cru01, Xua12, Fou13, Fro17], whose gel networks form through chemical and/or physical cross-linking of polymeric chains. In contrast, LMWG molecules self-assemble into gel networks through non-covalent interactions (physical). In the thesis at

hand, the goal is to combine the novel concept of forming gelled bicontinuous microemulsions via orthogonal self-assembly with the formulation of non-toxic microemulsions and explore their potentials in transdermal drug delivery (Figure 1.2).

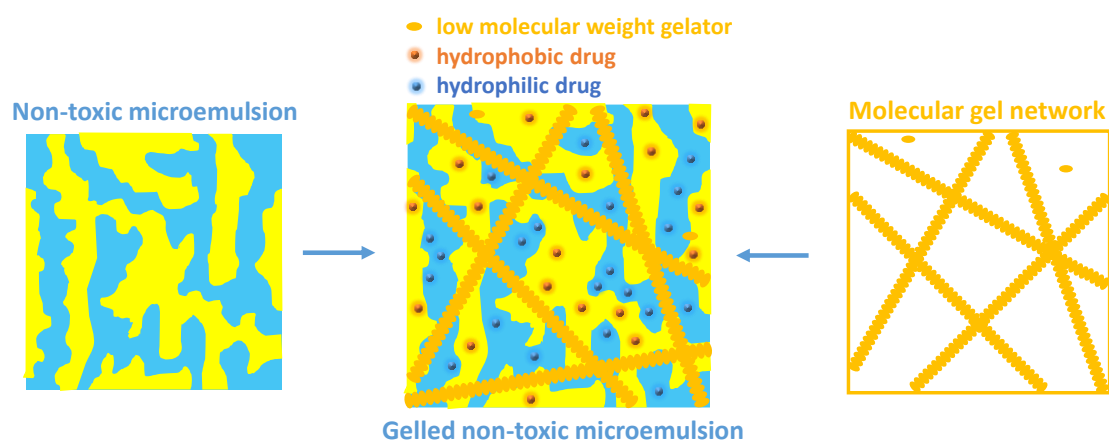


Figure 1.2: Schematic presentation of a drug-loaded gelled non-toxic microemulsion.

1.2 Task Description

In order to study the formation of gelled non-toxic microemulsions via orthogonal self-assembly and their potential use as a drug delivery system, three tasks need to be dealt with:

- (1) Formulation of non-toxic microemulsions with biocompatible components and model drugs.
- (2) Identification of a suitable low molecular weight gelator (LMWG) for the gelation of the microemulsion.
- (3) Examination of whether the orthogonality of the two structures is maintained, *i.e.* whether the system is formed via orthogonal self-assembly of the surfactant and the gelator.

(1) Regarding the formulation of non-toxic microemulsions, one first needs to find a biocompatible surfactant. Sugar surfactants, such as *n*-alkanoyl-*N*-methylglucamides (MEGA-*n*, Figure 1.3) and alkyl polyglucosides (APGs, denoted as C_nG_m , an example of C_nG_1 is given in Figure 1.3), are dermatologically safe, commercially available, and exhibit excellent surface activity [Hil99]. Due to their hydrophilicity, sugar surfactants form bicontinuous microemulsions only with the addition of co-surfactants. The APG-based model system $H_2O - n\text{-octane} - n\text{-octyl-}\beta\text{-D-glucopyranoside} (\beta\text{-}C_8G_1) - 1\text{-octanol}$ was extensively studied with

respect to its phase behavior, interfacial composition, interfacial tension, and microstructure [Klu00, Klu01, Sot02, Rei03]. As the oil *n*-octane and the co-surfactant 1-octanol are irritating to human bodies, they must be replaced by non-toxic saturated fatty acid esters, such as isopropyl myristate (IPM, Figure 1.3) and alkanediols (one example is given in Figure 1.3) [Kah96, Kah97]. Both IPM and alkanediols are bio-compatible and act as permeation enhancers in transdermal drug delivery [Kog06, Joh12, Wil12].

Based on the quoted previous studies, the tasks of the present thesis are the following: (a) Restudy the phase behavior of the scouting system $\text{H}_2\text{O} - n\text{-octane} - \beta\text{-C}_8\text{G}_1 - 1\text{-octanol}$ at $T = 25\text{ }^\circ\text{C}$ with equal volumes of water and oil to ensure a bicontinuous structure. (b) Replace the oil *n*-octane and the co-surfactant 1-octanol of the scouting system with non-toxic components, namely the oil IPM and the co-surfactant 1,2-octanediol. (c) Search for a more efficient and less expensive sugar surfactant, *e.g.* technical-grade APGs with longer carbon chains. (d) Formulate model drugs in the non-toxic bicontinuous microemulsions, namely the hydrophobic model drug lidocaine and the hydrophilic model drug diclofenac sodium salt (Figure 1.3). (e) Vary the oil-to-water ratios systematically along the trajectory of the middle phase to extend the application potential of the gelled non-toxic microemulsions.

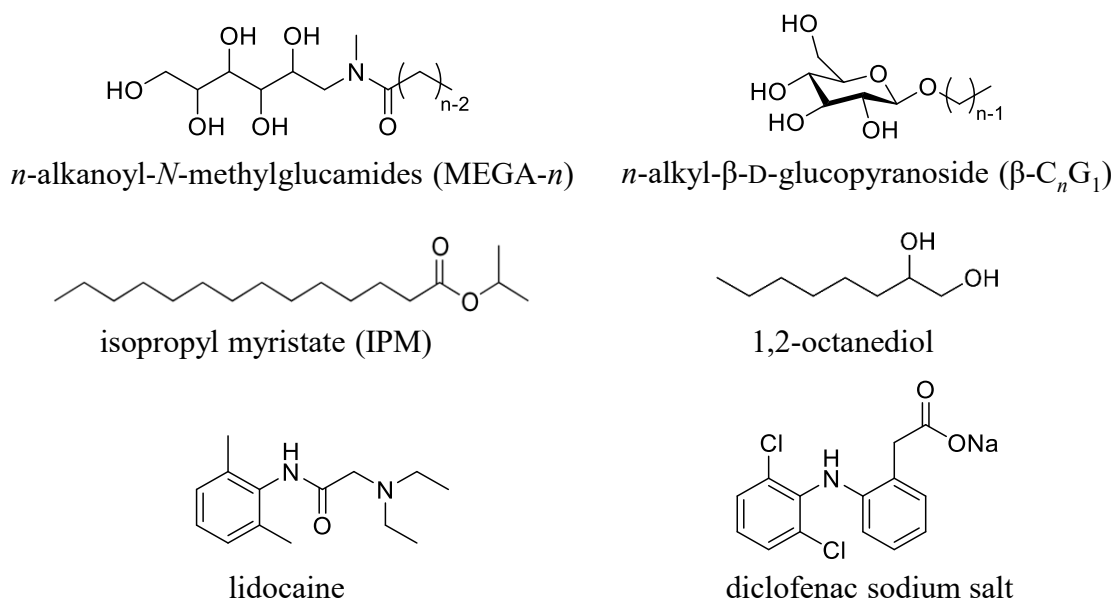


Figure 1.3: Molecular structures of used chemicals.

(2) Since the bicontinuous microemulsion contains equal volumes of oil and water, theoretically, both organogelator and hydrogelator could be suitable to gel the microemulsion. The chosen candidates are organogelators 12-hydroxyoctadecanoic acid (12-HOA) and 1,3:2,4-dibenzylidene-D-sorbitol (DBS), and hydrogelators *N,N'*-dibenzoyl-L-cystine (DBC) and DBS derivatives, namely 1,3:2,4-dibenzylidene-D-sorbitol-*p,p'*-dicarboxylic acid (DBS-COOH) and DBS-CONHNH₂ (Figure 2.8). 12-HOA is surface-active [Lau13], which thus might act as both gelator and co-surfactant, and ideally no additional co-surfactant other than 12-HOA would be needed for the formation of a microemulsion. In contrast, DBS and DBC are not surface-active, and the phase boundaries of gelled microemulsions should be consistent with those of the non-gelled counterparts. These gelators are first to be tested in the scouting system and then in the non-toxic system. With the variation of the oil-to-water ratios of the non-toxic microemulsion, two questions are to be answered: (a) Does the same gelator gel both water-rich and oil-rich microemulsions? (b) If not, does a hydrogelator gel the water-rich microemulsion and an organogelator the oil-rich microemulsion? The gel properties of the gelled non-toxic microemulsions are to be characterized by oscillation shear rheometry. The storage modulus G' and the loss modulus G'' are to be measured by frequency sweeps and the sol-gel transition temperature $T_{\text{sol-gel}}$ by temperature sweeps.

(3) In order to characterize the orthogonality of the gelled non-toxic microemulsion, the gelled non-toxic microemulsion is to be compared with the non-gelled counterpart. Firstly, the phase diagrams of both systems are to be compared to see whether the gelator affects the phase behavior of the bicontinuous microemulsion. Secondly, small-angle neutron scattering (SANS) is to be used to characterize the microstructure of the two systems. Thirdly, freeze-fracture electron microscopy (FFEM) is to be used to (i) visualize the coexistence of the bicontinuous microemulsion and the fibrillar gel network, and (ii) confirm the length scales of the microemulsion domains and of the gel network.

2 Theoretical Background

In the following sections, the two base systems of gelled non-toxic microemulsions are introduced, namely microemulsions and molecular gels. If not otherwise stated, the theory of microemulsions was taken from [Sot05, Sot08] and that of molecular gels from [Wei06, Geo06, Zwe13]. Additionally, the theoretical principles of rheology are introduced, of which the theory was taken from [Mez06, Bla18].

2.1 Microemulsions

A microemulsion consists of at least three components, namely a hydrophilic, a hydrophobic, and an amphiphilic one. In most cases, these three components are water, oil, and surfactant. Microemulsions have two characteristics: they are thermodynamically stable, and they have various nanostructures, which distinguish them from emulsions. The domain size of microemulsions is around 3–100 nm [Str94], whereas the droplet size of emulsions is within the μm range.

Phase Behavior

Phase behavior studies of microemulsions are necessary to determine the conditions where the surfactant solubilizes the maximum amounts of water and oil. The ternary systems consist of water, oil, and the nonionic surfactant n -alkyl polyglycol ethers (C_iE_j , where i denotes the hydrophobic carbon chain length, and j denotes the number of ethylene oxide groups) [Kah85]. These ternary nonionic microemulsions have been extensively studied [Kah87], and they are taken as an example to illustrate the general phase behavior of microemulsions.

To understand the complex behavior of the ternary system, one first needs to understand the binary base systems. Figure 2.1 depicts phase diagrams of the three binary systems. The binary system water – oil has a large miscibility gap. In the binary system oil – nonionic surfactant, the upper critical point cp_α is typically located below 0 °C, which means that the nonionic

of $\underline{2} - 3 - \bar{2}$. Below T_1 , the sample consists of an o/w-microemulsion (lower phase) and an oil excess phase (upper phase), denoted as “ $\underline{2}$ ” since the surfactant-rich phase is the lower phase. Between T_1 and T_u , a bicontinuous microemulsion middle phase coexists with a water (lower phase) and an oil excess (upper phase) phase, denoted as “3”. Above T_u , the sample consists of a water excess phase (lower phase) and a w/o-microemulsion (upper phase), accordingly denoted as “ $\bar{2}$ ” because the surfactant-rich phase is the upper phase. At a γ higher than $\tilde{\gamma}$, $\underline{2}$ and $\bar{2}$ still exist, but the three-phase region transforms into an isotropic bicontinuous phase without excess oil and water (denoted as “1”). The fishtail point \tilde{X} has the coordinates $\tilde{\gamma}$ and \tilde{T} . $\tilde{\gamma}$ represents the minimal mass fraction of surfactant needed to solubilize equal amounts of water and oil completely, which is a measure of the surfactant efficiency. \tilde{T} is called phase inversion temperature (PIT).

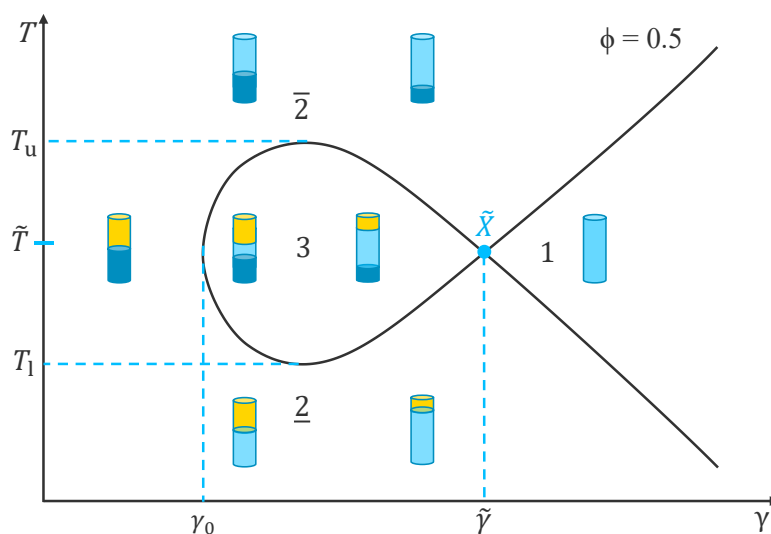


Figure 2.2: Schematic $T(\gamma)$ -section (“fish-cut”) at a constant oil/(oil + water) volume fraction $\phi = 0.5$. The test tubes illustrate the relative volumes of phases.

Another type of nonionic surfactant is sugar surfactants, whose phase behavior differs from that of C_iE_j type surfactants. Sugar surfactants are of great interest because of their nontoxicity and biodegradability. They are widely used in personal care, pharmaceuticals, and detergents [Hil99], and they can be manufactured from renewable resources. Sugar surfactants consist of a hydrophobic alkyl chain and a hydrophilic sugar head group. The bond between the alkyl

chain and the sugar head group can be an ester, an ether, an amine, or an amide. Alkyl glycosides are the most extensively studied sugar surfactants because of their excellent surface activities. They are often denoted as C_nG_m , where n denotes the alkyl chain length and m denotes the number of glucose units.

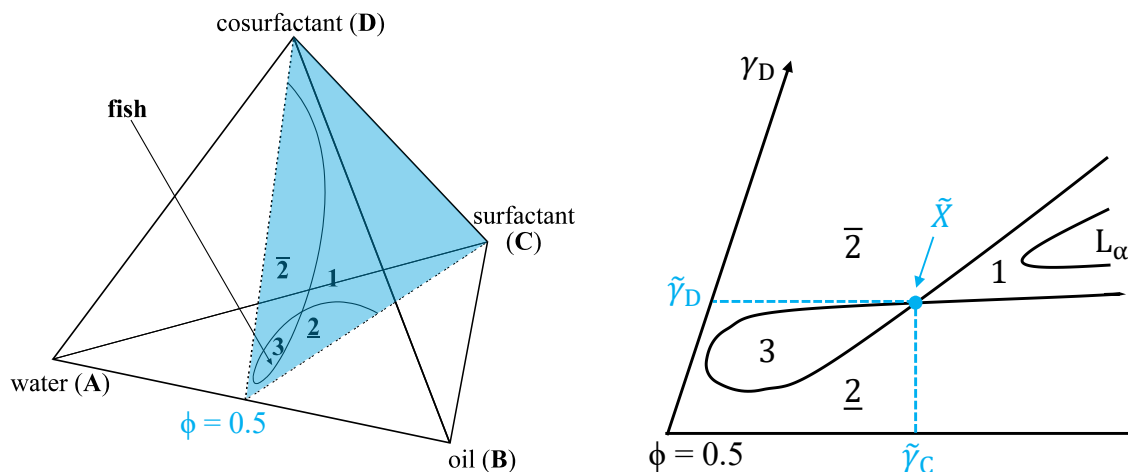


Figure 2.3: (Left) A schematic phase tetrahedron of quaternary system H_2O – oil – surfactant – co-surfactant at a constant temperature (modified from [Klu01]). (Right) A schematic section through the phase tetrahedron of the quaternary system H_2O – oil – C_nG_m surfactant – co-surfactant at $\phi = 0.5$ and a constant T .

One characteristic property of C_nG_m is that microemulsions stabilized with C_nG_m surfactants are less temperature-sensitive than those stabilized with C_iE_j surfactants. This is due to the strong hydrogen bonds between hydroxyl groups and water molecules, making dehydration difficult, even at high temperatures [Stu01]. Due to the temperature insensitivity, the phase behavior cannot be tuned by changes of temperature. The sugar head group is so hydrophilic that in the ternary system H_2O – oil – C_nG_m only o/w-microemulsions form. Therefore, a relatively hydrophobic co-surfactant (such as long-chain alcohol) is necessary to reach the middle point of a fish-cut, *i.e.* to form a bicontinuous microemulsion. In contrast to the phase prism of the ternary system of H_2O – oil – C_iE_j surfactant, the phase behavior of the quaternary system of H_2O – oil – C_nG_m surfactant – co-surfactant is depicted in an isothermal phase tetrahedron (Figure 2.3 (left)), which consists of four Gibbs phase triangles of the corresponding ternary systems. At a constant oil-to-water ratio ϕ , a $\gamma_D(\gamma_C)$ -section through the phase tetrahedron can be obtained, ($\phi = 0.5$ as an example in Figure 2.3 (right)). The two axes

present the mass fractions of the surfactant (C) and the co-surfactant (D), γ_C and γ_D , respectively. The fishtail point \tilde{X} has the coordinates $\tilde{\gamma}_C$ and $\tilde{\gamma}_D$. When γ_C is smaller than $\tilde{\gamma}_C$, phase transitions occur in the sequence of $\underline{2} - 3 - \bar{2}$ along with the addition of a co-surfactant. When γ_C is larger than $\tilde{\gamma}_C$, the increase of γ_D induces the phase transition sequence of $\underline{2} - 1 - \bar{2}$. At high surfactant concentrations, the lamellar phase exists in the 1-phase region.

Microstructure

Microemulsions are macroscopically homogeneous but heterogeneous on the nanoscopic scale. The main parameter determining the microstructure is the mean curvature H of the interfacial surfactant monolayer, which is defined as

$$H = \frac{c_1 + c_2}{2} \quad (2.1)$$

with $c_1 = 1/R_1$ and $c_2 = 1/R_2$ being the principal curvatures given by the two principal radii of curvature R_1 and R_2 of the surfactant monolayer. The curvatures are positive if the surfactant monolayer bends towards oil (o/w-microemulsion) and negative if it bends towards water (w/o-microemulsion). The mean curvature H , which can be experimentally determined [Str94], is closely related to the spontaneous curvature H_0 , *i.e.* the curvature of the interfacial surfactant monolayer if no external forces, thermal fluctuations, or conservation constraints exists. Another important parameter is the Gaussian curvature K , which is given by

$$K = c_1 c_2. \quad (2.2)$$

The variation of the mean curvature H of the interfacial surfactant monolayer can be induced by the change of temperature T , co-surfactant ratio δ , or salinity, *etc.* Figure 2.4 (left) illustrates the variation of the mean curvature H for the temperature-sensitive ternary system of $\text{H}_2\text{O} - \text{oil} - \text{C}_i\text{E}_j$. At low temperatures, the ethylene oxide head groups of C_iE_j surfactants are strongly hydrated, so the volume of the hydrophilic head groups in water is larger than the volume of the hydrophobic tails in oil, leading to a positive mean curvature. Thus, the surfactant

monolayer tends to enclose water, and o/w-microemulsions form. With increasing temperatures, the ethylene oxide head groups become less and less hydrated, which decreases the volume of the head groups, while the volume of the hydrophobic tails remains the same, resulting in a lower mean curvature H . When $H = 0$, the microstructure of the system transforms from discontinuous droplets in a continuous phase into two continuous phases. As the temperature increases further, the head groups become completely dehydrated so that H eventually turns into negative values. The surfactant monolayer tends to enclose oil, and w/o-microemulsions form. The same principle applies to the less temperature-sensitive quaternary system consisting of $\text{H}_2\text{O} - \text{oil} - \text{C}_n\text{G}_m - \text{co-surfactant}$ (Figure 2.4 (right)). The strong hydration of the sugar surfactant leads to large head groups and thus to a positive mean curvature H . The more hydrophobic co-surfactant has a smaller head group. Therefore, the addition of co-surfactants leads to the incorporation of the co-surfactant molecules into the surfactant monolayer, which causes a decrease of the mean curvature from $H > 0$ to $H < 0$. Here, the composition of the interfacial surfactant monolayer $\delta_{v,i}$ [Sot02] is the tuning parameter of the mean curvature.

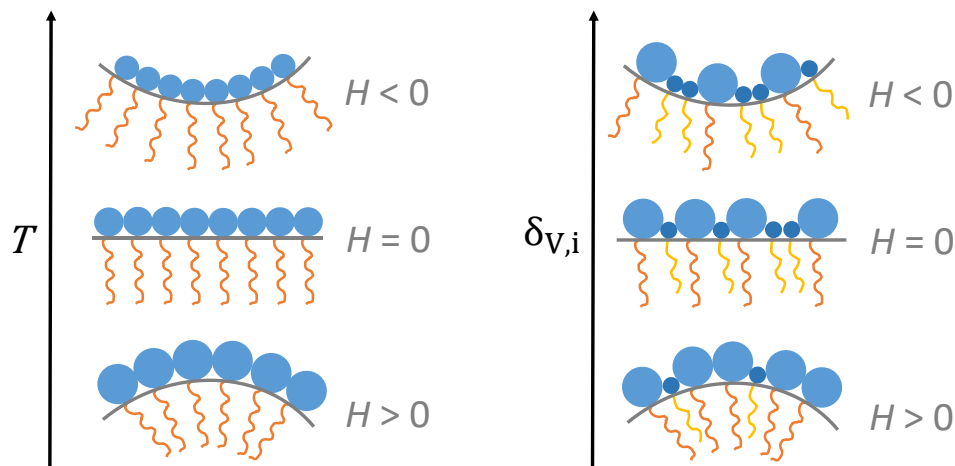


Figure 2.4: Mean curvature H of a nonionic surfactant monolayer at the water–oil interface as a function of (left) temperature T and (right) composition of the interfacial surfactant monolayer $\delta_{v,i}$.

Various experimental methods are available to characterize the microstructure quantitatively. Transmission electron microscopy provides direct and local information on the nanoscale [Jah88, Bur03]. Small-angle X-ray/neutron scattering (SAXS/SANS) determines the statistical length scales [Hel08]. NMR self-diffusion [Lin96] and electrical conductivity measurements

[Kah87] provide valuable information on the connectivity and on structural transitions. With the help of these experimental methods, extensive microstructure studies bring together an overview of the microstructure transitions caused by the change of the temperature and the surfactant concentration in the ternary systems $\text{H}_2\text{O} - \text{oil} - \text{C}_i\text{E}_j$ (Figure 2.5). At the phase inversion temperature \tilde{T} , the microemulsion always has a mean curvature of $H = 0$. At low surfactant concentrations near the \tilde{X} -point, bicontinuous structure exists in the middle phase of the 3-phase region and in the 1-phase region. The bicontinuous structure consists of two continuous sub-phases – water and oil – which are separated by a surfactant monolayer. The two domains interweave with each other and form a sponge-like structure, which has a mean curvature of $H = 0$ but a Gaussian curvature of $K < 0$ because c_1 and c_2 have opposite signs. As the surfactant concentration increases, the structure length scale becomes smaller because the total area of the internal interface increases. At high surfactant concentrations, the lamellar phase L_α is observed with a zero-curvature structure, being $H = 0$ and $K = 0$ ($c_1 = c_2 = 0$). Moving away from the \tilde{X} -point, $\gamma > \tilde{\gamma}$, o/w- or w/o-droplets appear at low or high temperatures, respectively. The droplet size decreases as γ further increases. During the transition from the bicontinuous structure to the droplet structure, one also observes elongated cylindrical domains.

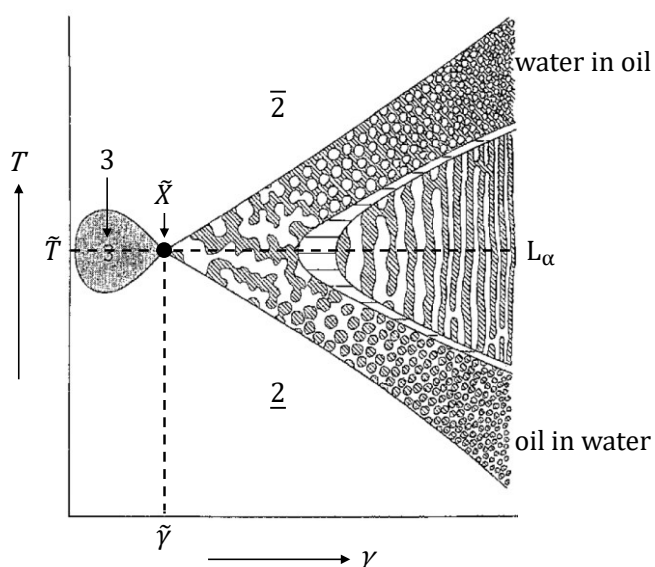


Figure 2.5: Schematic overview of the microstructures induced by the variation of temperature and surfactant concentration in nonionic microemulsions consisting of $\text{H}_2\text{O} - \text{oil} - \text{C}_i\text{E}_j$. The white regions represent water, and the shaded regions represent oil. Modified from [Str94].

2.2 Molecular Gels

Definition and Characteristics

Gels have been discovered for more than 150 years [Gra61]. Over the years, the definition of gels continues evolving. Generally, a substance is regarded as a gel if it (i) has a continuous microscopic structure that is permanent on the time scale of analytical experiments and (ii) has solid-like rheological behavior despite consisting mostly of a fluid. A gaseous or liquid system consisting of at least two components forms a gel if one of the components forms a three-dimensional (3D) entangled solid network within the bulk gas or liquid phase. The solid network restricts the flow of the remaining fluid bulk phase, which macroscopically appears as a solid.

There are several possibilities to classify gels, *e.g.*, according to the physical state of the bulk phase or the chemical nature of the components. A practical classification is to distinguish between chemical and physical gels. In chemical gels, *e.g.* cross-linked polymeric systems, the formation of a 3D network occurs through covalent cross-linking of polymers. The network structure is permanent unless the covalent cross-links are broken. In physical gels, the formation of a 3D network occurs through non-covalent interactions, such as hydrogen bonds, van der Waals forces, dipolar interactions, and π - π stackings. Thus, the formation of physical gels is thermoreversible. Physical gels can be formed with various substances, *e.g.* clays, polymers, proteins, colloids, and certain small organic compounds. Molecular gels are physical gels formed by small organic compounds called low molecular weight gelators (LMWGs). LMWG molecules have a molecular weight of less than 2000 Da, and they can gel organic solvents or water. If an LMWG gels organic solvents, it is called an organogelator. If an LMWG gels water, it is called a hydrogelator.

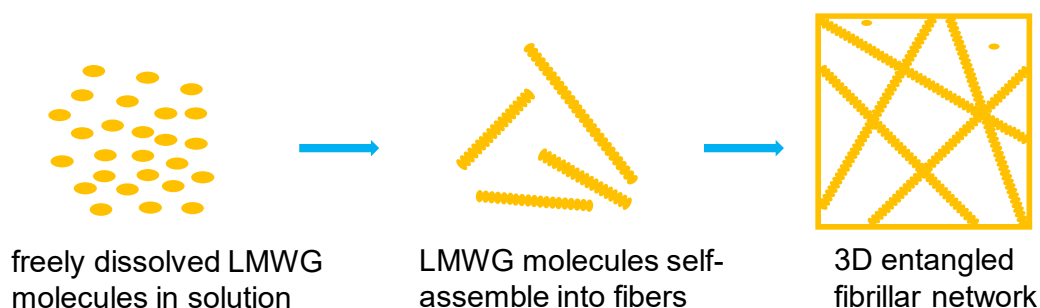


Figure 2.6: Schematic depiction of the molecular gel formation process.

The formation process of molecular gels is schematically depicted in Figure 2.6. Molecular gels are most commonly prepared by cooling a solution (or sol) with a low concentration of an LMWG (frequently ≤ 2 wt.%) in the solvent to be gelled below the characteristic gelation temperature. Thus, the solution is supersaturated, and microscopic phase separation occurs, which leads to the crystallization of LMWG molecules. The LMWG molecules self-assemble in stochastic nucleation events, and highly specific non-covalent interactions allow preferential one-dimensional nuclei growth into crystal-like fibers. These fibers have the same function as polymers in polymer gels and aggregate into a fibrous 3D entangled network. The essential formation of so-called “junction zones” (nodes) [Ter95] provides rigidity to the 3D network and distinguishes it from an aggregate of 1D fibrillar objects which do not interact. The shapes of junction zones range from strands, tapes, chiral ribbons, and tubules to other various aggregates with large aspect ratios. Note that the aggregation of gelator molecules and gel fibers occurs through non-covalent interactions, which are considerably weaker than covalent bonds.

Two important characteristics of LMWGs are the minimum gelation concentration (*mgc*) and the gel–sol phase transition temperature $T_{\text{sol-gel}}$. The minimum gelation concentration, also called the critical gelation concentration (*cgc*), is the minimum amount of the gelator to gel a specific solvent. The gel–sol phase transition temperature $T_{\text{sol-gel}}$ is the temperature at which the gel loses its structural integrity. $T_{\text{sol-gel}}$ depends on the molecular structure of the gelator, the nature of the solvent, and the total gelator concentration. With the determination of $T_{\text{sol-gel}}$ in a solvent over a range of gelator concentrations, one can establish a phase diagram for the

gelator–solvent combination (Figure 2.7). The sol phase is the solution of gelators in the solvent, while the gel phase consists of the gelator solution and the 3D gel network (solid). Thus, the gel-to-sol transition line is a measure of the gelator solubility in the solvent c_{sol} [Chr18]. As the gelator concentration increases, $T_{\text{sol-gel}}$ also increases until it reaches a plateau. Above the gelator concentration threshold, where the $T_{\text{sol-gel}}$ reaches a plateau, the melted gelator and the solvent are no longer miscible, corresponding to a monotectic transformation [Chr16].

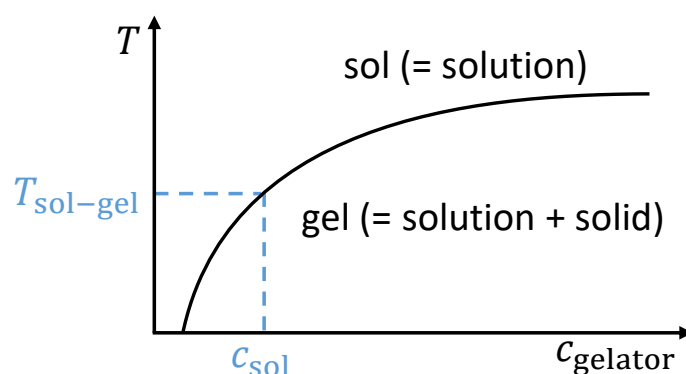


Figure 2.7: Example of a phase diagram for a gelator in a solvent.

Versatile experimental techniques are available to determine phase diagrams and to characterize the macroscopic behavior of molecular gels. The “tabletop” rheology can be carried out in a laboratory without sophisticated equipment, which gives a “quick and dirty” overview of the general properties such as mgc and $T_{\text{sol-gel}}$. One can thus quickly establish a phase diagram of a specific solvent–gelator system. The most common methods are *tube inversion* and *dropping ball* [Rag06]. A more precise yet simple method to map the phase diagram is liquid NMR, which yields the gelator solubility as a function of temperature with a single sample [Chr18]. Quantitative characterizations of the viscoelastic properties can be obtained by oscillatory rheology (see Section 2.3 for more details). Depending on the measuring programs, oscillatory rheology characterizes the yield point, the gel–sol transition temperature $T_{\text{sol-gel}}$, and the recovery time after destructive stress (thixotropy). Differential scanning calorimetry (DSC) determines the gel–sol transition temperature (both on heating and cooling) and the phase-change enthalpy ($\Delta H_{\text{gel-sol}}$), which provides insight into the thermodynamics of intermolecular actions [Rag06]. On the nanoscale, the fiber and gel

morphology can be visualized with transmission electron microscopy (TEM) and scanning electron microscopy (SEM). Additionally, atomic force microscopy (AFM) can provide information on fiber width and height [Neb13, Gue18]. Instead of the bundled/aggregated gel fibers observed in electron microscopy images, small-angle X-ray/neutron scattering (SAXS/SANS) provides averaged information about the dimensions of molecular fibrils [Ter06].

Low molecular weight gelators (LMWGs)

In the thesis at hand, five LMWGs with a wide variety of molecular structures were chosen (see Figure 2.8 for molecular structures). We chose two organogelators, namely 12-hydroxyoctadecanoic acid (12-HOA) and 1,3:2,4-dibenzylidene-D-sorbitol (DBS). In addition, we studied three hydrogelators, namely *N,N'*-dibenzoyl-L-cystine (DBC) and the derivatives of DBS, 1,3:2,4-dibenzylidene-D-sorbitol-*p,p'*-dicarboxylic acid (DBS-COOH) and 1,3:2,4-dibenzylidene-D-sorbitol-*p,p'*-dihydrazide (DBS-CONHNH₂). The gelation demands a meticulous balance between solubility and crystallinity of LMWGs. If the gelator is highly soluble in the solvent, gelation does not occur. If the gelator is too insoluble, it precipitates or crystallizes rapidly. Therefore, although the chemical properties and the molecular structures of the LMWGs do play a role, it remains trial and error to know which gelator gels which solvent. In the following, the properties of the five gelators will be briefly described.

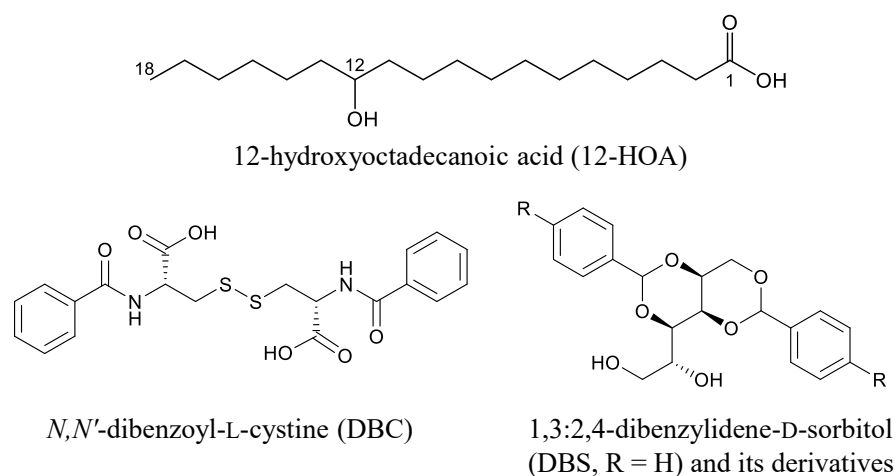


Figure 2.8: Molecular structures of the chosen LMWGs.

12-Hydroxyoctadecanoic/hydroxystearic acid (12-HOA/12-HSA) is one of the most widely studied LMWGs, which belongs to the long-chain saturated fatty acid type. The unique self-assembly behavior of 12-HOA originates from its chemical structures of a carboxylic head group and a secondary hydroxyl group. The presence of a hydroxyl group at position 12 on the C₁₈-fatty acid chain induces interaction possibilities and molecular chirality. Hence, 12-HOA can gel various organic solvents, such as vegetable oils, long-chain alkanes, cycloalkanes, long-chain aldehydes, ethers, short-chain alkanediols, nitriles, and thiols [Gao12, Lan15]. The intermolecular interactions of 12-HOA are mainly hydrogen bonding. The carboxylic acid head group of the molecule forms cyclic dimers with the adjacent molecule, meanwhile facilitating interactions between hydroxyl groups. Both interactions lead to unidirectional hydrogen bonding sequences along the fiber axis [Ter94, Sat08, Sat11]. Furthermore, 12-HOA with alkali metals or alkanolamines as counterions also gels aqueous solutions [Fam20]. Various structures are reported, such as fibers, tubes, and helical ribbons [Lau15]. The structures depend on the enantiomer purity of 12-HOA, the type of counterions, and the molar ratio between 12-HOA and counterions.

DBC as an amino acid derivative is an efficient hydrogelator. It gels water at a very low gelator content of 0.1 wt.% (2 mM) and forms a firm, translucent gel at a concentration of 4 mM in ethanol (5%)/water. The self-assembly of DBC is caused by hydrogen bonds between amide-NH and carboxyl-CO functionalities. Besides, π - π stacking of the aromatic rings promotes the formation of gel fibers. Furthermore, the disulfide linkage -S-S- is critical for the gelation, presumably because the disulfide linkage forms a linear backbone, and its conformational rigidity favors hydrogen-bonding contacts. Overall, gel fibers are held together by a favorable backbone orientation enhanced by hydrogen bonding and π - π stacking or hydrophobic interactions [Men95, Men00]. Note that the gelation of DBC only occurs when the pH is below 5 [Zie13]. At basic conditions, the ionized carboxyl groups destroy the gel due to electrostatic repulsion.

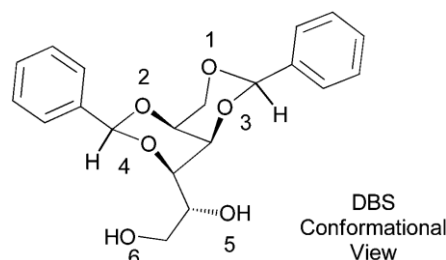


Figure 2.9: A conformational perspective of the molecular structure of 1,3:2,4-dibenzylidene-D-sorbitol (DBS, taken from [Oke15]).

DBS is a well-known organogelator of the sorbitol derivative type. It has been widely used in cosmetics, biomedical materials, and electronic devices. DBS has a chiral butterfly-shaped conformation – the D-sorbitol backbone is the “body,” and the phenyl rings are the “wings”. The butterfly-like DBS has two potential gelation mechanisms: (1) hydrogen bonding of the “body” with 5-OH/6-OH groups (see Figure 2.9) of one molecule being hydrogen bond donor and the 5-OH/6-OH or the cyclic acetals of another being hydrogen bond acceptor, and (2) π - π stacking or solvophobic interactions between the aromatic “wings” of two molecules. Experimental and theoretical results reveal that (a) in non-polar solvents, intermolecular hydrogen bonding, mainly from the 6-OH group, plays a key role in self-assembly; (b) in polar or protic solvents, intermolecular hydrogen bonding becomes less significant, while π - π stacking or solvophobic interactions between the aromatic “wings” become more dominant [Oke15]. To increase the solubility of DBS in water, one can modify DBS with additional functional groups on the aromatic rings. The resulting DBS derivatives can act as hydrogelators. DBS-COOH requires protonation of the carboxyl groups to gel. Thus the gelation is induced by slow acidification of DBS-COOH in a basic solution [Cor13]. The other hydrogelator DBS-CONHNH₂ is pH-tolerant, which is potentially easier to use than DBS-COOH [Oke13].

2.3 Rheology

Rheology is essential to characterize quantitatively the mechanical properties of gels. Rheological measurements provide information about the flow behavior of liquids and the deformation behavior of solids caused by shear forces. All types of rheological behavior are

between the two extreme cases: the flow behavior of ideally viscous liquids and the deformation behavior of ideally elastic solids.

Viscous behavior

The Two-Plates-Model is used to define the fundamental rheological parameters (Figure 2.10 (left)). An upper plate with a shear area A is set in motion by the shear force F , resulting in a velocity v to be measured. The distance between the upper plate and the stationary lower plate ($v = 0$) is the shear gap z . The sample is sheared in this shear gap. If there are no wall-slip effects, the sample adheres to both plates, and if the flow is laminar, the shear stress is defined as

$$\tau = F/A \text{ [Pa]}. \quad (2.3)$$

The shear rate is defined as

$$\dot{\gamma} = dv/dz = v/z \text{ [s}^{-1}\text{]}, \quad (2.4)$$

given laminar flow conditions ($dv = \text{const.}$, $dz = \text{const.}$). Accordingly, the shear viscosity is given by

$$\eta = \tau/\dot{\gamma} \text{ [Pa}\cdot\text{s]}. \quad (2.5)$$

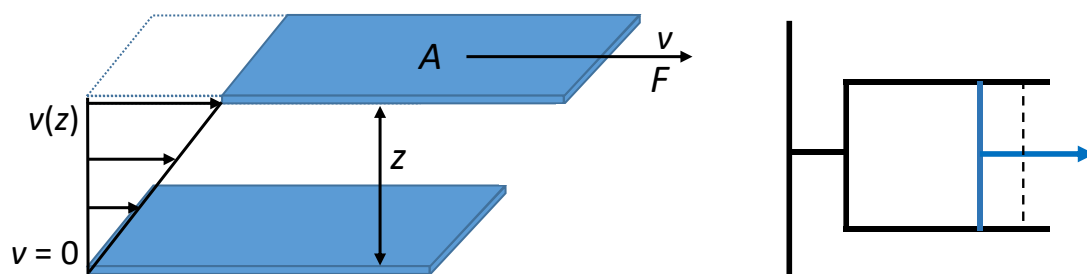


Figure 2.10: Schematic presentations of (left) the Two-Plates-Model for flow behavior, (right) the dashpot model.

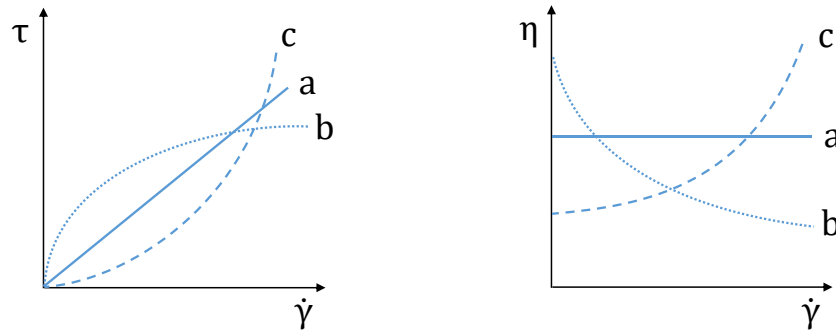


Figure 2.11: Flow curves (left) and viscosity functions (right) of the three types of flow behaviors: a = ideally viscous, b = shear-thinning, c = shear-thickening.

The ideally viscous (or Newtonian) flow behavior fulfills Newton's law

$$\tau(t) = \eta \cdot \dot{\gamma}(t), \quad (2.6)$$

i.e., the $\tau(\dot{\gamma})$ -flow curve is a straight line and has a constant slope (Figure 2.11 (left)). Analogously, the viscosity function $\eta(\dot{\gamma})$ -curve of an ideally viscous or Newtonian fluid is a flat line (Figure 2.11 (right)) since the shear viscosity is independent of the magnitude and duration of the shear load applied. The flow behavior of a Newtonian fluid can be represented by the dashpot model (Figure 2.10 (right)). Under a constant force, the piston and the dashpot fluid move with a constant velocity or deformation rate, and the velocity is proportional to the force strength. The proportionality corresponds to the internal friction of the dashpot, *i.e.* the viscosity. Once the force is removed, the piston stops moving immediately, and thus the ideally viscous fluid remains deformed. During the flow or deformation process, the applied deformation energy is converted to frictional heating (also called viscous heating) between molecules. The resulting thermal energy partially heats up the fluid and partially goes to the surrounding environment. Therefore, the deformation process is irreversible. In ideally viscous fluids, such as water, oils, and pure solvents, there are no strong interactions between molecules. However, there are also other types of fluids, namely shear-thinning and shear-thickening fluids (Figure 2.11). For shear-thinning fluids, the viscosity decreases with increasing shear rate, and the slope of the $\tau(\dot{\gamma})$ -flow curve decreases with increasing $\dot{\gamma}$. Vice versa, for shear-thickening fluids, the viscosity increases with increasing shear rate, and the slope of the $\tau(\dot{\gamma})$ -flow curve increases.

Elastic Behavior

The Two-Plates-Model can also be used to define the elastic behavior of solids (Figure 2.12 (left)). A shear force F is applied on the upper plate with a shear area A while the lower plate is stationary ($s = 0$), resulting in a deflection s and a deflection angle φ . The sample is sheared in the shear gap z . If there are no wall-slip effects, the sample adheres to both plates, and if the sample is deformed homogeneously throughout the shear gap, the shear deformation or shear strain is defined as

$$\gamma = s/z = \tan \varphi. \quad (2.7)$$

The shear rate $\dot{\gamma}$ defined in *Flow Behavior* can be interpreted as the time derivative of γ , which writes

$$\dot{\gamma} = d\gamma/dt \text{ [s}^{-1}\text{]}. \quad (2.8)$$

At a constant temperature, the ratio of the shear stress τ and the corresponding shear strain γ is a material constant if the measuring conditions are within the reversible-elastic deformation range (linear-elastic range). This ratio is called shear modulus or rigidity modulus G and gives information about the rigidity of a material. It holds

$$G = \tau/\gamma \text{ [Pa]}. \quad (2.9)$$

If the molecules of the material have strong intermolecular or crystalline cohesive forces, it exhibits high rigidity and a high G -value.

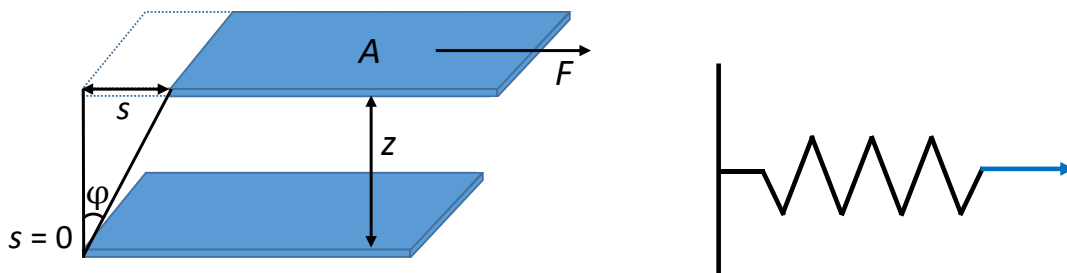


Figure 2.12: Schematic presentations of (left) the Two-Plates-Model for elastic behavior, (right) the spring model.

The ideally elastic (or Hookean) deformation behavior fulfills Hooke's law, namely

$$\tau(t) = G \cdot \gamma(t). \quad (2.10)$$

The deformation of an elastic solid is proportional to the applied force (shear stress) within the linear-elastic range, and the $\tau(\gamma)$ -function has a constant slope, *i.e.* the shear modulus G . The shear modulus is independent of the magnitude and duration of the applied shear load. The ideally elastic behavior can be illustrated by the spring model (Figure 2.12 (right)). If a constant force is applied, the spring deforms immediately and remains deformed as long as the force is present. The deformation disappears immediately after the removal of the force and returns to the initial state. In contrast to the dashpot model of the ideally viscous liquid, the spring has no viscous behavior at all. During the shear process, the applied deformation energy is entirely stored within the deformed material. The stored energy enables a complete reformation of the material once the load is removed. Thus, the deformation process is reversible for ideally elastic solids. The ideally elastic deformation behavior requires relatively strong interactions between atoms or molecules of the material, such as stone and steel. However, beyond the linear-elastic range, brittle fractures occur.

Viscoelastic Behavior

Viscoelastic materials exhibit both viscous and elastic behavior. The viscous portion follows Newton's law, while the elastic portion behaves according to Hooke's law. Viscoelastic materials show a time-dependent and delayed response to stress or strain when applied and removed. The rheological behavior of viscoelastic liquids differs from that of viscoelastic solids. To illustrate the difference, we use the Maxwell model to represent viscoelastic liquids and the Kelvin/Voigt model to represent viscoelastic solids.

The Maxwell model combines a dashpot and a spring in serial connection (Figure 2.13 (left)). Upon applying a constant force, the spring deforms immediately and reaches a constant deflection value, which is proportional to the applied force. Subsequently, the piston of the

dashpot starts to move with a constant velocity until the deformation reaches a constant value, which correlates to the applied force and the duration of time. When removing the force, the spring bounces back to its initial state immediately, while the dashpot remains at its deformed position. As a result, the elastic portion shows a reformation while the viscous portion leads to permanent deformation. The overall behavior resembles a liquid, thus the Maxwell model represents viscoelastic liquids.

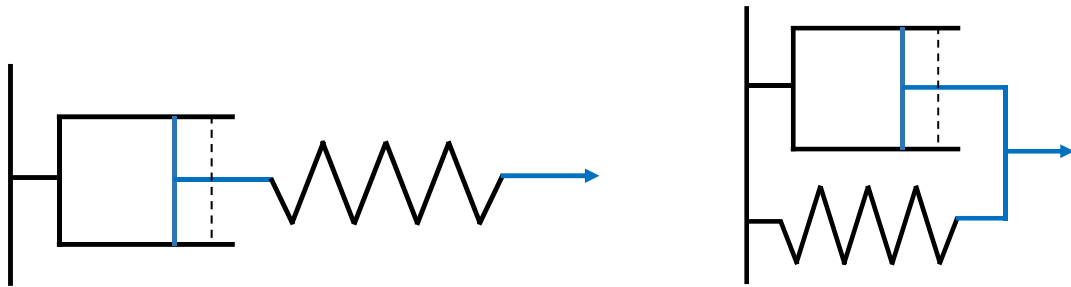


Figure 2.13: Schematic presentation of (left) the Maxwell model for viscoelastic liquids, (right) the Kelvin/Voigt model for viscoelastic solids.

The Kelvin/Voigt model is a parallel combination of a spring and a dashpot connected by a rigid frame (Figure 2.13 (right)). Since the two components are connected by a rigid frame, they must move simultaneously and to the same extent. Therefore, upon applying a constant force, the spring cannot deform instantly. Instead, the shear strain increases as a time-dependent exponential function until it reaches the maximum. When removing the force, the spring tends to bounce back immediately. However, the dashpot slows down the process, leading to a time-dependent decreasing exponential function $\gamma(t)$. After a sufficiently long time, the reformation completes, and both the spring and the dashpot go back to the starting position ($\gamma = 0$). Overall, the Kelvin/Voigt model displays a reversible but delayed deformation process, which behaves essentially like a solid. Thus, the Kelvin/Voigt represents viscoelastic solids.

Oscillating Shear Rheometry

Oscillatory shear rheometry is used to examine the rheological properties of all kinds of viscoelastic materials, including gels. Other types of rheometry, such as rotational rheometry that characterizes the flow behavior of liquids, are left out from this section since they are less

relevant. The same shear conditions of the Two-Plates-Model as in *Elastic Behavior* are assumed: (1) There are no wall-slip effects, and the sample adheres to both plates. (2) The sample is deformed homogeneously throughout the shear gap. Additionally, the applied shear load (either shear stress or shear strain) oscillates sinusoidally, causing a deflection path of $\pm s$, while the lower plate stays stationary (deflection $s = 0$, Figure 2.14).

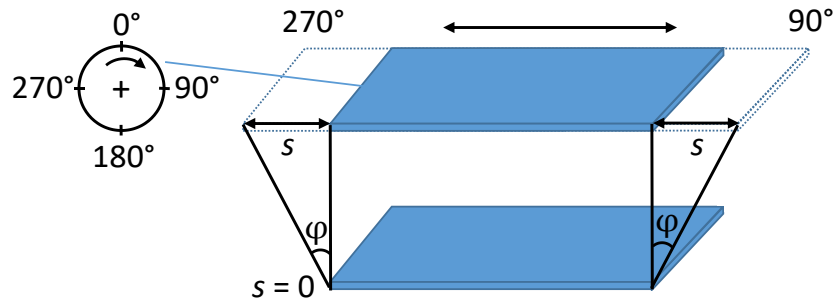


Figure 2.14: Schematic presentation of the Two-Plates-Model for oscillatory tests.

There are two preset modes for oscillatory tests: (1) Preset the shear strain γ as a sinusoidal function

$$\gamma(t) = \gamma_A \cdot \sin \omega t, \quad (2.11)$$

where γ_A is the shear strain amplitude, and ω is the angular frequency. This test method is called the controlled shear rate/deformation (CSR/CSD) test. (2) Preset the shear stress τ as a sinusoidal function

$$\tau(t) = \tau_A \cdot \sin \omega t \quad (2.12)$$

with τ_A being the shear stress amplitude, which is called the controlled shear stress (CSS) test. Here we preset the shear strain γ as a sinusoidal function (CSR test) to deduce the response functions: (a) For ideally elastic behavior, Hooke's law applies. Combining Equation 2.10 and 2.11, one obtains

$$\tau(t) = G \cdot \gamma(t) = G \cdot \gamma_A \cdot \sin \omega t. \quad (2.13)$$

Thus, there is no delay between the resulting $\gamma(t)$ -curve and the preset $\tau(t)$ -curve, *i.e.*, the phase shift angle (or loss angle) δ between the preset and the resulting curve is 0° (Figure 2.15). The

shear rate is

$$\dot{\gamma}(t) = d\gamma(t)/dt = \gamma_A \cdot \omega \cdot \cos \omega t, \quad (2.14)$$

which is shifted by 90° compared to the $\gamma(t)$ -curve. (b) For ideally viscous behavior, Newton's law applies. Combining Equation 2.6 and 2.14, one obtains

$$\tau(t) = \eta \cdot \dot{\gamma}(t) = \eta \cdot \gamma_A \cdot \omega \cdot \cos \omega t. \quad (2.15)$$

Therefore, both the $\dot{\gamma}(t)$ -curve and the $\tau(t)$ -curve have a phase shift angle of $\delta = 90^\circ$ compared to the preset $\gamma(t)$ -curve (Figure 2.15). (c) For viscoelastic behavior, the $\tau(t)$ -curve has a phase shift angle δ compared to the preset $\gamma(t)$ -function:

$$\tau(t) = \tau_A \cdot \sin(\omega t + \delta). \quad (2.16)$$

Overall, it always stands that for ideally elastic behavior $\delta = 0^\circ$, for ideally viscous behavior $\delta = 90^\circ$, and for viscoelastic behavior $0^\circ < \delta < 90^\circ$ (Figure 2.15).

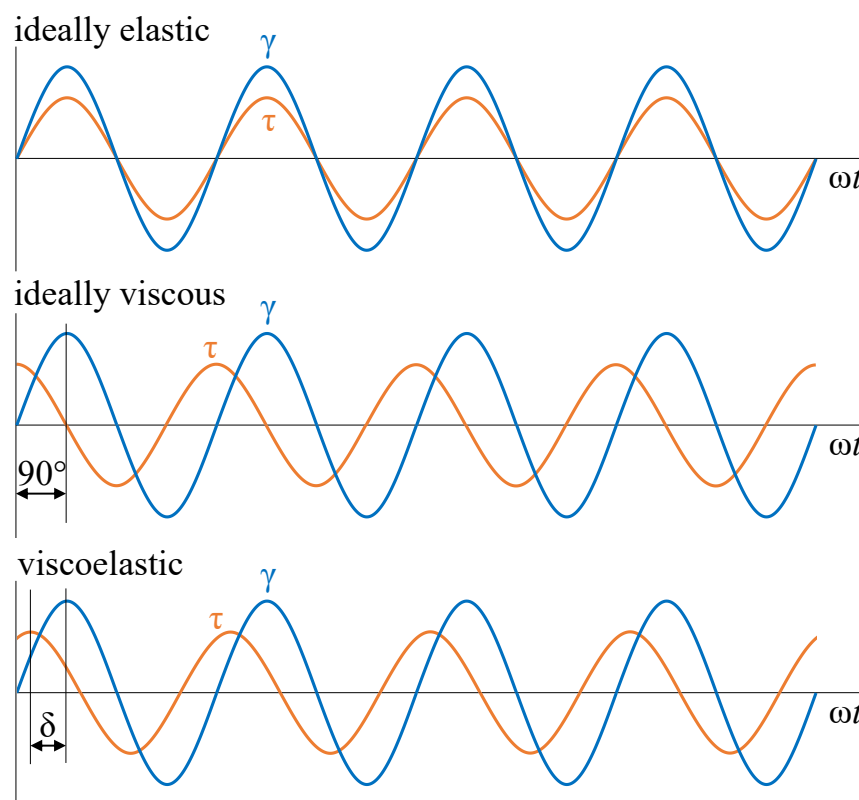


Figure 2.15: The oscillating curves of ideally elastic, ideally viscous, and viscoelastic behaviors. Preset is a sinusoidal shear strain $\gamma(t)$, and the shear stress $\tau(t)$ is the resulting response.

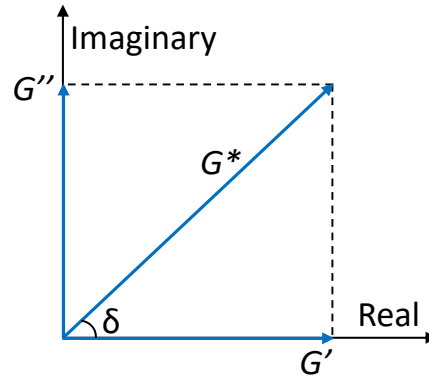


Figure 2.16: The vector diagram of the complex shear modulus G^* .

Through the oscillatory tests, the complex shear modulus is obtained:

$$G^* = \tau(t)/\gamma(t) \text{ [Pa]}. \quad (2.17)$$

On the complex plane in Figure 2.16, it gives

$$G^* = G' + iG'', \quad (2.18)$$

with the imaginary unit $i = \sqrt{-1}$. Then the real component

$$G' = G^* \cdot \cos \delta = (\tau_A/\gamma_A) \cdot \cos \delta \quad (2.19)$$

is the storage modulus, and the imaginary component

$$G'' = G^* \cdot \sin \delta = (\tau_A/\gamma_A) \cdot \sin \delta \quad (2.20)$$

is the loss modulus. The storage modulus G' is a measure of the deformation energy stored by the sample during the shear process, which is the driving force for reformation when the load is removed. Thus, the storage modulus G' represents the elastic behavior of the material. The loss modulus G'' is a measure of the deformation energy consumed by the sample for frictional heating during the shear process and represents the viscous behavior of the tested material. The loss factor or damping factor is defined as

$$\tan \delta = G'/G''. \quad (2.21)$$

It reveals the ratio of the viscous and the elastic portion of the viscoelastic behavior. Since the

phase shift angle has the range of $0^\circ \leq \delta \leq 90^\circ$, it holds $0 \leq \tan \delta \leq \infty$. When a sol forms a gel, its elastic behavior exceeds the flow behavior. The sol–gel transition point is where the storage modulus G' equals the loss modulus G'' , and it holds for the damping factor $\tan \delta = 1$ and the phase shift angle $\delta = 45^\circ$.

For molecular gels, rheology is often used to characterize the linear viscoelasticity, the gel–sol transition temperature $T_{\text{sol-gel}}$, the kinetics of gelation, the material failure modes, and the timescale of viscoelastic recovery. In this thesis, rheological measurements are focused on the linear viscoelasticity and $T_{\text{sol-gel}}$.

When the moduli are measured as a function of the applied shear strain or stress at a fixed frequency, gels typically show a linear regime or plateau called the linear viscoelastic range (LVE range) until the magnitude of the storage modulus G' drops considerably and falls below the loss modulus G'' (Figure 2.17). This measurement is called an amplitude sweep. In the LVE range, it always holds that $G' > G''$, and the power-law applies $G', G'' \sim (\gamma, \tau)^0$. Moreover, there is no significant internal structure change, *i.e.*, the elasticity is reversible. The limiting point of the LVE range is called the yield point. At higher shear strains or stresses, the material loses its gel character. The point where $G' = G''$ is called the flow point, and the range between the yield point and the flow point is called the yield zone. In this range, although the sample still has gel behavior, the elasticity is irreversible. Nevertheless, instant recovery behavior has been observed for some molecular gels due to their physical bond reformation of the gel network [Ohs14, Mal16].

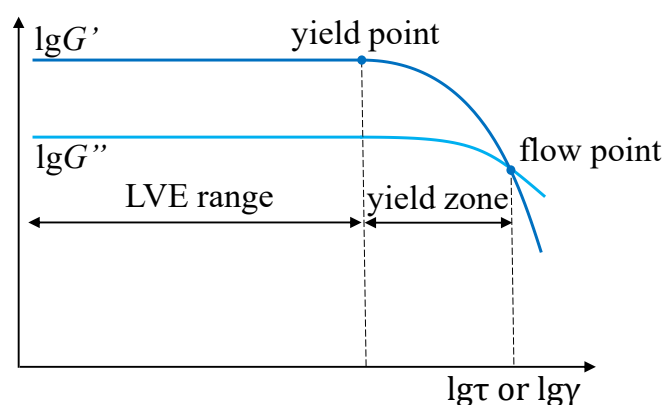


Figure 2.17: Schematic presentation of an amplitude sweep curve, showing a double-logarithmic scale of the storage modulus G' and the loss modulus G'' as a function of shear stress/strain.

After having determined the LVE range from amplitude sweeps, frequency sweeps can be used to investigate the time-dependent deformation behavior of gels since the frequency is the inverse value of time. G' and G'' are measured at fixed shear stress or strain within the LVE range and constant temperature as a function of frequency. The short-term behavior can be obtained at high frequencies and the long-term behavior at low frequencies. For gels, it always holds $G' > G''$ over the entire frequency range, and the G' -curve and the G'' -curve are parallel to each other. In most cases, the power-law applies $G' \sim \omega^\beta$. Figure 2.18 (left) shows frequency sweeps of the organogel liquid paraffin/DBS at various gelator concentrations (G'' -curves omitted) [Liu13]. When the gelator concentration increases above 0.35 wt.%, the shape of the $G'(\omega)$ -curve is less steep compared to those at low gelator concentrations, and the magnitude of G' is much larger, which means decently strong gels are formed.

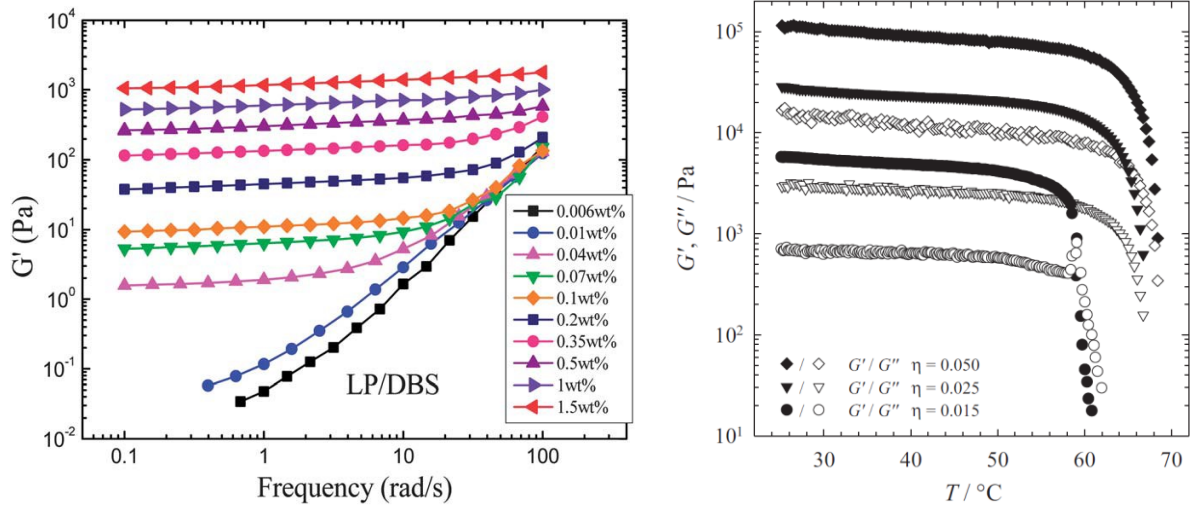


Figure 2.18: (left) Dependence of G' on the angular frequency ω of the organogel liquid paraffin/DBS at various DBS concentrations [Liu13]. (right) Storage modulus G' and loss modulus G'' of the organogel *n*-decane/12-HOA with 1.5 wt.%, 2.5 wt.%, and 5.0 wt.% gelator as a function of temperature [Lau15].

The gel–sol transition temperature $T_{\text{sol-gel}}$ can be determined by a temperature sweep. G' and G'' are measured as a function of temperature T at a fixed frequency and fixed shear stress or strain, which is within the LVE range. At low temperatures, it holds $G' > G''$ as the sample is a solid-like gel with elasticity. As the temperature increases, the gel starts to lose its elasticity and transforms into a less viscous liquid sol since gelator molecules are dissolved. At $T_{\text{sol-gel}}$, which is actually a temperature range of 5–10 °C, the storage modulus G' drops sharply and crosses over with the loss modulus G'' . Increasing the temperature further, $G'' > G'$, which means the viscous behavior dominates over the elastic behavior, and the sample becomes liquid. Figure 2.18 (right) shows temperature sweeps of the organogel *n*-decane/12-HOA [Lau15]. As described in Section 2.2, the $T_{\text{sol-gel}}$ -value as well as the G' - and G'' -values increase with increasing gelator concentration.

3 Methods

3.1 Chemicals, Sample Preparation and Visual Phase Studies

Chemicals

All chemicals used in this study are listed in Table 3.1. The chemicals were used without further purification. Plantacare contains a tiny amount of Mg^{2+} (< 500 ppm) and has basic pH values for preservative purposes, which caused the microemulsion samples to be slightly turbid. For a clear visual observation, the Plantacare surfactant was neutralized by adding citric acid anhydrous before use, leading to transparent microemulsions. Note that the effect of Mg^{2+} and citric acid on the phase behavior of microemulsions is negligible.

Table 3.1: Chemicals used in this study.

Name	Abbreviation	Supplier	Purity
water	H_2O		bidistilled
deuterium oxide	D_2O	Eurisotpo	> 99.9%
sodium chloride	NaCl	Merck	$\geq 99.5\%$
<i>n</i> -octane		Alfa Aesar	> 98%
1-octanol		Aldrich	99%
isopropyl myristate	IPM	TCI	> 98%
1,2-octanediol		Acros	> 98%
<i>n</i> -octyl- β -D-glucopyranoside	$\beta\text{-C}_8\text{G}_1$	GLYCON Biochemicals	> 99.5%
Plantacare 810 UP (technical-grade alkyl polyglucosides with an average composition of $\text{C}_{8/10}\text{G}_{1.5}$)		BASF	active content ~ 64%, water as solvent
Plantacare 2000 UP ($\text{C}_{10}\text{G}_{1.5}$)		BASF	active content ~ 53%, water as solvent
Plantacare 1200 UP ($\text{C}_{12}\text{G}_{1.4}$)		BASF	active content ~ 52%, water as solvent

MEGA-8/10 (C _{8/10} -methylglucamide)		Clariant	active content ~ 50% with 45% water and 5% propylene glycol
MEGA-12/14-HC (C _{12/14} -methylglucamide)		Clariant	active content ~ 64% with 22% water, 10% ethanol, and 4.5% propylene glycol
MEGA-12/14-PC (C _{12/14} -methylglucamide)		Clariant	active content ~ 35% with 60% water, 4% propylene glycol, and 0.8% sorbic acid
citric acid anhydrous		Sigma-Aldrich	≥ 99.5%
12-hydroxyoctadecanoic acid	12-HOA	Alfa Aesar	95%
<i>N,N'</i> -dibenzoyl-L-cystine	DBC	Santa Cruz	> 98%
1,3:2,4-dibenzylidene-D-sorbitol	DBS	NJC Europe	n/a
1,3:2,4-dibenzylidene-D-sorbitol- <i>p,p'</i> -dicarboxylic acid	DBS-COOH	synthesized by the group of Prof. Dr. David K. Smith	n/a
1,3:2,4-dibenzylidene-D-sorbitol- <i>p,p'</i> -dihydrazide	DBS-CONHNH ₂	from the University of York, UK	
lidocaine		TCI	> 99%
diclofenac sodium salt		Sigma-Aldrich	≥ 98%

Sample Preparation

Four kinds of samples were prepared: the non-gelled and gelled microemulsions for SANS measurements and phase studies. Non-gelled microemulsions for small-angle neutron scattering (SANS) measurements were prepared by weighing in surfactant (C), co-surfactant (D), oil (B), and water (A) in the mentioned order with an analytical balance into glass tubes, which were then sealed by polyethylene stoppers. Subsequently, the samples were heated up to 50 °C in a water bath while being stirred to homogenize. Afterward, the samples were equilibrated at 25 °C and then ready to use. For phase studies, the surfactant (C), oil (B), and water (A) were first weighed in, and the samples were homogenized at 50 °C. Afterward, phase studies were carried out at 25 °C titrating the co-surfactant (see Section *Visual Phase Studies*).

The preparation of gelled microemulsions was similar to that of non-gelled microemulsions, but a gelator was additionally added to the samples. The samples were firstly heated above 92 °C to dissolve the gelator. A heat gun was utilized when necessary. Subsequently, the samples were quickly transferred to an ice bath directly from the 92 °C water bath with manual shaking to ensure homogeneous gelation. Afterward, the samples were transferred to a 25 °C water bath and allowed to equilibrate.

Sample compositions were defined by the volume fraction of oil (B) in the solvent mixture

$$\phi = \frac{V_{\text{oil}}}{V_{\text{water}} + V_{\text{oil}}}, \quad (3.1)$$

the mass fraction of surfactant (C)

$$\gamma_{\text{C}} = \frac{m_{\text{surf.}}}{m_{\text{total}}}, \quad (3.2)$$

and the mass fraction of the co-surfactant (D)

$$\gamma_{\text{D}} = \frac{m_{\text{co-surf.}}}{m_{\text{total}}}. \quad (3.3)$$

When using technical-grade surfactants, $m_{\text{surf.}}$ is the weight of the active component in the original surfactant formulation, and m_{total} is the total mass of water, oil, the total mass of the technical-grade surfactant (including solvent and additives), co-surfactant, and gelator (if the sample is gelled microemulsion). When salt was added, the salinity of the microemulsion sample is defined as

$$\varepsilon = \frac{m_{\text{salt}}}{m_{\text{water}} + m_{\text{salt}}}. \quad (3.4)$$

In the case of gelled microemulsions, the gelator concentration is calculated according to

$$\eta = \frac{m_{\text{gelator}}}{m_{\text{total}}}. \quad (3.5)$$

Visual Phase Studies

The microemulsion phase behavior was investigated at a constant temperature of $T = 25.0\text{ }^{\circ}\text{C}$ using a house-built setup (Figure 3.1). The water basin was equipped with a thermostat and a cooling system to maintain a constant temperature with a precision of $\pm 0.1\text{ K}$. The non-gelled microemulsion samples were firstly prepared without co-surfactant (D). After equilibration in the water bath, the stopper was removed, and a co-surfactant (D) was titrated to the sample dropwise by a syringe. The added amount of co-surfactant was recorded using an analytical balance with a precision of $\pm 0.001\text{ g}$. After adding the co-surfactant, the sample was shaken and stirred vigorously before it was left to equilibrate. Then the phase behavior was visually determined. Birefringence of lyotropic liquid crystalline phases was observed via crossed polarizers. Since the phase transitions of sugar surfactant-based microemulsions were induced by the addition of a co-surfactant, the phase behavior was presented in a phase tetrahedron (Figure 2.3). The phase behavior of these microemulsions was studied at a constant oil-to-water ratio, *i.e.*, recording a two-dimensional section through the tetrahedron.

After measuring the phase boundaries, 1-phase microemulsion samples of different oil-to-water ratios (ϕ) were prepared to study the gelation behavior of LMWGs. We first determined the minimum gelation concentration (*mgc*) by adding a gelator to the microemulsion sample until the whole sample was gelled. The sample is considered gelled if the material does not flow in the inverted test tube. After knowing the *mgc*, the phase behavior of gelled microemulsions can be measured. The gelled microemulsion sample was first prepared without a co-surfactant, then the co-surfactant was titrated dropwise to the gelled sample at $25\text{ }^{\circ}\text{C}$. The sample was then heated above the gel–sol transition temperature, where the sample was melted and could thus be mixed. After the gelation process described in Section *Sample Preparation*, the phase behavior was recorded. A gelled 1-phase microemulsion is transparent, while a gelled 2-phase microemulsion is turbid. The titration, melting, and gelation procedures were repeated until the gelled microemulsion sample crossed the 2–1 and 1–2 phase boundaries.



Figure 3.1: The house-built experimental setup for visual phase studies: A – thermostat, B – water basin, C – microscopy lamp, D – crossed polarizers, E – digital thermometer, F – magnetic stirrer, G – house-made sample holder with the sample, H – co-surfactant bottle with a syringe, I – balance for recording the amount of added co-surfactant.

3.2 Oscillatory Shear Rheometry

Oscillatory shear rheometry was carried out to characterize the rheological properties of gelled microemulsions. The characteristic rheological behavior of molecular gels is described in Section 2.3. We used the rheometer Physica MCR 501 from Anton Paar, Austria, and a plate–plate geometry with the upper plate of 25 mm diameter. The gap size between the two plates was chosen to be 1 mm according to a previous study [Lau13]. The temperature was controlled via an external thermostat with a precision of $\Delta T = \pm 0.1$ K. Firstly, an amplitude sweep was carried out at $T = 25$ °C with an angular frequency of $\omega = 10$ s⁻¹ and a controlled shear stress τ to determine the limit of the linear viscoelastic range (LVE range). The shear stress for the subsequent measurements should be within the limit of the LVE range. Hence, for the gelled

microemulsions, the shear stress was kept constant at $\tau = 10$ Pa except for the samples with $\phi = 0.20$ and $\phi = 0.35$ at $\eta = 0.002$ in Publication IV, which were measured at a shear stress of $\tau = 1$ Pa. Secondly, an oscillation frequency sweep was performed at $T = 25$ °C as a function of the angular frequency ω . Lastly, a temperature sweep was carried out at an angular frequency of $\omega = 10$ s⁻¹ from $T = 25$ °C to $T = 100$ °C with a heating rate of 1 K·min⁻¹ to determine the gel–sol transition temperature $T_{\text{sol-gel}}$. Note that the storage modulus G' and the loss modulus G'' were measured only once for each sweep due to large deviations (10 – 50%) of repeated measurements [Ste19, Ste19b]. Thus, the absolute values should be considered carefully while the trends are discussable. We distinguish between “strong” and “weak” gel by the magnitude difference of the storage modulus G' and the loss modulus G'' . A sample is considered to be “rigid” if it is frequency-independent and “soft” if frequency-dependent.

3.3 Small-Angle Neutron Scattering

Small-angle neutron scattering (SANS) provides quantitative characterizations of the microstructure and the length scale of microemulsions [Hel08]. For the sample preparation, we replaced H₂O with D₂O to adjust bulk contrast. The phase boundaries of the deuterated system were measured again using the titration procedure, and the SANS sample was prepared in a composition close to the middle of the 1-phase region. Both non-gelled and gelled microemulsions were first prepared in test tubes and then loaded into Hellma quartz QS glass cells (optical path length of 1 mm). The non-gelled microemulsions were transferred to the measuring cell at $T = 25$ °C in the 1-phase state. The gelled microemulsion was transferred at $T = 95$ °C with stirring so that the sample was in the sol state and a homogeneous mixture, and the cell was rapidly cooled down in an ice bath and then equilibrated at $T = 25$ °C to form a transparent gel. Before the SANS measurement, the measuring cell was transferred to a house-built cell holder with high temperature precision and stability ($\Delta T = \pm 0.02$ K). It was ensured that samples were in the homogeneous 1-phase state during measurements by checking each sample before and after the measurement via visual inspection.

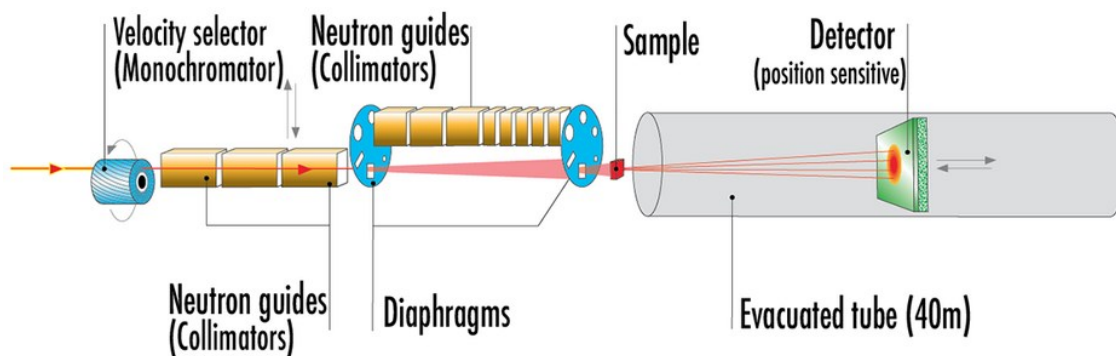


Figure 3.2: Schematic illustration of the instrument layout for SANS (taken from [www01]).

In Publication I, the glucose-containing non-gelled and gelled microemulsions were measured on the D11 spectrometer at the Institut Laue-Langevin (ILL) in Grenoble, France. The instrument layout is depicted in Figure 3.2. A neutron wavelength of $\lambda = 5.5 \text{ \AA}$ with a wavelength spread of $\Delta\lambda/\lambda = 9\%$ (full width at half-maximum) was used. To cover a q -range from 0.0016 to 0.47 \AA^{-1} , where

$$q = 4\pi \cdot \sin(\theta/2)/\lambda \quad (3.6)$$

is the absolute value of the scattering vector, we chose the detector/collimation distances of 39.0 m/40.5 m, 8.0 m/8.0 m, and 1.5 m/20.0 m. The recorded scattering intensity was normalized to absolute scale using the incoherent scattering of H_2O as a reference with a differential scattering cross section of 0.956 cm^{-1} at $\lambda = 5.5 \text{ \AA}$. The raw data treatment, including the subtraction of the dark current and the empty cell scattering, masking, and radial averaging, was performed using the analysis software program LAMP provided by the ILL. The detector dead time and sample transmission were also considered. The measurements were performed by our colleagues, Kristina Schneider, Shih-Yu Tseng, and Diana Zauser.

In Publication II, the glucamide-containing microemulsions were measured on the spectrometer NG7 at the National Institute of Standards and Technology (NIST), the USA, and on the instrument KWS-1 at the Heinz Maier-Leibniz Zentrum (MLZ) in Munich, Germany. The microemulsion samples of $\gamma_C = 0.0521$, $\gamma_D = 0.0878$ with $\varepsilon = 0$ and $\gamma_C = 0.0689$, $\gamma_D = 0.0927$ with $\varepsilon = 0.0009$ were measured on NG7, NIST. A neutron wavelength of $\lambda = 6 \text{ \AA}$ with

a wavelength spread of $\Delta\lambda/\lambda = 13.8\%$ was used. We chose the detector/collimation distances of 13.17 m/14.72 m, 4 m/8.52 m, and 1.33 m/5.42 m to cover a q -range from 0.002 to 0.48 Å. The microemulsion samples of $\gamma_C = 0.0232$, $\gamma_D = 0.0737$ with $\varepsilon = 0$ and $\gamma_C = 0.0522$, $\gamma_D = 0.0878$ with $\varepsilon = 0.0009$ were measured on KWS-1, MLZ. Neutron wavelengths of $\lambda = 5$ and 10 Å with a wavelength spread of $\Delta\lambda/\lambda = 10\%$ were used to cover a q -range from 0.001 to 0.66 Å. The detector/collimation distances were 20 m/20 m, 8 m/20m, and 1.5 m/8m. The recorded scattering intensity was normalized to the absolute scale using the empty beam (for the data from NIST) and the plexiglass (for the data from MLZ) as a reference. The raw data treatment, including the subtraction of the dark current and the empty cell scattering, masking, and radial averaging, was performed using IGOR Pro (for the data from NIST) and QtiSAS (for the data from MLZ). The detector dead time and sample transmission were also considered. The measurements were performed by our colleagues, Shih-Yu Tseng, Karina Abitaev, and Diana Zauser.

Obtained data were fitted with the Teubner–Strey model [Teu87], which describes the characteristic peak of a bicontinuous microemulsion with

$$I(q) = \frac{8\pi c_2 \phi_a \phi_b (\Delta\rho)^2 / \xi_{TS}}{a_2 + c_1 q^2 + c_2 q^4} + I_{\text{incoh}}, \quad (3.7)$$

where I_{incoh} is the incoherent background, $\Delta\rho$ is the scattering length density difference of the two subphases, and ϕ_a and ϕ_b are their respective volume fractions. The parameters a_2 , c_1 and c_2 are coefficients derived from a Landau–Ginzburg order parameter expansion of the local free energy density, where the order parameter is the water-to-oil ratio. After determining the values of a_2 , c_1 and c_2 , two characteristic length scales of the Teubner–Strey model can be calculated, namely the correlation length

$$\xi_{TS} = \left[\frac{1}{2} \left(\frac{a_2}{c_2} \right)^{\frac{1}{2}} + \frac{c_1}{4c_2} \right]^{-\frac{1}{2}}, \quad (3.8)$$

and the periodicity of the oil and water domains, *i.e.* the domain spacing

$$d_{\text{TS}} = 2\pi \left[\frac{1}{2} \left(\frac{a_2}{c_2} \right)^{\frac{1}{2}} - \frac{c_1}{4c_2} \right]^{-\frac{1}{2}}. \quad (3.9)$$

The amphiphilicity factor [Sch94] can be calculated by

$$f_a = \frac{c_1}{\sqrt{4a_2c_2}}. \quad (3.10)$$

3.4 Freeze-Fracture Electron Microscopy

The liquid mixtures of a microemulsion can be solidified via cryofixation, and then the microstructure can be visualized by transmission electron microscopy (TEM). In freeze-fracture electron microscopy (FFEM), the samples are prepared in a protected fashion in a sandwich. Subsequently, they are rapidly frozen, fractured, shadowed with metal, and replicated with a thin carbon film. The replica of the fractured surface is then studied by TEM [Sot08]. The sample preparation and operation of FFEM are sophisticated and demand rich experience to obtain decent images. Thus, the FFEM images were taken by Dr. Natalie Preisig, an expert in this field. The experimental details are briefly described here.

Replicas of gelled and non-gelled microemulsions were prepared using the Freeze-Fracture and Etching System BAF060 from Leica. A small amount of the gelled microemulsion was transferred from the test tube to two copper grids between two copper plates (4.5 mm × 3.0 mm), which were then assembled into a so-called sandwich. In the case of non-gelled microemulsion, the sandwich was immersed in the liquid sample with a tweezer for several minutes. Afterward, the sandwiches were quickly frozen in liquid ethane. After fracturing in liquid nitrogen, the grids with the frozen fractured specimen were fixed on a house-made specimen holder (with a metal cover plate to prevent contamination in the air) and quickly transferred into the vacuum chamber of the BAF060 ($T = -150$ °C). The frozen fractured surface of the specimens was shadowed with platinum-carbon (~2 nm) at 45° and covered by a layer of pure carbon (~20 nm) at 90°. The replicas were then cleaned with warm ethanol and

acetone, dried, and examined with an EM10 transmission electron microscope from *Zeiss* operated at 60 kV.

3.5 Electrical Conductivity

Electrical conductivity measurements were performed to monitor the structural change from water-rich to oil-rich microemulsions in Publication IV. Since water domains with salt have high electrical conductivity while oil domains have low conductivity, the structural change can be observed by the conductivity change [Sot05]. The experimental setup consisted of the conductivity cell TetraCon 925/LV from WTW (Xylem Analytics GmbH, Weilheim, Germany) integrated with a temperature sensor and the conductivity meter Multi 3510 IDS from WTW. The conductivity measuring cell was placed in a test tube, which contained the sample to be measured. The temperature was adjusted to a constant value of $T = (25.0 \pm 0.1) \text{ }^\circ\text{C}$ by placing the test tube in a water bath regulated by a thermostat DC30 from Thermo Electron GmbH (Karlsruhe, Germany). For a detectable conductivity, the water of the microemulsion sample was replaced by 0.1 wt.% of NaCl solution. Note that the effect of salt on the phase behavior of nonionic microemulsions is negligible at this low concentration. The electrical conductivity was measured through the titration procedure as described in Section 3.1. The sample was continuously stirred with a Teflon-coated magnetic stirring bar, and the co-surfactant was added to the sample dropwise. Thus, $\kappa(\gamma_D)$ -curves were established by recording the conductivities after each drop of co-surfactant and 3 min of waiting time.

4 Summary of Research

The results have been published in four publications [Pen19 (Publication I), Pen20 (Publication II), Pen21a (Publication III), Pen21b (Publication IV)]. In Publication I & II, we formulated non-toxic bicontinuous microemulsions using different types of surfactants, including alkyl polyglucosides (APGs) and alkanoyl methylglucamide (MEGA), and identified a suitable low molecular weight gelator (LMWG) for gelling non-toxic microemulsions. In Publication III, we loaded both hydrophilic and hydrophobic model drugs in the gelled non-toxic microemulsion for its potential application as a transdermal drug delivery carrier. In Publication IV, we studied the non-toxic microemulsions at various oil-to-water ratios and identified suitable LMWGs for both water-rich and oil-rich microemulsions. These studies broaden the application potentials of gelled non-toxic microemulsions and reveal information about the interactions between gelators and solvents (in our case, microemulsions). The most important findings and the connections between these publications will be described in the following sections.

4.1 Gelled Non-Toxic Microemulsions: Phase Behavior & Rheology (Publication I)

We intended to formulate non-toxic microemulsions with biocompatible sugar surfactants, namely alkyl polyglucosides (APGs, denoted as $\beta\text{-C}_n\text{G}_m$, see Figure 1.3 for molecular structure) [Stu01]. The phase behavior, interfacial composition, interfacial tension, and microstructure of the quaternary microemulsion $\text{H}_2\text{O} - n\text{-octane} - n\text{-octyl-}\beta\text{-D-glucopyranoside} (\beta\text{-C}_8\text{G}_1) - 1\text{-octanol}$ were extensively studied before [Klu00, Klu01, Sot02, Rei03]. Thus, we used this system as the scouting system and replaced both the oil $n\text{-octane}$ and the co-surfactant 1-octanol with non-toxic components. Our focus was on the location of the fishtail point \tilde{X} (where the 1-phase region meets the 3-phase region), where the microstructure is bicontinuous.

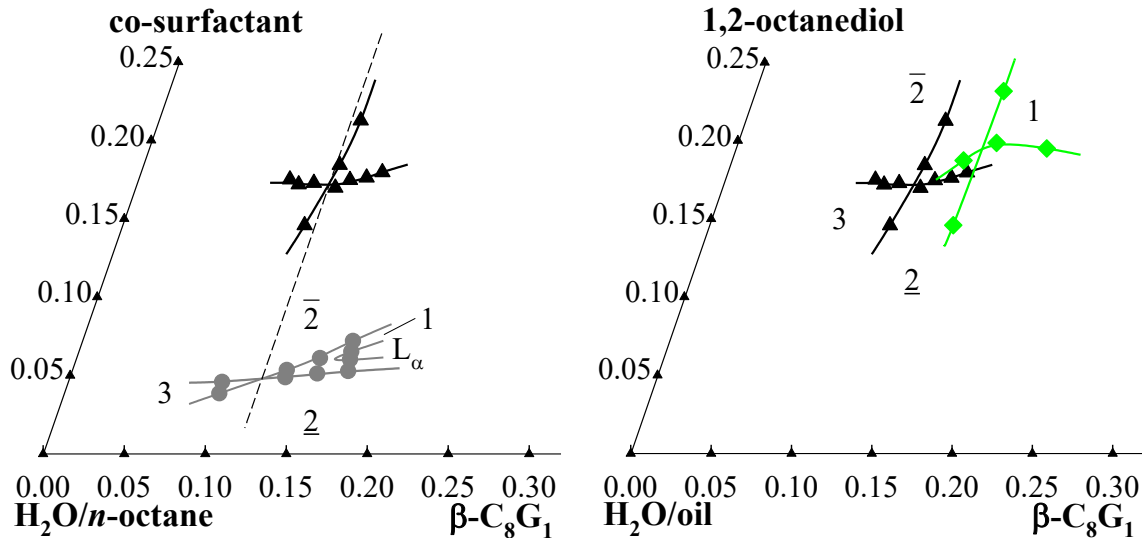


Figure 4.1: (left) Phase diagrams of the quaternary systems $\text{H}_2\text{O} - n\text{-octane} - \beta\text{-C}_8\text{G}_1 - 1\text{-octanol}$ (gray circles) and $\text{H}_2\text{O} - n\text{-octane} - \beta\text{-C}_8\text{G}_1 - 1,2\text{-octanediol}$ (black triangles up) at $T = 25\text{ }^\circ\text{C}$, $\phi = 0.50$. (right) Phase diagrams of quaternary system $\text{H}_2\text{O} - n\text{-octane} - \beta\text{-C}_8\text{G}_1 - 1,2\text{-octanediol}$ (black triangles up), and $\text{H}_2\text{O} - \text{IPM} - \beta\text{-C}_8\text{G}_1 - 1,2\text{-octanediol}$ (green diamonds) at $T = 25\text{ }^\circ\text{C}$, $\phi = 0.50$. Reproduced from [Pen19] with permission from the Royal Society of Chemistry.

We restudied the phase behavior of the scouting system $\text{H}_2\text{O} - n\text{-octane} - \beta\text{-C}_8\text{G}_1 - 1\text{-octanol}$ (Figure 4.1 (left), gray circles). One sees that the addition of 1-octanol induces phase transitions in the sequence of $\underline{2} - 3 - \bar{2}$ and $\underline{2} - 1 - \bar{2}$, respectively. Then we replaced the co-surfactant 1-octanol with the biocompatible 1,2-octanediol (Figure 4.1 (left), black triangles up). 1,2-Octanediol is much more hydrophilic than 1-octanol, and its effect on the phase behavior is similar to that of 1-butanol [Kah96]. Thus, the amount of 1,2-octanediol needed to form a 1-phase microemulsion $\tilde{\gamma}_C$ is considerably higher than that of 1-octanol. However, since the oil component remains the same, the amount of $\beta\text{-C}_8\text{G}_1$ needed to form a 1-phase microemulsion $\tilde{\gamma}_D$ does not change (\tilde{X} points of the two systems are shifted parallel to the co-surfactant axis). The more hydrophobic 1,2-dodecanediol was also examined. However, the sample solidified at $25\text{ }^\circ\text{C}$ due to its high melting point. Subsequently, $n\text{-octane}$ was replaced by isopropyl myristate (IPM, Figure 4.1 (right)). The shift of the \tilde{X} point to the right upper side of the phase diagram can be explained by two reasons: (1) IPM has a longer carbon chain compared to $n\text{-octane}$, which decreases the efficiency of the surfactant (an increase in $\tilde{\gamma}_D$). (2) 1,2-Octanediol has a higher solubility in IPM than in $n\text{-octane}$, so a slightly higher amount of 1,2-octanediol is

needed (an increase in $\tilde{\gamma}_C$).

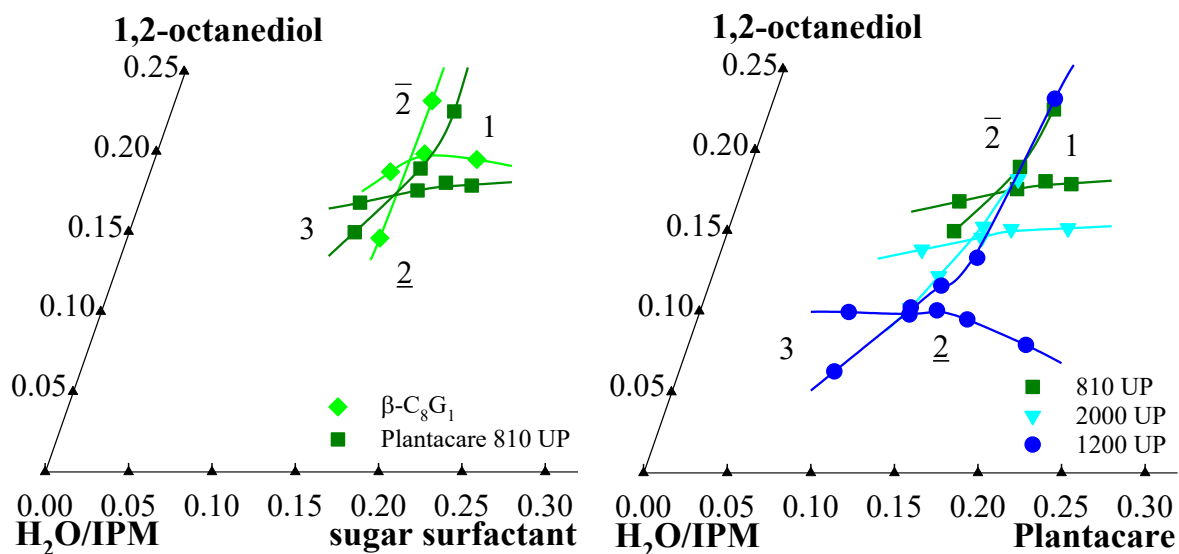


Figure 4.2: (left) Phase diagrams of $\text{H}_2\text{O} - \text{IPM} - \beta\text{-C}_8\text{G}_1 - 1,2\text{-octanediol}$ (green diamonds) and $\text{H}_2\text{O} - \text{IPM} - \text{Plantacare 810 UP} - 1,2\text{-octanediol}$ (dark green squares) at $T = 25\text{ }^\circ\text{C}$, $\phi = 0.50$. (right) Phase diagrams of $\text{H}_2\text{O} - \text{IPM} - \text{Plantacare 810 UP (C}_{8/10}\text{G}_{1.5}) - 1,2\text{-octanediol}$ (dark green squares), $\text{H}_2\text{O} - \text{IPM} - \text{Plantacare 2000 UP (C}_{10}\text{G}_{1.5}) - 1,2\text{-octanediol}$ (cyan triangles down), and $\text{H}_2\text{O} - \text{IPM} - \text{Plantacare 1200 UP (C}_{12}\text{G}_{1.4}) - 1,2\text{-octanediol}$ (blue hexagons) at $T = 25\text{ }^\circ\text{C}$, $\phi = 0.50$. Reproduced from [Pen19] with permission from the Royal Society of Chemistry.

Since the efficiency ($\tilde{\gamma}_C + \tilde{\gamma}_D$) of the non-toxic microemulsion $\text{H}_2\text{O} - \text{IPM} - \beta\text{-C}_8\text{G}_1 - 1,2\text{-octanediol}$ largely decreased compared to the scouting system $\text{H}_2\text{O} - n\text{-octane} - \beta\text{-C}_8\text{G}_1 - 1\text{-octanol}$ and because the pure surfactant $\beta\text{-C}_8\text{G}_1$ is quite expensive, the next step was to replace $\beta\text{-C}_8\text{G}_1$ with technical-grade APGs. Firstly, $\beta\text{-C}_8\text{G}_1$ was replaced by Plantacare 810 UP ($\text{C}_{8/10}\text{G}_{1.5}$, Figure 4.2 (left)). One sees that the \tilde{X} point is slightly shifted to a position where less surfactant and co-surfactant are needed. It also indicates that the longer carbon chain of Plantacare 810 UP compensates for its larger number of glucoside units, and the overall efficiency is slightly improved. In order to further increase the efficiency, technical-grade APGs with longer carbon chains were investigated (Figure 4.2 (right)), including Plantacare 2000 UP ($\text{C}_{10}\text{G}_{1.5}$) and Plantacare 1200 UP ($\text{C}_{12}\text{G}_{1.4}$). One sees that the longer the carbon chain is, the more efficient the system becomes. Simultaneously, the required co-surfactant amount decreases considerably due to the increased surfactant hydrophobicity. Therefore, the non-toxic

system H₂O – IPM – Plantacare 1200 UP (C₁₂G_{1.4}) – 1,2-octanediol with the highest efficiency of $\tilde{\gamma}_C = 0.121$, $\tilde{\gamma}_D = 0.098$ was chosen for further investigations.

After having formulated non-toxic microemulsions, we needed to find a suitable gelator. Since the microemulsions contain equal volumes of water and oil, theoretically, both hydrogelator and organogelator should be suitable to gel the system. Three LMWGs were tested, namely the organogelators 12-hydroxyoctadecanoic acid (12-HOA) and 1,3:2,4-dibenzylidene-D-sorbitol (DBS), and the hydrogelator *N,N'*-dibenzoyl-L-cystine (DBC) (for molecular structures see Figure 2.8).

We first tested these gelators in the scouting system H₂O – *n*-octane – β -C₈G₁ – 1-octanol, expecting to obtain some preliminary knowledge that can be transferred to the final non-toxic system. The organogelator 12-HOA gels the 1-phase microemulsion of the scouting system with a minimum gelation concentration (*mgc*) of 1.5 wt.%. However, the 1-phase boundaries are slightly shifted downwards, which indicates that 12-HOA is surface active. The role of 12-HOA as a co-surfactant was also observed in a previous study [Ste18]. The surface activity of 12-HOA is not strong enough to entirely replace the co-surfactant yet increases the complexity of the system. The second organogelator DBS does not dissolve in the scouting system even at a concentration as low as 0.1 wt.%. On the other hand, the hydrogelator DBC gels the 1-phase microemulsion at 1.0 wt.%, resulting in an isotropic and transparent gel. Moreover, the phase boundaries remain unchanged compared to the non-gelled microemulsion. Therefore, DBC is the gelator of choice for the scouting system.

Then we tested the three gelators in the non-toxic microemulsion H₂O – IPM – Plantacare 1200 UP – 1,2-octanediol. Surprisingly, DBC only gels the 1-phase non-toxic microemulsion at a considerably higher *mgc* of 2.4 wt.% than that in the scouting system, and the gelator precipitated overnight. For simplicity, we measured the phase behavior of the non-toxic microemulsion with 2 wt.% DBC (not gelled; Figure 4.3 (left), black open triangles). The phase boundaries are shifted to a larger amount of co-surfactant in the presence of 2 wt.% DBC. On the other hand, 12-HOA gels the non-toxic microemulsion at *mgc* of 2 wt.%. However, the

phase boundaries are also shifted. As shown in Figure 4.3 (left, green open squares), the phase boundaries are shifted to a smaller amount of co-surfactant since 12-HOA acts as an additional co-surfactant. Finally, DBS, which does not dissolve in the scouting system, turned to be a very potent gelator for our non-toxic microemulsion. The m_{gc} of DBS is as low as 0.14 wt.%, yet the gel is relatively weak. We used 0.3 wt.% DBS in the gelled non-toxic microemulsion for further investigations to have decent gel strengths. As shown in Figure 4.3 (right), DBS does not change the phase boundaries, and the gelled 1-phase microemulsion is transparent.

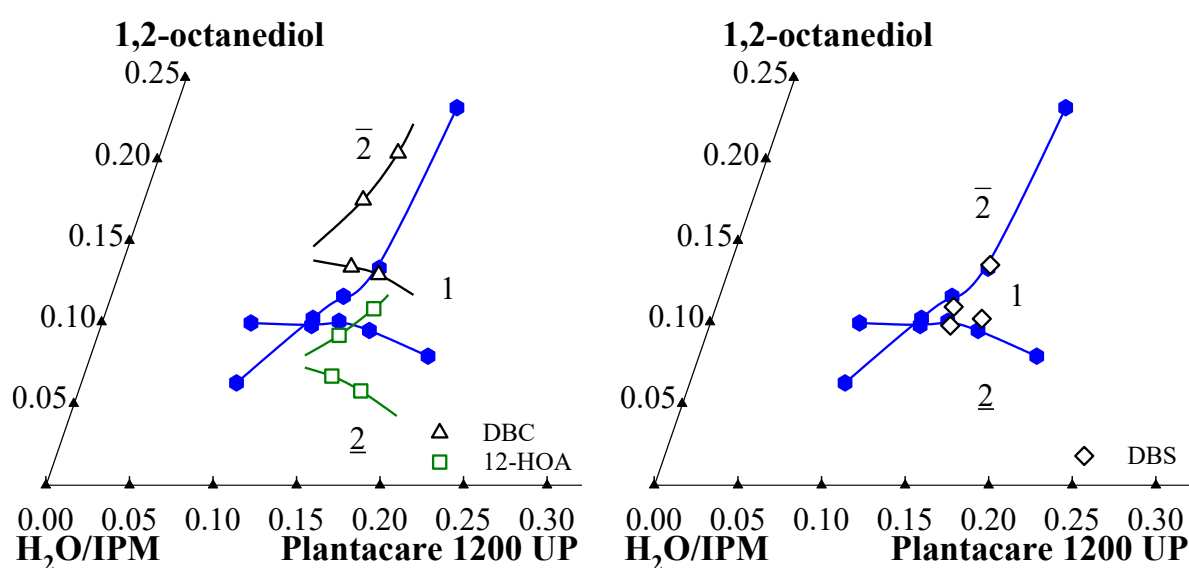


Figure 4.3: Phase diagrams of the quaternary system H_2O – IPM – Plantacare 1200 UP – 1,2-octanediol (blue closed hexagons) with (left) the non-gelled system in the presence of DBC (black open triangles) at $\eta = 0.02$ and the non-gelled system in the presence of 12-HOA (green open squares) at $\eta = 0.015$, (right) the gelled system in the presence of DBS (black open diamonds) at $\eta = 0.003$. All samples were studied at $T = 25$ °C and $\phi = 0.50$. Reproduced from [Pen19] with permission from the Royal Society of Chemistry.

Unexpectedly, the gelation behavior of the three gelators is quite different in the scouting system and the non-toxic final system. 12-HOA shifts phase boundaries in both systems. DBC is the ideal gelator for the scouting system while it precipitates in the non-toxic system. DBS does not dissolve in the scouting system but nicely gels the non-toxic system. So far, there is no paradigm for knowing (a) which gelator will gel the solvent or (b) the properties of the formed gel [Wei14, Dra17]. Our results also confirm that the gelator search for a certain solvent (in our case, the microemulsions) remains trial and error. Overall, the final gelled non-toxic

microemulsion was chosen to be H₂O – IPM – Plantacare 1200 UP – 1,2-octanediol in the presence of 0.3 wt.% DBS. Although this system has five components, the existence of the gelator does not alter the phase behavior, which provides convenience and simplicity for potential applications.

We subsequently performed oscillatory shear rheometry to examine the rheological properties of the gelled non-toxic microemulsions. The sample composition is located in the middle of the 1-phase region. The frequency sweep (Figure 4.4 (left)) indicates that the storage modulus G' is about one order of magnitude larger than the loss modulus G'' over the entire frequency range, and both moduli show a weak dependence on the frequency. The temperature sweep (Figure 4.4 (right)) shows a crossover of G' and G'' at 78 °C, which is assigned to the gel–sol transition temperature $T_{\text{sol-gel}}$. Thus, one can conclude that the sample is a relatively strong and rigid gel.

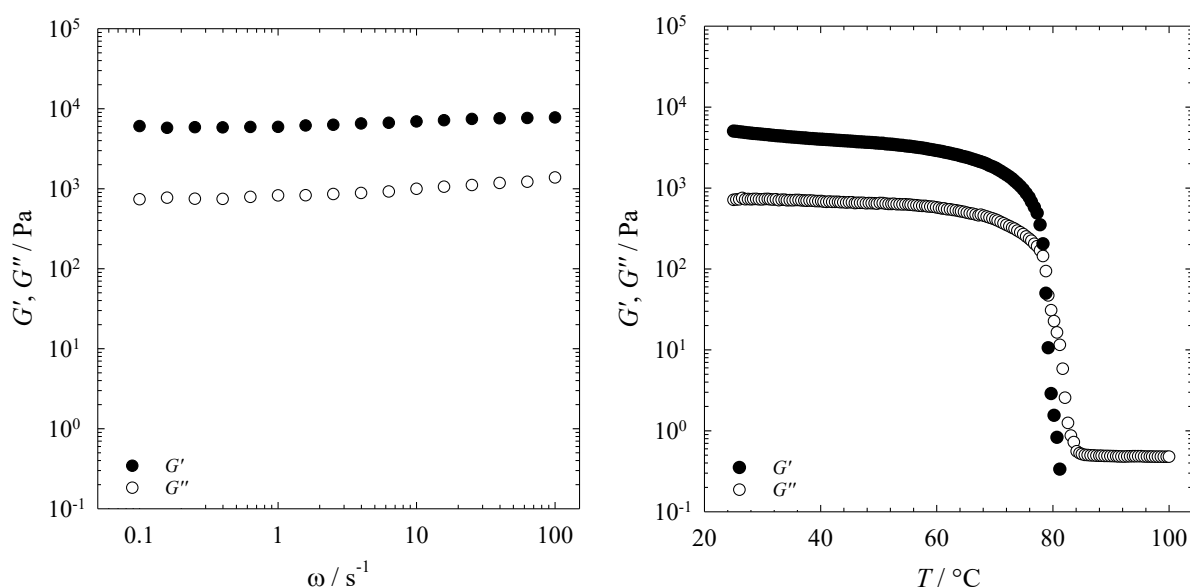


Figure 4.4: Storage modulus G' (filled symbols) and loss modulus G'' (open symbols) of the gelled microemulsion H₂O – IPM – Plantacare 1200 UP – 1,2-octanediol in the presence of DBS at $\eta = 0.003$, $\tau = 10$ Pa (left) as a function of ω at $T = 25$ °C with $\gamma_C = 0.1583$, $\gamma_D = 0.1204$, $\phi = 0.50$ and (right) as a function of T at $\omega = 10$ s⁻¹ with a heating rate of 1 °C·min⁻¹, $\gamma_C = 0.1588$, $\gamma_D = 0.1194$, $\phi = 0.50$. Reproduced from [Pen19] with permission from the Royal Society of Chemistry.

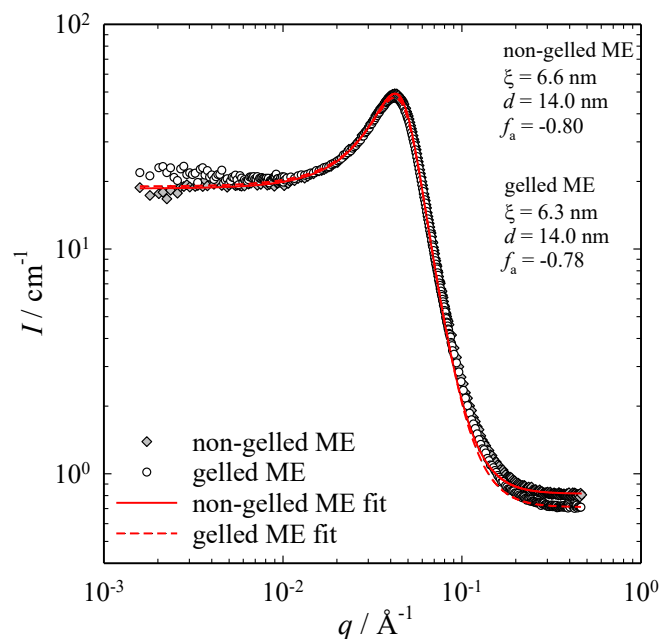


Figure 4.5: SANS data of the non-gelled microemulsion D₂O – IPM – Plantacare 1200 UP – 1,2-octanediol ($\gamma_C = 0.1571$, $\gamma_D = 0.1092$, $\phi = 0.50$; grey squares) and the gelled microemulsion ($\gamma_C = 0.1581$, $\gamma_D = 0.1100$, $\phi = 0.50$; open circles) in the presence of DBS at $\eta = 0.003$, $T = 25$ °C. Reproduced from [Pen19] with permission from the Royal Society of Chemistry.

Since we want to use bicontinuous microemulsions to solubilize both hydrophilic and hydrophobic drugs, it is essential to study the microstructure of the non-toxic microemulsions and see whether the microstructure is changed by the gel network. To this end, small-angle neutron scattering (SANS) measurements were carried out. In analogy to the rheological studies, the sample composition is located in the middle of the 1-phase region. H₂O was replaced by D₂O to adjust the bulk contrast. As one can see in Figure 4.5, the scattering curves of the non-gelled microemulsion and of the gelled microemulsion fall almost on top of each other, indicating that the microemulsion structure is retained in the gelled sample. Moreover, both curves have the typical peak for bicontinuous structure in the middle q -range, and the intensity decrease with q^{-4} in the high q -range. The two scattering curves were fitted with the Teubner–Strey model [Teu87], which describes the characteristic peak of a bicontinuous microemulsion (Figure 4.5). The fitting gives a periodicity of $d = 14.0$ nm for both non-gelled and gelled microemulsions. The non-gelled microemulsion has the correlation length of $\xi_{TS} = 6.6$ nm and

the amphiphilic factor of $f_a = -0.80$, while the gelled counterpart has $\xi_{TS} = 6.3$ nm and $f_a = -0.78$. These results indicate that the non-gelled microemulsion is slightly better structured than the gelled microemulsion. The gelled sample has a higher scattering intensity in the low q -range ($q < 0.01 \text{ \AA}^{-1}$) than the non-gelled sample. This is in line with a previous SANS study on gelled bicontinuous microemulsions, where it was shown that the characteristic scattering peak of a gel network appears in the low q -range [Lau14]. However, the gelator concentration of the current study is 5-fold lower than the gelator concentration used in the previous study. The low gelator concentration makes it difficult to quantitatively characterize the slight intensity increase in the low q -range.

In Publication I, we formulated a non-toxic bicontinuous microemulsion and gelled it with an LMWG for the first time. The system $\text{H}_2\text{O} - \text{IPM} - \text{Plantacare 1200 UP} - 1,2\text{-octanediol}$ in the presence of 0.3 wt.% DBS was examined with oscillatory shear rheometry for rheological properties. Furthermore, we characterized the bicontinuous microstructure of the microemulsion with SANS and evidenced that the microemulsion structure was not changed by the presence of the gel network.

4.2 Formulation of Gelled Non-Toxic Bicontinuous Microemulsions Stabilized by Highly Efficient Alkanoyl Methylglucamides (Publication II)

In Publication I, we formulated the gelled non-toxic bicontinuous microemulsion $\text{H}_2\text{O} - \text{IPM} - \text{Plantacare 1200 UP} - 1,2\text{-octanediol}$ in the presence of 0.3 wt.% DBS. However, at least 12.1 wt.% Plantacare 1200 UP and 9.8 wt.% 1,2-octanediol are needed for forming a bicontinuous microemulsion. In Publication II, we aimed to improve the system's efficiency by using a new class of sugar surfactants, n -alkanoyl- N -methylglucamides (denoted as MEGA- n , see Figure 1.3 for molecular structure), which are also called glucamides. Both glucamides and alkyl polyglucosides are biodegradable, dermatologically safe, and made from renewable sources [Hil99]. The glucamide molecule contains an open-ring glucose unit connected to the alkyl chain by an amide bond. The methyl group at the nitrogen atom contributes to the water

solubility of the surfactant [Soe00]. So far, there are only limited studies about the phase behavior of glucamide-containing microemulsions [Yan07, Yan08, Yan13]. Therefore, phase studies of glucamide-based microemulsions are essential. We chose three technical-grade glucamide surfactants, namely MEGA-8/10, MEGA-12/14-PC, and MEGA-12/14-HC, which differ in the carbon chain length and product composition (see Section 3.1).

First, we measured the system $\text{H}_2\text{O} - n\text{-octane} - \text{MEGA-8/10} - 1\text{-octanol}$ and compared it with the phase behavior of Plantacare 810 UP ($\text{C}_{8/10}\text{G}_{1.5}$) in the system with the same oil and co-surfactant. The system with MEGA-8/10 has a $\tilde{\gamma}_D$ -value of 0.146, which is substantially higher than the $\tilde{\gamma}_D$ -value of 0.051 in the system with Plantacare 810 UP. This result indicates that MEGA-8/10 is more hydrophilic than the glucoside, which can be explained by the fact that the hydrophobic chain of MEGA-8/10 has one carbon less than Plantacare 810 UP. Thus, we used MEGA-12/14-PC and MEGA-12/14-HC, which have a longer carbon chain length than MEGA-8/10 for the formulation of non-toxic microemulsion (Figure 4.6 (left)). The phase diagrams of the non-toxic microemulsions $\text{H}_2\text{O} - \text{IPM} - \text{Plantacare} - 1,2\text{-octanediol}$ are presented in Figure 4.6 (right) for comparison. One sees in Figure 4.6 (right) that with an increasing hydrophobic chain length of the Plantacare surfactant, the fishtail point shifts downward to the left on the phase diagram, which indicates an efficiency increase of the system. The efficiency of MEGA-12/14-PC is similar to Plantacare 1200 UP in the non-toxic system with fishtail \tilde{X} points of (0.118, 0.094) and (0.121, 0.098), respectively. Although MEGA-12/14-PC has a slightly longer hydrophobic chain than Plantacare 1200 UP, the more hydrophilic head group of the former compensates for the hydrophobic effect and results in a similar efficiency. On the other hand, the phase behavior of MEGA-12/14-HC is completely different from the other surfactants. A 3-phase region was not observed in the microemulsion $\text{H}_2\text{O} - \text{IPM} - \text{MEGA-12/14-HC} - 1,2\text{-octanediol}$. Instead, the 1-phase region expands down to at least $\gamma_C = 0.0187$ and $\gamma_D = 0.0611$. The efficiency of MEGA-12/14-HC ($\tilde{\gamma}_C + \tilde{\gamma}_D \leq 0.08$) is surprisingly high compared to the efficiency of MEGA-12/14-PC ($\tilde{\gamma}_C + \tilde{\gamma}_D \approx 0.21$), even though both products have the same main active component.

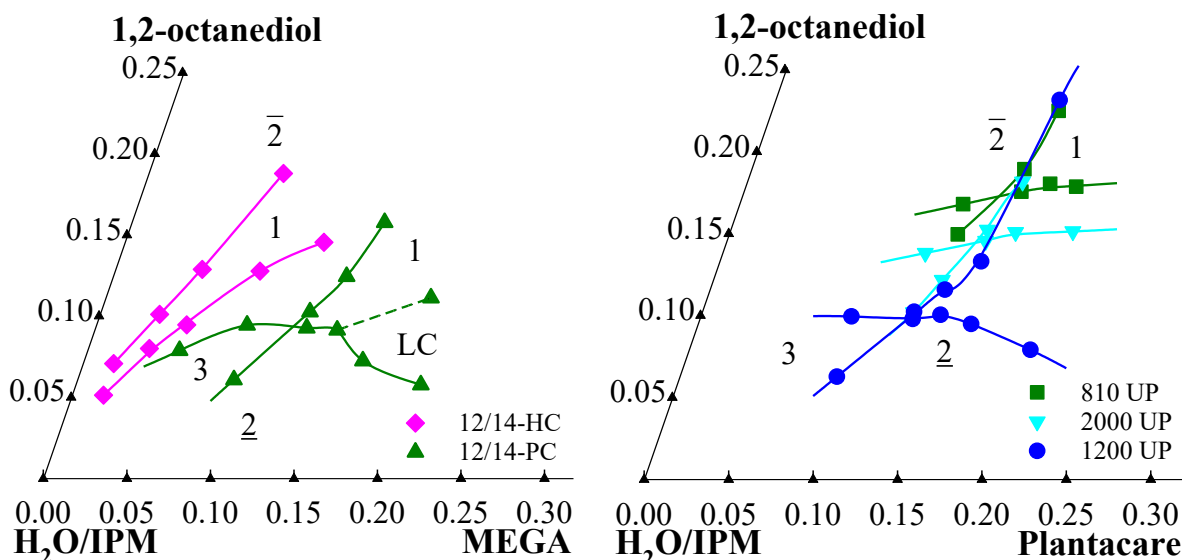


Figure 4.6: (left) Phase diagrams of H₂O – IPM – MEGA-12/14-PC – 1,2-octanediol (green triangles up) and H₂O – IPM – MEGA-12/14-HC – 1,2-octanediol (pink diamonds) at $T = 25\text{ }^{\circ}\text{C}$, $\phi = 0.50$. (right) Phase diagrams of H₂O – IPM – Plantacare 810 UP (C_{8/10}G_{1.5}) – 1,2-octanediol (green squares), H₂O – IPM – Plantacare 2000 UP (C₁₀G_{1.5}) – 1,2-octanediol (cyan triangles down), and H₂O – IPM – Plantacare 1200 UP (C₁₂G_{1.4}) – 1,2-octanediol (blue circles) at $T = 25\text{ }^{\circ}\text{C}$, $\phi = 0.50$. Adapted with permission from [Pen20]. Copyright 2020 American Chemical Society.

The phenomenon of an enormous efficiency improvement and the disappearance of the 3-phase region was previously observed by Kaler and Silas [Sil01]. With 2% of the cationic surfactant didodecyl dimethylammonium bromide (DDAB) in the surfactant mixture C₈E₃/DDAB, the surfactant efficiency was increased by a factor of 4 compared to that of the C₈E₃-only microemulsion H₂O – *n*-decane – C₈E₃, and the 3-phase region was not observed either. However, by adding a tiny amount of salt (NaBr) to the microemulsion H₂O – *n*-decane – C₈E₃/DDAB, the efficiency decreased to almost the same as that of H₂O – *n*-decane – C₈E₃, and the 3-phase region appeared again. Kaler and Silas proposed that this phenomenon was due to electrostatic stiffening of elastic surfactant monolayers induced by DDAB (an increase of efficiency), which is counterbalanced by the addition of NaBr (decrease in efficiency). Inspired by this work, we hypothesize that the technical-grade surfactant MEGA-12/14-HC contains traces of ionic components, which cause a similar electrostatic stiffening effect (efficiency increase) in the microemulsion H₂O – IPM – MEGA-12/14-HC – 1,2-octanediol. If this were the case, the addition of salt would lead to an efficiency decrease and the appearance of a 3-

phase region.

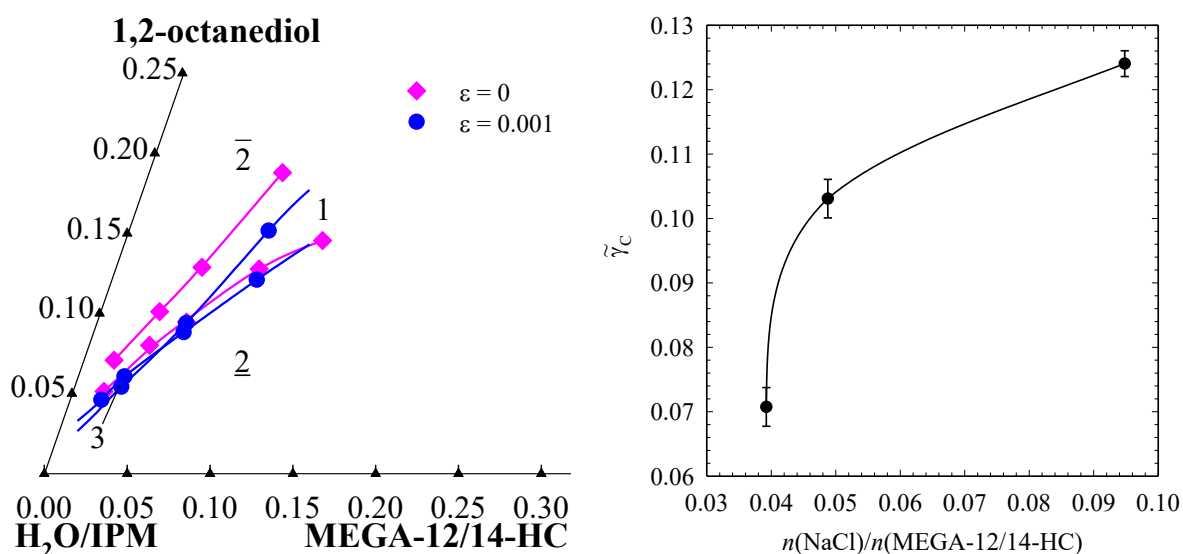


Figure 4.7: (left) Phase diagrams of H₂O – IPM – MEGA-12/14-HC – 1,2-octanediol (pink diamonds) and H₂O/NaCl – IPM – MEGA-12/14-HC – 1,2-octanediol with $\epsilon = 0.001$ (blue circles) at $T = 25$ °C, $\phi = 0.50$. (right) Plot of $\tilde{\gamma}_c$ -values against the molar ratio of NaCl over MEGA-12/14-HC for the microemulsion H₂O/NaCl – IPM – MEGA-12/14-HC – 1,2-octanediol. Reproduced with permission from [Pen20]. Copyright 2020 American Chemical Society.

In order to verify the hypothesis, we measured the phase boundaries of the microemulsion H₂O/NaCl – IPM – MEGA-12/14-HC – 1,2-octanediol with salinities of $\epsilon = 0.001$, 0.002, and 0.005. For the sake of clarity, only the results of $\epsilon = 0$ and $\epsilon = 0.001$ are shown in Figure 4.7 (left). With the addition of a tiny amount of salt, the 3-phase channel appeared. With $\epsilon = 0.002$ and 0.005, the phase boundaries have a similar shape but shift to the right upper part of the phase diagram. $\tilde{\gamma}_c$ -values at different salinities are plotted against the molar ratio of NaCl over MEGA-12/14-HC in Figure 4.7 (right). One sees that the system efficiency decreases as the salinity increases and tends to level off approaching the $\tilde{\gamma}_c$ -value of the microemulsion H₂O – IPM – MEGA-12/14-PC – 1,2-octanediol. These results indicate that the salt might counterbalance the charge effects in the microemulsion and support our hypothesis that the exceptional efficiency of MEGA-12/14-HC is caused by a tiny amount of unknown ionic components contained in the surfactant formulation.

It is known that a bicontinuous microstructure forms in the 1-phase region near the fishtail point. Since the system $\text{H}_2\text{O} - \text{IPM} - \text{MEGA-12/14-HC} - 1,2\text{-octanediol}$ has neither a 3-phase region nor an \tilde{X} point, it is hard to say whether a bicontinuous microstructure exists in the 1-phase microemulsion. Thus, SANS measurements are essential to investigate the microstructure and to observe the structural change induced by the composition change. We chose four samples with low γ located in the 1-phase region: two for the microemulsion $\text{D}_2\text{O} - \text{IPM} - \text{MEGA-12/14-HC} - 1,2\text{-octanediol}$ without salt ($\gamma_{\text{C}} = 0.0521$, $\gamma_{\text{D}} = 0.0878$, $\phi = 0.50$ and $\gamma_{\text{C}} = 0.0232$, $\gamma_{\text{D}} = 0.0737$, $\phi = 0.50$), and two for the microemulsion $\text{D}_2\text{O/NaCl} - \text{IPM} - \text{MEGA-12/14-HC} - 1,2\text{-octanediol}$ with $\varepsilon = 0.0009$ ($\gamma_{\text{C}} = 0.0689$, $\gamma_{\text{D}} = 0.0927$, $\phi = 0.50$ and $\gamma_{\text{C}} = 0.0522$, $\gamma_{\text{D}} = 0.0878$, $\phi = 0.50$). Note that H_2O was replaced with D_2O to adjust bulk contrast, and the salinity of $\varepsilon = 0.0009$ in D_2O is equivalent to $\varepsilon = 0.001$ in H_2O . In Figure 4.8, all four scattering curves have the typical shape known for bicontinuous microemulsions [Str94, Sot97] as described in Section 4.1. The scattering peaks were analyzed with the Teubner–Strey model [Teu87], yielding the periodicity of the oil and water domains d_{TS} , the correlations length ξ_{TS} and the amphiphilicity factor f_{a} . For the two samples without salt (Figure 4.8 (left)) and the two samples with salt (Figure 4.8 (right)), the same trend applies: the correlation peak shifts to larger q -values as the surfactant mass fraction γ_{C} increases. This is expected since the distance between surfactant monolayers becomes smaller with an increased surfactant concentration. Accordingly, the periodicity and the correlation length decrease. Meanwhile, the surfactant monolayers are softened due to a weaker influence of thermal fluctuations and the better-ordered microstructure [Mor94], which leads to a more negative amphiphilicity factor f_{a} .

The very efficient microemulsion sample ($\gamma_{\text{C}} = 0.0232$) has higher scattering intensities than the other samples, which result in double and multiple scattering contributions visible at $q \approx 2 \cdot q_{\text{max}}$. Nevertheless, the bicontinuous microstructure is retained. Its large length scale ($\xi_{\text{TS}} = 18.0$ nm, $d_{\text{TS}} = 48.5$ nm) might be caused by an increased bending rigidity of the surfactant monolayer. We speculate that the increased bending rigidity might be induced by an electrostatic repulsion [Sil01], which is caused by a tiny amount of ionic amphiphilic components contained in the surfactant formulation. Last but not least, comparing the scattering

curves of the samples with nearly the same surfactant mass fraction but without and with salt ($\gamma_C = 0.0521$, $\gamma_D = 0.0878$, $\varepsilon = 0$ and $\gamma_C = 0.0522$, $\gamma_D = 0.0878$, $\varepsilon = 0.0009$), one sees similar values for the periodicity, the correlation length, and the amphiphilicity. This indicates that with the addition of salt, although the system efficiency of the microemulsion decreases, the microstructure remains the same. The addition of salt only counterbalances the electrostatic effect.

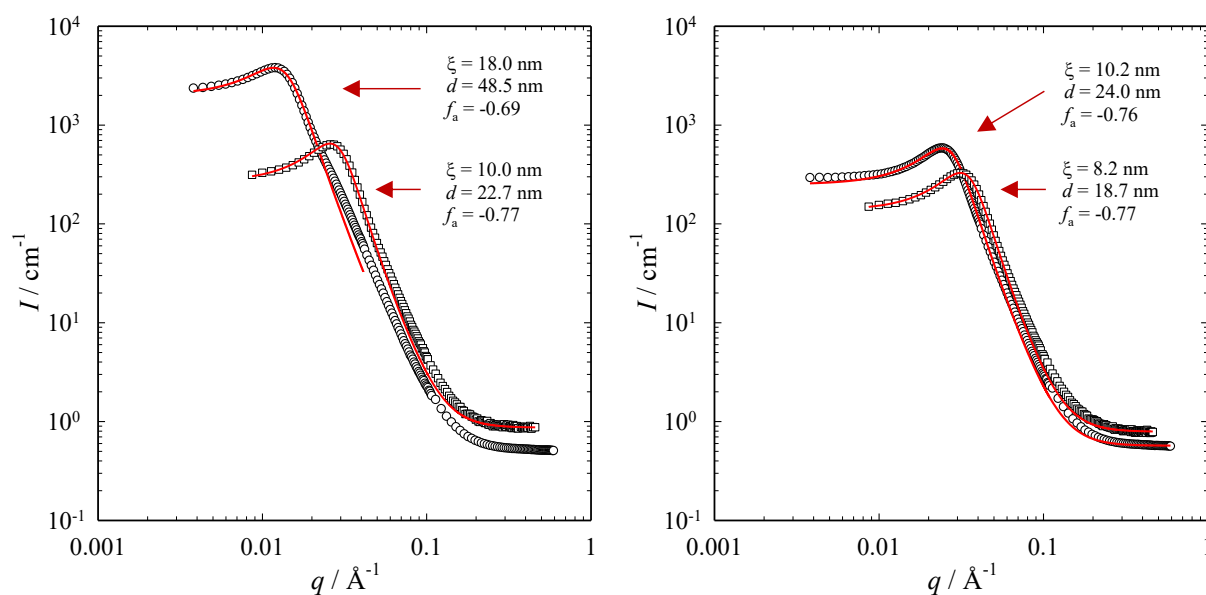


Figure 4.8: SANS curves of (left) $\text{D}_2\text{O} - \text{IPM} - \text{MEGA-12/14-HC} - 1,2\text{-octanediol}$ with $\gamma_C = 0.0232$, $\gamma_D = 0.0737$, $\phi = 0.50$ at $T = 24.7\text{ }^\circ\text{C}$ (empty circles) and $\gamma_C = 0.0521$, $\gamma_D = 0.0878$, $\phi = 0.50$ at $T = 27.0\text{ }^\circ\text{C}$ (empty squares); (right) $\text{D}_2\text{O/NaCl} - \text{IPM} - \text{MEGA-12/14-HC} - 1,2\text{-octanediol}$ with $\gamma_C = 0.0522$, $\gamma_D = 0.0878$, $\varepsilon = 0.0009$, $\phi = 0.50$ at $T = 25.4\text{ }^\circ\text{C}$ (empty circles) and $\gamma_C = 0.0689$, $\gamma_D = 0.0927$, $\varepsilon = 0.0009$, $\phi = 0.50$ at $T = 27.0\text{ }^\circ\text{C}$ (empty squares). Red solid lines are Teubner-Strey fits [Teu87]. Reproduced with permission from [Pen20]. Copyright 2020 American Chemical Society.

After having formulated the non-toxic microemulsions with MEGA-12/14-PC and MEGA-12/14-HC, the next step was to gel the microemulsion and examine its rheological properties. The results are quite consistent with those of glucoside-containing microemulsions. For the microemulsion $\text{H}_2\text{O} - \text{IPM} - \text{MEGA-12/14-PC} - 1,2\text{-octanediol}$, the hydrogelator DBC does not gel the system even at a gelator concentration as high as 3.0 wt.% but shifts the phase boundaries to a larger amount of co-surfactant. On the other hand, the organogelator DBS gelled

the microemulsion H₂O – IPM – MEGA-12/14-HC – 1,2-octanediol without changing the phase boundaries. The choice of gelator concentration is 0.3 wt.%, the same as that of the glucoside-containing microemulsion. Subsequently, we chose two samples in the middle of the 1-phase region of the gelled microemulsion H₂O – IPM – MEGA-12/14-HC – 1,2-octanediol for rheological measurements, namely $\gamma_C = 0.0363$, $\gamma_D = 0.0885$ and $\gamma_C = 0.0538$, $\gamma_D = 0.1042$ in the presence of DBS at $\eta = 0.003$. The two samples have almost the same rheological behavior, which is quite similar to that of glucoside-containing microemulsions. The storage modulus G' ($\sim 10^3$ Pa) from the frequency sweep is about one order of magnitude larger than the loss modulus G'' over the entire frequency range, and both moduli show only a very weak frequency dependence. A temperature sweep allowed to determine the gel–sol transition temperature, which is $T_{\text{sol-gel}} \approx 82$ °C. These results support our assumption that the gelled non-toxic microemulsion is an orthogonal self-assembled system: (1) The gelator does not change the phase behavior. (2) The microemulsion “only” acts as a solvent for the gelator, *i.e.*, the composition of the microemulsion does not influence the rheological properties.

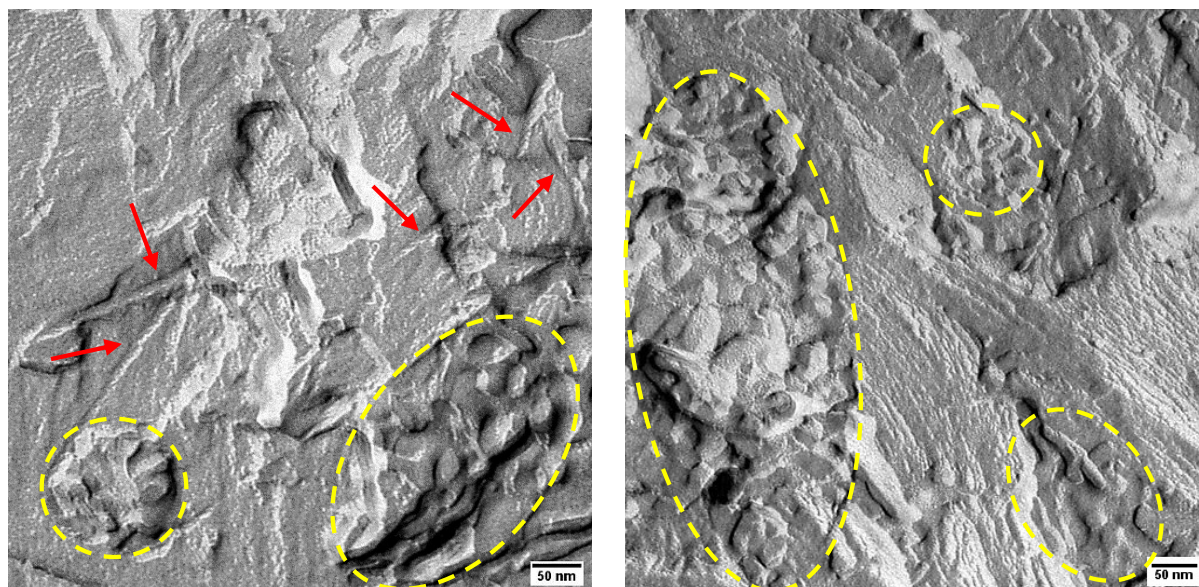


Figure 4.9: FFEM pictures of the gelled bicontinuous microemulsion H₂O – IPM – MEGA-12/14-HC – 1,2-octanediol in the presence of DBS at $\eta = 0.003$ with the composition of $\gamma_C = 0.0276$, $\gamma_D = 0.0774$, $\phi = 0.50$. The red arrows point at the gel fibers, and the yellow circles surround the bicontinuous domains. Reproduced with permission from [Pen20]. Copyright 2020 American Chemical Society.

For visualizing the structure of the gelled microemulsion, FFEM was used to characterize the system H₂O – IPM – MEGA-12/14-HC – 1,2-octanediol with a composition of $\gamma_C = 0.0276$, $\gamma_D = 0.0774$, $\phi = 0.50$ in the presence of DBS at $\eta = 0.003$. Figure 4.9 (left) clearly shows the coexistence of twisted gel fibers (red arrows) and bicontinuous regions (yellow circles). The gel fibers have diameters of $d_{\text{fibril}} \approx 8\text{--}12$ nm and are sparsely distributed due to a very low gelator concentration ($\eta = 0.003$). Furthermore, the length scale of the bicontinuous structure agrees with the domain size of $d_{\text{TS}}/2 \approx 24$ nm obtained from SANS of a sample with a similar composition. In Figure 4.9 (right), the lamellar structured regions suggest a partial phase separation of the sample during the FFEM sample preparation process.

In summary, we studied a new class of sugar surfactants, namely *n*-alkanoyl-*N*-methylglucamides, and formulated a very efficient gelled non-toxic microemulsion consisting of H₂O – IPM – MEGA-12/14-HC – 1,2-octanediol and the gelator DBS. The system efficiency is $\tilde{\gamma}_C + \tilde{\gamma}_D \leq 0.08$, which is substantially higher than the efficiency of Plantacare-based microemulsions. This exceptional efficiency might be caused by the electrostatic stiffening effect induced by a tiny amount of ionic amphiphilic components in the surfactant formulation. All experimental results suggest that the gelled non-toxic microemulsion is an orthogonal self-assembled system: (1) The gelator does not influence the phase behavior of the microemulsion. (2) The rheological properties depend on the gelator and are independent of the microemulsion composition. (3) The FFEM pictures indicate the coexistence of twisted gel fibers and bicontinuous water and oil domains.

4.3 Gelled Non-Toxic Bicontinuous Microemulsions as Promising Transdermal Drug Carriers (Publication III)

Although we found an ultra-efficient gelled non-toxic microemulsion (Publication II), the glucamide-containing microemulsions are sensitive to salinity, and glucamide surfactants are less available than APGs. Therefore, we decided to continue the study with Plantacare-based microemulsions consisting of H₂O – IPM – Plantacare 1200 UP (C₁₂G_{1.4}) – 1,2-octanediol,

whose phase behavior is more predictable and reproducible. In Publication III, we aimed to load both hydrophobic and hydrophilic model drugs in the gelled non-toxic microemulsion (base system) and thus to formulate a model drug delivery carrier for further application tests.

We chose two commonly used model drugs [Kog06], namely the hydrophobic lidocaine and the hydrophilic diclofenac sodium salt (for molecular structures, see Figure 1.3). Lidocaine is a local anesthetic, and diclofenac is a nonsteroidal anti-inflammatory drug (NSAID) for pain relief. It was found that the combination of lidocaine and diclofenac has a synergistic analgesic effect [Lin18]. Referring to the active content of commercial gel-based medical ointments, we chose two dosages for each model drug, namely 2.0 and 4.0 wt.% for lidocaine and 1.0 and 2.3 wt.% for diclofenac sodium salt. The first step was to investigate the effect of each model drug on the phase boundaries of the base microemulsion.

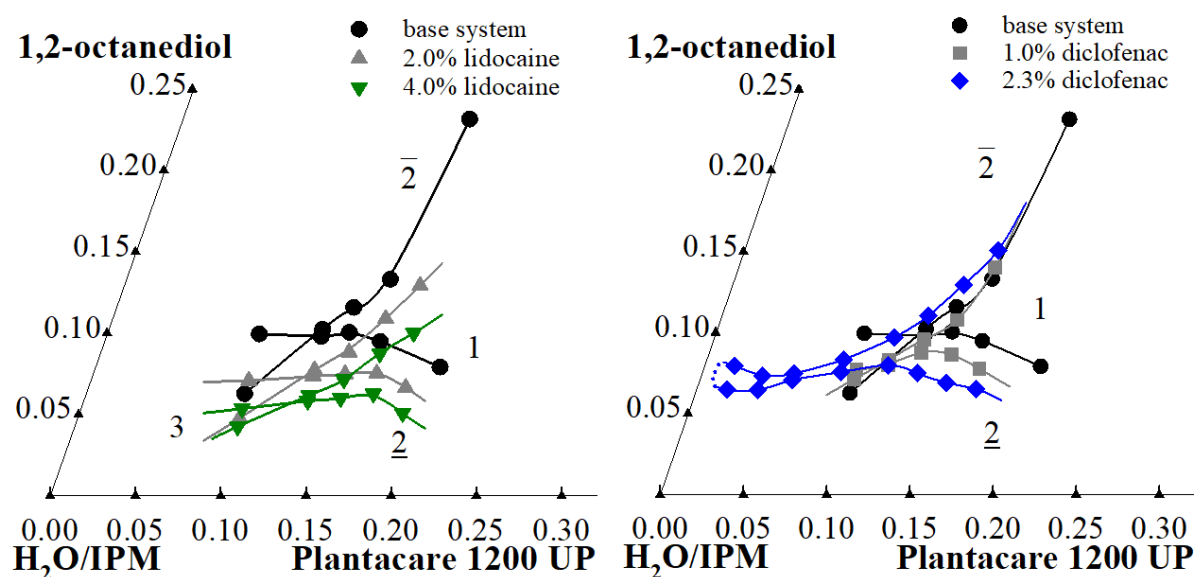


Figure 4.10: Phase diagrams of the base system $\text{H}_2\text{O} - \text{IPM} - \text{Plantacare 1200 UP (C}_{12}\text{G}_{1.4}) - 1,2\text{-octanediol}$ without drugs (black circles) and (left) with 2.0 wt.% (grey triangles up) and 4.0 wt.% lidocaine (green triangles down) at $T = 25\text{ }^\circ\text{C}$, $\phi = 0.50$; (right) with 1.0 wt.% (grey squares) and 2.3 wt.% diclofenac sodium salt (blue diamonds) at $T = 25\text{ }^\circ\text{C}$, $\phi = 0.50$. Reproduced with permission from [Pen21a]. Copyright 2021 Taylor & Francis Group.

As one can see in Figure 4.10 (left), the shape of the phase boundaries remains the same as the base system, but the phase diagram shifts downward with the addition of lidocaine. The more lidocaine is added, the less co-surfactant ($\tilde{\gamma}_D$) is needed to form a 1-phase microemulsion, while

the amount of the main surfactant ($\tilde{\gamma}_C$) stays constant. Considering the facts that (a) lidocaine has a high solubility in IPM (> 15 wt.%), (b) less co-surfactant is needed in the presence of lidocaine, (c) lidocaine has a similar carbon number as IPM but with an aromatic ring, one can conclude that lidocaine is mainly dissolved in the oil phase thus rendering the oil less hydrophobic. A previous study has shown that a cyclic oil with an aromatic ring behaves less hydrophobic than the saturated cyclic oil and the n -alkane with the same carbon number in the microemulsion [Bur00], which supports our conclusion.

As for the effect of diclofenac sodium salt, one sees in Figure 4.10 (right) that it is concentration-dependent. With 1.0 wt.% diclofenac, the shape of the phase boundaries does not change significantly, but the solubilization efficiency increases, *i.e.*, both $\tilde{\gamma}_C$ and $\tilde{\gamma}_D$ are smaller than those of the base system. Interestingly, with 2.3 wt.% diclofenac, the 1-phase channel extends to the very left edge of the phase diagram ($\gamma_C \leq 0.019$), while no 3-phase region was observed. This phenomenon is similar to Kaler and Silas' observation [Sil01] and to what we observed in Publication II [Pen20]. Since diclofenac sodium salt has an amphiphilic structure and a negative charge, we expect it to partly adsorb in the surfactant monolayer (interface) and induce an electrostatic stiffening effect, which increases the bending rigidity of the surfactant monolayer and stabilizes the microemulsion. On the other hand, we found that 5 wt.% diclofenac sodium salt also dissolves in the mixture of 10 wt.% 1,2-octanediol and 90 wt.% IPM, which resembles the oil phase composition. Therefore, diclofenac sodium salt might go to both the interface and the oil phase. In other words, diclofenac sodium salt acts as both co-surfactant and co-oil in the microemulsion, although it is specified as a "hydrophilic drug".

Having studied the individual effect of the model drugs on the microemulsion phase behavior, the next step was to add both drugs to the microemulsion. In order to have more representative results, we took the higher dosage of each drug, namely 4.0 wt.% lidocaine and 2.3 wt.% diclofenac sodium salt. The results are shown in Figure 4.11 (right), and the phase diagrams of the base system with each drug separately are shown in Figure 4.11 (left) for comparison. The phase behavior of the base system containing both drugs combines the effects observed for the

“single drug” systems: (1) The phase boundaries further shift downward compared to the system with 2.3 wt.% diclofenac due to the function of lidocaine as co-oil. (2) The 1-phase channel extends to the left edge of the phase diagram. This surfactant-free 1-phase mixture has strong opalescence, as shown in the two photos (Figure 4.11 (right)) taken in transmitted light and without illumination, respectively. This unexpected stabilization of such a mixture might be caused by the electrostatic stiffening effect from diclofenac sodium salt or might be due to the proximity of a critical point in the surfactant-free system. Nevertheless, in summary, our non-toxic microemulsion (the base system) can solubilize the designated amounts of both model drugs. Moreover, the model drugs help to stabilize the microemulsion and increase the overall efficiency.

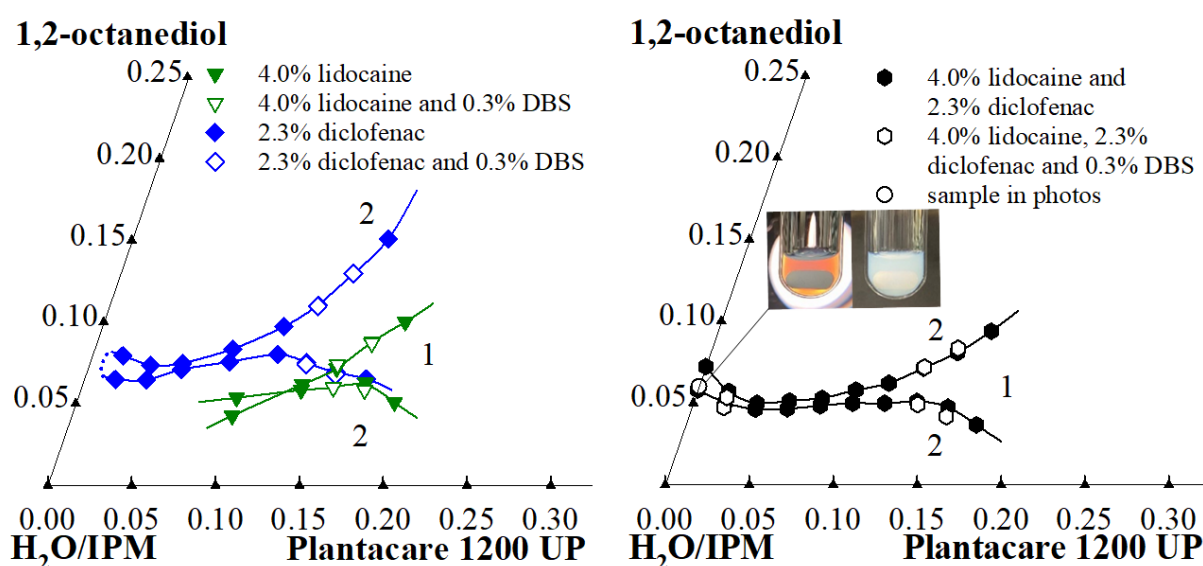


Figure 4.11: (Left) Phase diagrams of the non-gelled base system with 4.0 wt.% lidocaine (green triangles), with 2.3 wt.% diclofenac sodium salt (blue diamonds) and the gelled counterparts in the presence of DBS at $\eta = 0.003$, $T = 25\text{ }^{\circ}\text{C}$, $\phi = 0.50$ (empty green triangles and empty blue diamonds, respectively). (Right) Phase diagrams of the non-gelled microemulsion with 4.0 wt.% lidocaine and 2.3 wt.% diclofenac sodium salt (black hexagons) and the gelled microemulsion (empty black hexagons) in the presence of DBS a $\eta = 0.003$, $T = 25\text{ }^{\circ}\text{C}$, $\phi = 0.50$. Two photos taken in transmitted light (left) and without illumination (right) show the strong opalescence of the surfactant-free 1-phase mixture. Adapted with permission from [Pen21a]. Copyright 2021 Taylor & Francis Group.

Subsequently, we intended to gel the drug-containing microemulsions to increase their mechanical stability. The three drug-containing microemulsions, namely the system with 4.0

wt.% lidocaine, the system with 2.3 wt.% diclofenac sodium salt, and the system with both drugs, are gelled with 0.3 wt.% of the organogelator DBS. Note that the phase boundaries are not changed upon gelation (Figure 4.11). These results are consistent with our findings in Publication I [Pen19] and II [Pen20]. Then we examined the rheological properties of the three drug-containing gelled microemulsions for samples located in the middle of the 1-phase region at $\gamma_C \sim 0.16$. We found that the three samples have almost the same rheological behavior: (1) Frequency sweeps show that the storage modulus G' is in the range of 10^3 Pa and the loss modulus G'' in the range of 10^2 Pa. Moreover, both moduli show only very weak frequency dependence. (2) The gel–sol transition temperatures $T_{\text{sol-gel}}$ are in the range of 72–80 °C. We note that the rheological properties of the drug-containing gelled microemulsions are quite similar to those of the drug-free gelled microemulsions, which again supports our hypothesis of orthogonal self-assembly: the gelled microemulsions are nearly the “same” gels with 0.3 wt.% organogelator DBS but consist of slightly different solvents.

To conclude, we dissolved both hydrophobic and hydrophilic model drugs, namely 4.0 wt.% lidocaine and 2.3 wt.% diclofenac sodium salt, in the gelled non-toxic microemulsion. Surprisingly, the addition of the model drugs helps to stabilize the microemulsion and to improve its efficiency.

4.4 From Water-Rich to Oil-Rich Gelled Non-Toxic Microemulsions (Publication IV)

In Publication I–III, we studied microemulsions with equal volumes of oil and water ($\phi = 0.5$). In Publication IV, we varied the oil-to-water ratios from $\phi = 0.20$ to $\phi = 0.80$ so that both oil- and water-soluble drugs can be solubilized and the gelled non-toxic microemulsions can be either water- or oil-based, depending on the specific application needs. The system of choice was the non-toxic system H₂O – IPM – Plantacare 1200 UP (C₁₂G_{1.4}) – 1,2-octanediol, for which a suitable LMWG must be identified for different oil-to-water ratios.

To measure the phase behavior at different oil-to-water ratios, sections through the isothermal phase tetrahedron were recorded at a constant temperature of $T = 25\text{ }^{\circ}\text{C}$ and five ϕ -ratios of 0.20, 0.35, 0.50, 0.65, and 0.80. The phase diagrams of $\phi = 0.20$, 0.50, and 0.80 are shown in Figure 4.12 (top). It always holds that the addition of 1,2-octanediol induces phase transitions in the sequence of $\underline{2} - 3 - \bar{2}$ and $\underline{2} - 1 - \bar{2}$, respectively. With increasing ϕ -ratios, the 1-phase region is broadened, and the fishtail \tilde{X} point shifts upward and to the right of the phase diagram.

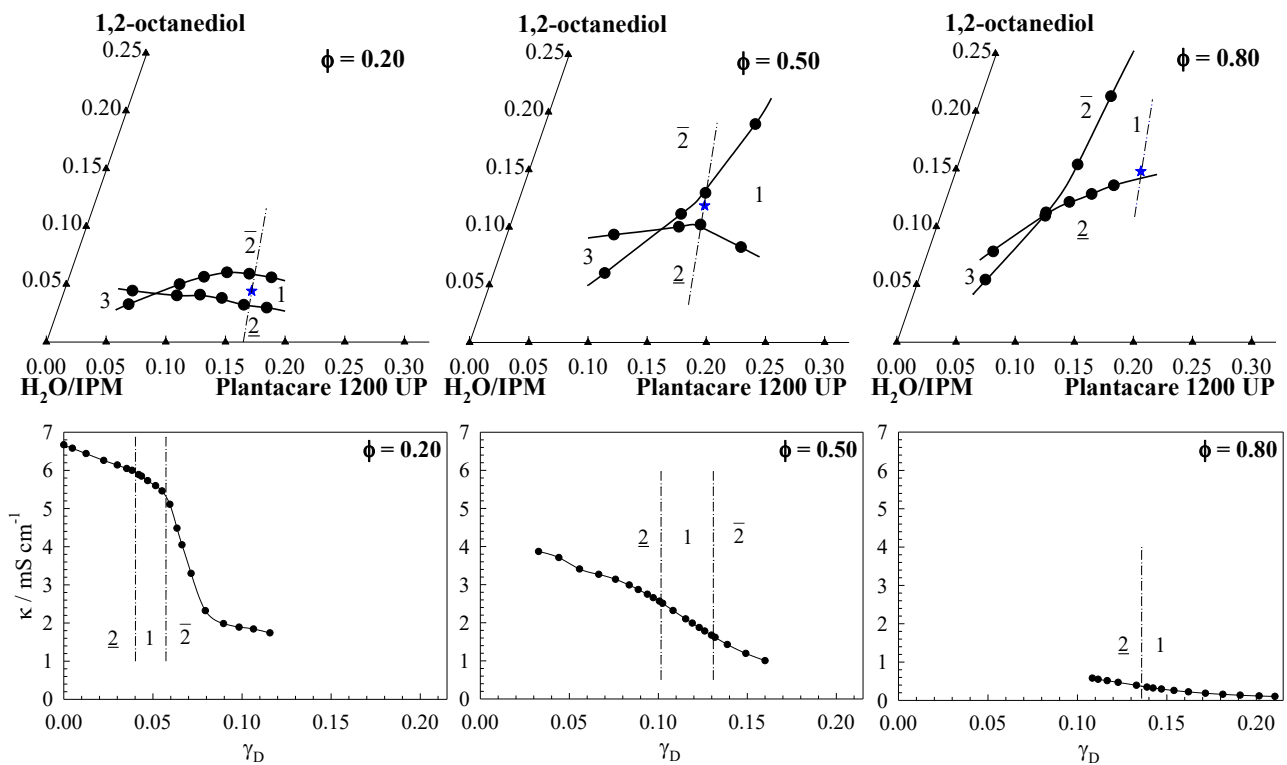


Figure 4.12: (top) Phase diagrams of the non-toxic system $\text{H}_2\text{O} - \text{IPM} - \text{Plantacare 1200 UP}$ ($\text{C}_{12}\text{G}_{1.4}$) – 1,2-octanediol at oil-to-water ratios of $\phi = 0.20$, 0.50 and 0.80 at $T = 25\text{ }^{\circ}\text{C}$. The sample compositions of gelled microemulsions for the rheological measurements and FFEM are marked with a blue star. (bottom) Electrical conductivities measured as a function of the co-surfactant mass fraction γ_D with $\phi = 0.20$, 0.50 and 0.80 at $T = 25\text{ }^{\circ}\text{C}$. The titration path for measuring the electrical conductivity is indicated by a dashed-dotted line in the phase diagrams. Instead of pure water, a 0.1 wt.% NaCl solution was used, which has a negligible effect on the phase behavior. Reproduced from [Pen21b] with permission from the PCCP Owner Societies.

In order to monitor the structural change that comes along with the co-surfactant addition, we measured electrical conductivities along a titration path (Figure 4.12 (top), dashed-dotted line). Note that water was replaced by 0.1 wt.% NaCl solution for conductivity measurements and

that the effect of brine on the phase behavior is negligible. Looking at the conductivity curve of the water-rich microemulsion ($\phi = 0.20$), one sees a sharp decrease in conductivity with increasing γ_D . The conductivities of the 1-phase region are relatively high, indicating a water-continuous structure with either discrete oil droplets or network-like oil structures. The conductivity curve of the symmetric microemulsion ($\phi = 0.50$) has a typical sigmoidal shape, and the curve in the 1-phase region has the steepest slope with intermediate conductivities, suggesting a bicontinuous structure. The bicontinuous structure was also shown by SANS in Publication I [Pen19]. Note that the conductivity decrease is not as significant as reported in the literature, where one finds a decrease by up to several orders of magnitude [Kah93b]. The moderate conductivity drop is partly due to the low salt concentration and partly due to the weak amphiphilicity of the sugar surfactants and the weakly structured nature of the non-toxic microemulsion [Kah93b, Pen19]. For the oil-rich microemulsion ($\phi = 0.80$), low and decreasing conductivity values indicate an oil-continuous structure with discrete spherical or cylindrical water droplets.

Having understood the phase behavior of the non-toxic microemulsion H₂O – IPM – Plantacare 1200 UP – 1,2-octanediol, a suitable LMWG must be found for each oil-to-water ratio ϕ . The goal was to formulate gelled 1-phase microemulsions, *i.e.* transparent gels. It is known that the organogelator DBS gels the non-toxic microemulsion at $\phi = 0.50$, so we tested DBS for other ϕ -ratios. DBS formed a transparent gel in the microemulsions with $\phi \geq 0.35$ at $\eta = 0.003$, but it could not be dissolved at $\eta = 0.0025$ in the microemulsion with $\phi = 0.20$. Nevertheless, DBS formed a weak transparent gel in the microemulsion with $\phi = 0.20$ at $\eta = 0.002$. Since our search for a more suitable gelator for the water-rich microemulsion was not successful, we continued working with DBS at all ϕ -ratios.

Having identified a suitable gelator, we investigated whether the oil-to-water ratio affects the rheological properties of the gelled microemulsions. We chose one sample for each ϕ -ratio located in the 1-phase region with nearly the same γ_C -value. A gelator concentration of $\eta = 0.002$ was used for the gelled microemulsion with $\phi = 0.20$ and of $\eta = 0.003$ for the samples

with other ϕ -ratios. For the sake of comparison, we also studied a sample with $\phi = 0.35$ and $\eta = 0.002$.

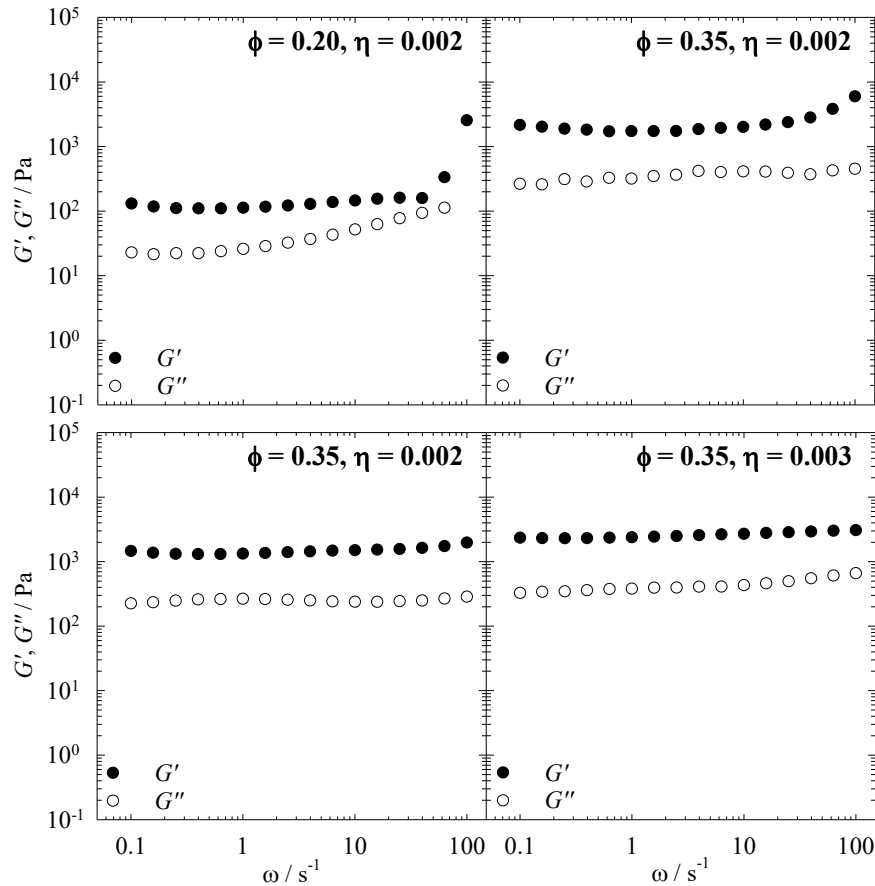


Figure 4.13: Storage modulus G' (filled symbols) and loss modulus G'' (open symbols) of the gelled microemulsion in the presence of DBS at $T = 25$ °C as a function of the angular frequency ω with (top) $\phi = 0.20$, $\eta = 0.002$ and $\phi = 0.35$, $\eta = 0.002$ at a shear stress of $\tau = 1$ Pa; (bottom) $\phi = 0.35$, $\eta = 0.002$ and $\phi = 0.35$, $\eta = 0.003$ at a shear stress of $\tau = 10$ Pa. Reproduced from [Pen21b] with permission from the PCCP Owner Societies.

On the water-rich side, frequency sweeps were carried out at $\tau = 1$ Pa for the samples with $\phi = 0.20$ and 0.35 , $\eta = 0.002$ (Figure 4.13 (top)) because the LVE limit of the sample with $\phi = 0.20$ is smaller than 10 Pa. The moduli G' and G'' of the sample with $\phi = 0.20$ are one order of magnitude smaller than those of the sample with $\phi = 0.35$, and the former sample shows stronger frequency dependence than the latter one. Temperature sweeps of both samples show a similar difference of moduli strengths, yet the gel–sol transition temperatures of the two samples are similar since both have the same gelator concentration of $\eta = 0.002$. These results indicate that the sample with $\phi = 0.20$ is a rather weak gel. The sample with $\phi = 0.35$, $\eta = 0.002$ was also

compared with a sample with $\phi = 0.35$, $\eta = 0.003$ at $\tau = 10$ Pa (Figure 4.13 (bottom)). Both samples show the typical behavior of a strong gel, *i.e.* the storage modulus G' is one order of magnitude higher than the loss modulus G'' and both moduli are independent of the frequency.

On the other hand, all other samples from $\phi = 0.35$ to $\phi = 0.80$ with $\eta = 0.003$ (including the sample with $\phi = 0.50$ measured in Publication I) have nearly the same rheological behavior: (1) the storage modulus G' is in the range of 10^3 Pa, while the loss modulus G'' is in the range of 10^2 Pa; (2) both moduli have very weak frequency dependence; (3) the gel–sol transition temperature $T_{\text{sol-gel}}$ is around 72 °C. Given the fact that $\eta = 0.002$ of DBS in the water-rich microemulsion with $\phi = 0.35$ forms a strong gel, one must ask the following question: Why is the gelled microemulsion with $\phi = 0.20$ a much weaker gel than all other samples? Note that the fibrillar gel network spans through both oil and water domains; otherwise, we would not observe a gel-like behavior. The fact that DBS is an organogelator and that the water-rich microemulsion does not contain enough oil cannot answer the question.

Hansen solubility parameters (HSPs) have been used to characterize the gelation behavior of LMWGs in various solvents [Ray11, Gao12, Die14]. HSPs quantify the cohesive energy density δ of a solvent from three types of weak interactions: dipole-dipole or polar interactions δ_P , hydrogen-bonding interactions δ_H , and van der Waals or dispersive interactions δ_D [Han07]. Each solvent is a point on the 3D Hansen space, where the three axes represent the three HSPs (δ_P , δ_H , $2\delta_D$), and the distance from the origin to that point is the total cohesive energy density δ of the solvent. For gelator–solvent interactions, we used a gelation model for DBS in a wide range of solvents developed by Raghavan *et al.* [Die14]. Raghavan *et al.* assume that the HSPs of DBS are close to those of the solvents in which DBS is soluble and different from those of the solvents in which DBS is insoluble. The interactions between the gelator and the solvents are categorized into four types: the gelator is soluble but no gelation occurs (S), slow gelation (SG), instant gelation (IG), and the gelator is insoluble (I). The four categories are represented by four concentric spheres sharing the same origin on the 3D Hansen space (Figure 4.14). The center of the sphere is the HSPs of 1% (weight/volume) DBS with $(\delta_P, \delta_H, 2\delta_D) = (13.6, 6.4,$

35.6), which was fitted from the gelation results of 1% DBS in 35 solvents [Die14].

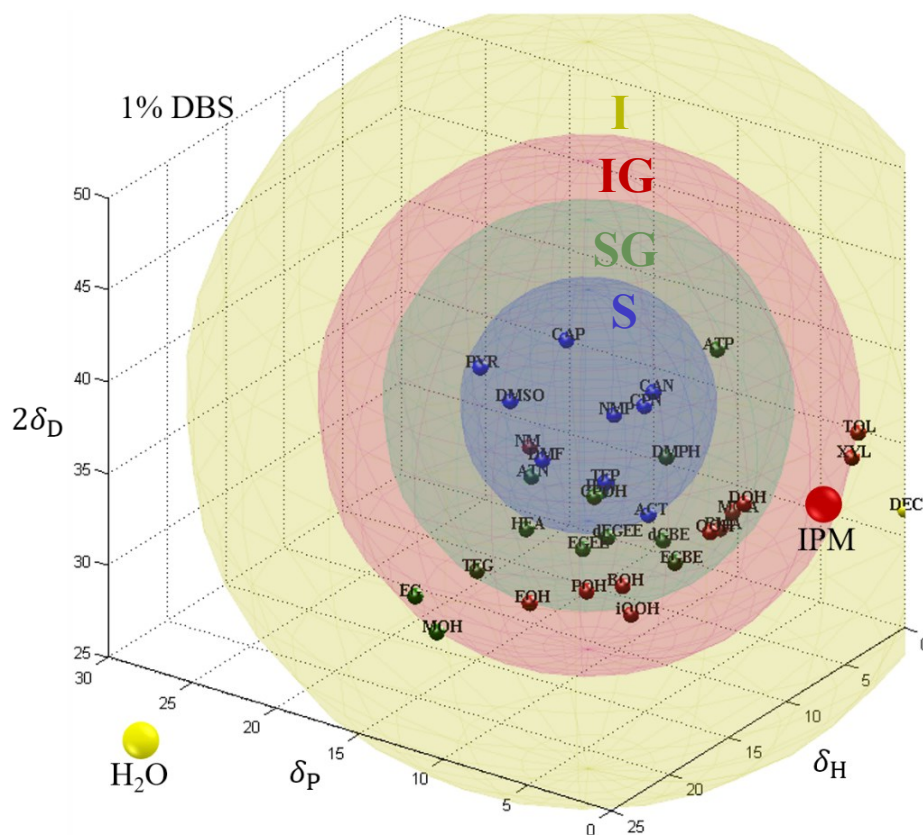


Figure 4.14: Hansen solubility parameters (HSPs) of 1% DBS (weight/volume) [Die14], water [Han07], and IPM [Yam21] plotted in the 3D Hansen space. The results show a pattern of concentric spheres, namely the central sol (S) sphere in blue, slow gelation (SG) in green, instant gelation (IG) in red, and insoluble (I) in yellow. The axes represent the three Hansen solubility parameters (δ_D = dispersive, δ_P = polar, and δ_H = hydrogen-bonding interactions). Reproduced from [Pen21b] with permission from the PCCP Owner Societies.

In our microemulsions with various oil-to-water ratios, the solvent properties mainly depend on the IPM-to-water ratio. We found the HSPs for water ($\delta_P = 16$, $\delta_H = 42.3$, $2\delta_D = 31$, [Han07]) and IPM ($\delta_P = 2$, $\delta_H = 4$, $2\delta_D = 32.4$, [www02]) and tested the gelation behavior of 1% DBS in water and IPM, respectively. Plotting water and IPM on the Hansen space (Figure 4.14), one sees that water and IPM are located on two different sides of the Hansen space, and the water is much farther away from the sphere center (HSPs of DBS) than IPM. Although we do not know the HSPs of the other components and the microemulsion domains, we suppose that changing the IPM-to-water ratio, one approaches the two inner spheres (IG and SG) from two different sides. This is in line with our observation that 35 vol.% IPM ($\phi = 0.35$) in the water-

rich microemulsion is needed to form a strong gel, while less than 20 vol.% water is needed in the oil-rich microemulsion. Raghavan *et al.* also found that the rheological properties of the gelled solvents in the IG sphere are very similar to each other, which agrees with our findings that all gelled microemulsions with $\phi \geq 0.35$ have nearly the same rheological behavior.

However, the HSP theory cannot explain why the gelled microemulsion with $\phi = 0.20$ is a rather weak gel. Since this water-rich microemulsion is close to the water side (Figure 4.14), it is probably located in the IG sphere rather than the SG sphere. Hence a strong gel should have been formed, which is not the case. We argue that besides gelator–solvent interactions, the microstructure also plays a role in the gelation behavior. For the microemulsion with $\phi = 0.20$, both the electrical conductivity scan and the FFEM image indicate polydisperse spherical and cylindrical oil droplets in a continuous water domain. For the microemulsion with $\phi = 0.50$, the electrical conductivity scan and the previous SANS measurements [Pen19] suggest a bicontinuous structure. For the microemulsion with $\phi = 0.80$, the FFEM image shows a continuous oil phase, whereas water droplets are hardly visible, and the low electrical conductivity also indicates an oil-continuous structure with discrete spherical or cylindrical water droplets. The structural change of our gelled microemulsions agrees with previous findings of a similar quaternary system $D_2O - n\text{-octane} - \beta\text{-C}_8\text{G}_1 - 1\text{-octanol}$ [Rei03]. NMR and SANS measurements varying from $\phi = 0.1$ to $\phi = 0.9$ by step of 0.1 suggest that the bicontinuous structure remains present between $\phi = 0.3$ and $\phi = 0.7$, while discrete droplets in a continuous phase are observed at lower and higher ϕ -ratios. Looking at our non-toxic microemulsions, the microstructure is either bicontinuous or oil-continuous at $\phi \geq 0.35$, *i.e.* an oil-continuous phase always exists. Only the microemulsion with $\phi = 0.20$ is water-continuous. Therefore, in the case of the organogelator DBS, the presence of an oil-continuous phase seems to be a prerequisite for a strong gel formation.

In conclusion, we formulated gelled non-toxic microemulsions with various oil-to-water ratios from $\phi = 0.2$ to $\phi = 0.8$ to expand their application potentials. Structural changes from the water-rich side to the oil-rich side were characterized by electrical conductivity scans and

complemented by FFEM measurements. Surprisingly, all gelled microemulsions with $\phi \geq 0.35$ have almost the same rheological behavior of strong gels, while the sample with $\phi = 0.20$ is a weak gel. We attribute the identical rheological behavior to gelator–solvent interactions described by Hansen solubility parameters (HSPs). However, DBS only forms a weak gel in the water-rich microemulsion with $\phi = 0.20$, indicating that an oil-continuous phase must be present for a strong gel formation with the organogelator DBS. In other words, the microstructure of the microemulsion must play a role in the gelation behavior. Overall, our hypothesis that gelled microemulsions are an orthogonal self-assembled system remains valid for $\phi \geq 0.35$, whereas the microstructure of the microemulsion affects the gel formation at $\phi = 0.20$.

5 Conclusion & Outlook

The thesis at hand aimed to study the formation of gelled non-toxic microemulsions and to explore their potential use as drug delivery systems. In the following, the findings are summarized in accordance with the three tasks: **(1)** Formulation of non-toxic microemulsions with biocompatible components and model drugs. **(2)** Identification of a suitable low molecular weight gelator (LMWG) for the gelation of the microemulsion. **(3)** Examination of whether the orthogonality of the two structures is maintained, *i.e.*, whether the system is formed via orthogonal self-assembly of the surfactant and the gelator.

We first restudied the scouting system $\text{H}_2\text{O} - n\text{-octane} - n\text{-octyl-}\beta\text{-D-glucopyranoside} (\beta\text{-C}_8\text{G}_1) - 1\text{-octanol}$ with equal volumes of water and oil at a constant temperature of $T = 25\text{ }^\circ\text{C}$, finding that the phase behavior is consistent with the literature [Sot02, Rei03]. Subsequently, we replaced the oil $n\text{-octane}$ and the co-surfactant 1-octanol with non-toxic components, namely isopropyl myristate (IPM) and 1,2-octanediol. The pure surfactant $\beta\text{-C}_8\text{G}_1$ was also replaced by more efficient technical-grade sugar surfactants, including Plantacare 1200 UP (alkyl polyglucosides with an average composition of $\text{C}_{12}\text{G}_{1.4}$) and MEGA-12/14-HC ($n\text{-alkanoyl-}N\text{-methylglucamides}$ with an average carbon chain length of 12–14). Surprisingly, the non-toxic microemulsion consisting of $\text{H}_2\text{O} - \text{IPM} - \text{MEGA-12/14-HC} - 1,2\text{-octanediol}$ has an ultra-high efficiency of $\tilde{\gamma}_C + \tilde{\gamma}_D \leq 0.08$, which is presumably due to the electrostatic stiffening effect. Nevertheless, in order to obtain predictable and reproducible results, we continued the investigation with the non-toxic microemulsion consisting of $\text{H}_2\text{O} - \text{IPM} - \text{Plantacare 1200 UP} - 1,2\text{-octanediol}$. Two model drugs, namely the hydrophobic lidocaine and the hydrophilic diclofenac sodium salt, were loaded to the non-toxic microemulsion. It turns out that 4.0 wt.% lidocaine and 2.3 wt.% diclofenac sodium salt stabilize the microemulsion and improve the system's efficiency. With this amount of drugs, a 1-phase mixture was observed even without surfactant. Last but not least, we varied the oil-to-water ratios from $\phi = 0.20$ to $\phi = 0.80$ so that both oil- and water-soluble drugs can be solubilized, and the gelled non-toxic microemulsions

can be either water- or oil-based, depending on the specific application needs.

After the formulation of non-toxic microemulsions, we tested three LMWGs, namely the organogelators 12-hydroxyoctadecanoic acid (12-HOA) and 1,3:2,4-dibenzylidene-D-sorbitol (DBS) and the hydrogelator *N,N'*-dibenzoyl-L-cystine (DBC), to first gel the scouting system and then the non-toxic system. The goal was to obtain a transparent gel and not to change the phase behavior. Surprisingly, the gelation behavior of the three gelators is quite different in the scouting system and in the non-toxic system, *i.e.*, identifying a suitable gelator is still a challenge. We chose the organogelator DBS as it does not change the phase boundaries and forms strong gels at a gelator concentration as low as 0.3 wt.%. DBS gels all non-toxic systems, namely H₂O – IPM – Plantacare 1200 UP – 1,2-octanediol without and with model drugs, and H₂O – IPM – MEGA-12/14-HC – 1,2-octanediol. Remarkably, DBS also gels the microemulsion consisting of H₂O – IPM – Plantacare 1200 UP – 1,2-octanediol at various oil-to-water ratios. We used 0.3 wt.% of DBS for $\phi \geq 0.35$ and 0.2 wt.% for $\phi = 0.2$ due to its poor solubility in the water-rich microemulsion (note that the hydrogelator derivatives of DBS did not gel the water-rich microemulsion). Frequency sweeps and temperature sweeps of oscillatory shear rheometry were performed to characterize the rheological properties. Surprisingly, all abovementioned systems except the one of H₂O – IPM – Plantacare 1200 UP – 1,2-octanediol with $\phi = 0.2$ show strong gel behavior: (1) the storage modulus G' is in the range of 10^3 Pa, while the loss modulus G'' is in the range of 10^2 Pa; (2) both moduli have very weak frequency dependence; (3) the gel–sol transition temperature $T_{\text{sol-gel}}$ is around 72–82 °C. These patterns are in line with our assumption of orthogonal self-assembly, *i.e.*, the microemulsion and the gel network form independently because these non-toxic microemulsions can be regarded as nearly the same solvent, and 0.3 wt.% of DBS forms similar gels in these solvents. However, DBS only forms a weak gel in the water-rich microemulsion with $\phi = 0.2$ since an oil-continuous phase is a prerequisite for DBS to form a strong gel, while the microemulsion with $\phi = 0.2$ has a water-continuous microstructure.

Finally, we compared the gelled non-toxic microemulsion with the non-gelled counterpart to

examine the orthogonality. For all systems, the phase boundaries remain unchanged upon gelation. Small-angle neutron scattering (SANS) curves of the gelled and non-gelled microemulsions consisting of H₂O – IPM – Plantacare 1200 UP – 1,2-octanediol with $\phi = 0.5$ were fitted with the Teubner–Strey model [Teu87], which gives nearly the same periodicity of $d = 14.0$ nm and the correlation length of $\xi_{TS} \approx 6.3$ – 6.6 nm. These results indicate that the non-toxic microemulsion has a bicontinuous microstructure and that the gel network does not alter the microstructure. However, the gelled microemulsion has slightly higher scattering intensities in the low q -range ($q < 0.01 \text{ \AA}^{-1}$), which is most likely due to the presence of the gel network but was not further investigated. The freeze-fracture electron microscopy (FFEM) images of the gelled microemulsion consisting of H₂O – IPM – Plantacare 1200 UP – 1,2-octanediol with 0.3 wt.% DBS show that the twisted rope-like gel fibers with diameters of $d_{\text{fibril}} \approx 6$ – 12 nm pass through the microemulsion domains. Consistently, the FFEM images of the gelled microemulsion consisting of H₂O – IPM – MEGA-12/14-HC – 1,2-octanediol with 0.3 wt.% DBS show the coexistence of bicontinuous microemulsion domains and the twisted rope-like gel fibers with diameters of $d_{\text{fibril}} \approx 8$ – 12 nm. The microemulsion domain size observed in FFEM agrees with the domain size of the non-gelled microemulsion determined by SANS. Moreover, one sees that the gel fibers formed by the organogelator DBS have the same shape and size in different systems. Overall, our observations indicate that except for the water-rich gelled microemulsion with $\phi = 0.2$, the non-toxic microemulsions and the gel network form independently but simultaneously, *i.e.*, the gelled non-toxic microemulsions are orthogonally self-assembled systems.

From the perspective of fundamental science, this study provides some insight into the interactions between the gelator and the microemulsion as complex fluids. So far, most studies on gelator–solvent interactions used pure organic solvents [Lan14] or binary solvent mixture [Die14]. The microemulsion in this study is a quaternary system with monomerically dissolved surfactant in water domains and a part of co-surfactant dissolved in oil domains, which cannot be described by a mixture of several solvents. Our study reveals that the solvent properties

represented by Hansen Solubility Parameters (HSPs) alone cannot explain the gelator–solvent interactions in the gelled water-rich microemulsion, and the microstructure might play a role in the gelation behavior.

This study substantially extends the application potentials of gelled microemulsions formed via orthogonal self-assembly. Future studies should address the following points: (1) Skin permeation studies should be performed using the system formulated in Publication III and compared with gel-based commercial products. (2) It is also worth investigating the microstructure of the surfactant-free 1-phase mixture (H₂O – IPM – 1,2-octanediol with 4.0 wt.% lidocaine and 2.3 wt.% diclofenac sodium salt) discovered in Publication III with SANS and FFEM. If the 1-phase mixture is structured without surfactant, it could be a very efficient drug delivery system. (3) A suitable LMWG should be identified for the water-rich microemulsion with $\phi = 0.2$ since a water-rich microemulsion is preferred to the oil-rich counterpart in drug delivery. (4) Moreover, stimuli-responsive LMWGs [Xio13] can be used to gel drug-loaded microemulsions so that topical active drug release could be possible. (5) More evidence is needed for proving or disproving the hypothesis that the microstructure of complex fluids plays a role in gelator–solvent interactions and thus in the gelation behavior. Combined dynamic light scattering (DLS) and static light scattering (SLS) could be helpful for this task.

References

- [Bla18] Blair, D. L. Viscoelastic Properties: The Rheology of Soft Solids. In *Molecular Gels: Structure and Dynamics*; Weiss, R. G., Ed.; The Royal Society of Chemistry, 2018; pp 28–56.
- [Boe16] Boekhoven, J.; Brizard, A. M.; Stuart, M. C. A.; Florusse, L.; Raffy, G.; Del Guerzo, A.; Van Esch, J. H. Bio-Inspired Supramolecular Materials by Orthogonal Self-Assembly of Hydrogelators and Phospholipids. *Chem. Sci.* **2016**, *7* (9), 6021–6031.
- [Bol98] Bolzinger, M. A.; Carduner, T. C.; Poelman, M. C. Bicontinuous Sucrose Ester Microemulsion: A New Vehicle for Topical Delivery of Niflumic Acid. *Int. J. Pharm.* **1998**, *176* (1), 39–45.
- [Bol99] Bolzinger-Thevenin, M. A.; Grossiord, J. L.; Poelman, M. C. Characterization of a Sucrose Ester Microemulsion by Freeze Fracture Electron Micrograph and Small Angle Neutron Scattering Experiments. *Langmuir* **1999**, *15* (7), 2307–2315.
- [Bri08] Brizard, A.; Stuart, M.; Van Bommel, K.; Friggeri, A.; De Jong, M.; Van Esch, J. Preparation of Nanostructures by Orthogonal Self-Assembly of Hydrogelators and Surfactants. *Angew. Chemie - Int. Ed.* **2008**, *47* (11), 2063–2066.
- [Bri09] Brizard, A. M.; Stuart, M. C. A.; van Esch, J. H. Self-Assembled Interpenetrating Networks by Orthogonal Self Assembly of Surfactants and Hydrogelators. *Faraday Discuss.* **2009**, *143*, 345–357.
- [Bri09b] Brizard, A. M.; Van Esch, J. H. Self-Assembly Approaches for the Construction of Cell Architecture Mimics. *Soft Matter* **2009**, *5* (7), 1320–1327.
- [Bur03] Burauer, S.; Belkoura, L.; Stubenrauch, C.; Strey, R. Bicontinuous Microemulsions Revisited: A New Approach to Freeze Fracture Electron Microscopy (FFEM). *Colloids Surfaces A Physicochem. Eng. Asp.* **2003**, *228* (1–3), 159–170.
- [Cal17] Callender, S. P.; Mathews, J. A.; Kobernyk, K.; Wettig, S. D. Microemulsion Utility in Pharmaceuticals: Implications for Multi-Drug Delivery. *Int. J. Pharm.* **2017**, *526* (1–2), 425–442.
- [Car91] Carlfors, J.; Blute, I.; Schmidt, V. Lidocaine in Microemulsion - a Dermal Delivery System. *J. Dispers. Sci. Technol.* **1991**, *12* (5–6), 467–482.
- [Chr16] Christ, E.; Blanc, C.; Al Ouahabi, A.; Maurin, D.; Le Parc, R.; Bantignies, J. L.; Guenet, J. M.; Collin, D.; Mésini, P. J. Origin of Invariant Gel Melting Temperatures in the C-T Phase Diagram of an Organogel. *Langmuir* **2016**, *32* (19), 4975–4982.
- [Chr18] Christ, E.; Collin, D.; Lamps, J. P.; Mésini, P. J. Variable Temperature NMR of Organogelators: The Intensities of a Single Sample Describe the Full Phase Diagram. *Phys. Chem. Chem. Phys.* **2018**, *20* (14), 9644–9650.

- [Cor13] Cornwell, D. J.; Okesola, B. O.; Smith, D. K. Hybrid Polymer and Low Molecular Weight Gels-Dynamic Two-Component Soft Materials with Both Responsive and Robust Nanoscale Networks. *Soft Matter* **2013**, *9* (36), 8730–8736.
- [Cru01] D’cruz, O. J.; Uckun, F. M. Gel-Microemulsions as Vaginal Spermicides and Intravaginal Drug Delivery Vehicles. *Contraception* **2001**, *64* (2), 113–123.
- [Die14] Diehn, K. K.; Oh, H.; Hashemipour, R.; Weiss, R. G.; Raghavan, S. R. Insights into Organogelation and Its Kinetics from Hansen Solubility Parameters. Toward a Priori Predictions of Molecular Gelation. *Soft Matter* **2014**, *10* (15), 2632–2640.
- [Dra17] Draper, E. R.; Adams, D. J. Low-Molecular-Weight Gels: The State of the Art. *Chem* **2017**, *3* (3), 390–410.
- [Dre97] Dreher, F.; Walde, P.; Walther, P.; Wehrli, E. Interaction of a Lecithin Microemulsion Gel with Human Stratum Corneum and Its Effect on Transdermal Transport. *J. Control. Release* **1997**, *45* (2), 131–140.
- [Fam20] Fameau, A. L.; Rogers, M. A. The Curious Case of 12-Hydroxystearic Acid — the Dr. Jekyll & Mr. Hyde of Molecular Gelators. *Curr. Opin. Colloid Interface Sci.* **2020**, *45*, 68–82.
- [Fou13] Fouad, S. A.; Basalious, E. B.; El-Nabarawi, M. A.; Tayel, S. A. Microemulsion and Poloxamer Microemulsion-Based Gel for Sustained Transdermal Delivery of Diclofenac Epolamine Using in-Skin Drug Depot: In Vitro/in Vivo Evaluation. *Int. J. Pharm.* **2013**, *453* (2), 569–578.
- [Fro17] Froelich, A.; Osmałek, T.; Snela, A.; Kunstman, P.; Jadach, B.; Olejniczak, M.; Roszak, G.; Białas, W. Novel Microemulsion-Based Gels for Topical Delivery of Indomethacin: Formulation, Physicochemical Properties and in Vitro Drug Release Studies. *J. Colloid Interface Sci.* **2017**, *507*, 323–336.
- [Gao12] Gao, J.; Wu, S.; Rogers, M. A. Harnessing Hansen Solubility Parameters to Predict Organogel Formation. *J. Mater. Chem.* **2012**, *22* (25), 12651–12658.
- [Gel96] Gelbart, W. M.; Ben-Shaul, A. The “New” Science of “Complex Fluids.” *J. Phys. Chem.* **1996**, *100* (31), 13169–13189.
- [Geo06] George, M.; Weiss, R. G. Low Molecular-Mass Organic Gelators. In *Molecular Gels: Materials with Self-Assembled Fibrillar Networks*; Weiss, R. G., Terech, P., Eds.; Springer Netherlands: Dordrecht, 2006; pp 449–551.
- [Gra61] Graham, T. X. Liquid Diffusion Applied to Analysis. *Philos. Trans. R. Soc. London* **1861**, No. 151, 183–224.
- [Gue18] Guenet, J.-M.; Mesini, P.; Schmutz, M. Structural Techniques at Different Length Scales. In *Molecular Gels: Structure and Dynamics*; Weiss, R. G., Ed.; The Royal Society of Chemistry, 2018; pp 227–299.
- [Han07] Hansen, C. M. Solubility Parameters — An Introduction. In *Hansen Solubility Parameters: A User’s Handbook*; CRC Press: Boca Raton, 2007; pp 1–26.

- [Hee03] Heeres, A.; Van Der Pol, C.; Stuart, M.; Friggeri, A.; Feringa, B. L.; Van Esch, J. Orthogonal Self-Assembly of Low Molecular Weight Hydrogelators and Surfactants. *J. Am. Chem. Soc.* **2003**, *125* (47), 14252–14253.
- [Hel08] Hellweg, T. Scattering Techniques to Study the Structure of Microemulsions. In *Microemulsions: Background, New Concepts, Applications, Perspectives*; Stubenrauch, C., Ed.; Wiley-Blackwell: Oxford, 2008; pp 48–83.
- [Heu08] Heuschkel, S.; Goebel, A.; Neubert, R. H. H. Microemulsions—Modern Colloidal Carrier for Dermal and Transdermal Drug Delivery. *J. Pharm. Sci.* **2008**, *97* (2), 603–631.
- [Hil99] Hill, K.; Rhode, O. Sugar-Based Surfactants for Consumer Products and Technical Applications. *Fett-Lipid* **1999**, *101* (1), 25–33.
- [Jah88] Jahn, W.; Strey, R. Microstructure of Microemulsions by Freeze Fracture Electron Microscopy. *J. Phys. Chem.* **1988**, *92* (8), 2294–2301.
- [Joh12] Johnson, W.; Bergfeld, W. F.; Belsito, D. V.; Hill, R. A.; Klaassen, C. D.; Liebler, D.; Marks, J. G.; Shank, R. C.; Slaga, T. J.; Snyder, P. W.; Andersen, F. A. Safety Assessment of 1,2-Glycols as Used in Cosmetics. *Int. J. Toxicol.* **2012**, *31*, 147S–168S.
- [Kah85] Kahlweit, M.; Strey, R. Phase Behavior of Ternary Systems of the Type H₂O–Oil–Nonionic Amphiphile (Microemulsions). *Angew. Chemie Int. Ed. English* **1985**, *24* (8), 654–668.
- [Kah87] Kahlweit, M.; Strey, R.; Haase, D.; Kunieda, H.; Schmeling, T.; Faulhaber, B.; Borkovec, M.; Eicke, H. F.; Busse, G.; Eggers, F.; Funck, T.; Richmann, H.; Magid, L.; Söderman, O.; Stilbs, P.; Winkler, J.; Dittrich, A.; Jahn, W. How to Study Microemulsions. *J. Colloid Interface Sci.* **1987**, *118* (2), 436–453.
- [Kah93b] Kahlweit, M.; Busse, G.; Winkler, J. Electric Conductivity in Microemulsions. *J. Chem. Phys.* **1993**, *99* (7), 5605–5614.
- [Kah95a] Kahlweit, M.; Busse, G.; Faulhaber, B. Preparing Microemulsions with Lecithins. *Langmuir* **1995**, *11* (5), 1576–1583.
- [Kah95b] Kahlweit, M.; Busse, G.; Faulhaber, B. Preparing Microemulsions with Alkyl Monoglucosides and the Role of N-Alkanols. *Langmuir* **1995**, *11* (9), 3382–3387.
- [Kah95c] Kahlweit, M.; Busse, G.; Faulhaber, B.; Eibl, H. Preparing Nontoxic Microemulsions. *Langmuir* **1995**, *11* (11), 4185–4187.
- [Kah96] Kahlweit, M.; Busse, G.; Faulhaber, B. Preparing Nontoxic Microemulsions with Alkyl Monoglucosides and the Role of Alkanediols as Cosolvents. *Langmuir* **1996**, *12* (4), 861–862.
- [Kah97] Kahlweit, M.; Busse, G.; Faulhaber, B. Preparing Nontoxic Microemulsions. 2.

- Langmuir* **1997**, *13* (20), 5249–5251.
- [Kan99] Kantaria, S.; Rees, G. D.; Lawrence, M. J. Gelatin-Stabilised Microemulsion-Based Organogels: Rheology and Application in Iontophoretic Transdermal Drug Delivery. *J. Control. Release* **1999**, *60* (2–3), 355–365.
- [Kat01] Kato, T.; Mizoshita, N.; Kanie, K. Hydrogen-Bonded Liquid Crystalline Materials: Supramolecular Polymeric Assembly and the Induction of Dynamic Function. *Macromol. Rapid Commun.* **2001**, *22* (11), 797–814.
- [Kat06] Kato, T.; Mizoshita, N.; Kishimoto, K. Functional Liquid-Crystalline Assemblies: Self-Organized Soft Materials. *Angew. Chemie - Int. Ed.* **2006**, *45* (1), 38–68.
- [Kat07] Kato, T.; Hirai, Y.; Nakaso, S.; Moriyama, M. Liquid-Crystalline Physical Gels. *Chem. Soc. Rev.* **2007**, *36* (12), 1857–1867.
- [Klu00] Kluge, K. Der Schlüssel Zum Verständnis von Mikroemulsionen Aus Zuckertensiden: Die Interne Grenzfläche (The Key to Understanding Microemulsions of Sugar Surfactants: The Interface), University of Cologne, 2000.
- [Klu01] Kluge, K.; Stubenrauch, C.; Sottmann, T.; Strey, R. Temperature-Insensitive Microemulsions Formulated from Octyl Monoglucoside and Alcohols: Potential Candidates for Practical Applications. *Tenside, Surfactants, Deterg.* **2001**, *38* (1), 30–40.
- [Kog06] Kogan, A.; Garti, N. Microemulsions as Transdermal Drug Delivery Vehicles. *Adv. Colloid Interface Sci.* **2006**, *123*, 369–385.
- [Koi17] Koitani, S.; Dieterich, S.; Preisig, N.; Aramaki, K.; Stubenrauch, C. Gelling Lamellar Phases of the Binary System Water–Didodecyldimethylammonium Bromide with an Organogelator. *Langmuir* **2017**, *33* (43), 12171–12179.
- [Kri09] Krieg, E.; Shirman, E.; Weissman, H.; Shimoni, E.; Wolf, S. G.; Pinkas, I.; Rybtchinski, B. Supramolecular Gel Based on a Perylene Diimide Dye: Multiple Stimuli Responsiveness, Robustness, and Photofunction. *J. Am. Chem. Soc.* **2009**, *131* (40), 14365–14373.
- [Kre02] Kreilgaard, M. Influence of Microemulsions on Cutaneous Drug Delivery. *Adv. Drug Deliv. Rev.* **2002**, *54* (Suppl. 1), 77–98.
- [Lai89] Laibinis, P. E.; Hickman, J. J.; Wrighton, M. S.; Whitesides, G. M. Orthogonal Self-Assembled Monolayers: Alkanethiols on Gold and Alkane Carboxylic Acids on Alumina. *Science* (80-.). **1989**, *245* (4920), 845–847.
- [Lan14] Lan, Y.; Corradini, M. G.; Liu, X.; May, T. E.; Borondics, F.; Weiss, R. G.; Rogers, M. A. Comparing and Correlating Solubility Parameters Governing the Self-Assembly of Molecular Gels Using 1,3:2,4-Dibenzylidene Sorbitol as the Gelator. *Langmuir* **2014**, *30* (47), 14128–14142.
- [Lan15] Lan, Y.; Rogers, M. A. 12-Hydroxystearic Acid SAFiNs in Aliphatic Diols—a Molecular Oddity. *CrystEngComm* **2015**, *17* (42), 8031–8038.

References

- [Lau13] Laupheimer, M.; Jovic, K.; Antunes, F. E.; da Graça Martins Miguel, M.; Stubenrauch, C. Studying Orthogonal Self-Assembled Systems: Phase Behaviour and Rheology of Gelled Microemulsions. *Soft Matter* **2013**, *9* (13), 3661.
- [Lau13b] Laupheimer, M. Gelled Bicontinuous Microemulsions: A New Type of Orthogonal Self-Assembled Systems, University of Stuttgart, 2013.
- [Lau14] Laupheimer, M.; Sottmann, T.; Schweins, R.; Stubenrauch, C. Studying Orthogonal Self-Assembled Systems: Microstructure of Gelled Bicontinuous Microemulsions. *Soft Matter* **2014**, *10* (43), 8744–8757.
- [Lau15] Laupheimer, M.; Preisig, N.; Stubenrauch, C. The Molecular Organogel N-Decane/12-Hydroxyoctadecanoic Acid: Sol-Gel Transition, Rheology, and Microstructure. *Colloids Surfaces A Physicochem. Eng. Asp.* **2015**, *469*, 315–325.
- [Law12] Lawrence, M. J.; Rees, G. D. Microemulsion-Based Media as Novel Drug Delivery Systems. *Adv. Drug Deliv. Rev.* **2012**, *64* (SUPPL.), 175–193.
- [Lin96] Lindman, B.; Olsson, U. Structure of Microemulsions Studied by NMR. *Berichte der Bunsengesellschaft für Phys. Chemie* **1996**, *100* (3), 344–363.
- [Lin18] Linares-Gil, M. J.; Valls, J.; Hereu-Boher, P.; Nebot, F. J.; De-Ramón, B.; Diaz-Munió, E.; Sanzol, R.; De-Oca, J.; Pérez-Lozano, P.; Suñé-Negre, J. M.; García-Montoya, E. Topical Analgesia with Lidocaine Plus Diclofenac Decreases Pain in Benign Anorectal Surgery: Randomized, Double-Blind, and Controlled Clinical Trial. *Clin. Transl. Gastroenterol.* **2018**, *9* (11).
- [Liu13] Liu, S.; Yu, W.; Zhou, C. Solvents Effects in the Formation and Viscoelasticity of DBS Organogels. *Soft Matter* **2013**, *9* (3), 864–874.
- [Mag09] Magno, M.; Tessoro, R.; Medronho, B.; Miguel, M. G.; Stubenrauch, C. Gelled Polymerizable Microemulsions. Part 3 Rheology. *Soft Matter* **2009**, *5* (23), 4763–4772.
- [Mal16] Mallia, V. A.; Blair, D. L.; Weiss, R. G. Oscillatory Rheology and Surface Water Wave Effects on Crude Oil and Corn Oil Gels with (*R*)-12-Hydroxystearic Acid as Gelator. *Ind. Eng. Chem. Res.* **2016**, *55* (4), 954–960.
- [Men95] Menger, F. M.; Yamasaki, Y.; Catlin, K. K.; Nishimi, T. X-Ray Structure of a Self-Assembled Gelating Fiber. *Angew. Chemie Int. Ed. English* **1995**, *34* (5), 585–586.
- [Men00] Menger, F. M.; Caran, K. L. Anatomy of a Gel. Amino Acid Derivatives That Rigidify Water at Submillimolar Concentrations. *J. Am. Chem. Soc.* **2000**, *122* (47), 11679–11691.
- [Mez06] Mezger, T. G. *The Rheology Handbook: For Users of Rotational and Oscillatory Rheometers*, 2nd ed.; Coatings compendia; Vincentz Network: Hannover, 2006.
- [Mor94] Morse, D. C. Topological Instabilities and Phase Behavior of Fluid Membranes.

- Phys. Rev. E* **1994**, *50* (4), R2423.
- [Neb13] Nebot, V. J.; Smith, D. K. Techniques for the Characterisation of Molecular Gels. In *Functional Molecular Gels*; Escuder, B., Miravet, J. F., Eds.; The Royal Society of Chemistry, 2013; pp 30–66.
- [Ohs14] Ohsedo, Y.; Oono, M.; Saruhashi, K.; Watanabe, H.; Miyamoto, N. A New Composite Thixotropic Hydrogel Composed of a Low-Molecular-Weight Hydrogelator and a Nanosheet. *RSC Adv.* **2014**, *4* (84), 44837–44840.
- [Oke13] Okesola, B. O.; Smith, D. K. Versatile Supramolecular PH-Tolerant Hydrogels Which Demonstrate PH-Dependent Selective Adsorption of Dyes from Aqueous Solution. *Chem. Commun.* **2013**, *49* (95), 11164–11166.
- [Oke15] Okesola, B. O.; Vieira, V. M. P.; Cornwell, D. J.; Whitelaw, N. K.; Smith, D. K. 1,3:2,4-Dibenzylidene-D-Sorbitol (DBS) and Its Derivatives – Efficient, Versatile and Industrially-Relevant Low-Molecular-Weight Gelators with over 100 Years of History and a Bright Future. *Soft Matter* **2015**, *11* (24), 4768–4787.
- [Pen19] Peng, K.; Sottmann, T.; Stubenrauch, C. Gelled Non-Toxic Microemulsions: Phase Behavior & Rheology. *Soft Matter* **2019**, *15* (41), 8361–8371.
- [Pen20] Peng, K.; Preisig, N.; Sottmann, T.; Stubenrauch, C. Formulation of Gelled Non-Toxic Bicontinuous Microemulsions Stabilized by Highly Efficient Alkanoyl Methylglucamides. *Langmuir* **2020**, *36* (42), 12692–12701.
- [Pen21a] (1) Peng, K.; Sottmann, T.; Stubenrauch, C. Gelled Non-Toxic Bicontinuous Microemulsions as Promising Transdermal Drug Carriers. *Mol. Phys.* **2021**, *119* (15–16), e1886363.
- [Pen21b] Peng, K.; Preisig, N.; Sottmann, T.; Stubenrauch, C. From Water-Rich to Oil-Rich Gelled Non-Toxic Microemulsions. *Phys. Chem. Chem. Phys.* **2021**, *23* (31), 16855–16867.
- [Rag06] Raghavan, S. R.; Cipriano, B. H. Gel Formation: Phase Diagrams Using Tabletop Rheology and Calorimetry. In *Molecular Gels: Materials with Self-Assembled Fibrillar Networks*; Weiss, R. G., Terech, P., Eds.; Springer Netherlands: Dordrecht, 2006; pp 241–252.
- [Ray11] Raynal, M.; Bouteiller, L. Organogel Formation Rationalized by Hansen Solubility Parameters. *Chem. Commun.* **2011**, *47* (29), 8271–8273.
- [Rei03] Reimer, J.; Söderman, O.; Sottmann, T.; Kluge, K.; Strey, R. Microstructure of Alkyl Glucoside Microemulsions: Control of Curvature by Interfacial Composition. *Langmuir* **2003**, *19* (26), 10692–10702.
- [Sat08] Sato, H.; Hori, K.; Sakurai, T.; Yamagishi, A. Long Distance Chiral Transfer in a Gel: Experimental and Ab Initio Analyses of Vibrational Circular Dichroism Spectra of R- and S-12-Hydroxyoctadecanoic Acid Gels. *Chem. Phys. Lett.* **2008**, *467* (1–3), 140–143.

- [Sat11] Sato, H.; Sakurai, T.; Yamagishi, A. Comparison of Vibrational Circular Dichroism between the Langmuir–Blodgett Films and Gels of 12-Hydroxyoctadecanoic Acid. *Chem. Lett.* **2011**, *40* (1), 25–27.
- [Sch94] Schubert, K. V.; Strey, R.; Kline, S. R.; Kaler, E. W. Small Angle Neutron Scattering near Lifshitz Lines: Transition from Weakly Structured Mixtures to Microemulsions. *J. Chem. Phys.* **1994**, *101* (6), 5343–5355.
- [Sil01] Silas, J. A.; Kaler, E. W. The Phase Behavior and Microstructure of Efficient Cationic–Nonionic Microemulsions. *J. Colloid Interface Sci.* **2001**, *243* (1), 248–254.
- [Soe00] Söderman, O.; Johansson, I. Polyhydroxyl-Based Surfactants and Their Physico-Chemical Properties and Applications. *Curr. Opin. Colloid Interface Sci.* **2000**, *4* (6), 391–401.
- [Sot97] Sottmann, T.; Strey, R. Ultralow Interfacial Tensions in Water–*n*-Alkane–Surfactant Systems. *J. Chem. Phys.* **1997**, *106* (20), 8606–8615.
- [Sot02] Sottmann, T.; Kluge, K.; Strey, R.; Reimer, J.; Söderman, O. General Patterns of the Phase Behavior of Mixtures of H₂O, Alkanes, Alkyl Glucosides, and Cosurfactants. *Langmuir* **2002**, *18* (8), 3058–3067.
- [Sot05] Sottmann, T.; Strey, R. *Microemulsions*, 1st ed.; Lyklema, Ed.; Academic Press: London, 2005; Vol. 5.
- [Sot08] Sottmann, T.; Stubenrauch, C. Phase Behaviour, Interfacial Tension and Microstructure of Microemulsions. In *Microemulsions. Background, New Concepts, Applications, Perspectives.*; Stubenrauch, C., Ed.; Wiley-Blackwell: Oxford, 2008; pp 1–42.
- [Ste18] Steck, K.; Schmidt, C.; Stubenrauch, C. The Twofold Role of 12-Hydroxyoctadecanoic Acid (12-HOA) in a Ternary Water—Surfactant—12-HOA System: Gelator and Co-Surfactant. *Gels* **2018**, *4* (3), 78.
- [Ste19] Steck, K.; van Esch, J. H.; Smith, D. K.; Stubenrauch, C. Tuning Gelled Lyotropic Liquid Crystals (LLCs) – Probing the Influence of Different Low Molecular Weight Gelators on the Phase Diagram of the System H₂O/NaCl–Genapol LA070. *Soft Matter* **2019**, *15* (15), 3111–3121.
- [Ste19b] Steck, K.; Stubenrauch, C. Gelling Lyotropic Liquid Crystals with the Organogelator 1,3:2,4-Dibenzylidene-D-Sorbitol Part I: Phase Studies and Sol–Gel Transitions. *Langmuir* **2019**, *35* (52), 17132–17141.
- [Ste19c] Steck, K.; Preisig, N.; Stubenrauch, C. Gelling Lyotropic Liquid Crystals with the Organogelator 1,3:2,4-Dibenzylidene-D-Sorbitol Part II: Microstructure. *Langmuir* **2019**, *35* (52), 17142–17149.
- [Ste20] Steck, K.; Dieterich, S.; Stubenrauch, C.; Giesselmann, F. Surfactant-Based

- Lytotropic Liquid Crystal Gels – the Interplay between Anisotropic Order and Gel Formation. *J. Mater. Chem. C* **2020**, 5335–5348.
- [Str94] Strey, R. Microemulsion Microstructure and Interfacial Curvature. *Colloid Polym. Sci.* **1994**, 272 (8), 1005–1019.
- [Str96] Strey, R. I. Experimental Facts: Water-nonionic Surfactant Systems, and the Effect of Additives. *Berichte der Bunsengesellschaft für Phys. Chemie* **1996**, 100 (3), 182–189.
- [Stu01] Stubenrauch, C. Sugar Surfactants - Aggregation, Interfacial, and Adsorption Phenomena. *Curr. Opin. Colloid Interface Sci.* **2001**, 6 (2), 160–170.
- [Stu07] Stubenrauch, C.; Tessendorf, R.; Strey, R.; Lynch, I.; Dawson, K. A. Gelled Polymerizable Microemulsions. 1. Phase Behavior. *Langmuir* **2007**, 23 (14), 7730–7737.
- [Stu08] Stubenrauch, C.; Tessendorf, R.; Salvati, A.; Topgaard, D.; Sottmann, T.; Strey, R.; Lynch, I. Gelled Polymerizable Microemulsions. 2. Microstructure. *Langmuir* **2008**, 24 (16), 8473–8482.
- [Stu16] Stubenrauch, C.; Gießelmann, F. Gelled Complex Fluids: Combining Unique Structures with Mechanical Stability. *Angew. Chemie - Int. Ed.* **2016**, 55 (10), 3268–3275.
- [Ter94] Térech, P.; Rodriguez, V.; Barnes, J. D.; McKenna, G. B. Organogels and Aerogels of Racemic and Chiral 12-Hydroxyoctadecanoic Acid. *Langmuir* **1994**, 10 (10), 3406–3418.
- [Ter95] Térech, P.; Furman, I.; Weiss, R. G. Structures of Organogels Based upon Cholesteryl 4-(2-Anthryloxy)Butanoate, a Highly Efficient Luminescing Gelator: Neutron and X-Ray Small-Angle Scattering Investigations. *J. Phys. Chem.* **1995**, 99 (23), 9558–9566.
- [Ter06] Térech, P. Molecular Gels and Small-Angle Scattering. In *Molecular Gels: Materials with Self-Assembled Fibrillar Networks*; Weiss, R. G., Terech, P., Eds.; Springer Netherlands: Dordrecht, 2006; pp 275–324.
- [Tes09] Tessendorf, R. Microemulsions as Templates for High Surface Area Polymers, University of Cologne, 2009.
- [Teu87] Teubner, M.; Strey, R. Origin of the Scattering Peak in Microemulsions. *J. Chem. Phys.* **1987**, 87 (5), 3195–3200.
- [Wei06] Weiss, R. G.; Térech, P. Introduction. In *Molecular Gels: Materials with Self-Assembled Fibrillar Networks*; Weiss, R. G., Terech, P., Eds.; Springer Netherlands: Dordrecht, 2006; pp 1–13.
- [Wei14] Weiss, R. G. The Past, Present, and Future of Molecular Gels. What Is the Status of the Field, and Where Is It Going? *J. Am. Chem. Soc.* **2014**, 136 (21), 7519–7530.

References

- [Wil12] Williams, A. C.; Barry, B. W. Penetration Enhancers. *Adv. Drug Deliv. Rev.* **2012**, *64*, 128–137.
- [www01] <https://www.ill.eu/users/instruments/instruments-list/d11/description/instrument-layout> (accessed Aug 16, 2021).
- [www02] Yamamoto, H. Hansen Solubility Parameters (HSP) Application Notes <https://pirika.com/NewHP/PirikaE2/Gallstone.html> (accessed May 21, 2021).
- [Xio13] Xiong, M.; Wang, C.; Zhang, G.; Zhang, D. Molecular Gels Responsive to Physical and Chemical Stimuli. In *Functional Molecular Gels*; Escuder, B., Miravet, J. F., Eds.; The Royal Society of Chemistry, 2013; pp 67–94.
- [Yan07] Yang, X. D.; Gao, Y. H.; Chai, J. L.; Wang, Z. N.; Qin, C. K. Studies on the Middle-Phase Microemulsion of Lauric-*N*-Methylglucamide. *Colloid J.* **2007**, *69* (2), 252–258.
- [Yan08] Yang, X.; Li, H.; Chai, J.; Gao, Y.; Chen, J.; Lou, A. Phase Behavior Studies of Quaternary Systems Containing *N*-Lauroyl-*N*-Methylglucamide/Alcohol/Alkane/Water. *J. Colloid Interface Sci.* **2008**, *320* (1), 283–289.
- [Yan13] Yang, X.; Zhang, H.; Shi, C.; Chai, J. Middle-Phase Microemulsions Formed by *n*-Dodecyl Polyglucoside and Lauric-*N*-Methylglucamide. *J. Dispers. Sci. Technol.* **2013**, *34* (2), 147–152.
- [Xua12] Xuan, X. Y.; Cheng, Y. L.; Acosta, E. Lecithin-Linker Microemulsion Gelatin Gels for Extended Drug Delivery. *Pharmaceutics* **2012**, *4* (1), 104–129.
- [Yam21] Yamamoto, H. Hansen Solubility Parameters (HSP) Application Notes <https://pirika.com/NewHP/PirikaE2/Gallstone.html> (accessed May 21, 2021).
- [Zie13] Ziemecka, I.; Koper, G. J. M.; Olive, A. G. L.; van Esch, J. H. Chemical-Gradient Directed Self-Assembly of Hydrogel Fibers. *Soft Matter* **2013**, *9* (5), 1556–1561.
- [Zwe13] Zweep, N.; van Esch, J. H. The Design of Molecular Gelators. In *Functional Molecular Gels*; Escuder, B., Miravet, J. F., Eds.; The Royal Society of Chemistry, 2013; pp 1–29.

Publication I

Gelled Non-Toxic Microemulsions: Phase Behavior & Rheology

Ke Peng, Thomas Sottmann, and Cosima Stubenrauch
Soft Matter **2019**, *15* (41), 8361–8371.

DOI: 10.1039/C9SM01350D

Reprinted from [Pen19] with permission from the Royal Society of Chemistry.

PAPER



Cite this: *Soft Matter*, 2019,
15, 8361

Gelled non-toxic microemulsions: phase behavior & rheology

Ke Peng,^{id} Thomas Sottmann^{id} and Cosima Stubenrauch^{id}*

Bicontinuous microemulsions gelled with a low molecular weight gelator have been shown to be an orthogonally self-assembled system. With the mechanical stability provided by the gel network, gelled non-toxic bicontinuous microemulsions have the potential to be an efficient transdermal drug delivery carrier. However, up to now no suitable system has been formulated for transdermal drug delivery. To fill this gap, we formulated and characterized a gelled non-toxic bicontinuous microemulsion suitable for the mentioned application. Starting from a previously studied scouting system, namely, H₂O–*n*-octane–*n*-octyl β-D-glucopyranoside (β-C₈G₁)–1-octanol, the co-surfactant and the oil were replaced by non-toxic components. Subsequently, the expensive pure surfactant was replaced by cheap technical-grade surfactants (Plantacare[®] series) to make the system economical. Having formulated the non-toxic microemulsion H₂O–IPM–Plantacare 1200 UP–1,2-octanediol, three low molecular weight gelators were studied with regard to the gelation of both the scouting system and the non-toxic system. The chosen gelators were 12-hydroxyoctadecanoic acid (12-HOA), 1,3:2,4-dibenzylidene-*D*-sorbitol (DBS), and *N,N'*-dibenzoyl-*L*-cystine (DBC). We found that only DBS gels the non-toxic microemulsion. The gelled non-toxic bicontinuous microemulsion H₂O–IPM–Plantacare 1200 UP–1,2-octanediol was characterized with oscillatory shear rheometry and small-angle neutron scattering (SANS) at a DBS concentration of 0.3 wt% to verify that the system is indeed a gel and that the microstructure of the microemulsion is not altered by the gel network.

Received 5th July 2019,
Accepted 27th September 2019

DOI: 10.1039/c9sm01350d

rsc.li/soft-matter-journal

1 Introduction

The simultaneous but independent formation of two self-assembled structures is called orthogonal self-assembly. The concept was first proposed by Laibinis *et al.* for the simultaneous and independent formation of two self-assembled monolayers.¹ One of the best-known examples of orthogonal self-assembly is mammalian cells, where the extracellular matrix and the cytoskeleton coexist independently. Orthogonal self-assembly was also used successfully in the field of gelled complex fluids, namely to combine the fibrillar gel network formed by low molecular weight gelators with various self-assembled colloidal nanostructures, *e.g.*, micelles, vesicles, liquid crystals.^{2–6} Such gelled complex fluids are promising systems for transdermal drug delivery, tissue healing, molecular electronics, or the synthesis of highly ordered materials.⁷

One particularly interesting type of gelled complex fluids is bicontinuous microemulsions gelled by low molecular weight gelators. Bicontinuous microemulsions contain two interweaving sub-domains of water and oil separated by an amphiphilic surfactant film. The length scale of the sponge-like domains

is 5 to 100 nm.⁸ Gelled bicontinuous microemulsions were first studied by Tessoro *et al.* by means of the system water–*n*-dodecane–Lutensol AO5 (technical-grade nonionic *n*-alkyl polyglycol ether), which was gelled with the low molecular weight organogelator 12-hydroxydecanoic acid (12-HOA).^{9–11} The aim was to use the “arrested” bicontinuous microstructure as a template for the synthesis of bicontinuous (sponge-like) nanoporous polymers. Laupheimer *et al.* studied a similar system, using this time a pure surfactant.^{12–14} The coexistence of two self-assembled structures—the gel fibrillar network and the bicontinuous microstructure—was shown with the help of freeze-fracture transmission electron microscopy and small-angle neutron scattering (SANS). It was found that the gel fibers pass through the whole microemulsion, *i.e.* through both water and oil domains. Therefore, one can conclude that it is possible to combine the mechanical stability of a gel with the unique bicontinuous microstructure,⁸ the latter being able to solubilize both hydrophilic and hydrophobic compounds.

Oil-in-water (o/w) microemulsions have been extensively studied for transdermal drug delivery as they provide a number of advantages.^{15–23} Due to the thermodynamic stability, the formulation and storage of microemulsions are trouble-free. The nanostructure (nanometer-sized oil droplets in a continuous aqueous phase) facilitates the transport through the skin barrier

Institute of Physical Chemistry, University of Stuttgart, Pfaffenwaldring 55,
70569 Stuttgart, Germany. E-mail: cosima.stubenrauch@ipc.uni-stuttgart.de

and enhances the solubilization of hydrophobic drugs. However, bicontinuous microemulsions, which provide the most effective solubilization and excellent wetting properties, have not been utilized in drug delivery yet. This may be due to the relatively high surfactant concentration that is often needed for their formulation. We also like to point out that in studies^{21,22} about microemulsion-based gels, water-soluble polymers were also used to gel the continuous aqueous phase, *i.e.* to formulate a hydrogel. Here we used molecular gelators—instead of polymers—to gel bicontinuous microemulsions which consist of equal amounts of water and oil, *i.e.*, they are neither hydro- nor organogels. Based on our previous studies on gelled bicontinuous microemulsion,^{12,14} the current project aims at the formulation of a gelled non-toxic bicontinuous microemulsion with a tolerable amount of surfactant and a molecular gelator. These systems have a high potential to be used as transdermal drug delivery carrier for both hydrophilic and hydrophobic drugs.

Regarding the formulation of non-toxic microemulsions, non-ionic and zwitterionic surfactants are more commonly used since they are less sensitive to salinity and pH than ionic surfactants. Kahlweit *et al.* formulated non-toxic microemulsions with the zwitterionic surfactant lecithin (Fig. 1 top, left), a biocompatible mixture of phosphoglycerolipids which widely exist in animals and plants.²⁴ However, *n*-alkanes were used as hydrophobic component, which cannot be used for drug delivery because of their toxicity. Another type of bio-compatible surfactant is alkyl polyglucosides (APGs, denoted as C_nG_m , Fig. 1 top, right). They are commercially available and exhibit a distribution in carbon chain lengths as well as glucose unit numbers.²⁵ Because of their hydrophilicity APG surfactants form bicontinuous microemulsions, with few exceptions, only after the addition of co-surfactants, normally medium-chain alkanols. Compared to the conventional *n*-alkyl polyglycol ether (C_iE_j) type microemulsions, APG-based microemulsions are less temperature sensitive.^{26,27} Moreover, APGs are widely used in cosmetics due to their biocompatibility.²⁸ The APG-based model system H_2O -*n*-octane- β -D-glucopyranoside (β - C_8G_1)-1-octanol has been comprehensively studied with respect to its phase behavior, interfacial composition, interfacial tension, and microstructure.^{29–31} Thus it is chosen as our scouting system. As the oil *n*-octane and the co-surfactant 1-octanol are irritating to human bodies, they

must be replaced by non-toxic saturated fatty acid esters, such as isopropyl myristate (IPM, Fig. 1 bottom, left) and alkanediols (one example is given in Fig. 1 bottom, right).^{32,33} Both IPM and alkanediols are bio-compatible and provide enhanced penetration effects in transdermal drug delivery.^{34,35}

To understand gelled microemulsions, one also needs to have in-depth knowledge about gels. Although a gel mainly consists of a solvent (in our case the bicontinuous microemulsion), the fluidity is restrained by the gel network. In contrast to polymeric gels, molecular gels form so-called self-assembled fibrillar networks.³⁶ The single gelator molecules, also referred to as low molecular weight gelators or molecular gelators, self-assemble through non-covalent interactions, *e.g.*, hydrogen bonds, van der Waals forces, and π - π interactions. The gelation process of these physical gels is thermo-reversible, *i.e.*, the sol-gel transition process can be manipulated by varying the temperature. Moreover, more biodegradable molecular than polymer gelators exist, namely, fatty acid derivatives,³⁷ steroid derivatives, and amino acid based molecular gelators.³⁸

In this study, we present a gelled non-toxic bicontinuous microemulsion. Starting with the scouting system H_2O -*n*-octane- β - C_8G_1 -1-octanol³⁰ which is not non-toxic, we replaced the oil and co-surfactant by non-toxic components, namely by isopropyl myristate (IPM) and 1,2-octanediol, respectively.^{26,32,33} Subsequently, we gelled the scouting system using different molecular gelators, and used these findings to gel our non-toxic microemulsions. Finally, we characterized the gelled non-toxic bicontinuous microemulsion by oscillatory shear rheometry and small-angle neutron scattering (SANS) to verify that the system is indeed a gel and that the microstructure of the microemulsion is not altered by the gel network. We were able to formulate a non-toxic bicontinuous microemulsion with a tolerable amount of surfactant and to gel it with a molecular gelator which allows one to “reversibly switch” between the gel and the sol state *via* a temperature change if need be.

2 Experimental section

2.1 Materials

Bidistilled water was used to prepare all protonated samples. For SANS measurements H_2O was replaced by D_2O (>99.9%) from

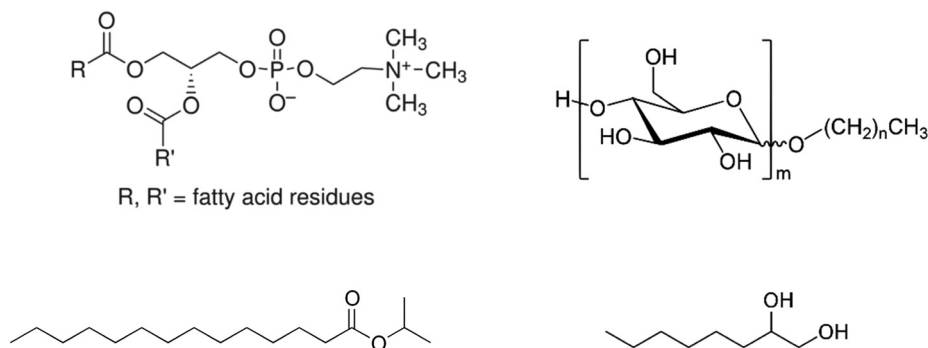


Fig. 1 Molecular structures of (top, left) lecithins, (top, right) alkyl polyglucosides (C_nG_m), (bottom, left) isopropyl myristate (IPM), (bottom, right) 1,2-octanediol.

Eurisotop, France. The pure surfactant *n*-octyl β -D-glucopyranoside (β -C₈G₁, >99.5%) was purchased from GLYCON Biochemicals, Germany. The technical grade sugar surfactants Plantacare[®] were supplied by BASF, Germany. The oil *n*-octane (>98%) was purchased from Alfa Aesar, Germany, and isopropyl myristate (IPM, >98%) was purchased from TCI, Japan. The co-surfactant 1-octanol (99%) was purchased from Aldrich, Germany, and 1,2-octanediol (>98%) from Acros, USA. The gelator 12-hydroxyoctadecanoic acid (12-HOA, 95%) was purchased from Alfa Aesar, Germany, *N,N'*-dibenzoyl-L-cystine (DBC, >98%) from Santa Cruz, the USA, and 1,3:2,4-dibenzylidene-D-sorbitol (DBS or Geniset[®] D) from NJC Europe.

Plantacare[®] contains glycosides with a wide distribution of carbon chain lengths and glucoside units. According to the product sheets of the Plantacare[®] series, the product contains only surfactants, water, and a tiny amount of Mg²⁺ (<500 ppm). For the used Plantacare[®] 810 UP, 2000 UP, and 1200 UP the weight fraction of the active components C_{8/10}G_{1.5}, C₁₀G_{1.5}, and C₁₂G_{1.4} are given as 0.64, 0.53 and 0.52, respectively. Note that the composition of the Plantacare[®] surfactants is taken into account calculating the oil mass fraction α in the solvent mixture (eqn (1)) and the surfactant mass fraction γ_C (eqn (2)). Microemulsion samples of Plantacare[®] were found to be slightly turbid. The turbidity is induced by Mg²⁺ (around 500 ppm) at basic pH values, which is contained in the product for the preservative purpose. Therefore, Plantacare[®] was neutralized by adding citric acid anhydrous (from Sigma Aldrich, Germany) before use, leading to transparent microemulsions.

2.2 Sample preparation

Non-gelled microemulsions for SANS measurements were prepared by weighing in surfactant (C), co-surfactant (D), oil (B), and water (A) with an analytical balance into glass tubes, which were then sealed by polyethylene stoppers. For monitoring phase diagrams we proceeded in a different way, *i.e.*, we chose a titration procedure (explained in Section 2.3). Subsequently, the samples were heated up to 50 °C in a water bath while being stirred by a magnetic stirrer in a water bath to homogenize.

In the case of gelled microemulsions, a gelator was additionally added to the samples. The samples were firstly heated above 90 °C to dissolve the gelator. A heat gun was also utilized when necessary. Afterwards, the sample was cooled down to 25 °C for gelation. With 12-HOA and DBC the gelation process takes 1–3 minutes, *i.e.*, there was time to stir the sample before gelation. With DBS the gelation process takes less than 30 seconds. Thus the samples were quickly transferred to an ice bath directly from the 90 °C water bath with manual shaking to ensure homogeneous gelation. Afterwards, the samples were transferred to a 25 °C water bath and allowed to equilibrate. It is essential to agitate the gelled microemulsion samples vigorously before gelling; otherwise, phase separation occurs, and the gelation process must be repeated.

2.3 Phase behavior

The phase behavior was investigated at a constant temperature of $T = 25.0$ °C. The water bath was equipped with a thermostat

and a cooling system to maintain a constant temperature with a precision of ± 0.1 K. The non-gelled microemulsion samples were firstly prepared without co-surfactant (D). After equilibration in the water bath, the stopper was removed, and a co-surfactant (D) was added to the sample dropwise by a syringe. The added amount of co-surfactant was recorded using an analytical balance. After adding the co-surfactant, the sample was shaken and left to reach equilibrium before the phase behavior was visually determined. Birefringence of lyotropic liquid crystalline phases was observed *via* crossed polarizers. Since the phase transitions of microemulsion systems stabilized by sugar surfactant are less sensitive to temperature changes, the phase behavior is typically presented in a phase tetrahedron (Fig. 2). The phase behavior of these microemulsions is most conveniently characterized at a constant oil-to-water ratio, *i.e.* recording a two-dimensional section through the tetrahedron as highlighted in Fig. 2. Hereby “2” denotes the coexistence of an oil-in-water (o/w)-microemulsion (lower phase) and an oil excess phase (upper phase). “1” means the isotropic one-phase bicontinuous microemulsion. “2” denotes the coexistence of an excess water phase (lower phase) and a water-in-oil (w/o)-microemulsion (upper phase). “3” is the coexistence of three phases, namely, an excess water phase (lower phase), a bicontinuous microemulsion (middle phase), and an excess oil phase (upper phase).

In the case of gelled microemulsions, we determined the minimum gelator concentration (mgc), also called critical gelator concentration (cgc), the lowest gelator concentration at which gels form at room temperature. Mgc can be determined by trial and error, *i.e.*, adding gelator to the microemulsion sample until the whole sample was gelled. After knowing the mgc, the phase behavior of gelled microemulsion can be measured. The co-surfactant was added to the gelled sample at 25 °C, which was then heated above the sol–gel transition temperature, where the sample was melted and could thus be mixed. After the gelation process (see Section 2.2) the phase behavior was recorded.

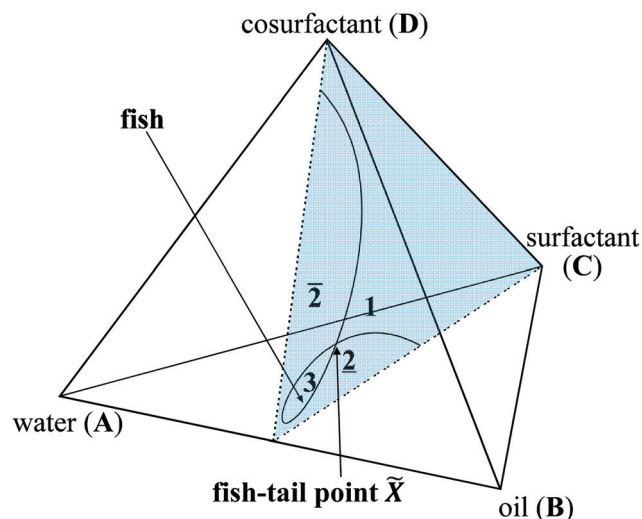


Fig. 2 Schematic phase tetrahedron of a quaternary system water–oil–surfactant–co-surfactant at a constant temperature.²⁹

While a gelled one-phase microemulsion appears transparent, the gelled two-phase samples are turbid.

In our experiments, the volume fraction of oil in the solvent mixture

$$\phi = \frac{V_{\text{oil}}}{V_{\text{water}} + V_{\text{oil}}} \quad (1)$$

was kept constant at 0.50. The mass fraction of surfactant (C) is defined as

$$\gamma_{\text{C}} = \frac{m_{\text{surf.}}}{m_{\text{water}} + m_{\text{oil}} + m_{\text{surf.}} + m_{\text{co-surf.}} + m_{\text{gelator}}}, \quad (2)$$

while the mass fraction of the co-surfactant (D) is denoted as

$$\gamma_{\text{D}} = \frac{m_{\text{co-surf.}}}{m_{\text{water}} + m_{\text{oil}} + m_{\text{surf.}} + m_{\text{co-surf.}} + m_{\text{gelator}}}. \quad (3)$$

The gelator mass fraction is calculated according to

$$\eta = \frac{m_{\text{gelator}}}{m_{\text{water}} + m_{\text{oil}} + m_{\text{surf.}} + m_{\text{co-surf.}} + m_{\text{gelator}}}. \quad (4)$$

2.4 Rheology

Oscillatory shear rheometry was carried out with a rheometer Physica MCR 501 from Anton Paar, Austria. We chose a plate-plate geometry, of which the upper plate has a diameter of 25 mm. The gap size between the two plates is kept constant at 1 mm according to previous experiments with gelled microemulsions.¹² A bigger gap size demands more material and induces more solvent evaporation, whereas a too-small gap size results in squeezing out the solvent thus increasing the moduli exponentially. For each measurement, the gelled sample was loaded on the lower plate and then the upper plate was lowered to the measurement position. Temperature can be controlled *via* an external thermostat with a precision of $\Delta T = \pm 0.1$ K.

Firstly, an amplitude sweep was carried out at $T = 25$ °C with an angular frequency of $\omega = 10$ s⁻¹ and a varied shear stress τ to determine the limit of the linear viscoelastic region (LVE region). As shown in Fig. 3, the limit of the LVE region is near $\tau = 40$ Pa. Hence, for subsequent measurements the shear stress is kept constant at $\tau = 10$ Pa. Secondly, oscillation frequency sweeps were performed at $T = 25$ °C and $\tau = 10$ Pa as a function of the angular frequency ω . Lastly, a temperature sweep was carried out at an angular frequency of $\omega = 10$ s⁻¹ and a shear stress of $\tau = 10$ Pa, from $T = 25$ °C to $T = 100$ °C with a heating rate of 1 K min⁻¹ to determine the sol-gel transition temperature $T_{\text{sol-gel}}$, *i.e.*, the temperature at which the values of G' and G'' decrease steeply.

2.5 Small-angle neutron scattering (SANS)

The microstructure of microemulsions and gelled microemulsions was investigated by small-angle neutron scattering (SANS) on the D11 spectrometer at the Institut Laue-Langevin (ILL) in Grenoble, France. A neutron wavelength of $\lambda = 5.5$ Å with a wavelength spread of $\Delta\lambda/\lambda = 9\%$ (full width at half-maximum) was used. To cover a q -range from 0.0016 to 0.47 Å⁻¹, where $q = 4\pi \cdot \sin(\theta/2)/\lambda$ is the absolute value of the scattering vector, we

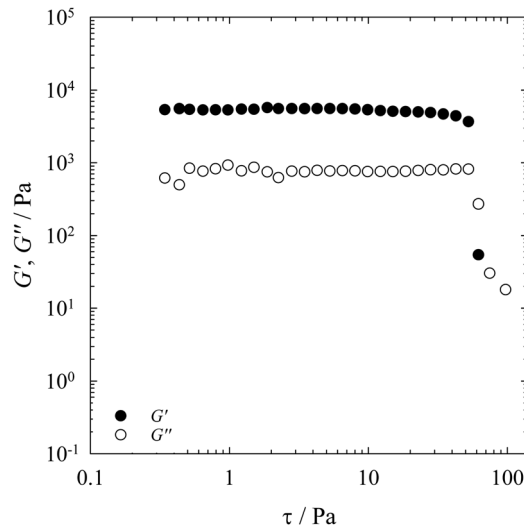


Fig. 3 Storage modulus G' (filled symbols) and loss modulus G'' (open symbols) of the gelled bicontinuous microemulsion H₂O–IPM–Plantacare 1200 UP–1,2-octanediol ($\gamma_{\text{C}} = 0.1590$, $\gamma_{\text{D}} = 0.1188$, $\phi = 0.50$) with 0.3 wt% DBS, measured with oscillatory shear rheometry at $T = 25$ °C and an angular frequency of $\omega = 10$ s⁻¹ as a function of the shear stress τ .

chose the detector/collimation distances of 39.0 m/40.5 m, 8.0 m/8.0 m, and 1.5 m/20.0 m. Samples were loaded into Hellma quartz QS glass cells (optical path length of 1 mm) and were then rapidly transferred to a home-built cell holder with a high temperature precision and stability ($\Delta T = \pm 0.02$ K). By checking each sample before and after the measurement *via* visual inspection, it is ensured that samples have been in the homogeneous one-phase state during measurements. The recorded scattering intensity was normalized to absolute scale using the incoherent scattering of H₂O as a reference with a differential scattering cross section of 0.956 cm⁻¹ at $\lambda = 5.5$ Å. The raw data treatment, including the subtraction of the dark current and the empty cell scattering, masking, and radial averaging, was performed using the analysis software program LAMP provided by the ILL. The detector dead time and sample transmission were also considered.

3 Formulating non-toxic microemulsions

As discussed in the Introduction, we aim to formulate non-toxic microemulsions which contain alkyl glycosides as main surfactant, saturated fatty acid esters as oil, and alkanediols as co-surfactant. We started with the scouting system H₂O–*n*-octane– β -C₈G₁–1-octanol, whose phase behavior, interfacial properties and microstructure were thoroughly studied.^{30,31} The phase diagrams of such quaternary system are typically characterized recording sections through the phase tetrahedron at a constant oil-to-water ratio (see Section 2.3). The two axes are the mass fractions of surfactant and co-surfactant, γ_{C} and γ_{D} , respectively. In addition to the notations defined in Section 2.3, “L _{α} ” denotes the presence of a birefringent lamellar phase (in coexistence with the microemulsion phase).

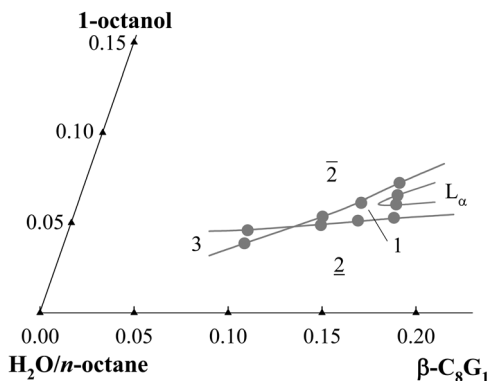


Fig. 4 Section through the phase tetrahedron of the quaternary system $\text{H}_2\text{O}-n\text{-octane}-\beta\text{-C}_8\text{G}_1\text{-1-octanol}$ (grey circles) at $\phi = 0.50$, $T = 25^\circ\text{C}$. Phase inversion was achieved by the addition of 1-octanol to the system.

Fig. 4 shows part of the section for $\phi = 0.50$ of the scouting system. Since we intend to gel the one-phase bicontinuous microemulsion, the location of the one-phase region and thus the location of the fish-tail point \bar{X} are of interest. We recall that the fish-tail point \bar{X} is a measure for the efficiency of a surfactant: the less surfactant is needed to mix water and oil in one phase, the higher is its efficiency. Looking at the phase diagram of the scouting system, one sees that the addition of 1-octanol induces phase transitions in the sequence $\underline{2}$ - $\underline{3}$ - $\bar{2}$ and $\underline{2}$ - $\underline{1}$ - $\bar{2}$, respectively. This is because the head group of $\beta\text{-C}_8\text{G}_1$ is so hydrophilic that the mean curvature of the amphiphilic film is positive (curved around the oil), thus forming o/w-microemulsions. The addition of an alcohol allows tuning the curvature since it acts as co-surfactant and as co-solvent.^{39,40} As co-surfactant, an alcohol has a smaller hydrophilic head and is thus more hydrophobic than glucosides. Thus, the incorporation of alcohol molecules in the amphiphilic film leads to a decreased mean curvature. A further decreasing mean curvature is induced as the alcohol molecules, which act as co-solvent, render the oil less hydrophobic. Therefore, the phase inversion from o/w-microemulsion ($\underline{2}$) to w/o-microemulsion ($\bar{2}$) over a bicontinuous microemulsion ($\underline{1}$) can be induced.

In order to replace both oil and co-surfactant by non-toxic components, the effects of the individual components on the

phase behavior must be examined. Firstly, 1-octanol was replaced by 1,2-octanediol due to its bio-compatibility³⁴ (Fig. 5 left). 1,2-Octanediol is much more hydrophilic compared to 1-octanol, and its effect on the phase behavior is similar to that of 1-butanol.³² Thus, the mass fraction of 1,2-octanediol needed to form a bicontinuous microemulsion is considerably higher than that of 1-octanol. However, since the oil component remains the same, the mass fraction of $\beta\text{-C}_8\text{G}_1$ needed to form a bicontinuous microemulsion does not change (\bar{X} points of the two systems are shifted parallel to the co-surfactant axis). The more hydrophobic 1,2-dodecanediol was also examined, expecting to lead to a lower co-surfactant fraction at the \bar{X} point. However, its melting point is so high that the microemulsion sample solidified at 25°C .

Secondly, with 1,2-octanediol being the new co-surfactant, $n\text{-octane}$ was replaced by isopropyl myristate (IPM). The resulting phase diagram is shown in Fig. 5 right. The shift of the \bar{X} point can be explained as follows. IPM has a longer carbon chain compared to $n\text{-octane}$, which decreases the efficiency of the surfactant $\beta\text{-C}_8\text{G}_1$. Furthermore, the 1,2-octanediol has a larger solubility in IPM, thus a slightly higher amount of 1,2-octanediol is needed.

In order to obtain low-cost non-toxic microemulsions, the expensive pure surfactant $\beta\text{-C}_8\text{G}_1$ was replaced by the technical-grade surfactant Plantacare 810 UP ($\text{C}_{8/10}\text{G}_{1.5}$), see Fig. 6 left. Note that for all technical-grade surfactants the mass fraction γ_c was calculated considering only the active part as specified by the supplier (see 2.1 Materials). As can be seen, using Plantacare 810 UP ($\text{C}_{8/10}\text{G}_{1.5}$) instead of the pure $\beta\text{-C}_8\text{G}_1$ shifts the \bar{X} point to slightly smaller mass fraction of surfactant and co-surfactant, indicating that the longer carbon chain compensates the larger number of glucoside units being present in the technical-grade Plantacare 810 UP surfactant. In order to increase the efficiency of the surfactant, technical-grade alkyl polyglucosides with longer carbon chains, namely Plantacare 2000 UP ($\text{C}_{10}\text{G}_{1.5}$) and Plantacare 1200 UP ($\text{C}_{12}\text{G}_{1.4}$), were utilized. In Fig. 6 right, it can be clearly seen that the longer the carbon chain is, the more efficient the surfactant becomes. At the same time, being more hydrophobic, the

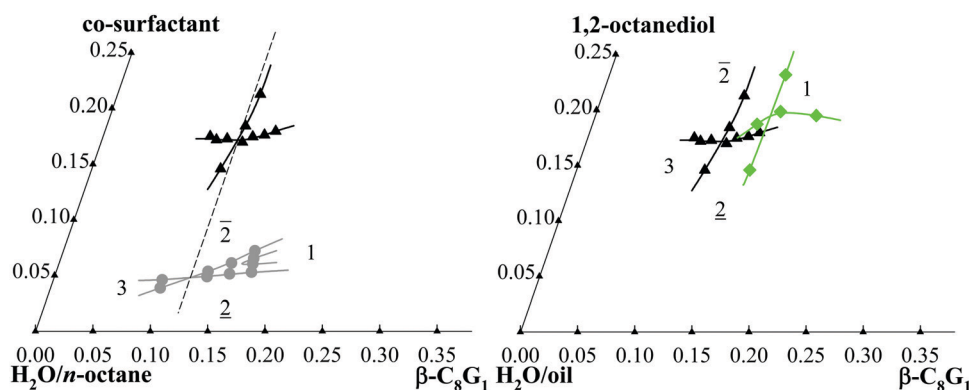


Fig. 5 (left) Phase diagrams of the quaternary systems $\text{H}_2\text{O}-n\text{-octane}-\beta\text{-C}_8\text{G}_1\text{-1-octanol}$ (gray circles) and $\text{H}_2\text{O}-n\text{-octane}-\beta\text{-C}_8\text{G}_1\text{-1,2-octanediol}$ (black triangles up) at $T = 25^\circ\text{C}$, $\phi = 0.50$. (right) Phase diagrams of quaternary system $\text{H}_2\text{O}-n\text{-octane}-\beta\text{-C}_8\text{G}_1\text{-1,2-octanediol}$ (black triangles up), and $\text{H}_2\text{O}-\text{IPM}-\beta\text{-C}_8\text{G}_1\text{-1,2-octanediol}$ (green diamonds) at $T = 25^\circ\text{C}$, $\phi = 0.50$.

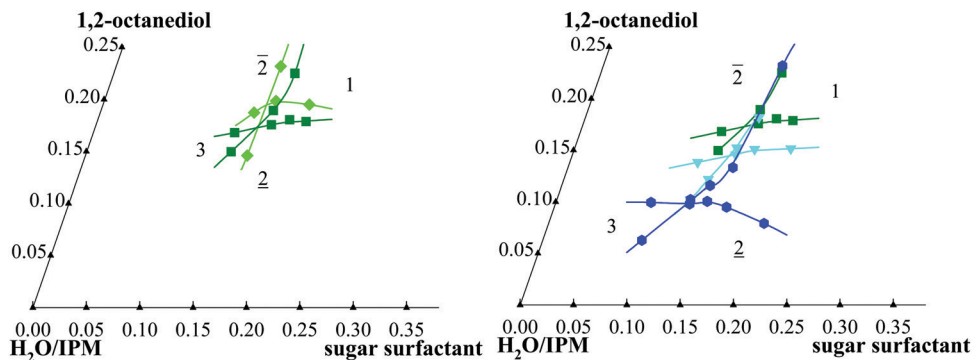


Fig. 6 (left) Phase diagrams of H₂O-IPM- β -C₈G₁-1,2-octanediol (green diamonds) and H₂O-IPM-Plantacare 810 UP-1,2-octanediol (dark green squares) at $T = 25$ °C, $\phi = 0.50$. (right) Phase diagrams of H₂O-IPM-Plantacare 810 UP-1,2-octanediol (dark green squares), H₂O-IPM-Plantacare 2000 UP-1,2-octanediol (cyan triangles down), and H₂O-IPM-Plantacare 1200 UP-1,2-octanediol (blue hexagons) at $T = 25$ °C, $\phi = 0.50$.

Table 1 Summary of the fish-tail \bar{X} points (the intersection point of the 3-phase and the 1-phase microemulsions) of all studied systems

Components				\bar{X} point	
	Oil	Surfactant	Co-Surfactant	γ_C	γ_D
H ₂ O	<i>n</i> -Octane	β -C ₈ G ₁	1-Octanol	0.118	0.047
	<i>n</i> -Octane	β -C ₈ G ₁	1,2-Octanediol	0.119	0.172
	Isopropyl myristate	β -C ₈ G ₁	1,2-Octanediol	0.154	0.195
	Isopropyl myristate	Plantacare 810 UP (C _{8/10} G _{1.5})	1,2-Octanediol	0.152	0.173
	Isopropyl myristate	Plantacare 2000 UP (C ₁₀ G _{1.5})	1,2-Octanediol	0.147	0.144
	Isopropyl myristate	Plantacare 1200 UP (C ₁₂ G _{1.4})	1,2-Octanediol	0.121	0.098

co-surfactant demand for the formation of a bicontinuous microemulsion is considerably decreased. In the quaternary system H₂O-IPM-Plantacare 1200 UP-1,2-octanediol the \bar{X} point is located at comparably small values of $\gamma_C = 0.121$ and $\gamma_D = 0.098$, which is why we chose this system for the next step, *i.e.* the gelation. For comparison the \bar{X} points of all measured systems are listed in Table 1.

4 Gelling non-toxic microemulsions

4.1 Gelling H₂O-*n*-octane- β -C₈G₁-1-octanol

In addition to formulating non-toxic microemulsions, we intended to gel the scouting system H₂O-*n*-octane- β -C₈G₁-1-octanol and transfer the gained knowledge to the final non-toxic system. It is important to note that there are no guiding

rules telling us which molecular gelator gels a specific solvent. Up to date, the gelation process remains empirical.^{36,41} Therefore, the difficulty of gelling a microemulsion is to choose a proper gelator. Since our microemulsions contain equal volumes of water and oil, theoretically both hydrogelator and organogelator could be suitable. In this study, three molecular gelators were used, namely, the organogelators 12-hydroxyoctadecanoic acid (12-HOA)³⁷ and 1,3:2,4-dibenzylidene-*D*-sorbitol (DBS)⁴² as well as the hydrogelator *N,N'*-dibenzoyl-*L*-cystine (DBC).⁴³ Their molecular structures are depicted in Fig. 7.

First, we used the organogelator 12-hydroxyoctadecanoic acid (12-HOA) as it gels the 1-phase microemulsion and the lamellar phase of the system water-*n*-decane-tetraethylene glycol monodecyl ether (C₁₀E₄) successfully.^{12,44} Furthermore, it gels the lamellar phase of the binary system water-didodecyl dimethylammonium bromide (2C₁₂DAB).⁶ Using 12-HOA for

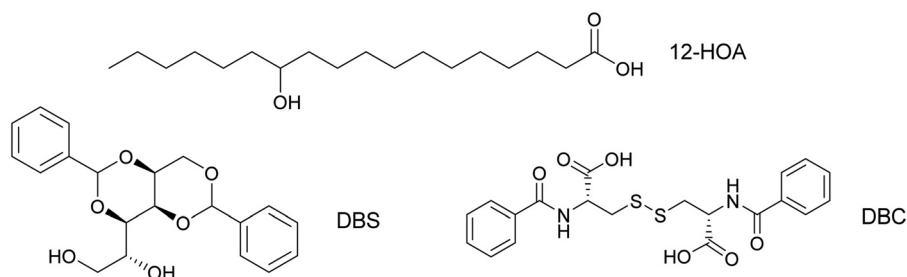


Fig. 7 Molecular structures of (top) 12-hydroxyoctadecanoic acid (12-HOA), (bottom, left) 1,3:2,4-dibenzylidene-*D*-sorbitol (DBS), (bottom, right) *N,N'*-dibenzoyl-*L*-cystine (DBC).

the gelation of the scouting system H_2O - n -octane- β - C_8G_1 -1-octanol, we found that it indeed gels the 1-phase microemulsion with a minimum gelator concentration (mgc) of 1.5 wt%. Nevertheless, there is a shift of the phase boundaries (see Fig. 8) leading to a decrease in surfactant efficiency. This can be explained by the dissolution of long-chain 12-HOA in the oil phase, which increases its hydrophobicity and makes the oil more difficult to be solubilized. On the other hand, the decreased amount of co-surfactant needed to form the 1-phase microemulsion is due to the surface activity of 12-HOA.¹² In conclusion, the threefold role of 12-HOA as gelator, co-solvent, and co-surfactant⁴⁵ increases the complexity of the system significantly.

Consequently, a molecular gelator acting solely as gelator had to be identified. DBS and DBC turned out to be potential candidates since they are not surface-active and do not affect the phase behavior of binary H_2O -surfactant systems.⁴⁶ However, DBS does not dissolve in the scouting system even at a concentration as low as 0.1 wt%. On the other hand, DBC gels the bicontinuous microemulsion at 1.0 wt%, leading to an isotropic and homogeneous sample (see Fig. 8 right). Furthermore, the phase boundaries remained unchanged compared to

the non-gelled microemulsion. Hence, DBC is the gelator of choice for the scouting system.

4.2 Gelling H_2O -IPM-Plantacare 1200 UP-1,2-octanediol

Having chosen DBC as gelator for the scouting system H_2O - n -octane- β - C_8G_1 -1-octanol, we expected DBC to gel the non-toxic microemulsion H_2O -IPM-Plantacare 1200 UP-1,2-octanediol as well. We found that the mgc (minimum gelator concentration) of DBC is 2.4 wt% in the non-toxic system as opposed to 1 wt% for the scouting system. After gelation, however, the gelator precipitated overnight. For simplicity, the phase diagram of the non-toxic system H_2O -IPM-Plantacare 1200 UP-1,2-octanediol was measured in the presence of DBC at a mass fraction of 2 wt% ($\eta = 0.02$, not gelled) in order to investigate the effect of DBC on the phase boundaries. As can be seen in Fig. 9, the phase boundaries shift to a larger amount of co-surfactant in the presence of 2 wt% DBC. Unfortunately, we have no explanation either for the higher demand of 1,2-octanediol or for the precipitation of DBC.

Since DBC turned out not to be a potent gelator for the system H_2O -IPM-Plantacare 1200 UP-1,2-octanediol, we used the organogelator 12-HOA whose mgc is 2 wt%. To investigate

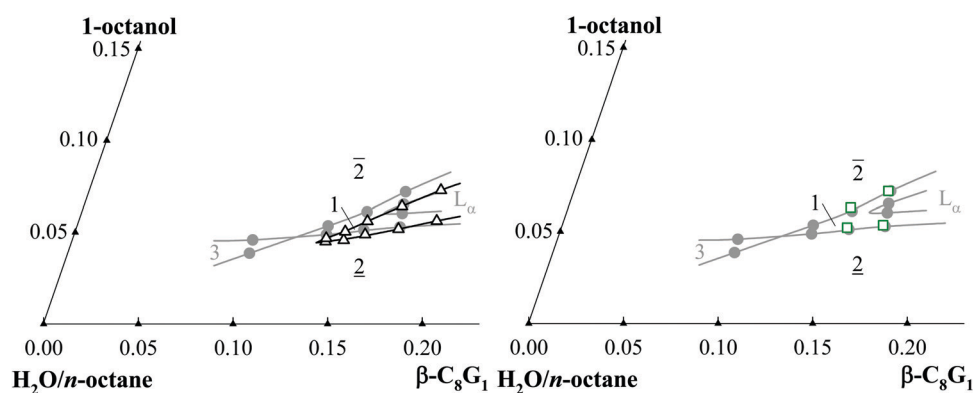


Fig. 8 Phase diagrams of the quaternary system H_2O - n -octane- β - C_8G_1 -1-octanol (gray closed circles) with (left) the gelled system with 12-HOA (black open triangles up) at $\eta = 0.015$, and (right) the gelled system with DBC (dark green open squares) at $\eta = 0.01$. For all samples $T = 25\text{ }^\circ\text{C}$ and $\phi = 0.50$ is adjusted.

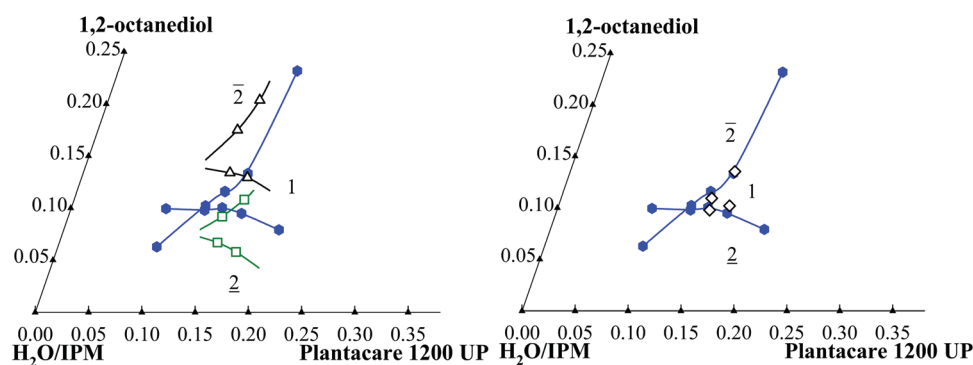


Fig. 9 Phase diagrams of the quaternary system H_2O -IPM-Plantacare 1200 UP-1,2-octanediol (blue closed hexagons) with (left) the non-gelled system in the presence of DBC (dark green open squares) at $\eta = 0.02$ and the non-gelled system in the presence of 12-HOA (black open triangles up) at $\eta = 0.015$; (right) the gelled system in the presence of DBS (black open diamonds) at $\eta = 0.003$. For all samples $T = 25\text{ }^\circ\text{C}$ and $\phi = 0.50$ is adjusted.

the effect of 12-HOA on the phase boundaries, we measured the phase diagram of the non-toxic microemulsion in the presence of 1.5 wt% 12-HOA ($\eta = 0.015$, not gelled). As depicted in Fig. 9, the phase boundaries shift to a smaller amount of 1,2-octanediol since 12-HOA acts as an additional co-surfactant.

Finally, we used DBS and found—as opposed to our scouting system—that it is a very potent gelator for the non-toxic microemulsion H₂O–IPM–Plantacare 1200 UP–1,2-octanediol: gels are formed at a mgc as low as of 0.14 wt%. As the gel is relatively weak at the mgc, we decided to use a DBS concentration of $\eta = 0.003$ (0.3 wt%) for further investigations. As can be seen in Fig. 9, the presence of DBS at $\eta = 0.003$ does not change the phase boundaries of the microemulsion. Therefore, we choose the gelled non-toxic microemulsion of the system H₂O–IPM–Plantacare 1200 UP–1,2-octanediol in the presence of DBS at $\eta = 0.003$ to be the final system.

Unexpectedly, DBC is an ideal gelator for the scouting system but not for the non-toxic “final” system. This phenomenon—namely that the gelling capacity of a gelator depends on the solvent, in our case the microemulsion—has also been reported by other researchers. Richard Weiss, an expert in molecular gels, commented: “there is no paradigm for discerning when a selected liquid will be gelled by a particular molecule (*i.e.*, a gelator) or even the properties of a molecular gel after it is formed.”³⁶ Another example is 12-HOA which gels the 1-phase microemulsion and the lamellar phase of the system water–*n*-decane–C₁₀E₄ at $\eta = 0.015$,^{12,44} but only gels the binary system H₂O–C₁₂E₇ at a mass fraction as high as $\eta = 0.05$.⁴⁵ In the former case it acts more as gelator (only to a minor extent as co-surfactant), while in the latter case it acts primarily as co-surfactant. As regards the organogelator DBS, it gels H₂O–C₁₂E₇ (technical-grade)⁴⁶ at relatively low gelator concentrations which is in agreement with our observations for the system H₂O–IPM–Plantacare 1200 UP–1,2-octanediol.

Having chosen the formulation of the gelled non-toxic microemulsion, we performed oscillatory shear rheometry in order to examine its rheological properties. For these measurements a

composition located in the middle of the 1-phase region was chosen. In a preliminary amplitude sweep (Fig. 3) the linear viscoelastic region (LVE) was determined, and a stress amplitude of $\tau = 10$ Pa was thus set for the frequency sweep. The frequency sweep of the gelled microemulsion (Fig. 10, left) indicates that the storage modulus G' is about one order of magnitude larger than the loss modulus G'' over the whole studied frequency range. Moreover, the two moduli depend only weakly on the frequency. Thus, one can conclude that even at a low gelator concentration of 0.3 wt% a rigid gel is formed. In the temperature sweep measurements (Fig. 10, right), both the storage modulus G' and the loss modulus G'' drop strongly and cross over at 78 °C, which can be assigned to the sol–gel transition temperature $T_{\text{sol-gel}}$. The sol–gel transition is the temperature-induced transformation of a highly viscous, solid-like gel into a lowly viscous, liquid sol with the gelator being dissolved in the sol. A sol–gel transition temperature $T_{\text{sol-gel}}$ of 78 °C is a good value for the application of gelled non-toxic microemulsions as transdermal drug delivery carrier since it is above the operating temperature range of 40 °C.

Since we want to use gelled non-toxic bicontinuous microemulsions to solubilize both hydrophobic and hydrophilic drugs, it is indispensable to show that the structure of the microemulsion remains unchanged in the gelled case. For this purpose, small-angle neutron scattering (SANS) was performed to investigate the microstructure of the gelled microemulsion. As reference, the non-gelled microemulsion was measured as well. In analogy to the rheological studies, a composition located in the middle of the 1-phase region was chosen. Note that for SANS measurements H₂O was replaced with D₂O to adjust the so-called bulk contrast. Thereby, the composition of SANS samples and H₂O microemulsions were the same with respect to volume fractions. Thus, samples of the non-gelled and the gelled microemulsions having almost identical composition were prepared, *i.e.* $\gamma_C = 0.1571$ and $\gamma_D = 0.1092$ as well as $\gamma_C = 0.1581$ and $\gamma_D = 0.1100$ with $\eta = 0.003$ DBS, respectively.

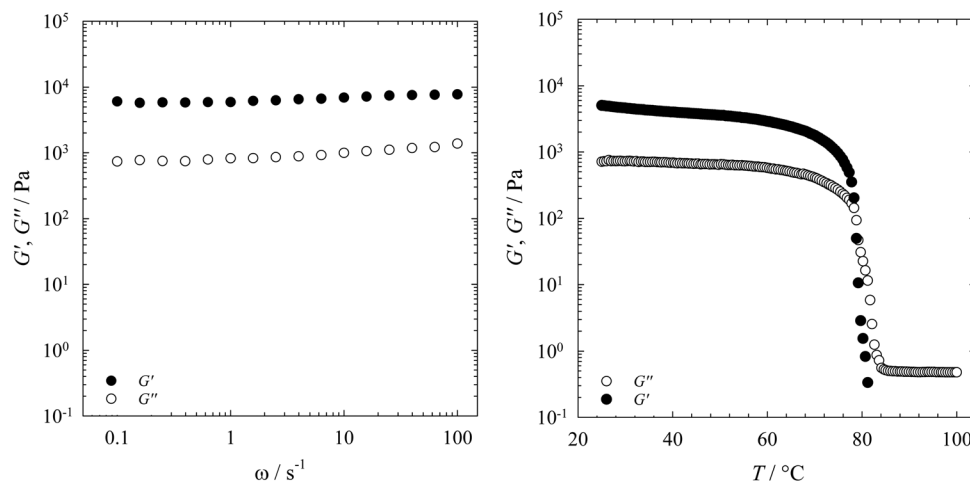


Fig. 10 Storage modulus G' (filled symbols) and loss modulus G'' (open symbols) of the gelled bicontinuous microemulsion H₂O–IPM–Plantacare 1200 UP–1,2-octanediol in the presence of DBS at $\eta = 0.003$, $\tau = 10$ Pa (left) as a function of ω at $T = 25$ °C, $\gamma_C = 0.1583$, $\gamma_D = 0.1204$, $\phi = 0.50$; (right) as a function of T at $\omega = 10$ s⁻¹, and a heating rate of 1 °C min⁻¹, $\gamma_C = 0.1588$, $\gamma_D = 0.1194$, $\phi = 0.50$.

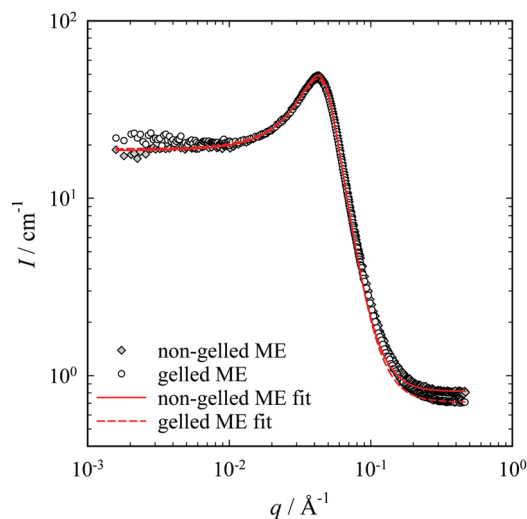


Fig. 11 SANS data of the bicontinuous microemulsion H₂O–IPM–Plantacare 1200 UP–1,2-octanediol ($\gamma_C = 0.1571$, $\gamma_D = 0.1092$, $\phi = 0.50$; closed squares) and the gelled bicontinuous microemulsion H₂O–IPM–Plantacare 1200 UP–1,2-octanediol ($\gamma_C = 0.1581$, $\gamma_D = 0.1100$, $\phi = 0.50$; open circles) in the presence of DBS at $\eta = 0.003$, $T = 25^\circ\text{C}$. The scattering curves were fitted with the Teubner–Strey model: solid line for the non-gelled and dashed line for the gelled microemulsion.

In Fig. 11, the scattering intensity is plotted as a function of the scattering vector q in a double-log plot. As can be seen, both curves fall almost on top of each other, which indicates that the structure of the microemulsion is retained in the gelled sample. Furthermore, both scattering curves have the typical shape found for bicontinuous microemulsions—a peak at intermediate q -values.⁴⁷ Starting from low q -values, the scattering intensity strongly increases, runs through a pronounced maximum at intermediate q -values before the intensity decreases with q^{-4} .

The scattering curves were fitted with the Teubner–Strey model,⁴⁷ which describes the characteristic peak of a bicontinuous microemulsion with

$$I(q) = \frac{8\pi c_2 \phi_a \phi_b (\Delta\rho)^2 / \xi_{\text{TS}}}{a_2 + c_1 q^2 + c_2 q^4} + I_{\text{incoh}}. \quad (5)$$

Where I_{incoh} is the incoherent background, $\Delta\rho$ the scattering length density difference of the two subphases, and ϕ_a and ϕ_b their volume fractions. The parameters a_2 , c_2 and c_1 are coefficients derived from a Landau–Ginzburg order parameter expansion of the local free energy density, where the order parameter is the water-to-oil ratio. After the determination of a_2 , c_2 and c_1 , two characteristic length scales of the Teubner–Strey model can be calculated, namely the correlation length

$$\xi_{\text{TS}} = \left[\frac{1}{2} \left(\frac{a_2}{c_2} \right)^{1/2} + \frac{c_1}{4c_2} \right]^{-1/2} \quad (6)$$

and the periodicity of the water and oil domains

$$d_{\text{TS}} = 2\pi \left[\frac{1}{2} \left(\frac{a_2}{c_2} \right)^{1/2} - \frac{c_1}{4c_2} \right]^{-1/2}. \quad (7)$$

By using this model a similar periodicity of $d = 14.0$ nm was found for both the non-gelled and the gelled microemulsions. The fact that the correlation length $\xi_{\text{TS}} = 6.6$ nm of the non-gelled sample is slightly larger than that of the gelled sample ($\xi_{\text{TS}} = 6.3$ nm) indicates that the non-gelled sample seems to be slightly better ordered. This observation goes hand in hand with the slightly higher scattering intensity observed for the gelled sample at low q -values. However, this increase might also originate from the gel fibrillar network. As previous small-angle neutron scattering (SANS) curves of gelled bicontinuous microemulsions¹⁴ proved that the main difference between gelled and non-gelled microemulsions is the scattering at low q ($< 0.01 \text{ \AA}^{-1}$). However, note that in the gelled microemulsion studied in this work the gelator mass fraction is a factor of 5 smaller compared to the gelled microemulsion systems studied previously.

5 Conclusion and outlook

In this study, we successfully formulated a gelled non-toxic bicontinuous microemulsion. On the one hand, the non-toxic bicontinuous microemulsion facilitates the solubilization of both hydrophilic and hydrophobic drugs, *e.g.*, for transdermal drug delivery. On the other hand, the gel network formed by a molecular gelator provides mechanical stability and thus facilitates the application of the drug-containing system.

Starting from the previously studied, not bio-compatible scouting system H₂O–*n*-octane– β -C₈G₁–1-octanol, the co-surfactant 1-octanol, and the oil *n*-octane were replaced by non-toxic components, namely 1,2-octanediol and isopropyl myristate (IPM). Replacing 1-octanol by 1,2-octanediol, one sees that the efficiency of the β -C₈G₁ surfactant remained the same, while the amount of co-surfactant required to form a 1-phase microemulsion is largely increased. Replacing the oil *n*-octane by IPM, one sees that the longer carbon chain of IPM compared to *n*-octane decreases the efficiency of β -C₈G₁. In order to increase the efficiency of surfactant and co-surfactant, the pure surfactant β -C₈G₁ was replaced by longer-chain technical-grade sugar surfactants. We found that the system becomes more efficient with increasing chain length and demands less co-surfactant to form the bicontinuous microemulsion. Thus, a symmetric non-toxic microemulsion of the type H₂O–IPM–Plantacare 1200 UP (C₁₂G_{1,4})–1,2-octanediol could be formulated using 12.1 wt% Plantacare 1200 UP and 9.8 wt% 1,2-octanediol.

Having formulated the non-toxic microemulsion, the gelation behavior of three molecular gelators [12-hydroxyoctadecanoic acid (12-HOA), 1,3:2,4-dibenzylidene-*D*-sorbitol (DBS), and *N,N'*-dibenzoyl-L-cystine (DBC)] was studied for both the scouting and the non-toxic system. As expected, 12-HOA was surface active in both systems and altered the phase behavior. Since our goal was to formulate an orthogonally self-assembled system we did not pursue the gelation with 12-HOA further. In case of the scouting system H₂O–*n*-octane– β -C₈G₁–1-octanol, DBS could not be dissolved, while DBC gelled the system without altering the phase behavior. However, in the case of the non-toxic system H₂O–IPM–Plantacare 1200 UP (C₁₂G_{1,4})–1,2-octanediol, DBC gelled the

system but precipitated overnight, while DBS gelled the system without altering the phase behavior. Thus the final system turned out to be H₂O–IPM–Plantacare 1200 UP–1,2-octanediol in the presence of 0.3 wt% DBS. The rheological properties of the gelled microemulsion were examined by oscillatory shear rheometry. Experimental evidence that the bicontinuous microstructure of the gelled microemulsion was not changed compared to the non-gelled microemulsion was provided by small-angle neutron scattering (SANS).

Future studies will focus on characterizing the structure of the gelled non-toxic bicontinuous microemulsion, *i.e.*, to show that our system is indeed orthogonally self-assembled. More specifically, we want to determine characteristic parameters of the gel network such as mesh size, fiber diameter, and fiber length. For this purpose, small-angle neutron scattering (SANS), light scattering, and freeze-fracture microscopy are the techniques of choice. Moreover, both hydrophobic and hydrophilic model drugs will be dissolved in the system, and skin permeability tests will be carried out.

Conflicts of interest

The authors declare no conflict of interest.

Acknowledgements

We thank Birgit Feucht for carrying out a part of the phase studies, and Katja Steck for her help with the rheological measurements. We also thank Sonja Dieterich for her help with the sample preparation of the gelled SANS sample and Krisitina Schneider, Diana Zauser and Shih-Yu Tseng for valuable help with the SANS measurements. Furthermore, we would like to acknowledge the Institut Laue Langevin (ILL) in Grenoble (France) in providing the facilities for the SANS measurements and the valuable support of the local contact Dr Ralf Schweins.

Notes and references

- 1 P. E. Laibinis, J. J. Hickman, M. S. Wrighton and G. M. Whitesides, *Science*, 1989, **245**, 845–847.
- 2 A. Heeres, C. Van Der Pol, M. Stuart, A. Friggeri, B. L. Feringa and J. Van Esch, *J. Am. Chem. Soc.*, 2003, **125**, 14252–14253.
- 3 A. Brizard, M. Stuart, K. Van Bommel, A. Friggeri, M. De Jong and J. Van Esch, *Angew. Chem., Int. Ed.*, 2008, **47**, 2063–2066.
- 4 A. M. Brizard, M. C. A. Stuart and J. H. van Esch, *Faraday Discuss.*, 2009, **143**, 345–357.
- 5 A. M. Brizard and J. H. Van Esch, *Soft Matter*, 2009, **5**, 1320–1327.
- 6 S. Koitani, S. Dieterich, N. Preisig, K. Aramaki and C. Stubenrauch, *Langmuir*, 2017, **33**, 12171–12179.
- 7 C. Stubenrauch and F. Gießelmann, *Angew. Chem., Int. Ed.*, 2016, **55**, 3268–3275.
- 8 R. Strey, *Colloid Polym. Sci.*, 1994, **272**, 1005–1019.
- 9 C. Stubenrauch, R. Tessendorf, R. Strey, I. Lynch and K. A. Dawson, *Langmuir*, 2007, **23**, 7730–7737.
- 10 C. Stubenrauch, R. Tessendorf, A. Salvati, D. Topgaard, T. Sottmann, R. Strey and I. Lynch, *Langmuir*, 2008, **24**, 8473–8482.
- 11 M. Magno, R. Tessendorf, B. Medronho, M. G. Miguel and C. Stubenrauch, *Soft Matter*, 2009, **5**, 4763–4772.
- 12 M. Laupheimer, K. Jovic, F. E. Antunes, M. da Graça Martins Miguel and C. Stubenrauch, *Soft Matter*, 2013, **9**, 3661.
- 13 M. Laupheimer, University of Stuttgart, 2013.
- 14 M. Laupheimer, T. Sottmann, R. Schweins and C. Stubenrauch, *Soft Matter*, 2014, **10**, 8744–8757.
- 15 M. Kreilgaard, E. J. Pedersen and J. W. Jaroszewski, *J. Controlled Release*, 2000, **69**, 421–433.
- 16 M. Kreilgaard, *Adv. Drug Delivery Rev.*, 2002, **54**, 77–98.
- 17 A. Kogan and N. Garti, *Adv. Colloid Interface Sci.*, 2006, **123**, 369–385.
- 18 S. Heuschkel, A. Goebel and R. H. H. Neubert, *J. Pharm. Sci.*, 2008, **97**, 603–631.
- 19 S. P. Callender, J. A. Mathews, K. Kobernyk and S. D. Wettig, *Int. J. Pharm.*, 2017, **526**, 425–442.
- 20 P. K. Ghosh, R. J. Majithiya, M. L. Umrethia and R. S. R. Murthy, *AAPS PharmSciTech*, 2006, **7**, E172.
- 21 S. A. Fouad, E. B. Basalious, M. A. El-nabarawi and S. A. Tayel, *Int. J. Pharm.*, 2013, **453**, 569–578.
- 22 K. Kim, M. Kim, J. Park, J. Lee, H. Cho, I. Yoon and D. Kim, *J. Ginseng Res.*, 2018, **42**, 512–523.
- 23 A. Froelich, T. Osmałek, A. Snela, P. Kunstman, B. Jadach, M. Olejniczak, G. Roszak and W. Białas, *J. Colloid Interface Sci.*, 2017, **507**, 323–336.
- 24 M. Kahlweit, G. Busse and B. Faulhaber, *Langmuir*, 1995, **11**, 1576–1583.
- 25 D. Nickel, C. Nitsch, P. Kurzendörfer and W. Von Rybinski, *Trends Colloid Interface Sci. VI*, 1992, **252**, 249–252.
- 26 M. Kahlweit, G. Busse and B. Faulhaber, *Langmuir*, 1995, **11**, 3382–3387.
- 27 M. Kahlweit, G. Busse, B. Faulhaber and H. Eibl, *Langmuir*, 1995, **11**, 4185–4187.
- 28 M. M. Fiume, B. Heldreth, W. F. Bergfeld, D. V. Belsito, R. A. Hill, C. D. Klaassen, D. Liebler, J. G. Marks, R. C. Shank, T. J. Slaga, P. W. Snyder and F. A. Andersen, *Int. J. Toxicol.*, 2013, **32**, 22S–48S.
- 29 K. Kluge, C. Stubenrauch, T. Sottmann and R. Strey, *Tenside, Surfactants, Deterg.*, 2001, **38**, 30–40.
- 30 T. Sottmann, K. Kluge, R. Strey, J. Reimer and O. Söderman, *Langmuir*, 2002, **18**, 3058–3067.
- 31 J. Reimer, O. Söderman, T. Sottmann, K. Kluge and R. Strey, *Langmuir*, 2003, **19**, 10692–10702.
- 32 M. Kahlweit, G. Busse and B. Faulhaber, *Langmuir*, 1996, **12**, 861–862.
- 33 M. Kahlweit, G. Busse and B. Faulhaber, *Langmuir*, 1997, **13**, 5249–5251.
- 34 W. Johnson, W. F. Bergfeld, D. V. Belsito, R. A. Hill, C. D. Klaassen, D. Liebler, J. G. Marks, R. C. Shank, T. J. Slaga,

- P. W. Snyder and F. A. Andersen, *Int. J. Toxicol.*, 2012, **31**, 147S–168S.
- 35 A. C. Williams and B. W. Barry, *Adv. Drug Delivery Rev.*, 2012, **64**, 128–137.
- 36 R. G. Weiss, *J. Am. Chem. Soc.*, 2014, **136**, 7519–7530.
- 37 M. Laupheimer, N. Preisig and C. Stubenrauch, *Colloids Surf., A*, 2015, **469**, 315–325.
- 38 P. Terech and R. G. Weiss, *Chem. Rev.*, 1997, **97**, 3133–3160.
- 39 H. Kunieda and K. Shinoda, *J. Colloid Interface Sci.*, 1985, **107**, 107–121.
- 40 C. Stubenrauch, B. Paeplow and G. H. Findenegg, *Langmuir*, 1997, **13**, 3652–3658.
- 41 E. R. Draper and D. J. Adams, *Chem*, 2017, **3**, 390–410.
- 42 B. O. Okesola, V. M. P. Vieira, D. J. Cornwell, N. K. Whitelaw and D. K. Smith, *Soft Matter*, 2015, **11**, 4768–4787.
- 43 F. M. Menger and K. L. Caran, *J. Am. Chem. Soc.*, 2000, **122**, 11679–11691.
- 44 Y. Xu, M. Laupheimer, N. Preisig, T. Sottmann, C. Schmidt and C. Stubenrauch, *Langmuir*, 2015, **31**, 8589–8598.
- 45 K. Steck, C. Schmidt and C. Stubenrauch, *Gels*, 2018, **4**, 78.
- 46 K. Steck, J. H. van Esch, D. K. Smith and C. Stubenrauch, *Soft Matter*, 2019, **15**, 3111–3121.
- 47 M. Teubner and R. Strey, *J. Chem. Phys.*, 1987, **87**, 3195–3200.

Publication II

Formulation of Gelled Non-Toxic Bicontinuous Microemulsions Stabilized by Highly Efficient Alkanoyl Methylglucamides

Ke Peng, Natalie Preisig, Thomas Sottmann, and Cosima Stubenrauch
Langmuir **2020**, *36* (42), 12692–12701.

DOI: 10.1021/acs.langmuir.0c02314

Reprinted with permission from [Pen20]. Copyright 2020 American Chemical Society.
<http://pubs.acs.org/articlesonrequest/AOR-EVUBMDMGJVCYSRSYM4KV>

Formulation of Gelled Non-toxic Bicontinuous Microemulsions Stabilized by Highly Efficient Alkanoyl Methylglucamides

Ke Peng, Natalie Preisig, Thomas Sottmann, and Cosima Stubenrauch*



Cite This: *Langmuir* 2020, 36, 12692–12701



Read Online

ACCESS |



Metrics & More

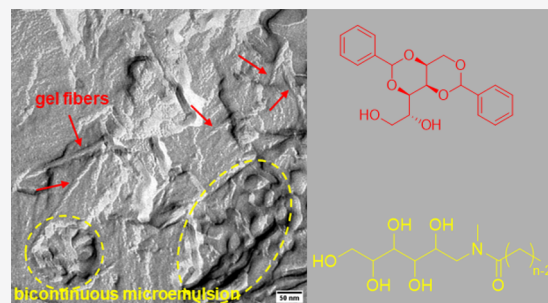


Article Recommendations



Supporting Information

ABSTRACT: Gelled non-toxic bicontinuous microemulsions have a great potential for transdermal drug delivery as the microemulsion facilitates the solubilization of both hydrophilic and hydrophobic drugs, while the gel network provides mechanical stability and thus an easy application on the skin. In our previous study, we formulated a gelled non-toxic bicontinuous microemulsion: we gelled the system H_2O –isopropyl myristate (IPM)–Plantacare 1200 UP ($C_{12}G_{1,4}$)–1,2-octanediol with the low molecular weight organogelator 1,3:2,4-dibenzylidene-D-sorbitol (DBS). However, a large amount of Plantacare 1200 UP (12 wt %) is needed to form a bicontinuous microemulsion. To solve this problem, we studied a new class of surfactants, namely, alkanoyl methylglucamides (MEGA), which have been rarely used for the formulation of microemulsions. The phase behavior of microemulsions stabilized by MEGA-8/10, MEGA-12/14-PC, and MEGA-12/14-HC was compared with that of systems stabilized by alkyl polyglucosides. We found that even with 2 wt % MEGA-12/14-HC, a bicontinuous microemulsion can be formed, which is 1/6 of the amount of Plantacare 1200 UP. The bicontinuous microstructure of the non-toxic microemulsion H_2O –IPM–MEGA-12/14-HC–1,2-octanediol was confirmed by small-angle neutron scattering. Furthermore, the phase boundaries remained unchanged when gelled by DBS. The rheological properties of the gel were studied by oscillatory shear rheometry. Finally, freeze-fracture electron microscopy images show the coexistence of gel fibers and bicontinuous oil and water domains. These results suggest that the new gelled non-toxic bicontinuous microemulsion is an orthogonal self-assembled system.



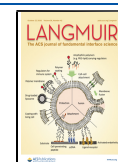
INTRODUCTION

Gelled bicontinuous microemulsions count among gelled complex fluids.¹ If the two self-assembled structures, namely, the gel fibrillar network and the bicontinuous microemulsion, form independently but simultaneously, this phenomenon is called orthogonal self-assembly.² The gelled bicontinuous microemulsion H_2O –*n*-decane–tetraethylene glycol mono-decyl ether ($C_{10}E_4$)–12-hydroxyoctadecanoic acid (12-HOA) was proven to be orthogonally self-assembled by means of freeze-fracture electron microscopy (FFEM) and small-angle neutron scattering (SANS).^{3,4} It was found that the gel fibers penetrate both the water and oil domains, even though the low molecular weight organogelator 12-HOA only dissolves in the oil phase. In contrast to polymeric gels, molecular gels form gel fibrillar networks via the self-assembly of single molecular gelators,⁵ which are also referred to as low molecular weight gelators.⁵ Due to the non-covalent interactions among gelator molecules, the gelation process is reversible. Thus, the sol–gel transition can be manipulated externally, for example, by a temperature change. Thermodynamically stable bicontinuous microemulsions contain two interweaving water and oil subdomains separated by an amphiphilic surfactant monolayer with domain sizes ranging from 5 to 100 nm.⁶ Bicontinuous microemulsions provide long-term stability as well as substantially high solubilization capacity for both hydrophobic

and hydrophilic components and enhance the permeation through skin barriers.⁷ Therefore, gelled bicontinuous microemulsions are of particular interest in the field of transdermal drug delivery as they combine the mechanical stability of the gel network and the abovementioned features of the bicontinuous microstructure.¹

In order to achieve transdermal drug delivery, biodegradable non-toxic microemulsions, which are suitable for biological organisms, must be formulated. Although non-toxic microemulsions as drug delivery systems have been extensively studied in pharmaceutical science,^{7–11} those were mostly oil-in-water (O/W) microemulsions. However, bicontinuous microemulsions, which exhibit the most efficient solubilization and excellent wetting properties, have not been studied in detail to date. Kahlweit et al. made a series of attempts to formulate non-toxic bicontinuous microemulsions. They started with the quaternary system H_2O –*n*-alkane–lecithin–

Received: August 6, 2020
Revised: September 7, 2020
Published: October 16, 2020



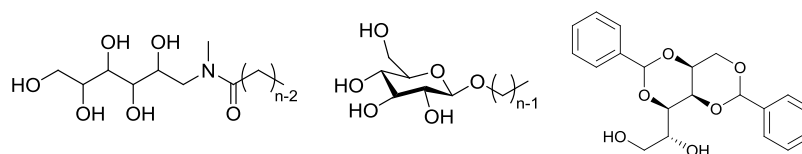


Figure 1. Molecular structures of (left) alkanoyl methylglucamide (MEGA-*n*) or *n*-alkanoyl-*N*-methylglucamine, (middle) *n*-alkanyl- β -D-glucopyranoside (β -C_{*n*}G₁), and (right) low molecular weight organogelator 1,3:2,4-dibenzylidene-D-sorbitol (DBS).

alkanol,¹² then replaced the zwitterionic surfactant lecithin with non-ionic alkyl polyglucosides (or glycosides).¹³ Since *n*-alkanes are not biocompatible, they replaced *n*-alkanes with unsaturated fatty acid ethyl esters.¹⁴ Subsequently, alkanol was replaced by 1,2-alkanediol, which is biocompatible yet surface-active enough to act as a cosurfactant.¹⁵ Finally, due to its sensitivity to light and oxygen, the unsaturated fatty acid ethyl esters were replaced by the saturated fatty acid ester isopropyl myristate (IPM). In this way, the non-toxic microemulsion H₂O–IPM–glycoside–alkanediol was successfully formulated.¹⁶

Following in the footsteps of Kahlweit et al., we also pursued the idea of formulating non-toxic microemulsions but extended it to a combination of non-toxic microemulsions and viscoelastic gel networks.¹⁷ We formulated a non-toxic bicontinuous microemulsion with a technical-grade glycoside surfactant (sugar surfactant, see Figure 1, middle) and gelled the microemulsion with the low molecular weight organogelator 1,3:2,4-dibenzylidene-D-sorbitol (DBS, see Figure 1, right),¹⁸ which did not change the phase boundaries of the microemulsion. We started the formulation of the non-toxic microemulsion with the scouting system H₂O–*n*-octane– β -C₈G₁–1-octanol,^{19,20} and replaced the oil *n*-octane and the cosurfactant 1-octanol with non-toxic isopropyl myristate (IPM) and 1,2-octanediol, respectively. However, the replacement of the oil and the cosurfactant led to a large decrease in the efficiency of the surfactant/cosurfactant mixture. Generally, there are two methods for improving the efficiency. The first method is to add efficiency boosters, e.g., amphiphilic block copolymers,^{21,22} which, however, are not biocompatible. The other method is to find a more efficient biocompatible surfactant. Besides glycosides, *n*-alkanoyl-*N*-methylglucamines (Figure 1, left), which are also called glucamides, fall into the category of sugar surfactants, too. The open-ring glucose unit is connected to the alkyl chain by an amide bond. The methyl group at the nitrogen contributes to the water solubility of the surfactant.²³ Glucamides and glycosides have comparable properties: they are both made from renewable sources, they are biodegradable, and they are dermatologically safe.²⁴ However, only limited studies about the phase behavior of glucamide-containing microemulsions can be found.^{25–27}

With a view to filling this gap as well as to finding a highly efficient surfactant for our gelled non-toxic bicontinuous microemulsions, we studied the solubilization capacity of technical-grade glucamide surfactants with C_{8/10}- and C_{12/14}-chain lengths (C_{8/10} = mixture of octyl and decyl chains; C_{12/14} = mixture of dodecyl and tetradecyl chains). We formulated quaternary systems consisting of H₂O–IPM–glucamide–1,2-octanediol and compared them with the glycoside-containing ones. One C_{12/14}-glucamide was found to be enormously efficient for the formation of bicontinuous microemulsions. We thus investigated this system via phase studies and small-angle neutron scattering (SANS). Finally, we gelled the non-toxic bicontinuous microemulsion with the low molecular weight

organogelator DBS, which was also used to gel the non-toxic glycoside-containing microemulsions in our previous study. The gelled bicontinuous microemulsion was subsequently characterized by rheological measurements and freeze-fracture electron microscopy (FFEM).

EXPERIMENTAL SECTION

Materials. Bi-distilled water was used to prepare all protonated samples. For SANS measurements, deuterated samples were prepared replacing bi-distilled water with deuterium oxide (>99.9%) from Eurisotop, France. The chemicals *n*-octane (Alfa Aesar, >99%), 1-octanol (Aldrich, 99%), isopropyl myristate (TCI, >98%), and 1,2-octanediol (Acros, >98%) were used as purchased. The low molecular weight organogelator 1,3:2,4-dibenzylidene-D-sorbitol (DBS) was purchased from NJC Europe under the product name “Geniset D”, and the low molecular weight hydrogelator *N,N'*-dibenzoyl-L-cystine (DBC, >98%) was purchased from Santa Cruz, USA. The technical-grade alkanoyl methylglucamides were provided by Clariant GmbH, Germany. Due to the solubility problem of glucamides in pure water, the original products contain cosolvents, and we used the surfactants as received without further purification. Three commercially available glucamides were studied during the experiments. They are named according to the main active components: (1) MEGA-8/10 (50% C_{8/10}-methylglucamide, 45% water, and 5% propylene glycol), (2) MEGA-12/14-HC (63% C_{12/14}-methylglucamide, 22% water, 10% ethanol, and 4.5% propylene glycol), (3) MEGA-12/14-PC (35% C_{12/14}-methylglucamide, 60% water, 4% propylene glycol, and 0.8% sorbic acid). The CMC value of (1) is about 0.26 g·L⁻¹, and the CMC of (2) is about 0.026 g·L⁻¹ (see Figure S1 in the Supporting Information). The CMC of (3) could not be measured due to the low solubility of the surfactant.

Sample Preparation. Non-gelled microemulsions were prepared by weighing in the surfactant (C), cosurfactant (D), oil (B), and water (A) with an analytical balance into glass tubes, which were then sealed by polyethylene stoppers. For monitoring phase diagrams, we used a titration procedure (explained in Section Phase Behavior) to reduce the amount of the material. Subsequently, the samples were heated up to 50 °C in a water bath while being stirred to homogenize.

In the case of gelled microemulsions, a gelator was additionally added to the samples. The samples were first heated above 95 °C to dissolve the gelator. A heat gun was utilized when necessary. With DBS, the gelation process takes less than 30 s; so, the samples were quickly transferred to an ice bath directly from the 95 °C water bath with manual shaking to ensure homogeneous gelation. Afterward, the samples were transferred to a 25 °C water bath and allowed to equilibrate. It is essential to agitate the gelled microemulsion samples vigorously before gelling; otherwise, phase separation occurs, and the gelation process must be repeated.

Phase Behavior. The phase behavior was investigated at a constant temperature of *T* = 25.0 °C in the water bath, which has a precision of ±0.1 K. The non-gelled microemulsion samples were first prepared without the cosurfactant (D). After equilibration in the water bath, a cosurfactant (D) was added to the sample dropwise by a syringe. The added amount of the cosurfactant was recorded by weight with an accuracy of ±0.001 g. After adding the cosurfactant, the sample was shaken and stirred vigorously before it was left to reach equilibrium. Then, the phase behavior was visually determined. Birefringence of lyotropic liquid crystalline phases was observed via crossed polarizers. Since the phase transitions of sugar surfactant-

based microemulsions were induced by a fourth component, namely, a cosurfactant, the phase behavior is presented in a phase tetrahedron (Figure 2). The phase behavior of these microemulsions is studied at

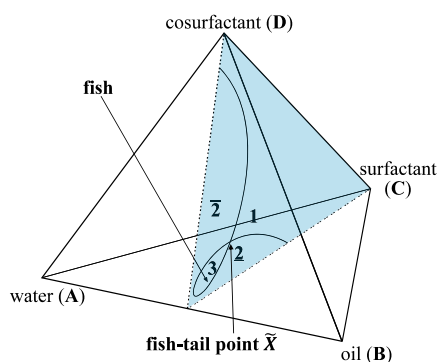


Figure 2. Schematic phase tetrahedron of a quaternary system water–oil–surfactant–cosurfactant at a constant temperature and a section (in blue) through the phase tetrahedron at a constant oil-to-water ratio as a function of the main surfactant mass fraction γ_C and the cosurfactant mass fraction γ_D .²⁸

a constant oil-to-water ratio, i.e., recording a two-dimensional section through the tetrahedron as highlighted in Figure 2. Hereby “2” means the coexistence of an oil-in-water (o/w)-microemulsion (lower phase) and an oil excess phase (upper phase). “1” denotes the isotropic one-phase microemulsion. “2” means the coexistence of an excess water phase (lower phase) and a water-in-oil (w/o)-microemulsion (upper phase). “3” denotes the coexistence of three phases, namely, an excess water phase (lower phase), a microemulsion (middle phase), and an excess oil phase (upper phase).

In the case of gelled microemulsions, the cosurfactant was added to the gelled sample at 25 °C, which was then heated above the sol–gel transition temperature, where the sample was melted and could thus be mixed. After the gelation process (see Section Sample Preparation), the phase behavior was recorded. While a gelled one-phase microemulsion appears transparent, the gelled two-phase samples are turbid.

In our experiments, the volume fraction of oil in the solvent mixture

$$\phi = \frac{V_{\text{oil}}}{V_{\text{water}} + V_{\text{oil}}} \quad (1)$$

was kept constant at 0.50. The mass fraction of the surfactant (C) is defined as

$$\gamma_C = \frac{m_{\text{surf.}}}{m_{\text{water}} + m_{\text{oil}} + m_{\text{surf. total}} + m_{\text{co-surf.}} + m_{\text{gelator}}} \quad (2)$$

where $m_{\text{surf.}}$ is the active content of alkanoyl methylglucamides in the original surfactant formulation, while $m_{\text{surf. total}}$ is the total mass of the technical-grade surfactant including cosolvents and additives. Then, the mass fraction of the cosurfactant (D) is calculated by

$$\gamma_D = \frac{m_{\text{co-surf.}}}{m_{\text{water}} + m_{\text{oil}} + m_{\text{surf. total}} + m_{\text{co-surf.}} + m_{\text{gelator}}} \quad (3)$$

The salinity of the microemulsion sample is defined as

$$\varepsilon = \frac{m_{\text{salt}}}{m_{\text{water}} + m_{\text{salt}}} \quad (4)$$

The gelator mass fraction is calculated according to

$$\eta = \frac{m_{\text{gelator}}}{m_{\text{water}} + m_{\text{oil}} + m_{\text{surf. total}} + m_{\text{co-surf.}} + m_{\text{gelator}}} \quad (5)$$

Small-Angle Neutron Scattering (SANS). The microstructure of selected microemulsions was investigated by small-angle neutron

scattering (SANS). The microemulsion samples of $\gamma_C = 0.0521$ and $\gamma_D = 0.0878$ with $\varepsilon = 0$ and $\gamma_C = 0.0689$ and $\gamma_D = 0.0927$ with $\varepsilon = 0.0009$ were measured with the spectrometer NG7 at the National Institute of Standards and Technology (NIST), USA. A neutron wavelength of $\lambda = 6 \text{ \AA}$ with a wavelength spread of $\Delta\lambda/\lambda = 13.8\%$ (full width at half-maximum) was used. To cover a q -range from 0.002 to 0.48 \AA^{-1} , where $q = 4\pi \cdot \sin(\theta/2)/\lambda$ is the absolute value of the scattering vector, we chose the detector/collimation distances of 13.17 m/14.72 m, 4 m/8.52 m, and 1.33 m/5.42 m. The microemulsion samples of $\gamma_C = 0.0232$ and $\gamma_D = 0.0737$ with $\varepsilon = 0$ and $\gamma_C = 0.0522$ and $\gamma_D = 0.0878$ with $\varepsilon = 0.0009$ were measured with the instrument KWS-1 at the Heinz Maier-Leibniz Zentrum (MLZ) in Munich, Germany. Neutron wavelengths of $\lambda = 5$ and 10 \AA with a wavelength spread of $\Delta\lambda/\lambda = 10\%$ were used to cover a q -range from 0.001 to 0.66 \AA^{-1} . The detector/collimation distances were 20 m/20 m, 8 m/20 m, and 1.5 m/8 m. All samples were loaded into 1 mm Hellma quartz QS glass cells and then transferred to a cell holder with a high temperature precision and stability ($\Delta T = \pm 0.02 \text{ K}$). It is ensured that samples have been in the homogeneous one-phase state during measurements by checking each sample before and after the measurement via visual inspection. The recorded scattering intensity was normalized to the absolute scale using the empty beam (for the data from NIST) and using the Plexiglass (for the data from MLZ) as a reference. The raw data treatment, including the subtraction of the dark current and the empty cell scattering, masking, and radial averaging, was performed using the analysis software program IGOR Pro (for the data from NIST) and QtiSAS (for the data from MLZ). The detector dead time and sample transmission were also considered.

Rheology. Oscillatory shear rheometry was carried out with a rheometer Physica MCR 501 from Anton Paar, Austria. We used a plate-plate geometry, of which the upper plate has a diameter of 25 mm. The gap size between the two plates was kept constant at 1 mm according to previous experiments with gelled microemulsions.³ Temperature can be controlled via an external thermostat with a precision of $\Delta T = \pm 0.1 \text{ K}$. First, an amplitude sweep was carried out at $T = 25 \text{ }^\circ\text{C}$ with an angular frequency of $\omega = 10 \text{ s}^{-1}$ and a varied shear stress τ to determine the limit of the linear viscoelastic region (LVE region). For our gelled microemulsion samples, the limit of the LVE region is near $\tau = 40 \text{ Pa}$. Hence, for subsequent measurements, the shear stress is kept constant at $\tau = 10 \text{ Pa}$. Second, oscillation frequency sweeps were performed at $T = 25 \text{ }^\circ\text{C}$ and $\tau = 10 \text{ Pa}$ as a function of the angular frequency ω . Lastly, a temperature sweep was carried out at an angular frequency of $\omega = 10 \text{ s}^{-1}$ and a shear stress of $\tau = 10 \text{ Pa}$, from $T = 25 \text{ }^\circ\text{C}$ to $T = 100 \text{ }^\circ\text{C}$ with a heating rate of 1 K/min to determine the sol–gel transition temperature $T_{\text{sol-gel}}$, i.e., the temperature at which the values of G' and G'' decrease steeply.

Freeze-Fracture Electron Microscopy (FFEM). In order to visualize the structure of the gelled non-toxic microemulsion with a transmission electron microscope, replicas of the specimen were prepared using the Freeze-Fracture and Etching System BAF060 from Leica. A small amount of the gelled microemulsion was placed on the two copper grids between two copper plates (4.5 mm \times 3.0 mm), which were assembled to a so-called sandwich. Sandwiches were quickly frozen in liquid ethane. After fracturing in the liquid nitrogen, the grids with the frozen fractured specimen were fixed on a house-made specimen holder (with a metal cover plate to protect the specimens from contamination in air) and quickly transferred into the vacuum chamber of the BAF060 ($T = -150 \text{ }^\circ\text{C}$). The frozen fractured surface of the specimens was shadowed with platinum-carbon ($\sim 2 \text{ nm}$) at 45° and covered by a layer of pure carbon ($\sim 20 \text{ nm}$) at 90°. The replicas were cleaned with warm ethanol, dried, and examined with an EM10 transmission electron microscope from Zeiss operated at 60 kV.

■ FORMULATING NON-TOXIC MICROEMULSIONS WITH ALKANOYL METHYLGLUCAMIDES

Phase Diagrams. The main task of this study was to formulate highly efficient non-toxic microemulsions using the relatively new class of alkanoyl methylglucamide surfactants.

We chose three technical-grade surfactants, namely, MEGA-8/10, MEGA-12/14-PC, and MEGA-12/14-HC, which differ in the hydrophobic chain length and the composition of the commercial products (see Section **Materials**). To study their ability to form microemulsions, we compare their phase diagrams with those of alkyl polyglucoside-containing microemulsions, which have been measured in our previous study.¹⁷ The used technical-grade alkyl polyglucosides have the trademark Plantacare, namely, Plantacare 810 UP ($C_{8/10}G_{1.5}$), Plantacare 2000 UP ($C_{10}G_{1.5}$), and Plantacare 1200 UP ($C_{12}G_{1.4}$). The influence of alkanoyl methylglucamides on the microemulsion phase behavior was first studied with the scouting system H_2O -*n*-octane-MEGA-8/10-1-octanol and then with the non-toxic system H_2O -isopropyl myristate (IPM)-MEGA-12/14-PC-1,2-octanediol and H_2O -IPM-MEGA-12/14-HC-1,2-octanediol. As explained in Section **Phase Behavior**, the phase behavior of quaternary microemulsion systems at $T = \text{const.}$ is represented in a phase tetrahedron (see Figure 2). We recall that the fishtail point \tilde{X} ($\tilde{\gamma}_C, \tilde{\gamma}_D$) is a measure of the efficiency: the less surfactant and cosurfactant ($\tilde{\gamma}_C + \tilde{\gamma}_D$) the system needs for the formation of the one-phase microemulsion, the higher the efficiency is. Since we intend to gel the one-phase bicontinuous microemulsion, the location of the fishtail point \tilde{X} is of particular interest.

In the scouting system H_2O -*n*-octane-MEGA-8/10-1-octanol (see Figure 3, left), the cosurfactant mass fraction $\tilde{\gamma}_D$ at

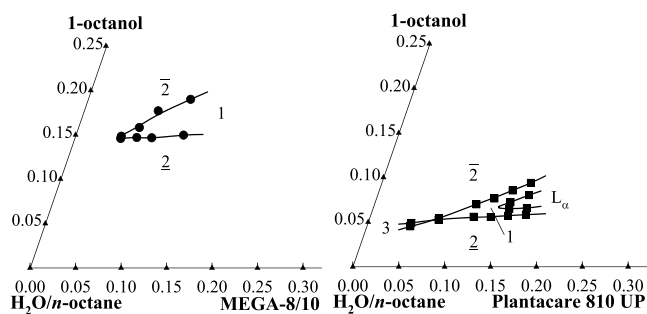


Figure 3. (left) Phase diagram of H_2O -*n*-octane-MEGA-8/10-1-octanol (circles) at $T = 25$ °C, $\phi = 0.50$. (right) Phase diagram of H_2O -*n*-octane-Plantacare 810 UP ($C_{8/10}G_{1.5}$)-1-octanol (squares) at $T = 25$ °C, $\phi = 0.50$.

the fishtail point \tilde{X} is 0.146, which is much higher than the value of 0.051 in the microemulsion H_2O -*n*-octane-Plantacare 810 UP ($C_{8/10}G_{1.5}$)-1-octanol (see Figure 3, right). This means that MEGA-8/10 is substantially more hydrophilic than Plantacare 810 UP. The strong hydrophilicity of MEGA-8/10 is due to the fact that (a) one carbon of the hydrophobic chain of MEGA-8/10 belongs to the amide bond (see Figure 1), i.e., the hydrophobic chain of MEGA-8/10 has one carbon less than Plantacare 810 UP, and (b) the head group is slightly more hydrophilic. However, the amount of the surfactant MEGA-8/10 ($\tilde{\gamma}_C = 0.045$) is smaller than that of Plantacare 810 UP ($\tilde{\gamma}_C = 0.070$). We suppose that the opening glucose head group of MEGA-8/10 allows for the formation of a denser surfactant film leading to a better shielding of the water/oil contact at the interface.

Having understood the influence of the glucamide surfactant on the microemulsion phase behavior in the scouting system, the next step was to study its influence on the non-toxic system. We have found the proper non-toxic components for

the formation of sugar surfactant-containing microemulsions, namely, IPM as the oil and 1,2-octanediol as the cosurfactant.¹⁷ The oil IPM is more polar but has a longer alkyl chain than *n*-octane, which results in a similar equivalent alkane chain number (EACN).²⁹ In addition, the cosurfactant mass fraction $\tilde{\gamma}_D$ should further increase due to the larger monomeric solubility of 1,2-octanediol in IPM. Thus, we used MEGA-12/14-PC and MEGA-12/14-HC with a longer carbon chain length than MEGA-8/10 for the formulation of the non-toxic microemulsion (Figure 4, left). The phase diagrams of

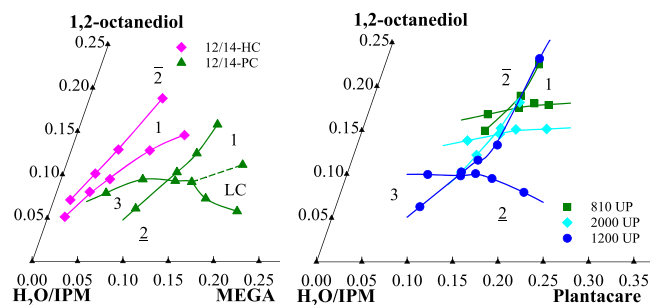


Figure 4. (left) Phase diagrams of H_2O -IPM-MEGA-12/14-PC-1,2-octanediol (green triangles) and H_2O -IPM-MEGA-12/14-HC-1,2-octanediol (pink diamonds) at $T = 25$ °C, $\phi = 0.50$. (right) Phase diagrams of H_2O -IPM-Plantacare 810 UP ($C_{8/10}G_{1.5}$)-1,2-octanediol (green squares), H_2O -IPM-Plantacare 2000 UP ($C_{10}G_{1.5}$)-1,2-octanediol (cyan diamonds), and H_2O -IPM-Plantacare 1200 UP ($C_{12}G_{1.4}$)-1,2-octanediol (blue circles) at $T = 25$ °C, $\phi = 0.50$.¹⁷

the non-toxic microemulsions H_2O -IPM-Plantacare-1,2-octanediol are presented for comparison (Figure 4, right).¹⁷ As the hydrophobic chain of the Plantacare surfactant gets longer, the fishtail points shift downward to the left of the phase diagram, which indicates an efficiency increase in the system. Although MEGA-12/14-PC has a longer alkyl chain than Plantacare 1200 UP both surfactants exhibit similar efficiencies, with fishtail \tilde{X} points of (0.118, 0.094) and (0.121, 0.098), respectively. This similarity can be explained by the molecular structure of MEGA-12/14-PC, i.e. (a) the C-atom that belongs to the head group and (b) the more hydrophilic head group compared to Plantacare 1200 UP (see also the CMC curves in Figure S1 of the Supporting Information, which clearly indicate that the two surfactants have similar surface activities although we could measure only two data points for MEGA-12/14-PC). On the other hand, MEGA-12/14-HC behaves completely different compared to MEGA-12/14-PC and Plantacare 1200 UP. The three-phase region was not found in the microemulsion H_2O -IPM-MEGA-12/14-HC-1,2-octanediol, and the one-phase microemulsion expands down to at least $\gamma_C = 0.0187$ and $\gamma_D = 0.0611$. Thus, compared to the MEGA-12/14-PC-containing microemulsion ($\tilde{\gamma}_C + \tilde{\gamma}_D \approx 0.21$), the efficiency of MEGA-12/14-HC is surprisingly high ($\tilde{\gamma}_C + \tilde{\gamma}_D \leq 0.08$) although both products have the same main active component (see Section **Materials**). Note that the MEGA-12/14-HC-containing samples were opaque at $\gamma_C \approx 0.019$ due to the strong scattering of the bicontinuous microemulsion.

An enormous efficiency improvement and the disappearance of the three-phase region were also observed by Kaler and Silas.³⁰ The surfactant efficiency increased by a factor of 4 in the microemulsion H_2O -*n*-decane- C_8E_3 /didodecyl dimethyl-

lammonium bromide (DDAB) with 2% non-ionic surfactant C_8E_3 in the microemulsion H_2O –*n*-decane– C_8E_3 being replaced by the cationic surfactant DDAB. However, adding a small amount of the salt NaBr to the microemulsion H_2O –*n*-decane– C_8E_3 /DDAB, the efficiency decreased to almost the same as that of the non-ionic surfactant. Thus, Kaler and Silas inferred that the charge of DDAB modified the bending rigidity of the C_8E_3 monolayer (increase in efficiency) and that the addition of NaBr counterbalanced this effect (decrease in efficiency). Inspired by the work of Kaler, we suppose that the technical-grade surfactant contains traces of an ionic component, which leads to a similar effect in the microemulsion H_2O –IPM–MEGA-12/14-HC–1,2-octanediol, i.e., which increases the efficiency compared to the microemulsion H_2O –IPM–MEGA-12/14-PC–1,2-octanediol. If this was the case, then the addition of small amounts of a salt would lead to a decrease in the efficiency.

In order to verify this assumption, microemulsions with salinities of $\epsilon = 0.001, 0.002,$ and 0.005 were prepared. For the sake of clarity, only phase diagrams of H_2O –IPM–MEGA-12/14-HC–1,2-octanediol and H_2O /NaCl–IPM–MEGA-12/14-HC–1,2-octanediol with $\epsilon = 0.001$ are presented in Figure 5,

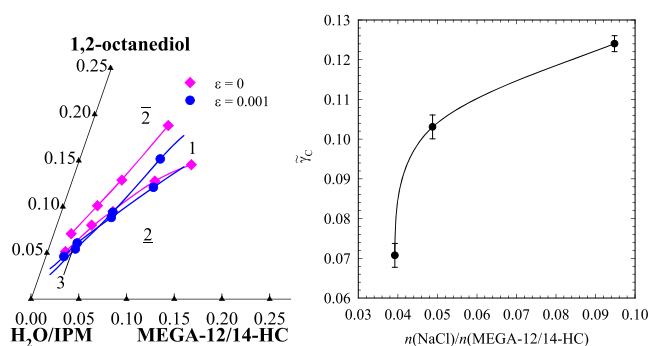


Figure 5. (left) Phase diagrams of H_2O –IPM–MEGA-12/14-HC–1,2-octanediol (pink diamonds) and H_2O /NaCl–IPM–MEGA-12/14-HC–1,2-octanediol with $\epsilon = 0.001$ (blue circles) at $T = 25$ °C, $\phi = 0.50$. (right) Plot of $\tilde{\gamma}_C$ values against the molar ratio of NaCl over MEGA-12/14-HC for the microemulsion H_2O /NaCl–IPM–MEGA-12/14-HC–1,2-octanediol.

left. The phase boundaries of H_2O /NaCl–IPM–MEGA-12/14-HC–1,2-octanediol with $\epsilon = 0.002$ and $\epsilon = 0.005$ have a similar shape to those with $\epsilon = 0.001$ but shift to the right

upper part of the phase diagram (see Figure S2 in the Supporting Information). Fishtail \tilde{X} points of all systems are summarized in Table 1. After adding a salt, the three-phase region appeared, which means that the salt indeed counterbalanced the charge effects in the microemulsion. Moreover, the efficiency of the system decreases as the salinity increases but seems to level off approaching the $\tilde{\gamma}_C$ value of the MEGA-12/14-PC (see Table 1). For a clear view of the efficiency decrease tendency, $\tilde{\gamma}_C$ values at different salinities are plotted against the molar ratio of NaCl over MEGA-12/14-HC (Figure 5, right). These results support our assumption that the exceptional efficiency of MEGA-12/14-HC is caused by an unknown but tiny amount of an ionic amphiphilic component present in the surfactant formulation.

Microstructure Determined via SANS. Since the system H_2O –IPM–MEGA-12/14-HC–1,2-octanediol does not have a three-phase region, it is hard to say whether a bicontinuous microstructure exists in the one-phase microemulsion. Therefore, we carried out small-angle neutron scattering (SANS) experiments to investigate the microstructure as well as to observe the structural change induced by the composition change. For SANS measurements, H_2O is replaced with D_2O to adjust bulk contrast. Generally, phase diagrams presented in volume fractions are supposed to remain almost the same in the deuterated system as in the protonated system. Hence, the salinity of $\epsilon = 0.001$ in the protonated system was adjusted to $\epsilon = 0.0009$ in the deuterated system. We checked the phase boundaries of the deuterated system to ensure that the measured sample exhibits indeed a similar phase behavior (see Figure S3 in the Supporting Information). Four samples with low γ located in the one-phase region were measured: two for the microemulsion D_2O –IPM–MEGA-12/14-HC–1,2-octanediol ($\gamma_C = 0.0521$, $\gamma_D = 0.0878$, and $\phi = 0.50$ and $\gamma_C = 0.0232$, $\gamma_D = 0.0737$, and $\phi = 0.50$) and two for the microemulsion D_2O /NaCl–IPM–MEGA-12/14-HC–1,2-octanediol with $\epsilon = 0.0009$ ($\gamma_C = 0.0689$, $\gamma_D = 0.0927$, and $\phi = 0.50$ and $\gamma_C = 0.0522$, $\gamma_D = 0.0878$, and $\phi = 0.50$). Figure 6 shows the scattering intensity plotted as a function of the scattering vector q in a double logarithmic representation. All four scattering curves have the typical shape known for bicontinuous microemulsions:^{6,31,32} starting from low q values, where the curves show a plateau, a scattering peak is found in the middle q -range before the intensity decreases proportional to q^{-4} , before the incoherent background is reached. The scattering peaks were analyzed with the Teubner–Strey model

Table 1. Summary of the Fishtail \tilde{X} Points (the Intersection Point of the Three-Phase and One-Phase Microemulsions) of All Studied Systems^a

components				\tilde{X} point	
H_2O	oil	surfactant	cosurfactant	$\tilde{\gamma}_C$	$\tilde{\gamma}_D$
	<i>n</i> -octane	MEGA-8/10	1-octanol	0.045	0.146
	<i>n</i> -octane	Plantacare 810 UP ($C_{8/10}G_{1.5}$)	1-octanol	0.070	0.051
	isopropyl myristate	MEGA-12/14-PC	1,2-octanediol	0.118	0.094
	isopropyl myristate	MEGA-12/14-HC	1,2-octanediol		
	isopropyl myristate	Plantacare 810 UP ($C_{8/10}G_{1.5}$)	1,2-octanediol	0.152	0.173
	isopropyl myristate	Plantacare 2000 UP ($C_{10}G_{1.5}$)	1,2-octanediol	0.147	0.144
	isopropyl myristate	Plantacare 1200 UP ($C_{12}G_{1.4}$)	1,2-octanediol	0.121	0.098
NaCl in H_2O ($\epsilon = 0.001$)	isopropyl myristate	MEGA-12/14-HC	1,2-octanediol	0.045	0.078
NaCl in H_2O ($\epsilon = 0.002$)	isopropyl myristate	MEGA-12/14-HC	1,2-octanediol	0.069	0.103
NaCl in H_2O ($\epsilon = 0.005$)	isopropyl myristate	MEGA-12/14-HC	1,2-octanediol	0.085	0.116

^aNote that the volume fraction of oil in the water/oil mixture was adjusted to $\phi = 0.50$.

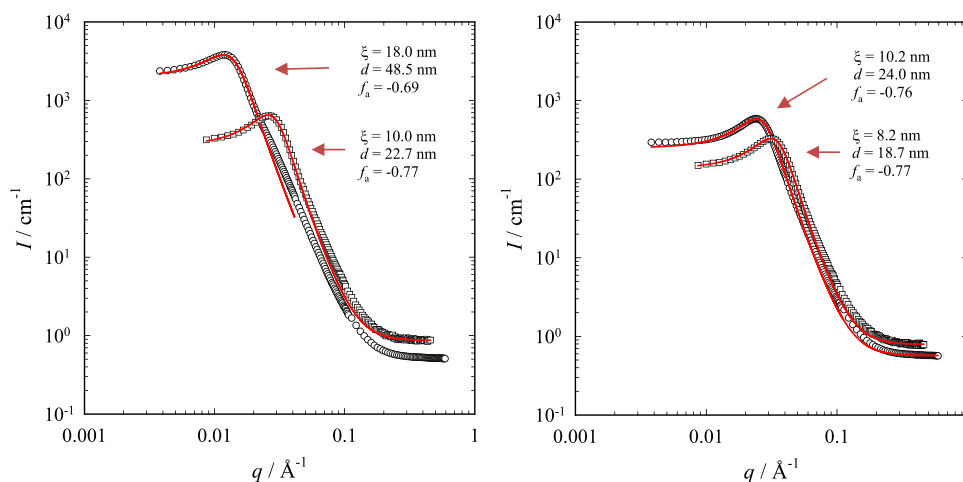


Figure 6. SANS curves of (left) D₂O–IPM–MEGA-12/14-HC–1,2-octanediol with $\gamma_C = 0.0232$, $\gamma_D = 0.0737$, and $\phi = 0.50$ at $T = 24.7$ °C (empty circles) and $\gamma_C = 0.0521$, $\gamma_D = 0.0878$, and $\phi = 0.50$ at $T = 27.0$ °C (empty squares); (right) D₂O/NaCl–IPM–MEGA-12/14-HC–1,2-octanediol with $\gamma_C = 0.0522$, $\gamma_D = 0.0878$, $\varepsilon = 0.0009$, and $\phi = 0.50$ at $T = 25.4$ °C (empty circles) and $\gamma_C = 0.0689$, $\gamma_D = 0.0927$, $\varepsilon = 0.0009$, and $\phi = 0.50$ at $T = 27.0$ °C (empty squares). Red solid lines are Teubner–Strey fits.³¹

Table 2. Composition of the Samples (Volume Fraction of Oil in the Solvent Mixture ϕ , Mass Fraction of the Main Surfactant γ_C , and Mass Fraction of the Cosurfactant γ_D) as well as the Correlation Length ξ_{TS} , the Periodicity d_{TS} , and the Amphiphilicity Factor f_a Obtained from Teubner–Strey Fits of the SANS Data

sample	ϕ	γ_C	γ_D	ξ_{TS}/nm	d_{TS}/nm	f_a
D ₂ O–IPM–MEGA-12/14-HC–1,2-octanediol	0.5017	0.0521	0.0878	10.0	22.7	−0.77
	0.5000	0.0232	0.0737	18.0	48.5	−0.69
D ₂ O/NaCl–IPM–MEGA-12/14-HC–1,2-octanediol ($\varepsilon = 0.0009$)	0.4992	0.0689	0.0927	8.2	18.7	−0.77
	0.5000	0.0522	0.0878	10.2	24.0	−0.76

(see the Supporting Information),³¹ yielding the periodicity of the oil and water domains d_{TS} , the correlation length ξ_{TS} , and the amphiphilicity factor f_a .

The obtained fitting parameters are summarized in Table 2 together with the composition of the samples. Considering at first the scattering curves recorded for the two samples without a salt (Figure 6, left), a strong shift of the correlation peak to larger q values is observed when the surfactant mass fraction is increased from $\gamma_C = 0.0232$ (empty circles) to $\gamma_C = 0.0521$ (empty squares). This result is expected as the distance between surfactant monolayers becomes smaller with increasing surfactant concentration. Accordingly, the periodicity d_{TS} decreases from 48.5 to 22.7 nm. Furthermore, the scattering peak of the sample at $\gamma_C = 0.0521$ is much more pronounced. This indicates that the microstructure is more ordered due to a weaker influence of thermal fluctuations, which softens the amphiphilic film,³³ and thus leads to a more negative amphiphilicity factor f_a . Note that the strong scattering of the very efficient microemulsion ($\gamma_C = 0.0232$) leads to double and multiple scattering contributions visible especially at $q \approx 2q_{\text{max}}$.

A similar trend is observed for the scattering curves of the two microemulsions with a salt (Figure 6, right), i.e., the correlation peak shifts to larger q values when the surfactant mass fraction increased from $\gamma_C = 0.0522$ (empty circles) to $\gamma_C = 0.0689$ (empty squares). Accordingly, both the periodicity and the correlation length decrease. However, due to the smaller difference in the surfactant mass fraction, the shift and the difference in d_{TS} and ξ_{TS} are much smaller. Last but not the least, comparing the scattering curves of the samples with almost the same surfactant mass fraction but without and with a salt ($\gamma_C = 0.0521$, $\gamma_D = 0.0878$, and $\varepsilon = 0$ and $\gamma_C = 0.0522$, γ_D

= 0.0878, and $\varepsilon = 0.0009$), one finds similar values for the periodicity, the correlation length, and the amphiphilicity factor. In summary, the recorded scattering curves indicate that even at very low surfactant mass fractions of $\gamma_C = 0.0232$ and $\gamma_D = 0.0737$, the microemulsion has a bicontinuous microstructure. The large length scale of the structure might be due to an increased bending rigidity of the amphiphilic film. We speculate that this increase is caused by an electrostatic repulsion, which, in turn, is induced by a tiny amount of an ionic amphiphilic component present in the surfactant formulation.³⁰

■ GELLING NON-TOXIC MICROEMULSIONS

Having formulated the highly efficient non-toxic bicontinuous microemulsion H₂O–IPM–MEGA-12/14-HC–1,2-octanediol, we intended to gel this microemulsion with a low molecular weight gelator and to examine its rheological properties. Finally, freeze-fracture electron microscopy (FFEM) was carried out to provide a direct image of the microstructure of the gelled microemulsion.

So far, there are no guiding rules on which low molecular weight gelators gel a specific solvent, i.e., finding a suitable gelator is still trial and error.^{5,34} Since our microemulsion contains equal volumes of water and oil, theoretically, both the hydrogelator and organogelator could be suitable. In our previous study, the hydrogelator *N,N'*-dibenzoyl-L-cystine (DBC) did not gel the non-toxic microemulsion H₂O–IPM–Plantacare 1200 UP–1,2-octanediol at 2 wt % but shifted the phase boundaries to a larger amount of the cosurfactant. On the other hand, the organogelator 1,3:2,4-dibenzylidene-D-sorbitol (DBS) gelled the non-toxic micro-

emulsion at 0.3 wt %, and the phase boundaries remained unchanged.¹⁷ In the non-toxic microemulsion studied here (H₂O–IPM–MEGA-12/14-PC–1,2-octanediol), the hydrogelator DBC also did not gel the system even at a gelator concentration as high as 3.0 wt % but shifted the phase boundaries to a larger amount of the cosurfactant (see Figure S4 in the Supporting Information), which is consistent with the results for the glucoside-containing microemulsion. On the other hand, DBS gelled the non-toxic microemulsion H₂O–IPM–MEGA-12/14-HC–1,2-octanediol, and the phase boundaries remain unchanged (Figure 7), which is also consistent

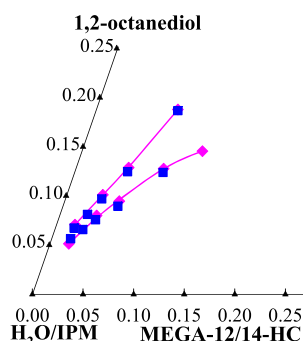


Figure 7. Phase diagrams of the non-gelled microemulsion H₂O–IPM–MEGA-12/14-HC–1,2-octanediol (pink diamonds) and the gelled microemulsion in the presence of DBS (blue squares) at $\eta = 0.003$, $T = 25$ °C, and $\phi = 0.50$.

with the results for the glucoside-containing microemulsion. The gelled microemulsion even forms at very low surfactant concentration ($\gamma_C = 0.019$ and $\gamma_D = 0.06$, the left bottom end on the phase diagram). As already mentioned in connection with Figure 4 (left), the sample was opaque due to the strong scattering of the bicontinuous microemulsion. Nevertheless, the gelled one-phase microemulsion was distinguishable from a gelled two-phase microemulsion.

After the formulation of the gelled non-toxic bicontinuous microemulsion, we performed oscillatory shear rheometry to examine the rheological properties. For this purpose, two compositions located in the middle of the one-phase region

were chosen, namely, $\gamma_C = 0.0363$ and $\gamma_D = 0.0885$ and $\gamma_C = 0.0538$ and $\gamma_D = 0.1042$ in the presence of DBS at $\eta = 0.003$. The linear viscoelastic region (LVE) was determined in the preliminary amplitude sweep, and the shear stress was set at $\tau = 10$ Pa for the subsequent frequency sweep (Figure 8). The storage modulus G' is about one order of magnitude larger than the loss modulus G'' over the entire frequency range, and both moduli show only very weak frequency dependence. The results show that the samples are indeed gelled. Subsequently, a temperature sweep was carried out to characterize the sol–gel transition temperature $T_{\text{sol-gel}}$ (Figure 9). For both samples, it is around 82 °C, where the storage modulus G' drops sharply and crosses the loss modulus G'' . We thus conclude that the sol–gel transition temperature is $T_{\text{sol-gel}} \approx 82$ °C. The rheological properties of both samples do not differ significantly, which supports our assumption that our gelled non-toxic microemulsion is an orthogonal self-assembled system: (a) the gelator does not influence the phase behavior; (b) the bicontinuous microemulsion “only” acts as a solvent for the gelator, i.e., the rheological properties are determined by the gelator.

To further study the microstructure of this new type of a gelled non-toxic bicontinuous microemulsion, we used freeze-fracture electron microscopy (FFEM). The system of choice was H₂O–IPM–MEGA-12/14-HC–1,2-octanediol ($\gamma_C = 0.0276$, $\gamma_D = 0.0774$, and $\phi = 0.50$) in the presence of DBS at $\eta = 0.003$. Note that the surfactant mass fraction was chosen to be slightly larger than the one used in the SANS experiment to provide a wider one-phase region for the FFEM sample preparation. The two representative FFEM pictures shown in Figure 10 clearly prove the coexistence of both twisted gel fibers (red arrows) and bicontinuously structured regions (yellow circles). The gel fibers have diameters of $d_{\text{fibril}} \approx 8$ –12 nm, which is consistent with the results obtained for the system H₂O–C₁₂E₇ in the presence of DBS at $\eta = 0.0075$ and $\eta = 0.015$.³⁵ However, unlike the dense bundles of gel fibers in the system H₂O–C₁₂E₇–DBS, the gel fibers in the system at hand are sparsely distributed (Figure 10, left) due to the very low gelator concentration ($\eta = 0.003$). Moreover, the length scale of the bicontinuous structure agrees almost quantitatively with the diameter of the water and oil domains, respectively,

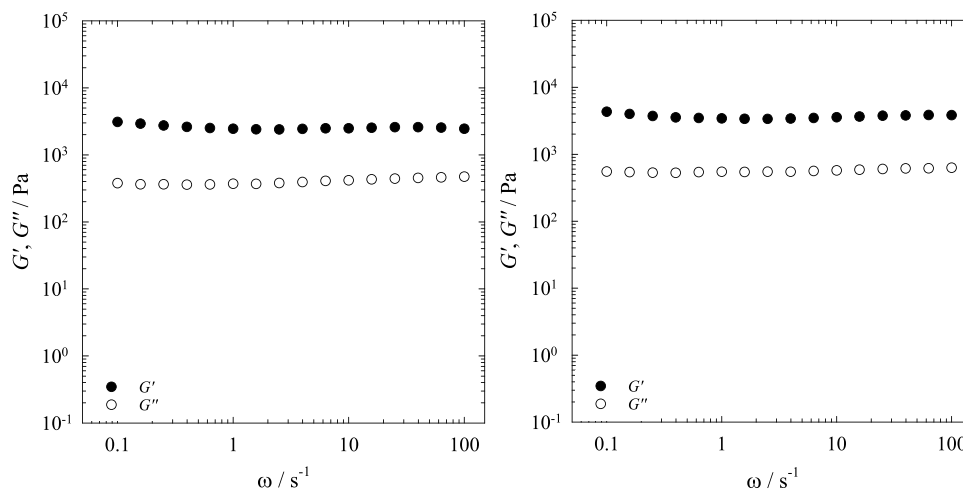


Figure 8. Storage modulus G' (filled symbols) and loss modulus G'' (open symbols) of the gelled bicontinuous microemulsion H₂O–IPM–MEGA-12/14-HC–1,2-octanediol in the presence of DBS at $\eta = 0.003$, $\tau = 10$ Pa, and $T = 25$ °C as a function of ω with the composition of (left) $\gamma_C = 0.0363$, $\gamma_D = 0.0885$, and $\phi = 0.50$ and (right) $\gamma_C = 0.0538$, $\gamma_D = 0.1042$, and $\phi = 0.50$.

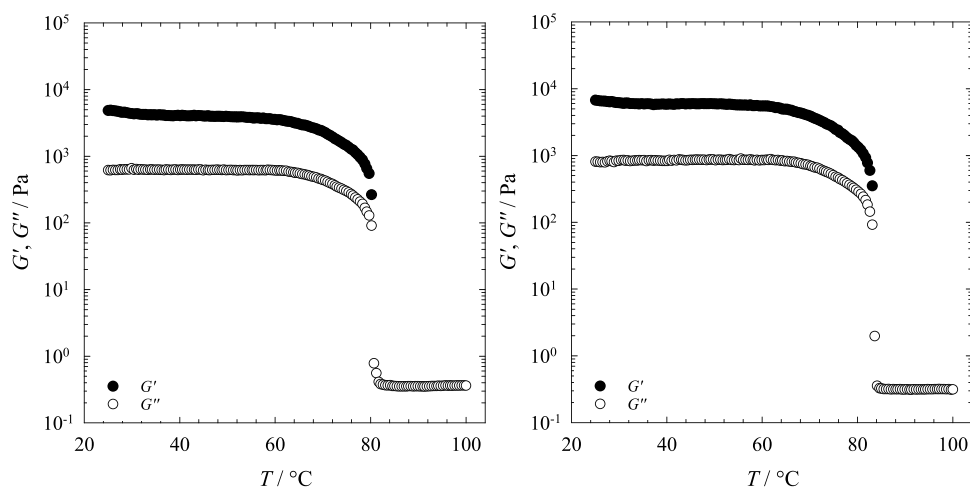


Figure 9. Storage modulus G' (filled symbols) and loss modulus G'' (open symbols) of the gelled bicontinuous microemulsion H_2O –IPM–MEGA-12/14-HC–1,2-octanediol in the presence of DBS at $\eta = 0.003$, $\tau = 10$ Pa, and $\omega = 10$ s $^{-1}$ as a function of T and a heating rate of 1 °C min $^{-1}$ with the composition of (left) $\gamma_C = 0.0363$, $\gamma_D = 0.0885$, and $\phi = 0.50$ and (right) $\gamma_C = 0.0538$, $\gamma_D = 0.1042$, and $\phi = 0.50$.

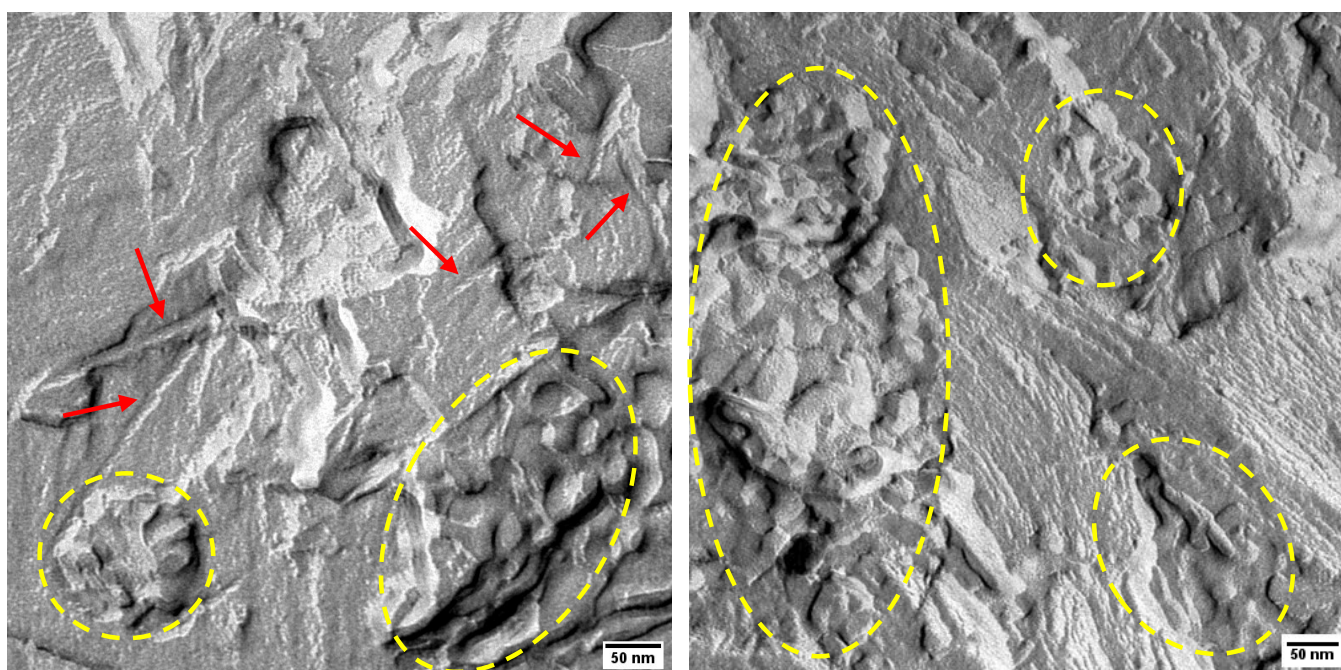


Figure 10. FFEM pictures of the gelled bicontinuous microemulsion H_2O –IPM–MEGA-12/14-HC–1,2-octanediol in the presence of DBS at $\eta = 0.003$ with the composition of $\gamma_C = 0.0276$, $\gamma_D = 0.0774$, and $\phi = 0.50$. The red arrows point at the gel fibers, and the yellow circles show the bicontinuous microstructure.

obtained from SANS ($d_{\text{TS}}/2 \approx 24$ nm for a very similar sample). A closer inspection of the FFEM picture on the right side of Figure 10 reveals the existence of lamellar structured regions with a smaller periodicity. This finding suggests a partial phase separation of the sample during the FFEM sample preparation.

To conclude, not only the rheological and SANS measurements but also the freeze-fracture electron microscopy (FFEM) pictures show that this new type of a gelled non-toxic bicontinuous microemulsion is an orthogonal self-assembled system, i.e., both the gel fibers and the microemulsion structure form simultaneously but independently.

CONCLUSION AND OUTLOOK

Gelled non-toxic bicontinuous microemulsions are interesting for transdermal drug delivery because the microemulsion facilitates the solubilization of both hydrophilic and hydrophobic drugs, while the gel network provides mechanical stability and an easy application. In our previous study, we formulated such a gelled system with H_2O –IPM–Plantacare 1200 UP ($\text{C}_{12}\text{G}_{1.4}$)–1,2-octanediol in the presence of 0.3 wt % DBS.¹⁷ However, a large amount of Plantacare 1200 UP (12 wt %) is needed to form a bicontinuous microemulsion. To overcome this drawback, we studied a relatively new class of surfactants, namely, alkanoyl methylglucamides. Unexpectedly, the efficiency increased largely, while both the bicontinuous microstructure and the gel fibrillar network remained unchanged.

Since there are only very few studies about the phase behavior of alkanoyl methylglucamide (MEGA), we first compared MEGA-8/10 with the alkyl polyglucoside surfactant Plantacare 810 UP ($C_{8/10}G_{1.5}$) in the scouting system H_2O -*n*-octane-surfactant-1-octanol. We found MEGA-8/10 to be substantially more hydrophilic than Plantacare 810 UP. Subsequently, we compared MEGA-12/14-PC and MEGA-12/14-HC (both have the same hydrophobic chain length but differ in the formulations) with Plantacare 1200 UP ($C_{12}G_{1.4}$) in the non-toxic microemulsions H_2O -IPM-surfactant-1,2-octanediol. Although the methylglucamide head group is more hydrophilic than the glucoside head group, MEGA-12/14-PC and Plantacare 1200 UP have similar efficiencies due to a slightly longer carbon chain length of MEGA-12/14-PC. On the other hand, MEGA-12/14-HC has an exceptional efficiency of $\tilde{\gamma}_C + \tilde{\gamma}_D \leq 0.08$ but, surprisingly, does not form a three-phase region. The three-phase region appears after adding a small amount of a salt, which, in turn, decreases the efficiency of the system. We thus speculate that the exceptional efficiency of MEGA-12/14-HC is caused by an electrostatic repulsion, which is induced by a tiny amount of an ionic amphiphilic component in the surfactant formulation.

After formulating the highly efficient non-toxic bicontinuous microemulsion, its bicontinuous microstructure was confirmed by small-angle neutron scattering (SANS) and freeze-fracture electron microscopy (FFEM), from which a periodicity of $d \approx 48$ nm could be determined. Furthermore, the system H_2O -IPM-MEGA-12/14-HC-1,2-octanediol was gelled by the low molecular weight organogelator 1,3:2,4-dibenzylidene-D-sorbitol (DBS) at 0.3 wt %. The phase boundaries of the gelled bicontinuous microemulsion remain unchanged compared to the non-gelled counterpart. The gelled bicontinuous microemulsions displayed the typical rheological behavior of gels with a sol-gel transition temperature of $T_{\text{sol-gel}} \approx 82$ °C. In conclusion, all experimental results suggest that the new type of an efficient gelled non-toxic bicontinuous microemulsion is an orthogonal self-assembled system, i.e., the gel fibrillar network and the bicontinuous microstructure form simultaneously but independently: (a) the gelator does not influence the phase behavior of the microemulsion; (b) the rheological properties of the gelled microemulsion are determined by the gelator and are independent of the microemulsion composition; (c) the bicontinuous oil and water domains coexist with twisted gel fibers as seen in the FFEM pictures.

In future studies, we will solubilize both hydrophilic and hydrophobic drugs in gelled non-toxic bicontinuous microemulsions and carry out skin permeability tests. Furthermore, we will investigate the rheological behavior and structure of gelled non-toxic bicontinuous microemulsions at various water-to-oil ratios. The main open question is whether DBS can be used for both water-rich and oil-rich microemulsions. If not, a proper gelator needs to be searched for in the first place. The final goal is to know how to formulate an efficient gelled non-toxic bicontinuous microemulsion whose water and oil content can be adjusted as required.

■ ASSOCIATED CONTENT

SI Supporting Information

The Supporting Information is available free of charge at <https://pubs.acs.org/doi/10.1021/acs.langmuir.0c02314>.

CMC curves of alkanoyl methylglucamides, phase diagrams of H_2O -IPM-MEGA-12/14-PC-1,2-octane-

diol at different salinities, location of SANS and FFEM samples on the phase diagram, Teubner-Strey model for SANS fittings, and gelling H_2O -IPM-MEGA-12/14-PC-1,2-octanediol with *N,N'*-dibenzoyl-L-cystine (DBC) (PDF)

■ AUTHOR INFORMATION

Corresponding Author

Cosima Stubenrauch – Institute of Physical Chemistry, University of Stuttgart, 70569 Stuttgart, Germany; orcid.org/0000-0002-1247-4006; Phone: +49-711-685 64470; Email: cosima.stubenrauch@ipc.uni-stuttgart.de

Authors

Ke Peng – Institute of Physical Chemistry, University of Stuttgart, 70569 Stuttgart, Germany
Natalie Preisig – Institute of Physical Chemistry, University of Stuttgart, 70569 Stuttgart, Germany
Thomas Sottmann – Institute of Physical Chemistry, University of Stuttgart, 70569 Stuttgart, Germany; orcid.org/0000-0003-3679-3703

Complete contact information is available at: <https://pubs.acs.org/10.1021/acs.langmuir.0c02314>

Author Contributions

The manuscript was written through contributions of all authors. All authors have given approval to the final version of the manuscript.

Notes

The authors declare no competing financial interest.

■ ACKNOWLEDGMENTS

We thank Dr. Natascha Schelero from Clariant GmbH for providing the alkanoyl methylglucamide surfactants. We also thank Shih-Yu Tseng, Karina Abitayev, and Diana Zauser for their valuable help with the SANS measurements. Furthermore, we would like to acknowledge the National Institute of Standards and Technology (NIST) in the USA and the Heinz Maier-Leibniz Zentrum (MLZ) in Munich, Germany for providing the facilities for the SANS measurements and the valuable support of the local contacts Dr. Yun Liu (NIST) and Dr. Henrich Frielinghaus (MLZ).

■ ABBREVIATIONS

CMC, critical micelle concentration; DBC, *N,N'*-dibenzoyl-L-cystine; DBS, 1,3:2,4-dibenzylidene-D-sorbitol; FFEM, freeze-fracture electron microscopy; IPM, isopropyl myristate; MEGA, alkanoyl methylglucamide; SANS, small-angle neutron scattering

■ REFERENCES

- Stubenrauch, C.; Gießelmann, F. Gelled Complex Fluids: Combining Unique Structures with Mechanical Stability. *Angew. Chem., Int. Ed.* **2016**, *55*, 3268–3275.
- Laibinis, P. E.; Hickman, J. J.; Wrighton, M. S.; Whitesides, G. M. Orthogonal Self-Assembled Monolayers: Alkanethiols on Gold and Alkane Carboxylic Acids on Alumina. *Science* **1989**, *245*, 845–847.
- Laupheimer, M.; Jovic, K.; Antunes, F. E.; da Graça Martins Miguel, M.; Stubenrauch, C. Studying Orthogonal Self-Assembled Systems: Phase Behaviour and Rheology of Gelled Microemulsions. *Soft Matter* **2013**, *9*, 3661.

- (4) Laupheimer, M.; Sottmann, T.; Schweins, R.; Stubenrauch, C. Studying Orthogonal Self-Assembled Systems: Microstructure of Gelled Bicontinuous Microemulsions. *Soft Matter* **2014**, *10*, 8744–8757.
- (5) Weiss, R. G. The Past, Present, and Future of Molecular Gels. What Is the Status of the Field, and Where Is It Going? *J. Am. Chem. Soc.* **2014**, *136*, 7519–7530.
- (6) Strey, R. Microemulsion Microstructure and Interfacial Curvature. *Colloid Polym. Sci.* **1994**, *272*, 1005–1019.
- (7) Heuschkel, S.; Goebel, A.; Neubert, R. H. H. Microemulsions—Modern Colloidal Carrier for Dermal and Transdermal Drug Delivery. *J. Pharm. Sci.* **2008**, *97*, 603–631.
- (8) Kreilgaard, M.; Pedersen, E. J.; Jaroszewski, J. W. NMR Characterisation and Transdermal Drug Delivery Potential of Microemulsion Systems. *J. Controlled Release* **2000**, *69*, 421–433.
- (9) Kreilgaard, M. Influence of Microemulsions on Cutaneous Drug Delivery. *Adv. Drug Delivery Rev.* **2002**, *54*, 77–98.
- (10) Kogan, A.; Garti, N. Microemulsions as Transdermal Drug Delivery Vehicles. *Adv. Colloid Interface Sci.* **2006**, *123-126*, 369–385.
- (11) Callender, S. P.; Mathews, J. A.; Kobernyk, K.; Wettig, S. D. Microemulsion Utility in Pharmaceuticals: Implications for Multi-Drug Delivery. *Int. J. Pharm.* **2017**, *526*, 425–442.
- (12) Kahlweit, M.; Busse, G.; Faulhaber, B. Preparing Microemulsions with Lecithins. *Langmuir* **1995**, *11*, 1576–1583.
- (13) Kahlweit, M.; Busse, G.; Faulhaber, B. Preparing Microemulsions with Alkyl Monoglucosides and the Role of N-Alkanols. *Langmuir* **1995**, *11*, 3382–3387.
- (14) Kahlweit, M.; Busse, G.; Faulhaber, B.; Eibl, H. Preparing Nontoxic Microemulsions. *Langmuir* **1995**, *11*, 4185–4187.
- (15) Kahlweit, M.; Busse, G.; Faulhaber, B. Preparing Nontoxic Microemulsions with Alkyl Monoglucosides and the Role of Alkanediols as Cosolvents. *Langmuir* **1996**, *12*, 861–862.
- (16) Kahlweit, M.; Busse, G.; Faulhaber, B. Preparing Nontoxic Microemulsions. 2. *Langmuir* **1997**, *13*, 5249–5251.
- (17) Peng, K.; Sottmann, T.; Stubenrauch, C. Gelled Non-Toxic Microemulsions: Phase Behavior & Rheology. *Soft Matter* **2019**, *15*, 8361–8371.
- (18) Okesola, B. O.; Vieira, V. M. P.; Cornwell, D. J.; Whitelaw, N. K.; Smith, D. K. 1,3:2,4-Dibenzylidene-D-Sorbitol (DBS) and Its Derivatives – Efficient, Versatile and Industrially-Relevant Low-Molecular-Weight Gelators with over 100 Years of History and a Bright Future. *Soft Matter* **2015**, *11*, 4768–4787.
- (19) Sottmann, T.; Kluge, K.; Strey, R.; Reimer, J.; Söderman, O. General Patterns of the Phase Behavior of Mixtures of H₂O, Alkanes, Alkyl Glucosides, and Cosurfactants. *Langmuir* **2002**, *18*, 3058–3067.
- (20) Reimer, J.; Söderman, O.; Sottmann, T.; Kluge, K.; Strey, R. Microstructure of Alkyl Glucoside Microemulsions: Control of Curvature by Interfacial Composition. *Langmuir* **2003**, *19*, 10692–10702.
- (21) Jakobs, B.; Sottmann, T.; Strey, R.; Allgaier, J.; Willner, L.; Richter, D. Amphiphilic Block Copolymers as Efficiency Boosters for Microemulsions. *Langmuir* **1999**, *15*, 6707–6711.
- (22) Sottmann, T. Solubilization Efficiency Boosting by Amphiphilic Block Co-Polymers in Microemulsions. *Curr. Opin. Colloid Interface Sci.* **2002**, *7*, 57–65.
- (23) Söderman, O.; Johansson, I. Polyhydroxyl-Based Surfactants and Their Physico-Chemical Properties and Applications. *Curr. Opin. Colloid Interface Sci.* **1999**, *4*, 391–401.
- (24) Hill, K.; Rhode, O. Sugar-Based Surfactants for Consumer Products and Technical Applications. *Fett-Lipid* **1999**, *101*, 25–33.
- (25) Yang, X. D.; Gao, Y. H.; Chai, J. L.; Wang, Z. N.; Qin, C. K. Studies on the Middle-Phase Microemulsion of Lauric-N-Methylglucamide. *Colloid J.* **2007**, *69*, 252–258.
- (26) Yang, X.; Li, H.; Chai, J.; Gao, Y.; Chen, J.; Lou, A. Phase Behavior Studies of Quaternary Systems Containing N-Lauroyl-N-Methylglucamide/Alcohol/Alkane/Water. *J. Colloid Interface Sci.* **2008**, *320*, 283–289.
- (27) Yang, X.; Zhang, H.; Shi, C.; Chai, J. Middle-Phase Microemulsions Formed by n-Dodecyl Polyglucoside and Lauric-N-Methylglucamide. *J. Dispersion Sci. Technol.* **2013**, *34*, 147–152.
- (28) Kluge, K.; Stubenrauch, C.; Sottmann, T.; Strey, R. Temperature-Insensitive Microemulsions Formulated from Octyl Monoglucoside and Alcohols: Potential Candidates for Practical Applications. *Tenside Surf. Det.* **2001**, *38*, 30–40.
- (29) Aubry, J. M.; Ontiveros, J. F.; Salager, J. L.; Nardello-Rataj, V. Use of the Normalized Hydrophilic-Lipophilic-Deviation (HLD_N) Equation for Determining the Equivalent Alkane Carbon Number (EACN) of Oils and the Preferred Alkane Carbon Number (PACN) of Nonionic Surfactants by the Fish-Tail Method (FTM). *Adv. Colloid Interface Sci.* **2020**, *276*, 102099.
- (30) Silas, J. A.; Kaler, E. W. The Phase Behavior and Microstructure of Efficient Cationic–Nonionic Microemulsions. *J. Colloid Interface Sci.* **2001**, *243*, 248–254.
- (31) Teubner, M.; Strey, R. Origin of the Scattering Peak in Microemulsions. *J. Chem. Phys.* **1987**, *87*, 3195–3200.
- (32) Sottmann, T.; Strey, R. Ultralow Interfacial Tensions in Water–n-Alkane–Surfactant Systems. *J. Chem. Phys.* **1997**, *106*, 8606–8615.
- (33) Morse, D. C. Topological Instabilities and Phase Behavior of Fluid Membranes. *Phys. Rev. E* **1994**, *50*, R2423.
- (34) Draper, E. R.; Adams, D. J. Low-Molecular-Weight Gels: The State of the Art. *Chem* **2017**, *3*, 390–410.
- (35) Steck, K.; Preisig, N.; Stubenrauch, C. Gelling Lyotropic Liquid Crystals with the Organogelator 1,3:2,4-Dibenzylidene-D-Sorbitol Part II: Microstructure. *Langmuir* **2019**, *35*, 17142–17149.

Formulation of gelled non-toxic bicontinuous microemulsions stabilized by highly efficient alkanoyl methylglucamides

*Ke Peng, Natalie Preisig, Thomas Sottmann, Cosima Stubenrauch**

Institute of Physical Chemistry, University of Stuttgart, Pfaffenwaldring 55, 70569 Stuttgart, Germany, *cosima.stubenrauch@ipc.uni-stuttgart.de

Table of Contents

S1. CMC curves of alkanoyl methylglucamides.....	2
S2. H ₂ O–IPM–MEGA-12/14-PC–1,2-octanediol at different salinities.....	3
S3. The location of SANS and FFEM samples on the phase diagram	3
S4. The Teubner–Strey Model for SANS fittings.....	4
S5. Gelling H ₂ O–IPM–MEGA-12/14-PC–1,2-octanediol with DBC	5

S1. CMC curves of alkanoyl methylglucamides

The surface tension isotherms were measured at room temperature with the Du Noüy ring method on an STA1 tensiometer from Sinterface Technologies. For each system, a 100 mL stock solution with a surfactant concentration above the CMC (critical micelle concentration) was prepared. All solutions were prepared with bi-distilled water. For each measurement, 10 mL stock solution was used for rinsing the glassware, and 20 mL stock solution was used for the measurement. The measuring time was set to 15 min. After each measurement, the stock solution flask was filled up with water, and the diluted surfactant solution was used for the next measurement. The CMC values are $\sim 0.26 \text{ g}\cdot\text{L}^{-1}$ for MEGA-8/10, $\sim 0.026 \text{ g}\cdot\text{L}^{-1}$ for MEGA-12/14-HC, and $\sim 0.016 \text{ g}\cdot\text{L}^{-1}$ for Plantacare 1200 UP. The CMC of MEGA-12/14-PC could not be measured due to the low solubility of the surfactant. The surface tension values at two concentrations only are shown in Figure S1.

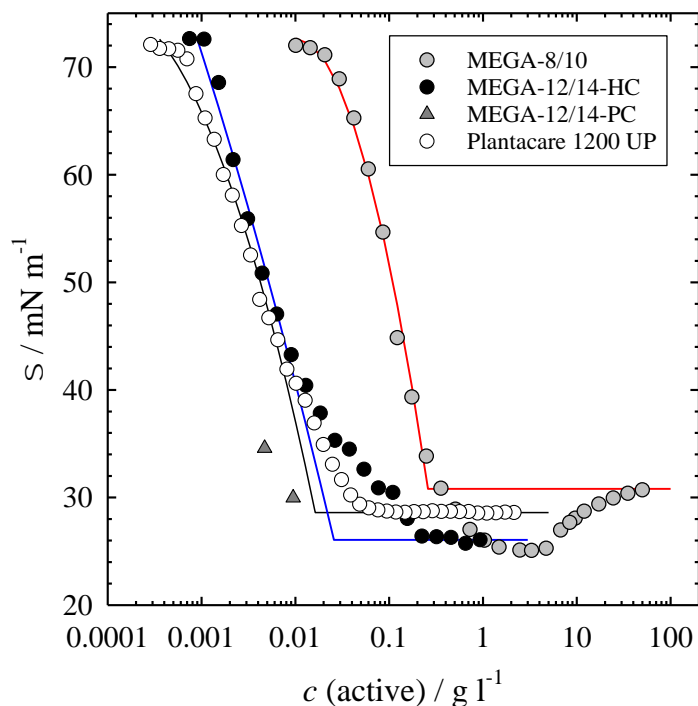


Figure S1. Surface tension σ as a function of the surfactant concentration c (calculated by active content) for aqueous solutions of MEGA-8/10 (light grey circles), MEGA-12/14-HC (black circles), MEGA-12/14-PC (dark grey triangles), and Plantacare 1200 UP (white circles). Solid lines below the CMC represent second-order polynomial fits of the experimental data.

S2. H₂O–IPM–MEGA-12/14-PC–1,2-octanediol at different salinities

A 1-phase microemulsion of H₂O–isopropyl myristate (IPM)–MEGA-12/14-HC–1,2-octanediol can be found even at very low surfactant concentrations. However, adding a small amount of salt ($\varepsilon = 0.002$) led to an efficiency decrease and the 3-phase region appeared (Figure S2). With more salt added to the system ($\varepsilon = 0.005$), the efficiency further decreased.

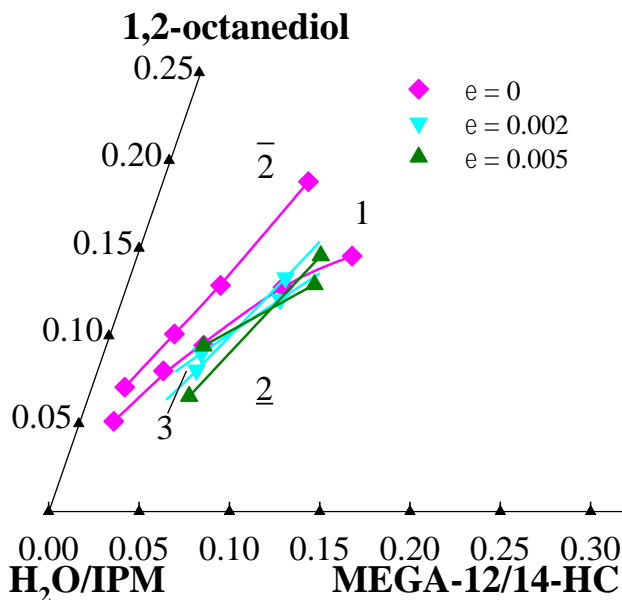


Figure S2. Phase diagrams of H₂O–IPM–MEGA-12/14-HC–1,2-octanediol (pink diamonds), H₂O/NaCl–IPM–MEGA-12/14-HC–1,2-octanediol with $\varepsilon = 0.002$ (cyan triangles down) and $\varepsilon = 0.005$ (green triangles up) at $T = 25^\circ\text{C}$, $\phi = 0.50$.

S3. The location of SANS and FFEM samples on the phase diagram

The phase boundaries of the deuterated system were measured to ensure that the prepared SANS sample was in the 1-phase region. Theoretically, the deuterated samples with equivalent volume fractions have the same phase behavior as the protonated samples. In

Figure S3 the phase boundaries of the protonated system and the deuterated system are presented in volume fractions, without salt (left) and with salt (right), respectively. The phase behavior of the deuterated system is consistent with that of the protonated system, but the 1-phase region is slightly narrowed down. The location of the SANS samples and the FFEM sample was marked in

the figure. Please note that $\varepsilon = 0.0009$ in the D_2O system is equivalent to $\varepsilon = 0.001$ in the H_2O system.

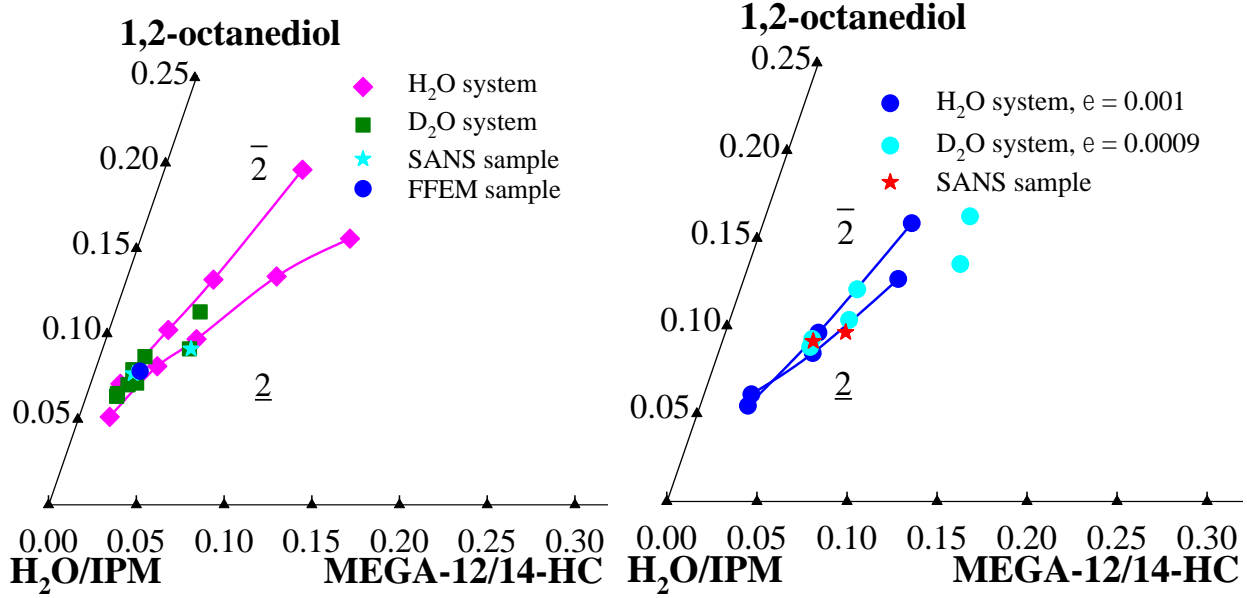


Figure S3. (left) Phase diagrams of H_2O –IPM–MEGA-12/14-PC–1,2-octanediol (pink diamonds) and D_2O –IPM–MEGA-12/14-HC–1,2-octanediol (green squares) presented in volume fractions at $T = 25^\circ C$, $\phi = 0.50$, the location of SANS samples are presented in cyan star and FFEM sample in blue circle; (right) Phase diagrams of $H_2O/NaCl$ –IPM–MEGA-12/14-PC–1,2-octanediol (blue circles) with $\varepsilon = 0.001$ and $D_2O/NaCl$ –IPM–MEGA-12/14-HC–1,2-octanediol (cyan circles) with $\varepsilon = 0.0009$ presented in volume fractions at $T = 25^\circ C$, $\phi = 0.50$, the location of SANS samples are presented in red star.

S4. The Teubner–Strey Model for SANS fittings

The Teubner–Strey Model³¹ describes the characteristic peak of a bicontinuous microemulsion with:

$$I(q) = \frac{8\pi c_2 \phi_a \phi_b (\Delta\rho)^2 / \xi_{TS}}{a_2 + c_1 q^2 + c_2 q^4} + I_{incoh}, \quad (1)$$

where I_{incoh} is the incoherent background, $\Delta\rho$ is the scattering length density difference of the two subphases, and ϕ_a and ϕ_b are their respective volume fractions. The parameters a_2 , c_1 and c_2 are coefficients derived from a Landau–Ginzburg order parameter expansion of the local free energy density, where the order parameter is the water-to-oil ratio. After determining the values of a_2 , c_1

and c_2 , two characteristic length scales of the Teubner–Strey model can be calculated, namely the correlation length

$$\xi_{\text{TS}} = \left[\frac{1}{2} \left(\frac{a_2}{c_2} \right)^{1/2} + \frac{c_1}{4c_2} \right]^{-1/2}, \quad (2)$$

the periodicity of the oil and water domains, i.e., the domain spacing

$$d_{\text{TS}} = 2\pi \left[\frac{1}{2} \left(\frac{a_2}{c_2} \right)^{1/2} - \frac{c_1}{4c_2} \right]^{-1/2}, \quad (3)$$

and the amphiphilicity factor

$$f_a = \frac{c_1}{\sqrt{4a_2c_2}}. \quad (4)$$

S5. Gelling H₂O–IPM–MEGA-12/14-PC–1,2-octanediol with DBC

The microemulsion H₂O–IPM–MEGA-12/14-PC–1,2-octanediol could not be gelled with *N, N'*-dibenzoyl-L-cystine (DBC), not even at a gelator content of 3 wt %. We only found that the phase boundaries were shifted upwards. The effect of DBC on the phase boundaries is consistent with that observed for the system H₂O–IPM–Plantacare 1200 UP (C₁₂G_{1.4})–1,2-octanediol.¹⁷

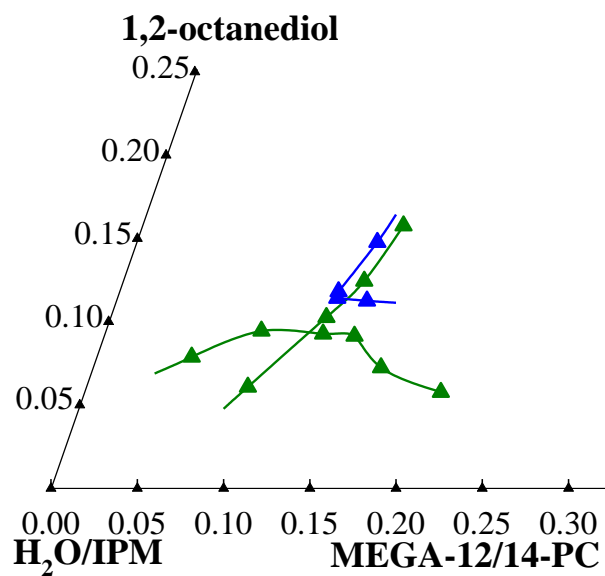


Figure S4. Phase diagrams of the microemulsion H₂O–IPM–MEGA-12/14-PC–1,2-octanediol in the absence (green triangles) and in the presence of DBC (blue triangles) at $\eta = 0.03$, $T = 25^\circ\text{C}$, $\phi = 0.50$.

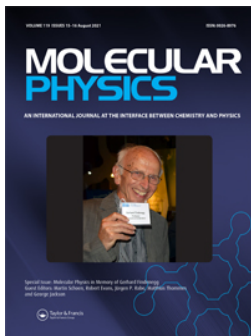
Publication III

Gelled Non-Toxic Bicontinuous Microemulsions as Promising Transdermal Drug Carriers

Ke Peng, Thomas Sottmann, Cosima Stubenrauch
Mol. Phys. **2021**, *119* (15–16), e1886363.

DOI: 10.1080/00268976.2021.1886363

Reprinted with permission from [Pen21a]. Copyright © 2021 Taylor & Francis Group.



Molecular Physics

An International Journal at the Interface Between Chemistry and Physics

ISSN: (Print) (Online) Journal homepage: <https://www.tandfonline.com/loi/tmph20>

Gelled non-toxic bicontinuous microemulsions as promising transdermal drug carriers

Ke Peng, Thomas Sottmann & Cosima Stubenrauch

To cite this article: Ke Peng, Thomas Sottmann & Cosima Stubenrauch (2021) Gelled non-toxic bicontinuous microemulsions as promising transdermal drug carriers, Molecular Physics, 119:15-16, e1886363, DOI: [10.1080/00268976.2021.1886363](https://doi.org/10.1080/00268976.2021.1886363)

To link to this article: <https://doi.org/10.1080/00268976.2021.1886363>



Published online: 18 Feb 2021.



Submit your article to this journal [↗](#)



Article views: 132



View related articles [↗](#)



View Crossmark data [↗](#)

Gelled non-toxic bicontinuous microemulsions as promising transdermal drug carriers

Ke Peng , Thomas Sottmann  and Cosima Stubenrauch 

Institute of Physical Chemistry, University of Stuttgart Stuttgart, Germany

ABSTRACT

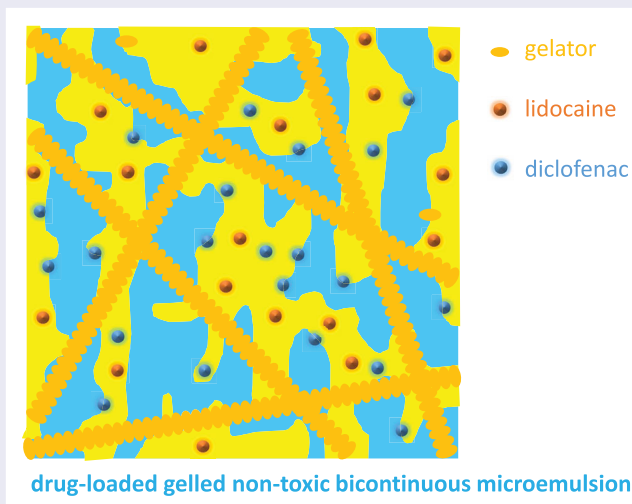
Gelled non-toxic bicontinuous microemulsions have great potentials in transdermal drug delivery. The bicontinuous microemulsion provides optimum drug solubilisation and promotes skin permeation, while the gel network provides mechanical stability and an easy application. For the first time, we have formulated such a gelled non-toxic bicontinuous microemulsion consisting of H₂O, isopropyl myristate (IPM), the non-ionic sugar-based surfactant Plantacare 1200 UP (C₁₂G_{1.4}), 1,2-octanediol, and the low molecular weight gelator 1,3:2,4-dibenzylidene-D-sorbitol (DBS). In this study, we solubilised both hydrophobic and hydrophilic model drugs in the non-toxic bicontinuous microemulsion, namely lidocaine and diclofenac sodium salt. We found that the microemulsion allows for the solubilisation of designated amounts of both model drugs in the same formulation. Interestingly, the combination of both drugs led to the unexpected stabilisation of a scattering one-phase formulation without adding the surfactant Plantacare 1200 UP. Furthermore, the drug-loaded microemulsions were gelled by DBS without altering the phase behaviour. Finally, we found the rheological behaviour of the drug-free and drug-loaded microemulsions to be quite similar. These results suggest that the drug-containing gelled bicontinuous microemulsion is an orthogonal self-assembled system with a high potential for the use in transdermal drug delivery.

ARTICLE HISTORY

Received 30 September 2020
Accepted 29 January 2021

KEYWORDS

Bicontinuous microemulsions; gels; drug delivery systems; orthogonal self-assembly



Introduction

Microemulsions are promising tools for transdermal drug delivery due to their thermodynamic stability (long shelf-life), optical clarity, and ease of preparation. Furthermore, they enable the solubilisation of both hydrophilic and hydrophobic drugs, and they promote

drug permeation through the stratum corneum [1–3]. Among all types of microemulsions, the bicontinuous microemulsion [4] provides the optimum solubilising capacity for drugs, and the ultra-low interfacial tension improves the wetting of the stratum corneum, which facilitates the drug permeation through the skin

barrier [5,6]. However, drug-containing bicontinuous microemulsions have been rarely used [5–8] or properly characterised [9,10]. Instead, most of the studied systems are oil-in-water (o/w) or water-in-oil (w/o) microemulsions [7,11].

Highly viscous microemulsion systems, e.g. gelled microemulsions, are preferred in transdermal drug delivery due to the mechanical stability which immobilises drugs on the applied surface [3]. So far, most of the gelled microemulsions are polymeric gels, whose gelation process is irreversible [10,12–16]. In this study we utilised low molecular weight gelators (LMWGs) to gel our drug-containing bicontinuous microemulsions. In general, LMWG molecules self-assemble into fibers. These fibers entangle and form a 3D gel network, which, in turn, is able to immobilise an appropriate solvent. Since all interactions are non-covalent (mainly H-bonds and π - π interactions) [17], the gelation process of these molecular gels is thermo-reversible, i.e. the sol-gel transition process can be conveniently controlled with the temperature. More importantly, with low molecular weight gelators the gelled bicontinuous microemulsion can become an orthogonal self-assembly system [18], i.e. the bicontinuous microstructure and the gel network form simultaneously but independently [19,20]. Gelled bicontinuous microemulsions could thus combine the function of an effective drug delivery carrier provided by the microemulsion and the mechanical stability provided by the gel network without interfering with each other [21].

For the first time, we formulated and characterised such a gelled non-toxic bicontinuous microemulsion, namely H₂O – isopropyl myristate (IPM) – Plantacare 1200 UP (technical-grade alkyl polyglucoside with the equivalent average composition of C₁₂G_{1.4}) – 1,2-octanediol – 1,3:2,4-dibenzylidene-D-sorbitol (DBS) [22]. In this system, (a) the main surfactant is a biodegradable alkyl polyglucoside [23], which is essential for drug delivery, (b) the oil IPM and the co-surfactant 1,2-octanediol act as permeation enhancers [24], (c) DBS (molecular structure see Figure 1) gels both water and oil domains although it is a low molecular weight organogelator [25].

In the study at hand, we chose two commonly used model drugs, namely the hydrophobic model drug lidocaine and the hydrophilic model drug diclofenac sodium salt [24]. Lidocaine is a local anaesthetic, and diclofenac is a nonsteroidal anti-inflammatory drug (NSAID) used to treat pain and inflammation. It has been shown that the combination of lidocaine and diclofenac has a synergistic analgesic effect, which can be very effective for pain relief [26]. We investigated the individual and the synergistic effects of drug solubilisation on the phase behaviour

of microemulsions and will discuss the possible locus of the drugs in the drug-loaded microemulsions. Finally, the drug-loaded microemulsions were gelled with the low molecular weight organogelator DBS and characterised by rheological measurements. As a result, we propose a novel gelled non-toxic bicontinuous microemulsion, which has the potential to be a transdermal drug delivery carrier.

Experimental section

Materials

We used bidistilled water to prepare all samples. The oil isopropyl myristate (IPM, > 98%) was purchased from TCI, Japan, and the co-surfactant 1,2-octanediol (> 98%) from Acros, USA. The low molecular weight organogelator 1,3:2,4-dibenzylidene-D-sorbitol (DBS or Geniset[®] D) was purchased from NJC Europe. The hydrophobic model drug lidocaine (> 99%) was purchased from TCI, Japan and the hydrophilic model drug diclofenac sodium salt (\geq 98%) from Sigma-Aldrich, Germany. The technical-grade sugar surfactant Plantacare[®] 1200 UP (C₁₂G_{1.4}) was supplied by BASF, Germany and consists of 52 wt.% of surfactants, 48 wt.% of water and a tiny amount of Mg²⁺ (< 500 ppm). Microemulsion samples of Plantacare[®] were found to be slightly turbid due to the presence of Mg²⁺ at basic pH values, which is contained in the product for preservative purposes. Therefore, the surfactant was neutralised by adding citric acid anhydrous (from Sigma Aldrich, Germany) before use, leading to transparent microemulsions. Furthermore, we have studied the effect of both Mg²⁺ and citric acid on the phase boundaries of the base microemulsion and found that their effect is negligible.

Sample preparation

The solubilities of the model drugs at 25°C in the non-toxic bicontinuous microemulsions as well as in the individual components of the microemulsion were checked before sample preparation to ensure proper solubilisation (see Table 1). Non-gelled microemulsions were prepared by weighing in surfactant (C), co-surfactant (D), oil (B), water (A) and model drugs with an analytical balance into glass tubes with an accuracy of ± 0.001 g, which were then sealed by polyethylene stoppers. Subsequently, the samples were heated up to 50°C in a water bath while being stirred to homogenise. For monitoring the phase diagrams, we used a titration procedure (explained in Section *Phase behaviour*) to reduce material consumption.

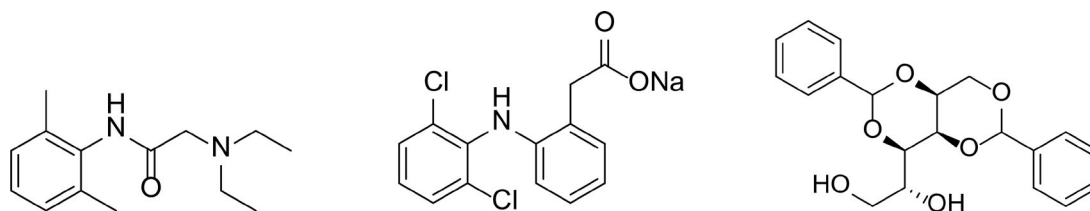


Figure 1. Molecular structures of (left) lidocaine, (middle) diclofenac sodium salt, (right) 1,3:2,4-dibenzylidene-D-sorbitol (DBS).

Table 1. The solubilities of the hydrophilic model drug diclofenac sodium salt and the hydrophobic model drug lidocaine in H₂O, IPM, 1,2-octanediol and in the bicontinuous microemulsion at 25°C.

	H ₂ O	IPM	1,2-octanediol	Bicontinuous microemulsion
Diclofenac sodium salt	< 0.63%	< 0.28%	> 13.5%	> 5.4%
Lidocaine	< 0.37%	> 15.2%	> 15.0%	> 10.6%

Results are given in mass fractions.

In the case of gelled microemulsions, a gelator was additionally added to the samples. The samples were firstly heated above 95°C to dissolve the gelator. A heat gun was utilised when necessary. Subsequently, the samples were directly transferred to an ice bath with manual shaking to ensure homogeneous gelation. Afterwards, the samples were transferred to a 25°C water bath and allowed to equilibrate. It is essential to agitate the gelled microemulsion samples vigorously before gelling; otherwise, phase separation occurs, and the gelation process must be repeated.

Phase behaviour

The phase behaviour was investigated at a constant temperature of $T = 25.0^\circ\text{C}$ in the water bath with a precision of $\pm 0.1\text{ K}$. The non-gelled microemulsion samples were firstly prepared without co-surfactant (D), and a co-surfactant (D) was added to the sample dropwise by a syringe after equilibration in the water bath. The added amount of co-surfactant was recorded by weight with an accuracy of $\pm 0.001\text{ g}$. Then the sample was shaken and stirred vigorously before it was left to equilibrate. The stirring was then stopped and the types of coexisting phases were determined by visual inspection of both transmitted and scattered light using crossed polarisers to recognise anisotropic phases. Since the phase transitions of the microemulsions are induced by a fourth component, namely a co-surfactant, the phase behaviour is presented in a phase tetrahedron (Figure 2). The phase behaviour of these microemulsions is studied at a constant oil-to-water ratio, i.e. a two-dimensional section through the tetrahedron as highlighted in Figure 2.

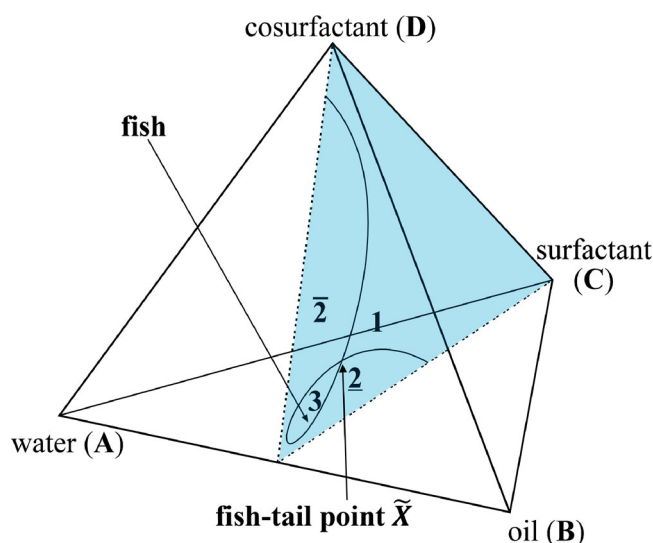


Figure 2. Schematic phase tetrahedron of a quaternary system water – oil – surfactant – co-surfactant at a constant temperature and a section (in blue) through the phase tetrahedron at a constant oil-to-water ratio [27].

Hereby ‘ $\underline{2}$ ’ means the coexistence of an oil-in-water (o/w)-microemulsion (lower phase) and an oil excess phase (upper phase). ‘1’ denotes the isotropic one-phase microemulsion. ‘ $\bar{2}$ ’ means the coexistence of an excess water phase (lower phase) and a water-in-oil (w/o)-microemulsion (upper phase). ‘3’ denotes the coexistence of three phases, namely, an excess water phase (lower phase), a microemulsion (middle phase), and an excess oil phase (upper phase).

In the case of gelled microemulsions, the co-surfactant was added to the gelled sample at 25°C, which was then heated above the sol–gel transition temperature, where the sample melted and could thus be mixed. After the gelation process (see Section *Sample preparation*), the phase behaviour was recorded. Gelled one-phase microemulsions appear transparent while gelled two-phase samples are turbid.

In our experiments, the volume fraction of oil in the solvent mixture

$$\phi = \frac{V_{\text{oil}}}{V_{\text{water}} + V_{\text{oil}}} \quad (1)$$

was kept constant at 0.50. The mass fraction of surfactant (C) is calculated as

$$\gamma_C = \frac{m_{\text{surf.}}}{m_{\text{total}}}, \quad (2)$$

where $m_{\text{surf.}}$ is the active content of alkyl polyglucosides in the original surfactant formulation, while m_{total} is the total mass of water, oil, total mass of the technical-grade surfactant (including solvent and additives), co-surfactant, gelator and drugs. The mass fraction of the co-surfactant (D) is calculated by

$$\gamma_D = \frac{m_{\text{co-surf.}}}{m_{\text{total}}}. \quad (3)$$

The gelator mass fraction is calculated by

$$\eta = \frac{m_{\text{gelator}}}{m_{\text{total}}}. \quad (4)$$

Rheology

Oscillatory shear rheometry was carried out with a rheometer Physica MCR 501 from Anton Paar, Austria. A plate-plate geometry was adopted with the upper plate of 25 mm diameter and 1 mm gap size between the two plates. An external thermostat ensures a temperature precision of $\Delta T = \pm 0.1$ K. Firstly, an amplitude sweep was carried out to determine the limit of the linear viscoelastic region (LVE region) at $T = 25^\circ\text{C}$ with an angular frequency of $\omega = 10\text{ s}^{-1}$ and a varied shear stress τ . For our gelled microemulsion samples, the limit of the LVE region is near $\tau = 40$ Pa. Hence, for subsequent measurements, the shear stress was kept constant at $\tau = 10$ Pa.

Secondly, oscillation frequency sweeps were performed as a function of the angular frequency ω at $T = 25^\circ\text{C}$ and $\tau = 10$ Pa. Lastly, a temperature sweep was carried out at an angular frequency of $\omega = 10\text{ s}^{-1}$ and a shear stress of $\tau = 10$ Pa, from $T = 25^\circ\text{C}$ to $T = 100^\circ\text{C}$ with a heating rate of 1°C min^{-1} to determine the sol-gel transition temperature $T_{\text{sol-gel}}$, i.e. the temperature where the values of G' and G'' decrease sharply.

Solubilising model drugs in non-toxic bicontinuous microemulsions

Since we intend to use the gelled non-toxic bicontinuous microemulsion base system H_2O – isopropyl myristate (IPM) – Plantacare 1200 UP – 1,2-octanediol – DBS [22] as a transdermal drug delivery carrier, it is essential to investigate the effects of drugs on the phase behaviour of the microemulsion, i.e. whether the 1-phase region still exists. We chose two dosages for each model drug: 2.0 and 4.0 wt.% for lidocaine, 1.0 and 2.3 wt.% for diclofenac sodium salt referring to the active content of commercially available gel products. Then we measured the phase boundaries of the drug-loaded microemulsions.

As shown in Figure 3 left, the lidocaine-containing microemulsions exhibit the phase behaviour well-known from quaternary microemulsions stabilised by a mixture of surfactant and co-surfactant [28]. The addition of lidocaine shifts the phase boundaries and accordingly the fishtail point \bar{X} downward, i.e. the amount of co-surfactant needed to form a bicontinuous microemulsion $\tilde{\gamma}_D$ decreases while the amount of main surfactant $\tilde{\gamma}_C$ stays roughly constant. The more lidocaine is added, the less co-surfactant ($\tilde{\gamma}_D$) is needed. Based on the facts that

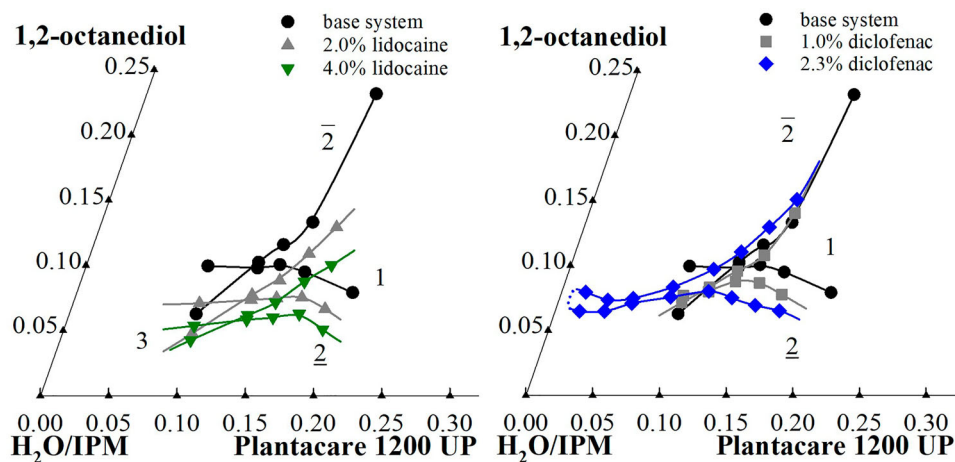


Figure 3. Left: Phase diagrams of the base system H_2O – IPM – Plantacare 1200 UP ($\text{C}_{12}\text{G}_{1,4}$) – 1,2-octanediol without drugs (black circles), with 2.0 wt.% lidocaine (grey triangles up) and with 4.0 wt.% lidocaine (green triangles down) in the overall microemulsion at $T = 25^\circ\text{C}$, $\phi = 0.50$. Right: Phase diagrams of the base system H_2O – IPM – Plantacare 1200 UP ($\text{C}_{12}\text{G}_{1,4}$) – 1,2-octanediol (black circles), with 1.0 wt.% diclofenac sodium salt (grey squares) and with 2.3 wt.% diclofenac sodium salt (blue diamonds) in the overall microemulsion at $T = 25^\circ\text{C}$, $\phi = 0.50$.

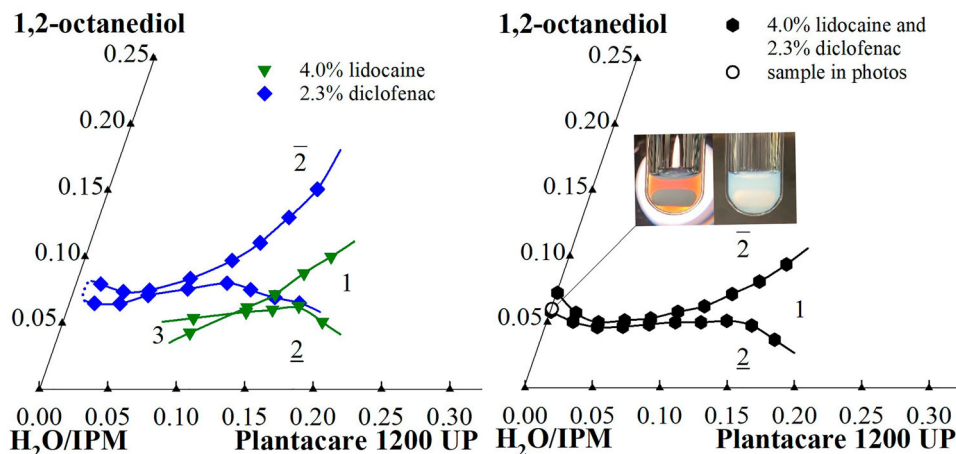


Figure 4. Left: Phase diagrams of the base system H_2O – IPM – Plantacare 1200 UP ($\text{C}_{12}\text{G}_{1.4}$) – 1,2-octanediol with 4.0 wt.% lidocaine (green triangles) and with 2.3 wt.% diclofenac sodium salt (blue diamonds) at $T = 25^\circ\text{C}$, $\phi = 0.50$. Right: Phase diagram of the base system H_2O – IPM – Plantacare 1200 UP ($\text{C}_{12}\text{G}_{1.4}$) – 1,2-octanediol with both drugs (black hexagons) at $T = 25^\circ\text{C}$, $\phi = 0.50$. Two photos taken both in transmitted light (left) and without illumination (right) show the strong opalescence of the surfactant-free one-phase mixture.

(1) lidocaine dissolves well in IPM (see Table 1), (2) lidocaine has a similar carbon number as IPM but with an aromatic ring, (3) less co-surfactant is needed in the presence of lidocaine, we speculate that lidocaine goes mostly into the oil phase and renders the oil less hydrophobic. The result of Burauer et al. also supports our speculation as they found that a cyclic oil with aromatic ring behaves less hydrophobic than the saturated cyclic oil and the n -alkane with the same number of carbon atoms in the microemulsion formation [29].

Considering the effect of diclofenac sodium salt on the phase behaviour of the base system, a strong dependence on the drug concentration is found. The shape of the phase boundaries of the system containing 1.0 wt.% diclofenac sodium salt resembles that of the base system (Figure 3 right). However, the solubilisation efficiency of the surfactant/co-surfactant mixture is considerably increased, i.e. both $\tilde{\gamma}_C$ and $\tilde{\gamma}_D$ are smaller than those of the base system. Interestingly, increasing the diclofenac sodium salt concentration to 2.3 wt.%, a 1-phase channel is observed which extends to the very left edge of the phase diagram, while no 3-phase region could be found. The huge efficiency increase, which enables the formulation of a microemulsion even at an extremely low surfactant concentration ($\gamma_C = 0.019$), might be caused by electrostatic interactions induced by diclofenac sodium salt. The electrostatic repulsion increases the bending rigidity of the surfactant monolayer and thus stabilises the microemulsion. A similar phenomenon has been observed and investigated by Kaler et al. [30] as well as in our previous study [31]. Since diclofenac sodium salt has an amphiphilic structure, we expect it to absorb partly in the interface, i.e. the surfactant monolayer. On the other

hand, we observed that 5 wt.% diclofenac sodium salt also dissolves in the mixture of 10 wt.% 1,2-octanediol and 90 wt.% IPM, which resembles the composition of the oil phase. Therefore, diclofenac sodium salt goes to the oil phase as well. In other words, although diclofenac sodium salt is specified as ‘hydrophilic drug’, it acts as both co-surfactant and co-oil in the microemulsion.

Having studied the individual effect of the model drugs on the phase behaviour of the microemulsion, the next step was to add both drugs to the microemulsion simultaneously. We took the higher dosage of each drug, i.e. 4.0 wt.% lidocaine and 2.3 wt.% diclofenac sodium salt, to obtain a more representative result. The phase diagram of the base system with both drugs is shown in Figure 4 right, while the phase diagrams of the base system with each drug separately are presented in Figure 4 left for comparison. The base system with both drugs combines the effects of both drugs: (1) the phase boundaries shift further to lower concentration of 1,2-octanediol compared to the base system with 2.3% diclofenac due to the lower hydrophobicity of lidocaine as a co-oil; (2) and more importantly the 1-phase channel extends to the left edge of the phase diagram. This surfactant-free one-phase mixture is characterised by a strong opalescence, which is shown by two photos taken in both transmitted light (left) and without illumination (right). Although rather unexpected, the stabilisation of such a mixture might be either related to the adsorption of diclofenac molecules in the amphiphilic film inducing strongly stabilising electrostatic interactions or the proximity of a critical point in the surfactant-free side system. Small-angle neutron scattering (SANS) and freeze fracture electron microscopy (FFEM) studies are underway

to elucidate the structure of this exciting surfactant-free one-phase mixture.

The fishtail \tilde{X} points of all studied systems are summarised in Table 2 for reference. In conclusion, our non-toxic base microemulsion system can solubilise the designated amounts of both model drugs, and the model drugs increase the efficiency of the microemulsion. Even more interestingly, a scattering one-phase mixture of H₂O – IPM – 1,2-octanediol containing 4.0 wt.% lidocaine and 2.3 wt.% diclofenac sodium salt can be formulated, which is less expensive and less skin-irritating than the alkyl polyglucoside-containing microemulsion.

Gelling drug-containing microemulsions

Having measured the phase behaviour of the bicontinuous microemulsion with the model drugs, we intended

to gel the drug-containing microemulsions to increase their mechanical stability. Previously we have gelled the base system with the low molecular organogelator 1,3:2,4-dibenzylidene-D-sorbitol (DBS) and found that the gelator does not change the phase behaviour of the microemulsion [22]. Hence, here we used the same gelator to gel the drug-containing microemulsions and examined their rheological properties.

The aforementioned three drug-containing microemulsions, namely the base system with 4.0 wt.% lidocaine, the base system with 2.3 wt.% diclofenac sodium salt, and the base system with both drugs, were gelled with 0.3 wt.% DBS (see Figure 5). The phase boundaries of these gelled systems remain unchanged compared to the non-gelled systems, which is in line with our previous study [22,31] and shows that the gelled bicontinuous microemulsion is an orthogonal self-assembly system. As

Table 2. Summary of the fishtail \tilde{X} points (the intersection point of the 3-phase and the 1-phase microemulsions) of all studied systems.

	Components					\tilde{X} point	
	Oil	Surfactant	Co-surfactant	Lidocaine	Diclofenac sodium salt	$\tilde{\gamma}_C$	$\tilde{\gamma}_D$
H ₂ O	Isopropyl myristate	Plantacare 1200 UP	1,2-octanediol	–	–	0.121	0.098
	Isopropyl myristate	Plantacare 1200 UP	1,2-octanediol	2%	–	0.124	0.073
	Isopropyl myristate	Plantacare 1200 UP	1,2-octanediol	4%	–	0.123	0.057
	Isopropyl myristate	Plantacare 1200 UP	1,2-octanediol	–	1%	0.104	0.079
	Isopropyl myristate	Plantacare 1200 UP	1,2-octanediol	–	2.3%	–	–
	Isopropyl myristate	Plantacare 1200 UP	1,2-octanediol	4%	2.3%	–	–

Note that the volume fraction of oil in the water/oil mixture was adjusted to $\phi = 0.50$.

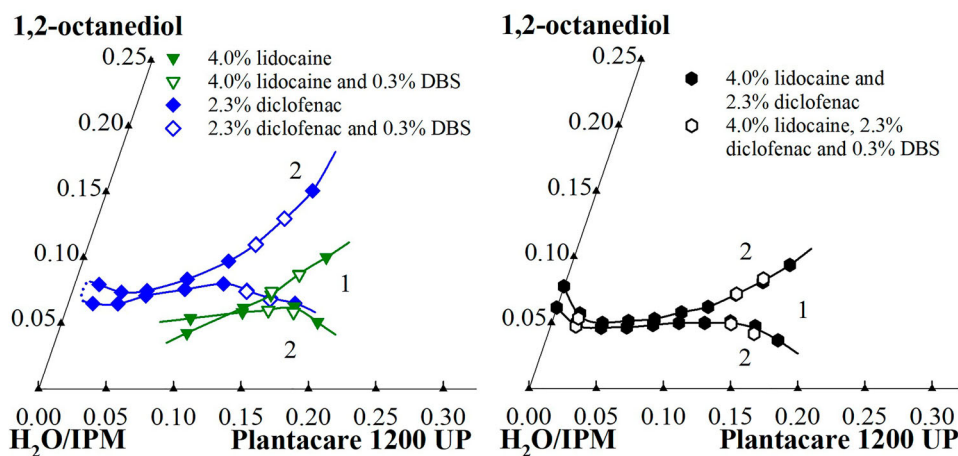


Figure 5. Left: Phase diagrams of the non-gelled microemulsion H₂O – IPM – Plantacare 1200 UP (C₁₂G_{1.4}) – 1,2-octanediol with 4.0 wt.% lidocaine (green triangles), with 2.3 wt.% diclofenac sodium salt (blue diamonds) and the gelled counterparts in the presence of DBS at $\eta = 0.003$, $T = 25^\circ\text{C}$, $\phi = 0.50$ (green empty triangles and blue empty diamonds respectively). Right: Phase diagrams of the non-gelled microemulsion H₂O – IPM – Plantacare 1200 UP (C₁₂G_{1.4}) – 1,2-octanediol with 4.0 wt.% lidocaine and 2.3 wt.% diclofenac sodium salt (black hexagons) and the gelled microemulsion (black empty hexagons) in the presence of DBS at $\eta = 0.003$, $T = 25^\circ\text{C}$, $\phi = 0.50$.

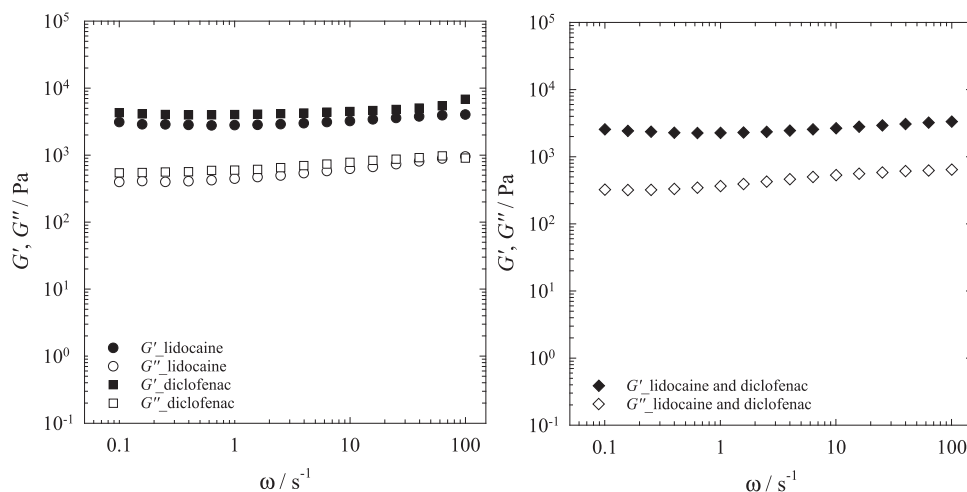


Figure 6. Storage modulus G' (filled symbols) and loss modulus G'' (open symbols) of the gelled bicontinuous microemulsion H_2O – IPM – Planacare 1200 UP – 1,2-octanediol in the presence of DBS at $\eta = 0.003$, $\tau = 10$ Pa, $T = 25^\circ\text{C}$ as a function of ω with the composition of (left) $\gamma_C = 0.1564$, $\gamma_D = 0.0700$, 4.3 wt.% lidocaine, $\phi = 0.50$ (circles) and $\gamma_C = 0.1605$, $\gamma_D = 0.1022$, 2.3 wt.% diclofenac sodium salt, $\phi = 0.50$ (squares); (right) $\gamma_C = 0.1582$, $\gamma_D = 0.0615$, 3.9 wt.% lidocaine and 2.3 wt.% diclofenac sodium salt, $\phi = 0.50$ (diamonds).

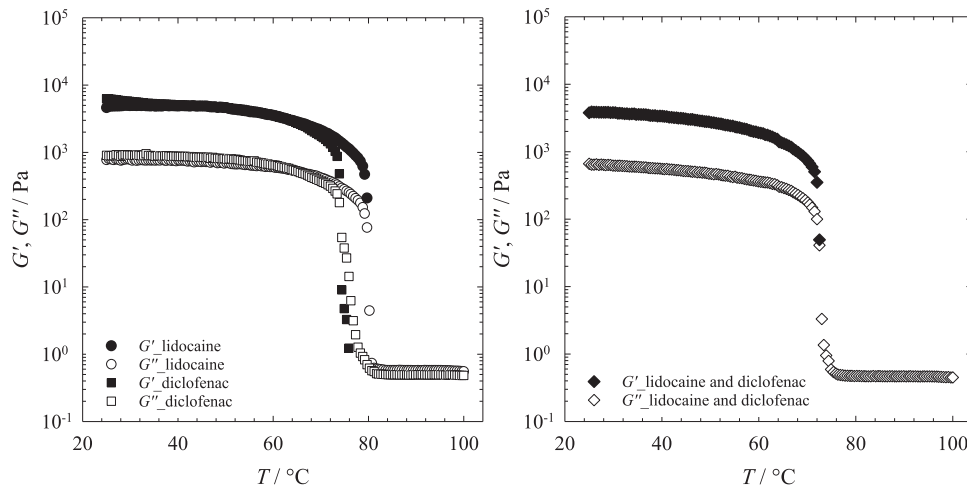


Figure 7. Storage modulus G' (filled symbols) and loss modulus G'' (open symbols) of the gelled bicontinuous microemulsion H_2O – IPM – Planacare 1200 UP – 1,2-octanediol in the presence of DBS at $\eta = 0.003$, $\tau = 10$ Pa, $\omega = 10$ s^{-1} as a function of T and a heating rate of 1°C min^{-1} with the composition of (left) $\gamma_C = 0.1564$, $\gamma_D = 0.0700$, 4.3 wt.% lidocaine, $\phi = 0.50$ (circles) and $\gamma_C = 0.1605$, $\gamma_D = 0.1022$, 2.3 wt.% diclofenac sodium salt, $\phi = 0.50$ (squares); (right) $\gamma_C = 0.1582$, $\gamma_D = 0.0615$, 3.9 wt.% lidocaine and 2.3 wt.% diclofenac sodium salt, $\phi = 0.50$ (diamonds).

a result, the microemulsion ‘only’ acts as a solvent for the gel and the incorporation of drugs into the microemulsion does not affect the gelling behaviour.

Subsequently, we examined the rheological properties of the three drug-containing gelled microemulsions with oscillatory shear rheometry. For each microemulsion, we chose one composition located in the middle of the 1-phase region at $\gamma_C \sim 0.16$. The linear viscoelastic region (LVE) was determined in the preliminary amplitude sweep, and the shear stress was set at $\tau = 10$ Pa for the subsequent frequency sweep (Figure 6). For all three samples, the storage modulus G' is about one order of magnitude larger than the loss modulus G'' over the

entire frequency range, and both moduli show only a very weak frequency dependence, i.e. the storage modulus G' and the loss modulus G'' increase slightly at high frequency. The results show that the samples are indeed gelled. Afterwards, a temperature sweep was carried out to characterise the sol–gel transition temperature $T_{\text{sol-gel}}$ (Figure 7), i.e. the temperature at which the storage modulus G' drops sharply and crosses the loss modulus G'' . For the base system with 4.3 wt.% lidocaine the $T_{\text{sol-gel}}$ is around $(80 \pm 1)^\circ\text{C}$, for the base system with 2.3 wt.% diclofenac sodium salt the $T_{\text{sol-gel}}$ is around $(74 \pm 1)^\circ\text{C}$, and for the base system with both drugs the $T_{\text{sol-gel}}$ is around $(72 \pm 1)^\circ\text{C}$.

We recall that the rheological properties of the base system without drugs were examined in our previous study [22], and they are consistent with the results at hand. The rheological behaviour of the drug-free and the drug-containing gelled microemulsions is quite similar: (1) the storage modulus G' is in the range of 10^3 Pa and the loss modulus G'' is in the range of 10^4 Pa; (2) both moduli only show very weak frequency dependence; (3) the sol–gel transition temperature $T_{\text{sol-gel}}$ is between 72 and 80°C. This again is in line with the formation of an orthogonal self-assembled system because the gelled microemulsions are nearly the ‘same’ gels, which contain 0.3 wt.% low molecular weight organogelator DBS but consist of slightly different solvents.

Conclusion and outlook

In the study at hand, we show that the non-toxic bicontinuous microemulsion (the base system) H_2O – IPM – Plantacare 1200 UP ($\text{C}_{12}\text{G}_{1.4}$) – 1,2-octanediol can solubilise two model drugs, namely the hydrophobic drug lidocaine and the hydrophilic drug diclofenac sodium salt. Moreover, we gelled the drug-loaded microemulsions successfully with the low molecular weight organogelator 1,3:2,4-dibenzylidene-D-sorbitol (DBS).

We first investigated the effects of the model drugs on the phase behaviour of the base system. Referring to commercially available products, we chose dosages of 2.0 and 4.0 wt.% for lidocaine and 1.0 and 2.3 wt.% for diclofenac sodium salt. The addition of lidocaine shifts the phase boundaries and accordingly the fishtail point \tilde{X} toward smaller amounts of the co-surfactant 1,2-octanediol, which implies that lidocaine goes mostly into the oil phase and renders the oil less hydrophobic. On the other hand, the addition of diclofenac increases the solubilisation efficiency of the Plantacare 1200 UP ($\text{C}_{12}\text{G}_{1.4}$)/1,2-octanediol mixture, which might be related to the adsorption of diclofenac molecules in the amphiphilic film inducing strongly stabilising electrostatic interactions. Based on experimental observations, we speculate that diclofenac sodium salt acts as both co-surfactant and co-oil in the microemulsion although it is specified as ‘hydrophilic drug’. The combination of both drugs led to the unexpected stabilisation of a one-phase formulation without adding the surfactant Plantacare 1200 UP. In this way, a strongly scattering one-phase mixture of H_2O – IPM – 1,2-octanediol containing 4.0 wt.% lidocaine and 2.3 wt.% diclofenac sodium salt could be formulated, and therewith not only less expensive but also less skin-irritating than the surfactant-containing system.

We then gelled three drug-containing microemulsions, namely the base system containing 4.0 wt.%

lidocaine, the base system containing 2.3 wt.% diclofenac, and the base system containing both drugs, with 0.3 wt.% DBS. All the phase boundaries remain unchanged compared to the non-gelled systems. Furthermore, the rheological properties of the drug-free and the drug-containing gelled microemulsions are quite similar. These findings can be attributed to the existence of an orthogonal self-assembled structure in which the bicontinuous microstructure and the gel network form simultaneously but independently.

In future studies, we will carry out *in vitro* skin permeation tests and compare the performance of the drug-containing gelled bicontinuous microemulsions with commercial products which contain the same active content of drugs. We expect the gelled bicontinuous microemulsions to be an efficient and effective drug delivery carrier. Furthermore, we will investigate the gelling behaviour and the structural change of the gelled non-toxic bicontinuous microemulsions at various water-to-oil ratios. By this means, we will know how to formulate efficient gelled non-toxic bicontinuous microemulsions whose water- and oil-content can be adjusted as wanted.

Disclosure statement

No potential conflict of interest was reported by the authors.

ORCID

Ke Peng  <http://orcid.org/0000-0001-9231-1954>

Thomas Sottmann  <http://orcid.org/0000-0003-3679-3703>

Cosima Stubenrauch  <http://orcid.org/0000-0002-1247-4006>

References

- [1] M. Kreilgaard, *Adv. Drug Deliv. Rev.* 54, 77 (2002). doi:10.1016/S0169-409X(02)00116-3
- [2] S. Heuschkel, A. Goebel and R.H.H. Neubert, *J. Pharm. Sci.* 97, 603 (2008). doi:10.1002/jps.20995
- [3] M.J. Lawrence and G.D. Rees, *Adv. Drug Deliv. Rev.* 64, 175 (2012). doi:10.1016/j.addr.2012.09.018
- [4] R. Strey, *Colloid Polym. Sci.* 272, 1005 (1994). doi:10.1007/BF00658900
- [5] M.A. Bolzinger, T.C. Carduner and M.C. Poelman, *Int. J. Pharm.* 176, 39 (1998). doi:10.1016/S0378-5173(98)00-292-0
- [6] M.A. Bolzinger-Thevenin, J.L. Grossiord and M.C. Poelman, *Langmuir* 15, 2307 (1999). doi:10.1021/la9804278
- [7] S.P. Callender, J.A. Mathews, K. Kobernyk and S.D. Wetzig, *Int. J. Pharm.* 526, 425 (2017). doi:10.1016/j.ijpharm.2017.05.005
- [8] J. Carlfors, I. Blute and V. Schmidt, *J. Dispers. Sci. Technol.* 12, 467 (1991). doi:10.1080/01932699108913146
- [9] M.A. Thevenin, J.L. Grossiord and M.C. Poelman, *Int. J. Pharm.* 137, 177 (1996). doi:10.1016/0378-5173(96)04-518-8

- [10] A. Froelich, T. Osmałek, A. Snela, P. Kunstman, B. Jadach, M. Olejniczak, G. Roszak and W. Białas, *J. Colloid Interface Sci.* 507, 323 (2017). doi:[10.1016/j.jcis.2017.08.011](https://doi.org/10.1016/j.jcis.2017.08.011)
- [11] P.P. Constantinides, *Pharm. Res. An Off. J. Am. Assoc. Pharm. Sci.* 12, 1561 (1995).
- [12] O.J. D'cruz and F.M. Uckun, *Contraception.* 64, 113 (2001). doi:[10.1016/S0010-7824\(01\)00233-5](https://doi.org/10.1016/S0010-7824(01)00233-5)
- [13] F. Dreher, P. Walde, P. Walther and E. Wehrli, *J. Control. Release.* 45, 131 (1997). doi:[10.1016/S0168-3659\(96\)01559-3](https://doi.org/10.1016/S0168-3659(96)01559-3)
- [14] S. Kantaria, G.D. Rees and M.J. Lawrence, *J. Control. Release.* 60, 355 (1999). doi:[10.1016/S0168-3659\(99\)00092-9](https://doi.org/10.1016/S0168-3659(99)00092-9)
- [15] S.A. Fouad, E.B. Basalious, M.A. El-Nabarawi and S.A. Tayel, *Int. J. Pharm.* 453, 569 (2013). doi:[10.1016/j.ijpharm.2013.06.009](https://doi.org/10.1016/j.ijpharm.2013.06.009)
- [16] X.Y. Xuan, Y.L. Cheng and E. Acosta, *Pharmaceutics.* 4, 104 (2012). doi:[10.3390/pharmaceutics4010104](https://doi.org/10.3390/pharmaceutics4010104)
- [17] R.G. Weiss, *J. Am. Chem. Soc.* 136, 7519 (2014). doi:[10.1021/ja503363v](https://doi.org/10.1021/ja503363v)
- [18] P.E. Laibinis, J.J. Hickman, M.S. Wrighton and G.M. Whitesides, *Science* (80-.). 245, 845 (1989). doi:[10.1126/science.245.4920.845](https://doi.org/10.1126/science.245.4920.845)
- [19] M. Laupheimer, K. Jovic, F.E. Antune, M. da Graça Martins Miguel and C. Stubenrauch, *Soft Matter.* 9, 3661 (2013). doi:[10.1039/c3sm27883b](https://doi.org/10.1039/c3sm27883b)
- [20] M. Laupheimer, T. Sottmann, R. Schweins and C. Stubenrauch, *Soft Matter.* 10, 8744 (2014). doi:[10.1039/C4SM01639D](https://doi.org/10.1039/C4SM01639D)
- [21] C. Stubenrauch and F. Gießelmann, *Angew. Chemie - Int. Ed.* 55, 3268 (2016). doi:[10.1002/anie.201506603](https://doi.org/10.1002/anie.201506603)
- [22] K. Peng, T. Sottmann and C. Stubenrauch, *Soft Matter.* 15, 8361 (2019). doi:[10.1039/C9SM01350D](https://doi.org/10.1039/C9SM01350D)
- [23] C. Stubenrauch, *Curr. Opin. Colloid Interface Sci.* 6, 160 (2001). doi:[10.1016/S1359-0294\(01\)00080-2](https://doi.org/10.1016/S1359-0294(01)00080-2)
- [24] A. Kogan and N. Garti, *Adv. Colloid Interface Sci.* 123, 369 (2006). doi:[10.1016/j.cis.2006.05.014](https://doi.org/10.1016/j.cis.2006.05.014)
- [25] B.O. Okesola, V.M.P. Vieira, D.J. Cornwell, N.K. Whitelaw and D.K. Smith, *Soft Matter.* 11, 4768 (2015). doi:[10.1039/C5SM00845J](https://doi.org/10.1039/C5SM00845J)
- [26] M.J. Linares-Gil, J. Valls, P. Hereu-Boher, F.J. Nebot, B. De-Ramón, E. Diaz-Munió, R. Sanzol, J. De-Oca, P. Pérez-Lozano, J.M. Suñé-Negre and E. García-Montoya, *Clin. Transl. Gastroenterol.* 9 (2018).
- [27] K. Kluge, C. Stubenrauch, T. Sottmann and R. Strey, *Tenside, Surfactants, Deterg.* 38, 30 (2001).
- [28] T. Sottmann, K. Kluge, R. Strey, J. Reimer and O. Söderman, *Langmuir.* 18, 3058 (2002). doi:[10.1021/la011665x](https://doi.org/10.1021/la011665x)
- [29] S. Burauer, T. Sottmann, R. Strey and S. Tenside, *Deterg.* 37, 8 (2000).
- [30] J.A. Silas and E.W. Kaler, *J. Colloid Interface Sci.* 243, 248 (2001). doi:[10.1006/jcis.2001.7874](https://doi.org/10.1006/jcis.2001.7874)
- [31] K. Peng, N. Preisig, T. Sottmann and C. Stubenrauch, *Langmuir.* 36, 12692 (2020). doi:[10.1021/acs.langmuir.0c02314](https://doi.org/10.1021/acs.langmuir.0c02314)

Publication IV

From Water-Rich to Oil-Rich Gelled Non-Toxic Microemulsions

Ke Peng, Natalie Preisig, Thomas Sottmann, and Cosima Stubenrauch
Phys. Chem. Chem. Phys. **2021**, *23* (31), 16855–16867.

DOI: 10.1039/D1CP02522H

Reproduced from [Pen21b] with permission from the PCCP Owner Societies.



Cite this: *Phys. Chem. Chem. Phys.*,
2021, **23**, 16855

From water-rich to oil-rich gelled non-toxic microemulsions†

Ke Peng,  Natalie Preisig, Thomas Sottmann  and Cosima Stubenrauch *

Gelled non-toxic microemulsions have great potential in transdermal drug delivery: the microemulsion provides an optimum solubilizing capacity for drugs and promotes drug permeation through the skin barrier, while the gel network provides mechanical stability. We have formulated such a gelled non-toxic microemulsion consisting of H₂O – isopropyl myristate (IPM) – Plantacare 1200 UP (technical-grade alkyl polyglucoside with an average composition of C₁₂G_{1.4}) – 1,2-octanediol in the presence of the low molecular weight gelator (LMWG) 1,3:2,4-dibenzylidene-*D*-sorbitol (DBS) at an oil-to-water ratio of $\phi = 0.50$. The study at hand aimed to develop gelled non-toxic microemulsions that can contain both oil- and water-soluble drugs and are either water- or oil-based, depending on the application. To accomplish this, we varied the oil-to-water ratio from being water-rich to oil-rich, *i.e.* $0.2 \leq \phi \leq 0.8$. Phase studies were carried out along the middle phase trajectory, and a suitable LMWG was identified for all ϕ -ratios. Electrical conductivity measurements showed that the structure can be tuned from water- to oil-continuous by adjusting the amount of 1,2-octanediol and ϕ -ratios. The existence of the gel network was visualized by freeze-fracture electron microscopy (FFEM) at three different ϕ -ratios. We found that all systems from $\phi = 0.35$ to $\phi = 0.80$ form strong gels with nearly the same rheological behavior, while the system with $\phi = 0.20$ is a much weaker gel. We attribute this behavior on the one hand to the microemulsion microstructure and on the other hand to the solvent-dependent gelation properties of DBS, which can be described by the Hansen solubility parameters (HSPs).

Received 5th June 2021,
Accepted 16th July 2021

DOI: 10.1039/d1cp02522h

rsc.li/pccp

1. Introduction

Orthogonal self-assembly¹ is the simultaneous but independent formation of two self-assembled structures and was discovered in gelled complex fluids^{2,3} only recently. It is reported that the fibrillar gel network formed by low molecular weight gelators (LMWG)⁴ coexists with various self-assembled colloidal nanostructures, namely micelles,⁵ vesicles,⁶ thermotropic liquid crystals,⁷ lyotropic liquid crystals,^{8–11} and microemulsions.^{12,13} Gelled bicontinuous microemulsions are of particular interest due to their potential use as transdermal drug delivery carriers. Bicontinuous microemulsions consist of two interweaving oil and water domains, which are separated by an amphiphilic surfactant monolayer and have a domain size ranging from 5 to 100 nm.¹⁴ Compared to oil-in-water and water-in-oil microemulsions, bicontinuous microemulsions provide the optimum solubilizing capacity for both hydrophilic and hydrophobic drugs.¹⁵ Moreover, the ultra-low interfacial tension facilitates the wetting of the stratum corneum, thus promoting the drug permeation through the skin barrier.¹⁶

Furthermore, the self-assembled fibrillar gel network provides mechanical stability to bicontinuous microemulsion and thus immobilizes drugs on the applied surface.¹⁷

In our previous studies, we formulated and characterized a gelled non-toxic bicontinuous microemulsion system consisting of H₂O – isopropyl myristate (IPM) – Plantacare 1200 UP (technical-grade alkyl polyglucoside with an average composition of C₁₂G_{1.4}) – 1,2-octanediol in the presence of the LMWG 1,3:2,4-dibenzylidene-*D*-sorbitol (DBS).¹⁸ Such a gelled non-toxic bicontinuous microemulsion was never formulated and studied before. The used surfactant belongs to the alkyl polyglucosides (APGs, denoted as C_{*n*}G_{*m*}), which are commercially available and are widely used in cosmetics due to low skin irritation.^{19,20} The oil IPM and the co-surfactant 1,2-octanediol also act as permeation enhancers.²¹ We recall that the LMWG DBS²² gels the bicontinuous microemulsion, which contains equal volumes of water and oil, although it is an organogelator. Moreover, small-angle neutron scattering (SANS) results provide evidence of the bicontinuous microstructure and indicate that the gel network does not alter the microstructure of the microemulsion. Since the bicontinuous microemulsion contains equal volumes of water and oil, the system should be able to carry both hydrophilic and hydrophobic drugs. Our subsequent study found that the system indeed solubilizes designated amounts of the hydrophilic model drug diclofenac

*Institute of Physical Chemistry, University of Stuttgart, Pfaffenwaldring 55,
70569 Stuttgart, Germany. E-mail: cosima.stubenrauch@ipc.uni-stuttgart.de*

† Electronic supplementary information (ESI) available. See DOI: 10.1039/d1cp02522h

sodium salt and the hydrophobic model drug lidocaine.²³ Furthermore, rheological data suggest that the drug-containing gelled bicontinuous microemulsion is an orthogonal self-assembled system.

In order to further extend the application of this promising system, the present work aimed to develop gelled non-toxic microemulsions that can contain both oil- and water-soluble drugs and are either water- or oil-based, depending on the applied surface. Therefore, we investigate whether it is possible to tune the continuity of the gelled microemulsions from water-rich to oil-rich by systematically varying the oil-to-water ratio along the trajectory of the middle phase. Studies of the nanostructure of a series of microemulsions using freeze-fracture electron microscopy,^{24,25} NMR self-diffusion,^{26–28} and small-angle neutron scattering¹⁴ have shown that the structure is essentially bicontinuous along this scalable trajectory.²⁹ However, when approaching small oil and water contents, discrete cylindrical oil or water droplets are often found in water or oil, respectively, in addition to bicontinuous elements.

In this study, we investigated the phase behavior of the non-toxic microemulsion H₂O – IPM – Plantacare 1200 UP (C₁₂G_{1.4}) – 1,2-octanediol at various oil-to-water ratios, *i.e.* not limiting to equal volumes of oil and water, because they provide a versatile toolbox for optimized drug solubilization. The continuity of the microemulsion structure upon the addition of 1,2-octanediol was examined by electrical conductivity measurements for three selected oil-to-water ratios. We applied various gelators to find proper LMWGs for both water-rich and oil-rich microemulsions and studied the rheological properties of the gelled microemulsions. Freeze-fracture electron microscopy (FFEM) was used to prove the presence of gel fibers in water-rich, symmetric, and oil-rich gelled microemulsions. The final goal is to know how to formulate gelled non-toxic microemulsions that are water- or oil-based and can thus be adapted to the specific application surface as needed.

2. Experimental section

2.1 Materials

We used bidistilled water to prepare all samples. The oil isopropyl myristate (IPM, >98%) was purchased from TCI, Japan, and the co-surfactant 1,2-octanediol (>98%) from Acros, USA. Sodium chloride was purchased from Merck, Germany. The low molecular weight gelator (LMWG) 12-hydroxyoctadecanoic acid (12-HOA, 95%) was purchased from Alfa Aesar, Germany, *N,N'*-dibenzoyl-L-cystine (DBC, >98%) from Santa Cruz, the USA, and 1,3:2,4-dibenzylidene-D-sorbitol (DBS or Geniset[®] D) from NJC Europe. The DBS-derivatives 1,3:2,4-dibenzylidene-D-sorbitol-*p,p'*-dicarboxylic acid (DBS-CO₂H) and DBS-CONHNH₂ were provided by Prof. Dr David K. Smith from the University of York, UK. The technical-grade sugar surfactant Plantacare[®] 1200 UP (C₁₂G_{1.4}) was supplied by BASF, Germany, and consists of 52 wt% of surfactants, 48 wt% of water, and a tiny amount of Mg²⁺ (<500 ppm). Water-rich microemulsion samples of Plantacare[®] were found to be slightly turbid due to the presence of

Mg²⁺ at basic pH values, which is contained in the product for preservative purposes. However, the surfactant was used as it is since the slight turbidity does not affect the phase studies.

2.2 Sample preparation

Non-gelled microemulsions were prepared by weighing in surfactant (C), co-surfactant (D), oil (B), and water (A) with an analytical balance into glass tubes, which were then sealed by polyethylene stoppers. For monitoring phase diagrams, we used a titration procedure (explained in section Phase studies) to reduce the amount of material. Subsequently, the samples were heated up to 50 °C in a water bath while being stirred to homogenize. In the case of gelled microemulsions, a gelator was additionally added to the samples. The samples were firstly heated above 92 °C to dissolve the gelator. A heat gun was utilized when necessary. Subsequently, the samples were quickly transferred to an ice bath directly from the 92 °C water bath with manual shaking to ensure homogeneous gelation. Afterward, the samples were transferred to a 25 °C water bath and allowed to equilibrate.

2.3 Phase studies

The microemulsion phase behavior was investigated at a constant temperature of $T = (25.0 \pm 0.1)$ °C in the water bath. The samples were firstly prepared without co-surfactant (D). After equilibration in the water bath, a co-surfactant (D) was added dropwise to the sample by a syringe. The added amount of co-surfactant was recorded by weight with an accuracy of ± 0.001 g. After adding the co-surfactant, the sample was shaken and stirred vigorously before it was left to equilibrate. Then the phase behavior was visually determined. Since the phase transitions of sugar surfactant-based microemulsions were induced by a fourth component, namely a co-surfactant, the phase behavior is presented in a phase tetrahedron. The phase behavior of these microemulsions is studied at a constant oil-to-water ratio, *i.e.*, recording a two-dimensional section through the tetrahedron.

After measuring the phase boundaries, 1-phase microemulsion samples of different oil-to-water ratios (ϕ) were prepared to study the gelation behavior of LMWGs. We first determined the minimum gelation concentration (mgc) by adding a gelator to the microemulsion sample until the whole sample was gelled. The sample is considered gelled if the material does not flow in the inverted test tube. Afterward, it was checked whether the gelled sample was transparent at the mgc or at higher gelator contents. A gelled 1-phase microemulsion is transparent, while a gelled 2-phase microemulsion is turbid.

In our experiments, the oil-to-water ratio is defined by the volume fraction of oil in the mixture of water and oil

$$\phi = \frac{V_{\text{oil}}}{V_{\text{water}} + V_{\text{oil}}} \quad (1)$$

The mass fraction of surfactant (C) is calculated by

$$\gamma_{\text{C}} = \frac{m_{\text{surf.}}}{m_{\text{total}}} \quad (2)$$

where $m_{\text{surf.}}$ is the active content of alkyl polyglucosides in the original surfactant formulation, while m_{total} is the total mass of water, oil, total mass of the technical-grade surfactant (including solvent and additives), co-surfactant, and gelator. Then the mass fraction of the co-surfactant (D) is calculated by

$$\gamma_{\text{D}} = \frac{m_{\text{co-surf.}}}{m_{\text{total}}}. \quad (3)$$

The gelator mass fraction is calculated according to

$$\eta = \frac{m_{\text{gelator}}}{m_{\text{total}}}. \quad (4)$$

2.4 Electrical conductivity

The experimental setup consisted of the conductivity cell TetraCon 925/LV from WTW (Xylem Analytics GmbH, Weilheim, Germany) containing a temperature sensor and the conductivity meter Multi 3510 IDS from WTW. The conductivity measuring cell was placed in a test tube, which contained the sample to be measured. The temperature was adjusted to a constant value of $T = (25.0 \pm 0.1)^\circ\text{C}$ by placing the test tube in a water bath regulated by a thermostat DC30 from Thermo Electron GmbH (Karlsruhe, Germany). For a detectable conductivity, the water of the microemulsion sample was replaced by 0.1 wt% of NaCl solution. Note that the effect of salt on the phase behavior of nonionic microemulsions is negligible at this low concentration. The electrical conductivity was measured through the titration procedure (see Section 2.3). The sample was continuously stirred with a Teflon-coated magnetic stirring bar. Then the co-surfactant was added into the sample dropwise. $\kappa(\gamma_{\text{D}})$ -curves were obtained, recording the conductivities after each drop of co-surfactant and 3 min of waiting time.

2.5 Rheology

Oscillatory shear rheometry was carried out with a rheometer Physica MCR 501 from Anton Paar, Austria. A plate-plate geometry was used with the upper plate of 25 mm diameter and a gap size of 1 mm between the two plates. The temperature was controlled *via* an external thermostat with a precision of $\Delta T = \pm 0.1$ K. Firstly, an amplitude sweep was carried out at $T = 25^\circ\text{C}$ with an angular frequency of $\omega = 10\text{ s}^{-1}$ and a controlled shear stress τ to determine the limit of the linear viscoelastic region (LVE region). The shear stress for the subsequent measurements should be within the limit of the LVE region. Hence, for the gelled microemulsions, the shear stress was kept constant at $\tau = 10$ Pa except for the samples with $\phi = 0.20$ and $\phi = 0.35$ at $\eta = 0.002$, which were measured at a shear stress of $\tau = 1$ Pa (for the amplitude sweeps see Fig. S2 in the ESI†). Secondly, an oscillation frequency sweep was performed at $T = 25^\circ\text{C}$ as a function of the angular frequency ω . Lastly, a temperature sweep was carried out at an angular frequency of $\omega = 10\text{ s}^{-1}$ from $T = 25^\circ\text{C}$ to $T = 100^\circ\text{C}$ with a heating rate of 1 K min^{-1} to determine the sol-gel transition temperature $T_{\text{sol-gel}}$. Note that the storage modulus G' and loss modulus G'' were measured only once due to large deviations (10–50%) of repeated measurements.^{30,31} The absolute values should thus be looked at with care while the trends are discussable.

2.6 Freeze-fracture electron microscopy (FFEM)

Replicas of gelled and non-gelled microemulsions were prepared using the Freeze-Fracture and Etching System BAF060 from Leica. A small amount of the gelled microemulsion was transferred from the test tube to two copper grids between two copper plates (4.5 mm \times 3.0 mm), which were then assembled into a so-called sandwich. In the case of non-gelled microemulsion, the sandwich was immersed in the liquid sample with a tweezer for several minutes. Afterward, the sandwiches were quickly frozen in liquid ethane. After fracturing in liquid nitrogen, the grids with the frozen fractured specimen were fixed on a house-made specimen holder (with a metal cover plate to prevent contamination in the air) and quickly transferred into the vacuum chamber of the BAF060 ($T = -150^\circ\text{C}$). The frozen fractured surface of the specimens was shadowed with platinum-carbon (~ 2 nm) at 45° and covered by a layer of pure carbon (~ 20 nm) at 90° . The replicas were then cleaned with warm ethanol and acetone, dried, and examined with an EM10 transmission electron microscope from Zeiss operated at 60 kV.

3. Phase studies & gelator search

3.1 Influence of oil-to-water ratio on the phase behavior of non-gelled microemulsions

A systematic study of the phase behavior is an absolute prerequisite to further extend the application of non-toxic gelled microemulsions towards water-rich and oil-rich gelled microemulsions. Therefore, sections through the isothermal phase tetrahedron of the system $\text{H}_2\text{O} - \text{IPM} - \text{Plantacare 1200 UP} (\text{C}_{12}\text{G}_{1.4}) - 1,2\text{-octanediol}$ were recorded at five oil-to-water ratios, namely $\phi = 0.20, 0.35, 0.50, 0.65,$ and 0.80 , and at $T = 25^\circ\text{C}$. At a fixed oil-to-water ratio, the phase diagrams were recorded by determining the phase boundaries as a function of the surfactant mass fraction γ_{C} and the co-surfactant mass fraction γ_{D} .

The phase diagrams obtained for $\phi = 0.20, 0.50,$ and 0.80 are shown in the upper part of Fig. 1, while those measured for $\phi = 0.35$ and 0.65 are included in Fig. S1 in the ESI.† As can be seen, the phase behavior resembles that of quaternary microemulsions stabilized by alkyl polyglucoside surfactants, where the phase inversion at constant temperature is induced by the addition of a hydrophobic co-surfactant.^{32,33} Along this path, the phase behavior of the system changes from “2” to “2̄”, *i.e.* from an oil-in-water (o/w) microemulsion (lower phase) coexisting with an excess oil phase (upper phase) to a water-in-oil (w/o) microemulsion (upper phase) coexisting with an excess water phase (lower phase). In between, separated by 2-phase boundaries, the isotropic 1-phase microemulsion “1” can be found. By reducing the mass fraction γ_{C} of Plantacare 1200 UP, the lower 2̄ \rightarrow 1 and upper 1 \rightarrow 2̄ phase boundaries converge until they then meet at the so-called \tilde{X} point. The latter is a measure of the system's efficiency since it denotes the minimum amount of surfactant and co-surfactant needed to solubilize water and oil, *i.e.* forming a 1-phase microemulsion. At even lower values of γ_{C} , the coexistence of three phases “3”, namely an excess water phase (lower phase), a

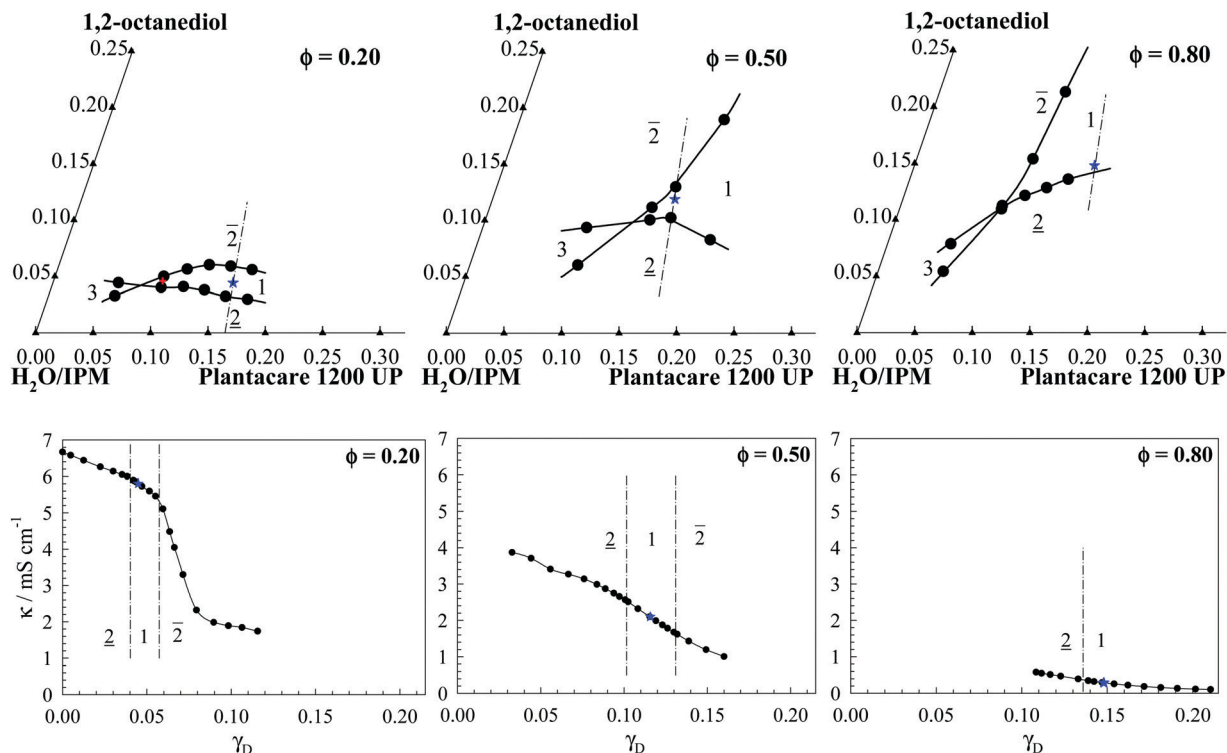


Fig. 1 (top) Phase diagrams of the non-toxic system H_2O – IPM – Plantacare 1200 UP ($\text{C}_{12}\text{G}_{1,4}$) – 1,2-octanediol at oil-to-water ratios of $\phi = 0.20, 0.50$ and 0.80 at $T = 25$ °C. The sample compositions of gelled microemulsions for the rheological measurements and FFEM are marked with a blue star, that of the non-gelled microemulsion at $\phi = 0.20$ for FFEM with a red cross. (bottom) Co-surfactant mass fraction γ_D -dependent electrical conductivities at $\phi = 0.20, 0.50$ and 0.80 at $T = 25$ °C. The titration path for measuring the electrical conductivity is indicated by a dashed-dotted line in the phase diagrams. The sample compositions for FFEM are marked with a blue star. Note that instead of pure water, a 0.1 wt% NaCl solution was used, which has a negligible effect on the phase behavior of the system.

microemulsion (middle phase), and an excess oil phase (upper phase), is observed between the two 2-phase regions.

When comparing the phase diagrams, one sees that the 1-phase region together with the \bar{X} point shifts to higher mass fractions γ_D of co-surfactant when the oil-to-water ratio increases. Furthermore, the mass fraction $\bar{\gamma}_C$ of surfactant passes through a maximum at the \bar{X} point around $\phi = 0.50$. Both trends can be explained mainly by the high monomeric solubility of 1,2-octanediol in IPM and the equal amounts of oil and water that need to be dissolved at $\phi = 0.50$. A more detailed discussion can be found in relation to the trajectory of \bar{X} points shown in Fig. 2.

Next, the continuity of the microemulsion structure was examined by electrical conductivity measurements. For this purpose, water was replaced by 0.1 wt% NaCl solution, which has a negligible effect on the phase behavior of the system, and the electrical conductivity was measured under vigorous stirring when 1,2-octanediol was added dropwise for each of the three oil-to-water ratios. In order to compare these results with the FFEM images, γ_C was chosen so that the titration path (dashed-dotted line in the phase diagrams) ran through the composition of the respective FFEM sample.

As can be seen in the bottom part of Fig. 1, the observed variation in electrical conductivity is typical for microemulsions stabilized by nonionic surfactants. The conductivity decreases with increasing co-surfactant mass fraction γ_D due to the

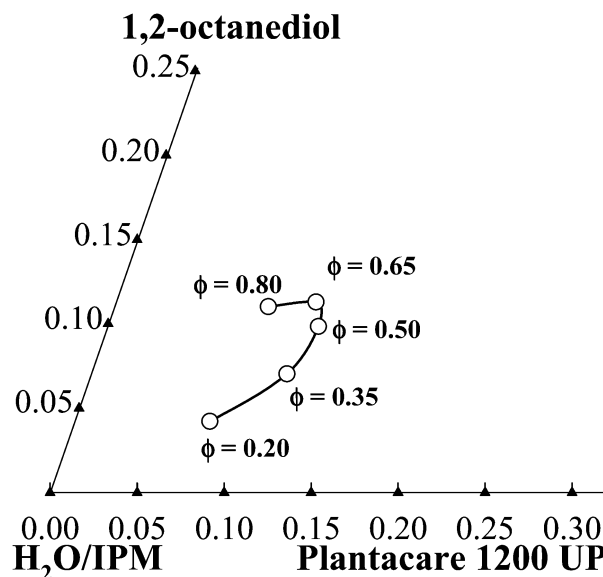


Fig. 2 The trajectory of the \bar{X} points (= intersection point of the 3-phase and the 1-phase regions in a fish cut) of the non-toxic system H_2O – IPM – Plantacare 1200 UP ($\text{C}_{12}\text{G}_{1,4}$) – 1,2-octanediol at $T = 25$ °C and various ϕ -ratios.

induced inversion from a water-continuous o/w microemulsion to an oil-continuous w/o microemulsion. Thereby, for the

studied non-toxic gelled microemulsions, the decrease in conductivity caused by the phase inversion is moderate. This is due, on the one hand, to the low salt concentration chosen and, on the other hand, to the relatively moderate microstructure formed. According to Kahlweit *et al.* the extent of the conductivity drop is systematically related to the amphiphilic nature of the surfactant and thus to the strength of the microstructure.³⁴

Discussing the electrical conductivity scans recorded for different oil-to-water ratios individually, one finds a sharp decrease in conductivity with increasing γ_D for the water-rich microemulsion ($\phi = 0.20$). In the 1-phase region, indicated by the dashed-dotted lines, the conductivity is high, indicating the existence of a water-continuous microemulsion. Note that one cannot deduce from this rather simple method to which extend discrete spherical or cylindrical oil droplets or network-like oil structures are present in the continuous water phase. However, since the focus of this work was on extending the application of the microemulsions, we refrained from using more advanced methods such as PFG-NMR or SANS to further elucidate the microstructure. The conductivity scan recorded for the symmetric microemulsion ($\phi = 0.50$) shows the typical sigmoidal shape. Within the 1-phase microemulsion region, the curve exhibits its steepest slope at an intermediate conductivity, strongly suggesting the presence of a bicontinuous structure, which was also proven by SANS.¹⁸ Looking now at the scan recorded for the oil-rich microemulsion ($\phi = 0.80$), one sees low and decreasing electrical conductivity values indicating the existence of an oil-continuous microemulsion, opposite to the water-continuous microemulsion observed at $\phi = 0.20$. Here, one could conclude from the low electrical conductivity values that discrete spherical or cylindrical water droplets are present in the continuous oil phase rather than network-like water structures. The electrical conductivity scans recorded at three different ϕ values agree with measurements of Kahlweit *et al.* on the ternary system $\text{H}_2\text{O}/\text{NaCl}-n\text{-octane}-\text{C}_{10}\text{E}_4$,³⁴ except that in the latter system, the phase inversion was induced by temperature rather than by the addition of a co-surfactant.

The systematic study of the phase behavior at different ϕ -values allows now to construct the trajectory of the middle phase microemulsion by connecting the \bar{X} points ($\bar{\gamma}_C$, $\bar{\gamma}_D$) (Fig. 2). Starting from the water-rich side at $\phi = 0.20$, the mass fractions of surfactant and co-surfactant needed to formulate an optimal microemulsion increase. The mass fraction $\bar{\gamma}_C$ of surfactant runs through a maximum between $\phi = 0.50$ and $\phi = 0.65$, which can be vividly explained by the fact that equal amounts of oil and water must be solubilized. Increasing the oil-to-water ratio further to $\phi = 0.80$ on the oil-rich side, the mass fraction of the surfactant decreases while the mass fraction of the co-surfactant remains nearly constant.

The finding that the maximum of the middle phase trajectory with respect to $\bar{\gamma}_C$ is located close to $\phi \approx 0.50$ was also found for other microemulsion systems, stabilized either by nonionic or ionic surfactant. The groups of Kahlweit and Strey recorded the trajectory of the \bar{X} points for ternary nonionic microemulsions

consisting of $\text{H}_2\text{O}-n\text{-alkane}-n\text{-alkyl polyglycol ether (C}_i\text{E}_j)$ ^{25,29,35-37} as well as for the quaternary ionic microemulsion $\text{D}_2\text{O}/\text{NaCl}-n\text{-decane}-\text{AOT}$.^{38,39} In both types of systems, the phase inversion is induced by a temperature change. While in the former, an increasing temperature leads to a transition from an oil-in-water to a water-in-oil microemulsion, the temperature trend is reversed in the ionic microemulsion system.

Related to the system studied in this work, the properties of a quaternary microemulsion stabilized by the sugar surfactant *n*-octyl- β -D-glucopyranoside ($\beta\text{-C}_8\text{G}_1$) have been studied along the middle phase trajectory using the co-surfactant 1-octanol to induce the phase inversion at constant temperature.^{28,33} Comparing the trajectory of the $\beta\text{-C}_8\text{G}_1$ -stabilized microemulsion with the non-toxic microemulsion studied here, one finds a very similar shape. In both systems the $\bar{\gamma}_D(\bar{\gamma}_C)$ -trajectory is nearly flat at the oil-rich side (*i.e.* the \bar{X} points have roughly the same content of co-surfactant for $\phi > 0.60$), whereas in the temperature-dependent microemulsions (without co-surfactant) the $\bar{T}(\bar{\gamma})$ -trajectory tends towards higher temperatures.

The different shapes of the $\bar{\gamma}_D(\bar{\gamma}_C)$ - and the $\bar{T}(\bar{\gamma})$ -trajectory can be explained if one keeps in mind that the main properties of microemulsions are determined by the interfacial film.⁴⁰ For quaternary microemulsions (with co-surfactant), the composition of the interfacial film changes along the trajectory due to an enrichment of co-surfactant molecules. This change results in a decreasing spontaneous curvature, which drives the microemulsion through phase inversion.^{28,41} Note that the determination of the composition of the interfacial film is not trivial since both the surfactant and the co-surfactant have a monomeric solubility in water and oil. Although not determined for the non-toxic microemulsion studied here, it can be concluded that along the trajectory, the fraction of 1,2-octanediol $\bar{\gamma}_D$ in the interfacial film increases sigmoidally, which is similar to the trend of the phase inversion temperature \bar{T} in temperature-dependent microemulsions (without co-surfactant).^{25,29,35-37} Furthermore, the mass fraction of Plantacare 1200 UP and 1,2-octanediol in the interfacial film is expected to vary in the form of an inverted parabola exhibiting a maximum slightly above $\phi \geq 0.5$. The almost flat shape of the $\bar{\gamma}_D(\bar{\gamma}_C)$ -trajectory at the oil-rich side can thus be explained by the fact that the fraction of 1,2-octanediol increases only slightly, while the total mass fraction of Plantacare 1200 UP and 1,2-octanediol decreases strongly in the internal interface.

3.2 Gelator search

Having investigated the phase behavior of the microemulsion $\text{H}_2\text{O} - \text{isopropyl myristate (IPM)} - \text{Plantacare 1200 UP (C}_{12}\text{G}_{1.4}) - 1,2\text{-octanediol}$, a proper low molecular weight gelator (LMWG) needed to be found for each oil-to-water ratio ϕ . The goal is to formulate gelled 1-phase microemulsions over a broad range of ϕ -ratios. In our previous study, we investigated the gelation behavior of the hydrogelator *N,N'*-dibenzoyl-L-cystine (DBC),⁴² the organogelator 12-hydroxyoctadecanoic acid (12-HOA),^{43,44} and of the organogelator 1,3:2,4-dibenzylidene-D-sorbitol (DBS)²² in a microemulsion that contains equal volumes of water and oil ($\phi = 0.50$).¹⁸ It was found that DBC and 12-HOA

shift the phase boundaries of the 1-phase microemulsion. On the other hand, DBS turned out to be the ideal gelator, which gelled the bicontinuous microemulsion at a minimum gelation concentration (mgc) of 0.0014 and did not shift the phase boundaries. In the final formulation, we chose $\eta = 0.003$ to have a relatively strong gel.

Based on our previous results, we investigated the three LMWGs mentioned above in microemulsions for other ϕ -ratios. A summary of the gelation behavior is listed in Table 1. The goal was to formulate transparent gelled 1-phase microemulsions. The organogelator DBS formed a strong transparent gel in microemulsions with oil-to-water ratios $\phi \geq 0.35$ at $\eta = 0.003$. However, DBS could not be dissolved at $\eta = 0.0025$ in the microemulsion with $\phi = 0.20$ but formed a weak transparent gel in the microemulsion with $\phi = 0.20$ at $\eta = 0.002$. Because of the weakness of the gel, we tried to find a better LMWG for the water-rich microemulsion (see Table 1). The first candidates were hydrogelator derivatives of DBS, namely 1,3:2,4-dibenzylidene-D-sorbitol-*p,p'*-dicarboxylic acid (DBS-CO₂H)⁴⁵ and DBS-CONHNH₂,⁴⁶ which we assumed to dissolve better in the water-rich microemulsion. Indeed, both hydrogelators dissolved in the water-rich microemulsion at $\eta = 0.002$ but did not gel the system. Up to $\eta = 0.005$, no gelation was observed: the samples were clear liquids containing precipitated gelator crystals. The hydrogelator DBC formed either turbid or transparent gels in the microemulsions with $\phi = 0.20, 0.50$, and 0.80 , but the gelator always precipitated after a while. The organogelator 12-HOA could only form a turbid gel at $\phi = 0.20$. A transparent gel was obtained with 12-HOA at $\phi = 0.50$, but the gelator concentration was eight times higher than that of DBS, and the phase boundaries were shifted. Moreover, 12-HOA could not gel the microemulsion at $\phi = 0.80$. These results confirm what is already known: the gelation behavior of LMWGs in different solvents is difficult to predict, and there is no guiding rule for a gelator search.^{4,18} Overall, DBS was chosen as the gelator for the microemulsion at all ϕ -ratios, although only a weak gel can be obtained in the water-rich microemulsion. We thus chose $\eta = 0.002$ for the system with $\phi = 0.20$ and $\eta = 0.003$ for the systems with all other ϕ -ratios. For the sake of comparison, we also studied a sample with $\phi = 0.35$ and $\eta = 0.002$ (see Section 4.1).

4. Rheology of DBS-containing samples

4.1 Water-rich side

We chose DBS as the gelator to gel microemulsions consisting of H₂O – IPM – Plantacare 1200 UP (C₁₂G_{1.4}) – 1,2-octanediol. The gelator concentration was chosen to be $\eta = 0.003$ for all samples with oil-to-water ratios $\phi > 0.2$. Due to the limitation that only $\eta = 0.002$ of DBS could be dissolved in the system with $\phi = 0.20$, another water-rich system with $\phi = 0.35$ was measured at $\eta = 0.002$ for comparison.

A strong gel should have a larger storage modulus G' than loss modulus G'' , and both moduli should be independent of the frequency ω .^{47,48} In addition, the higher the absolute G' - and G'' -values, the stronger the gel is. Comparing the samples with $\phi = 0.20, \eta = 0.002$ and $\phi = 0.35, \eta = 0.002$ (Fig. 3, top), one sees that for both it indeed holds $G' > G''$. However, the moduli G' and G'' of the former sample are one order of magnitude smaller than those of the latter sample. Besides, the sample with $\phi = 0.20, \eta = 0.002$ shows stronger dependence of the frequency ω than the sample with $\phi = 0.35, \eta = 0.002$. These two samples contain the same amount of surfactants and co-surfactants and only differ in the oil-to-water ratio ϕ . However, the sample with $\phi = 0.20$ is a much weaker gel than the sample with $\phi = 0.35$. The reason will be discussed in Sections 4.3 and 5.

Comparing the frequency sweeps of the sample with $\phi = 0.35, \eta = 0.002$ measured at $\tau = 1$ Pa (Fig. 3, top right) and at $\tau = 10$ Pa (Fig. 3, bottom left), one sees that the G' - and G'' -values are slightly larger at $\tau = 1$ Pa than those at $\tau = 10$ Pa. This makes sense since, at higher shear stress, the gel sample is more “deformed”, and the mechanical properties are weaker. Additionally, the results measured at $\tau = 1$ Pa show a frequency dependence at $\omega > 40$ s⁻¹, which is not the case at $\tau = 10$ Pa. Since the frequency sweep is carried out at shear stress near the end of the LVE region (see Fig. S2 in the ESI[†]), the measurement at $\tau = 10$ Pa provides more reliable data.

The frequency sweeps of the samples with $\phi = 0.35, \eta = 0.002$ and $\phi = 0.35, \eta = 0.003$ show the typical behavior of a strong gel (Fig. 3, bottom). The storage modulus G' is one order of magnitude larger than the loss modulus G'' , and both are independent of the

Table 1 Summary of the gelation behavior of LMWGs on the non-toxic microemulsion at various ϕ -ratios. “HG” stands for hydrogelator, and “OG” stands for organogelator

ϕ	DBS (OG)	DBS-CO ₂ H, DBS-CONHNH ₂ (HG derivatives of DBS)	DBC (HG)	12-HOA (OG)
0.20	<ul style="list-style-type: none"> Weak transparent gel at $\eta = 0.002$ DBS could not be dissolved at $\eta = 0.0025$ 	<ul style="list-style-type: none"> $\eta = 0.002$ could be dissolved at 90 °C but no gelation $\eta = 0.005$, no gelation, clear liquid plus gelator crystals 	<ul style="list-style-type: none"> Turbid gel at $\eta = 0.0125$ (mgc) Transparent gel at $\eta = 0.015$, but gelator precipitated after 1 h 	<ul style="list-style-type: none"> Turbid gel at $\eta = 0.02$
0.35	<ul style="list-style-type: none"> Transparent gel at $\eta = 0.003$ 		<ul style="list-style-type: none"> Turbid gel at $\eta = 0.024$ (mgc), gelator precipitated overnight 	<ul style="list-style-type: none"> Transparent gel at $\eta = 0.025$ (mgc = 0.02)
0.50	<ul style="list-style-type: none"> Transparent gel at $\eta = 0.003$ (mgc = 0.0014) 			
0.65	<ul style="list-style-type: none"> Transparent gel at $\eta = 0.003$ 			
0.80	<ul style="list-style-type: none"> Transparent gel at $\eta = 0.003$ 		<ul style="list-style-type: none"> Transparent weak gel $\eta = 0.02$, but gelator precipitated after 1 hour; or could transparent liquid and gelator flocculates 	<ul style="list-style-type: none"> no gelation at $\eta = 0.02$, gelator not be dissolved completely

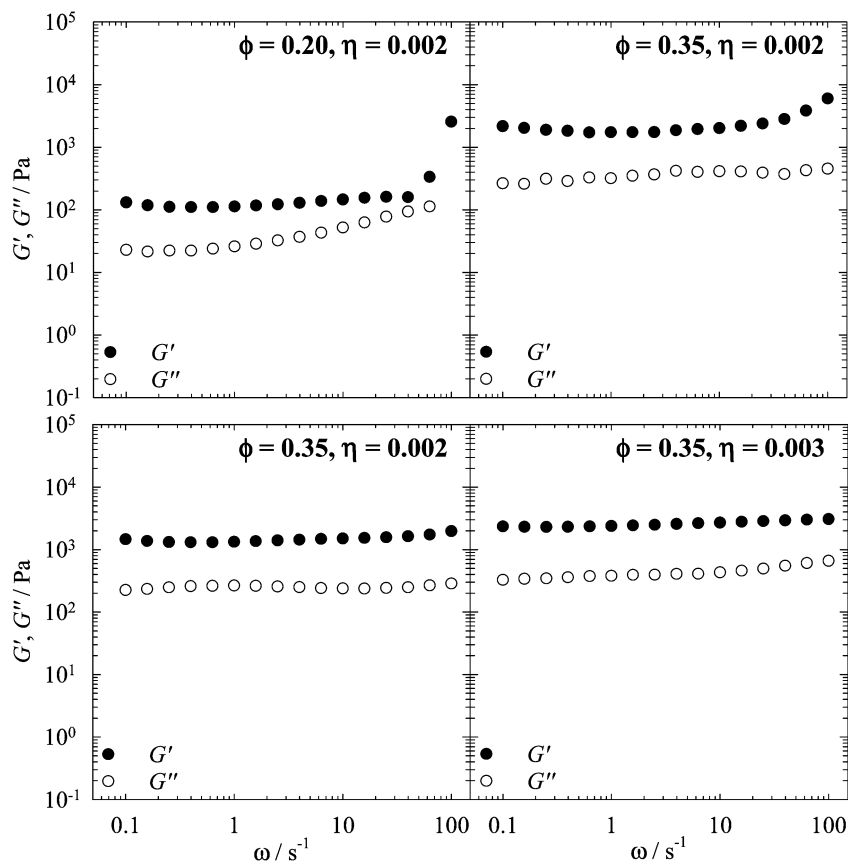


Fig. 3 Storage modulus G' (filled symbols) and loss modulus G'' (open symbols) of the gelled microemulsion in the presence of DBS at $T = 25\text{ }^{\circ}\text{C}$ as a function of the angular frequency ω with (top) $\phi = 0.20$, $\eta = 0.002$ and $\phi = 0.35$, $\eta = 0.002$ at a shear stress of $\tau = 1\text{ Pa}$; (bottom) $\phi = 0.35$, $\eta = 0.002$ and $\phi = 0.35$, $\eta = 0.003$ at a shear stress of $\tau = 10\text{ Pa}$.

frequency ω . The only difference is that the moduli G' and G'' of the sample with $\eta = 0.003$ are slightly larger than those with $\eta = 0.002$ due to the slightly higher gelator concentration.

Subsequently, temperature sweeps were carried out to characterize the sol-gel transition temperature $T_{\text{sol-gel}}$, *i.e.* the temperature at which the storage modulus G' drops sharply and crosses the loss modulus G'' . All values for $T_{\text{sol-gel}}$ are listed in Table 2. Because the sample with $\phi = 0.20$ and $\eta = 0.002$ could only be measured at $\tau = 1\text{ Pa}$, we first compared the systems with $\phi = 0.20$ and $\phi = 0.35$ at the same low gelator concentration of $\eta = 0.002$ at a shear stress of $\tau = 1\text{ Pa}$ (Fig. 4, top). The G' - and G'' -values of the sample with $\phi = 0.20$ are one order of magnitude smaller than the sample with $\phi = 0.35$, *i.e.* the former is a much weaker gel. However, the two samples have similar sol-gel transition temperatures, namely $T_{\text{sol-gel}} = (81 \pm 1)\text{ }^{\circ}\text{C}$ and $T_{\text{sol-gel}} = (84 \pm 1)\text{ }^{\circ}\text{C}$ (see Table 2). This indicates that the $T_{\text{sol-gel}}$ depends on the gelator concentration since both samples have $\eta = 0.002$, while the difference of mechanical strengths only slightly influences the $T_{\text{sol-gel}}$. Comparing the $T_{\text{sol-gel}}$ of the sample with $\phi = 0.35$, $\eta = 0.002$ measured at $\tau = 1\text{ Pa}$ (Fig. 4, top right) and at $\tau = 10\text{ Pa}$ (Fig. 4, bottom left), one sees that the $T_{\text{sol-gel}}$ is $20\text{ }^{\circ}\text{C}$ lower at $\tau = 10\text{ Pa}$ than at $\tau = 1\text{ Pa}$. We speculate that the higher shear stress starts “destroying” and weakens the gel because the shear stress at $\tau = 10\text{ Pa}$ is close to the yield point (see Fig. S2 in ESI†). This also reveals that the $T_{\text{sol-gel}}$ values measured at $\tau = 1\text{ Pa}$ are not directly

comparable with the results of the other samples measured at $\tau = 10\text{ Pa}$ (see Table 2). For the system with $\phi = 0.35$, we compared two gelator concentrations, $\eta = 0.002$ and $\eta = 0.003$, respectively, at $\tau = 10\text{ Pa}$ (Fig. 4, bottom). The $T_{\text{sol-gel}}$ of the sample with $\eta = 0.002$ is around $(64 \pm 1)\text{ }^{\circ}\text{C}$, and the $T_{\text{sol-gel}}$ of the sample with $\eta = 0.003$ is around $(72 \pm 1)\text{ }^{\circ}\text{C}$. As expected, the higher gelator concentration leads to a higher sol-gel transition temperature $T_{\text{sol-gel}}$.^{43,49}

4.2 Oil-rich side

On the oil-rich side, DBS can be dissolved well in the 1-phase microemulsion $\text{H}_2\text{O} - \text{IPM} - \text{Plantacare 1200 UP} (\text{C}_{12}\text{G}_{1.4}) - 1,2$ -octanediol. Thus three samples were compared with $\eta = 0.003$, namely $\phi = 0.50, 0.65$ and 0.80 . The frequency sweeps of the three samples (Fig. 5) are very similar and indicate that all three samples

Table 2 Summary of the composition and the rheological data of all gelled microemulsions

ϕ	γ_{C}	γ_{D}	η	τ/Pa	$T_{\text{sol-gel}}/^{\circ}\text{C}$	G'/Pa	G''/Pa
0.20	0.1572	0.0442	0.002	1	81	146	52
0.35	0.1557	0.0810	0.002	1	84	2010	412
0.35	0.1557	0.0810	0.002	10	64	1500	239
0.35	0.1553	0.0818	0.003	10	72	2700	431
0.50	0.1590	0.1188	0.003	10	72	2990	493
0.65	0.1584	0.1400	0.003	10	71	2320	442
0.80	0.1570	0.1480	0.003	10	73	3830	593

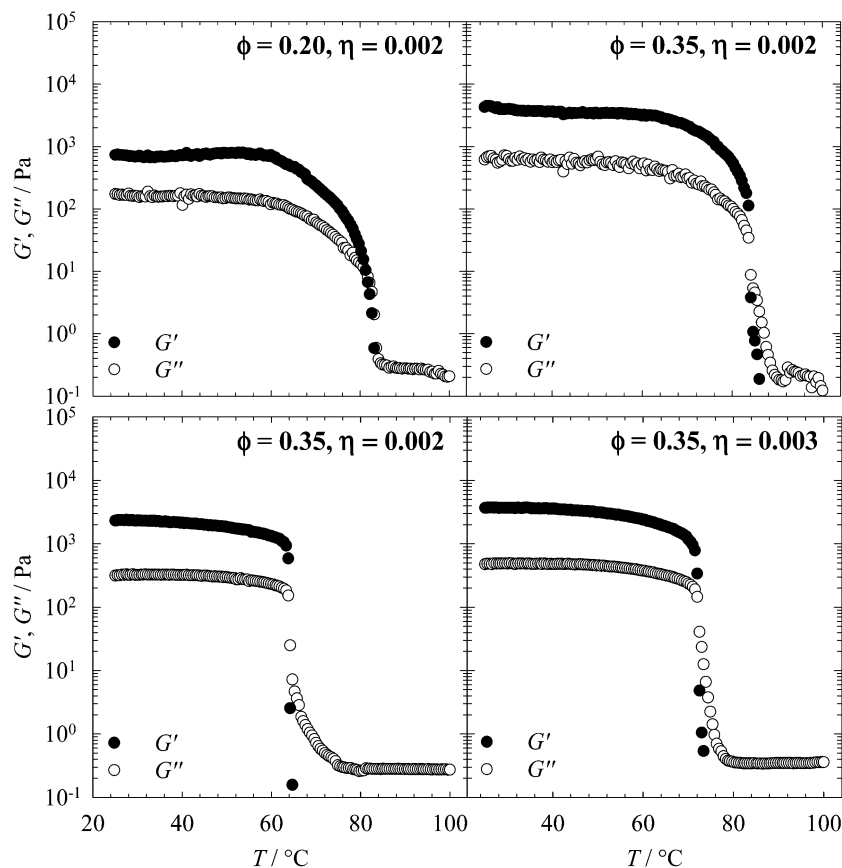


Fig. 4 Storage modulus G' (filled symbols) and loss modulus G'' (open symbols) of the gelled microemulsion in the presence of DBS at an angular frequency of $\omega = 10 \text{ s}^{-1}$ as a function of T . Heating rate 1 °C min^{-1} . (top) $\phi = 0.20$, $\eta = 0.002$ and $\phi = 0.35$, $\eta = 0.002$ at a shear stress of $\tau = 1 \text{ Pa}$; (bottom) $\phi = 0.35$, $\eta = 0.002$ and $\phi = 0.35$, $\eta = 0.003$ at a shear stress of $\tau = 10 \text{ Pa}$.

are strong gels: (a) the storage modulus G' is in the range of 10^3 Pa , while the loss modulus G'' is in the range of 10^2 Pa ; (b) both moduli only have very weak frequency dependence. The temperature sweeps (Fig. 6) tell the same story as the frequency sweeps: there is hardly any difference. The $T_{\text{sol-gel}}$ for the sample with $\phi = 0.50$ is around $(72 \pm 1) \text{ °C}$, for the sample with $\phi = 0.65$ around $(71 \pm 1) \text{ °C}$,

and for the sample with $\phi = 0.80$ around $(73 \pm 1) \text{ °C}$. Again, all values for $T_{\text{sol-gel}}$ are listed in Table 2.

4.3 Discussion

Table 2 provides the key rheological data of the studied gelled microemulsions. The sample compositions are marked in the

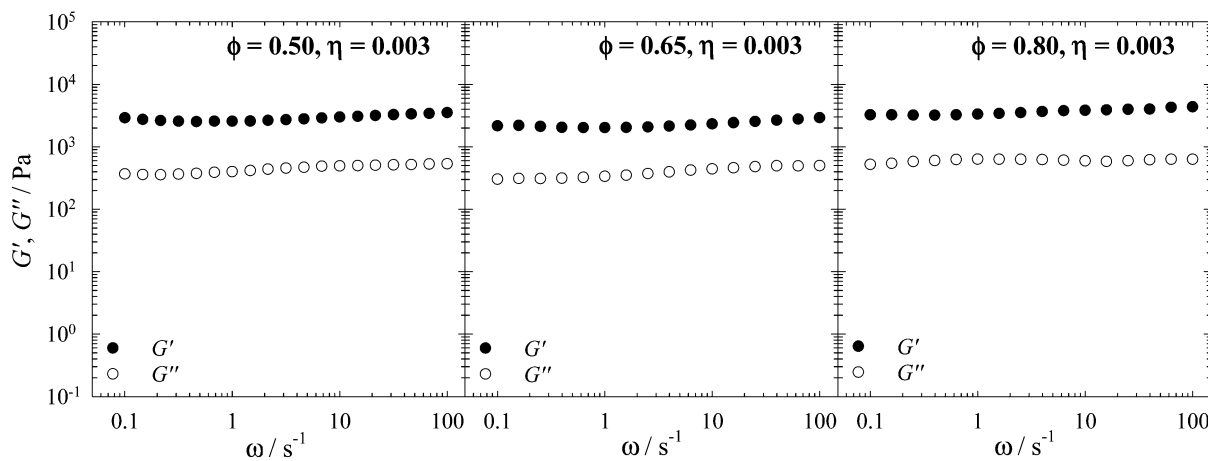


Fig. 5 Storage modulus G' (filled symbols) and loss modulus G'' (open symbols) of the gelled microemulsion in the presence of DBS at $\eta = 0.003$, $\tau = 10 \text{ Pa}$, $T = 25 \text{ °C}$ as a function of the angular frequency ω with $\phi = 0.50$ (left), $\phi = 0.65$ (middle), $\phi = 0.80$ (right).

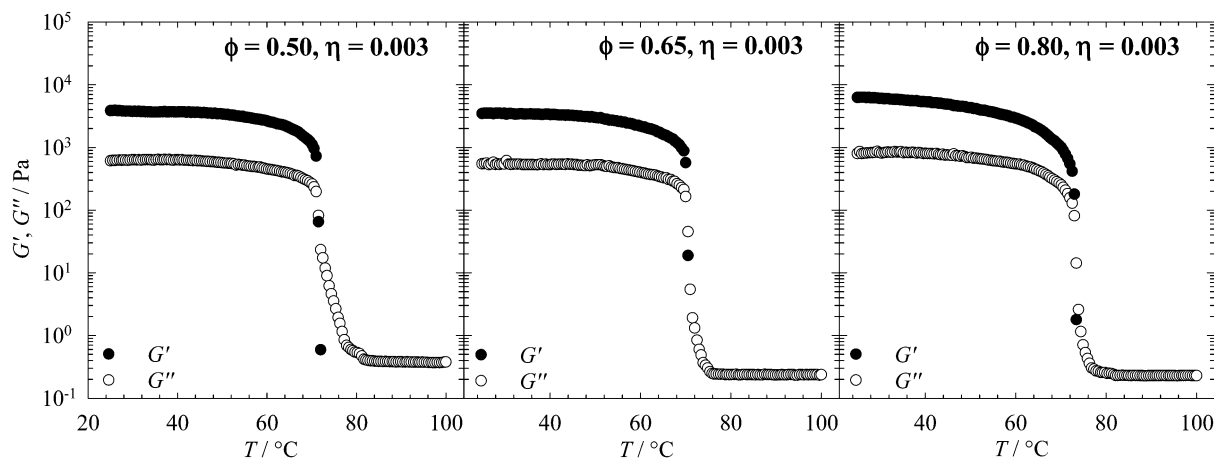


Fig. 6 Storage modulus G' (filled symbols) and loss modulus G'' (open symbols) of the gelled microemulsion in the presence of DBS at $\eta = 0.003$, $\tau = 10$ Pa, $\omega = 10$ s $^{-1}$ as a function of T and a heating rate of 1 °C min $^{-1}$ with $\phi = 0.50$ (left), $\phi = 0.65$ (middle), $\phi = 0.80$ (right).

corresponding phase diagrams (see Fig. 1 and Fig. S1 in the ESI†). The sample with $\phi = 0.20$, $\eta = 0.002$ is a much weaker gel than the sample with $\phi = 0.35$, $\eta = 0.002$ measured at $\tau = 1$ Pa according to the G' - and G'' -values. Surprisingly, except for the system with $\phi = 0.20$, all other systems from $\phi = 0.35$ to $\phi = 0.80$ with $\eta = 0.003$ measured at $\tau = 10$ Pa have nearly the same rheological behavior: (1) the storage modulus G' is in the range of 10^3 Pa, while the loss modulus G'' is in the range of 10^2 Pa; (2) both moduli only have very weak frequency dependence; (3) the $T_{\text{sol-gel}}$ is around 72 °C. Despite the fact that DBS is an organogelator and that the system with $\phi = 0.35$ is water-rich, its rheological behavior does not differ from that of the other systems with $\phi > 0.35$. Having said this, one can ask the question: Why is the gelled microemulsion with $\phi = 0.20$ a much weaker gel than all other samples?

One explanation could be the fact that DBS is an organogelator and thus the system simply needs more oil than water to form a gel. However, in this case, DBS would not gel the water-rich microemulsion with $\phi = 0.35$ either. Note that the gel fibrils are not only formed in the oil-rich (oil-continuous) regions of the microemulsion. A gel is a sample-spanning three-dimensional fiber network, *i.e.* the fibers must pass both oil domains and water domains.

Another explanation is based on the solvent properties. Hansen solubility parameters (HSPs) have been used to quantitatively characterize the gelation behavior of LMWGs in various solvents since the 2010s.^{50–52} HSPs quantify the cohesive energy density δ of a solvent from three types of weak interactions: dipole–dipole or polar interactions δ_p , hydrogen-bonding interactions δ_H , and van der Waals or dispersive interactions δ_D .⁵³ Each solvent is a point on the 3D Hansen space in which the axes represent the three HSPs (δ_p , δ_H , $2\delta_D$), and the distance from the origin to that point represents the total cohesive energy density δ of the solvent. Raghavan *et al.* proposed a powerful predictive gelation model for DBS for a wide range of organic solvents.⁵² According to Raghavan *et al.*, the HSPs of DBS are close to those of the solvents in which it is soluble and different from those of the solvents in which it is insoluble.

The interactions between gelator and solvent are divided into four categories: the gelator is soluble (S), a slow gel is formed (SG), a gel is formed instantaneously (IG), and the gelator is insoluble (I). The four categories are visualized by four concentric spheres sharing the same origin on the 3D Hansen space (Fig. 2 in ref. 52). The inner sphere contains the solvents in which DBS is soluble (S), the outer contains the solvents in which DBS is insoluble (I), and the two spheres in between contain the solvents which can be gelled by DBS (SG and IG). The center of the sphere is the HSPs of 1% (weight/volume) DBS with $(\delta_p, \delta_H, 2\delta_D) = (13.6, 6.4, 35.6)$, which was fitted from the gelation results of 1% DBS in 35 solvents.

Looking at our microemulsions at various oil-to-water ratios, one can argue that the solvent properties mainly depend on the IPM-to-water ratio. We found the following HSPs for IPM and water, namely $\delta_p = 2$, $\delta_H = 4$, $2\delta_D = 32.4$ for IPM⁵⁴ and $\delta_p = 16$, $\delta_H = 42.3$, $2\delta_D = 31$ for water⁵³ and we note that 1% DBS forms an instant gel in IPM but is insoluble in water. Plotting the results on the Hansen space (see Fig. S3 in the ESI†), one sees that IPM and water are located on two different sides of the Hansen space and that the distance between the center of the sphere (HSPs of DBS) and water is much larger than the distance between DBS and IPM. If we now change the solvent properties and thus the HSPs by changing the amount of surfactant, co-surfactant, water, and IPM, we approach the two inner spheres (in which gelation occurs) from two different sides. For additional gelation tests with DBS in other components of our microemulsion, we refer to Table S1 in the ESI.† Although we do not know the HSPs of our microemulsion domains (the water domains contain monomerically dissolved surfactant molecules and the oil domains a considerable amount of the co-surfactant 1,2-octanediol) and although the domains are separated by a surfactant film, we can argue that 35 vol% oil needs to be added to water ($\phi = 0.35$) to change the HSPs of the microemulsion such that instant gelation to a strong gel occurs, while it is enough to add 20 vol% water to the oil phase ($\phi = 0.80$) to reach this situation. According to Raghavan *et al.*, the rheological properties of the gelled solvents in the IG sphere are

very similar, which is in line with our findings that all gelled microemulsions with $\phi \geq 0.35$ have similar rheological behavior.

However, there is one problem when using the HSPs theory to explain our results: the gelled microemulsion with $\phi = 0.20$ is close to the water side (see Fig. S3 in the ESI†) and thus very likely located in the IG sphere. According to the HSPs theory, this sample should be a strong gel, which is not the case. Therefore, we argue that not only the gelator–solvent interactions, but also the microstructure plays a role in the gelation behavior, as will be further discussed in Section 5.

5 FFEM

To visualize the coexistence of the gel network and the microemulsion and to gain insight into the structural change from water-rich to oil-rich microemulsions, freeze-fracture electron microscopy (FFEM) of three gelled microemulsion samples with oil-to-water ratios of $\phi = 0.20$, 0.50, and 0.80, respectively, was performed (Fig. 7). The sample compositions are the same as those chosen for the rheological measurements and are marked in the phase diagrams with blue stars.

Looking at Fig. 7, one clearly sees gel fibers of DBS (marked with red arrows) in all samples. Regardless of the ϕ -value, the rope-like twisted gel fibers have diameters of $d_{\text{fibril}} \approx 6\text{--}12$ nm, while the length of gel fibers varies between 150 and 300 nm. Note that the d_{fibril} -range is consistent with previous studies: (1) in a similar alkanoyl methylglucamide-based gelled non-toxic microemulsion system, the DBS gel fibers have diameters of $d_{\text{fibril}} \approx 8\text{--}12$ nm and the same appearance.⁵⁵ (2) In lyotropic liquid crystals consisting of H_2O and C_{12}E_7 and equally gelled with DBS, the gel fibers have diameters of $d_{\text{fibril}} \approx 8\text{--}18$ nm.⁵⁶

Opposed to the gel fibers, the structure of the coexisting microemulsions is difficult to see in Fig. 7. (i) For the sample with $\phi = 0.20$, a non-gelled microemulsion sample with $\phi = 0.20$ was additionally investigated (Fig. S4 in the ESI†). The FFEM image shows polydisperse spherical and cylindrical oil droplets in a continuous water domain, confirming the results from electrical conductivities (Fig. 1), which clearly indicate a water-continuous microemulsion structure. (ii) For the sample with

$\phi = 0.50$, both the electrical conductivity scan and the previous small-angle neutron scattering (SANS) measurements suggest the existence of a bicontinuous structure with a periodicity of $d = 14.0$ nm and a correlation length of $\xi_{\text{TS}} \approx 6.3$ nm.¹⁸ (iii) For $\phi = 0.80$, the FFEM image shows a continuous oil phase, whereas water droplets are hardly visible. This result agrees with the detected low values of electrical conductivity, which also strongly indicate the presence of an oil-continuous microemulsion with discrete spherical or cylindrical water droplets. In any case, the structural change of the coexisting microemulsion is in line with that of the quaternary system D_2O –*n*-octane– β - C_8G_1 –1-octanol. NMR and SANS results varying from $\phi = 0.1$ to $\phi = 0.9$ by step of 0.1 indicate that the bicontinuous structure almost remains invariant between $\phi = 0.3$ and $\phi = 0.7$, while more and more discrete droplet-like structures are observed at lower and higher ϕ -ratios, respectively.²⁸

The dependence of the microemulsion structure on the oil-to-water ratio may explain the rheological results. We recall that the gelled microemulsion with $\phi = 0.20$ is a much weaker gel than all other samples with higher oil contents. Taking the water-continuous structure of the microemulsion into account, one can argue as follows. At $\phi = 0.20$, we basically have a water-continuous solvent for our organogelator. At all other oil-to-water ratios, the microemulsion is either bicontinuous or oil-continuous – in both cases, an oil-continuous phase is present. Obviously, the presence of an oil-continuous phase is a prerequisite for the formation of a strong gel in the case of the organogelator DBS.

6 Conclusion & outlook

In a previous study, we have formulated and characterized a gelled non-toxic bicontinuous microemulsion consisting of H_2O – IPM – Plantacare 1200 UP ($\text{C}_{12}\text{G}_{1.4}$) – 1,2-octanediol in the presence of the low molecular weight organogelator DBS with equal volumes of water and oil ($\phi = 0.50$).¹⁸ In the study at hand, we aimed to develop gelled non-toxic microemulsions which are either water- or oil-rich for the dissolution of both oil- and water-soluble drugs. For this purpose, we varied the

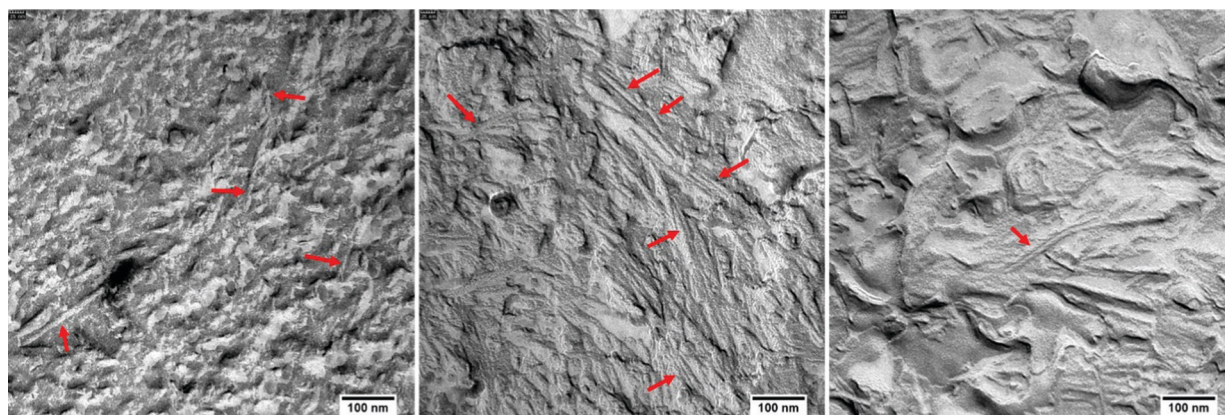


Fig. 7 FFEM images of the gelled non-toxic system H_2O – IPM – Plantacare 1200 UP ($\text{C}_{12}\text{G}_{1.4}$) – 1,2-octanediol in the presence of DBS with (left) $\phi = 0.20$, $\eta = 0.002$, (middle) $\phi = 0.50$, $\eta = 0.003$, (right) $\phi = 0.80$, $\eta = 0.003$. Red arrows point at the gel fibers.

oil-to-water ratios from water-rich ($\phi = 0.20$) to oil-rich ($\phi = 0.80$) and measured the respective phase diagrams. Complementary measurements of the electrical conductivities allowed us to study the continuity of the microemulsion structure at $\phi = 0.20$, 0.50, and 0.80.

Subsequently, a suitable low molecular weight gelator (LMWG) needed to be found for all ϕ -ratios. The organogelator 1,3:2,4-dibenzylidene-D-sorbitol (DBS) gelled the microemulsions with $\phi = 0.35$, 0.65 and 0.80 at a gelator mass fraction of $\eta = 0.003$. However, on the water-rich side at $\phi = 0.20$, DBS could only be dissolved up to $\eta = 0.002$, resulting in a weak gel. Thus, several LMWGs were tested to find a better gelator for the water-rich microemulsion, but none of them was able to gel the sample with $\phi = 0.20$. These results again confirm that the gelation behavior of LMWGs in different solvents is difficult to predict.^{4,18}

Then we characterized the rheological properties of the gelled microemulsions. Surprisingly, except for the system with $\phi = 0.20$, all systems from $\phi = 0.35$ to $\phi = 0.80$ with $\eta = 0.003$ have nearly the same rheological behavior. We explain the same rheological behavior with the location of our microemulsions in the Hansen space, while we attribute the different behavior of the sample with $\phi = 0.20$ to the microstructure of the microemulsion, which is water-continuous according to electrical conductivity values and FFEM images. In other words, for our microemulsions an oil-continuous phase is obviously required for the formation of a strong gel with DBS.

In future studies, a good gelator for the water-rich system with $\phi \leq 0.20$ needs to be found. Second, with the knowledge of how to formulate gelled microemulsions at a desired oil-to-water ratio, tailor-made drug-containing gelled non-toxic microemulsions will be formulated for various pharmaceutical purposes. Skin permeation measurements will be carried out to study the performance of these drug-containing gelled non-toxic microemulsions. Furthermore, with stimuli-responsive gelators (light, pH, temperature, salt, *etc.*), a controlled release of drugs from gelled non-toxic microemulsions would be possible.

Conflicts of interest

There are no conflicts to declare.

Acknowledgements

The authors thank Ms Nadine Schnabel for her instructions on electrical conductivity measurements, and sincere thanks to Prof. Dr Srinivasa R. Raghavan for sharing their valuable datasets of DBS in various solvents and the MATLAB program for calculations.

References

- 1 P. E. Laibinis, J. J. Hickman, M. S. Wrighton and G. M. Whitesides, Orthogonal self-assembled monolayers: alkanethiols on gold and alkane carboxylic acids on alumina, *Science*, 1989, **245**, 845–847.
- 2 C. Stubenrauch and F. Gießelmann, Gelled Complex Fluids: Combining Unique Structures with Mechanical Stability, *Angew. Chem., Int. Ed.*, 2016, **55**, 3268–3275.
- 3 A. M. Brizard and J. H. Van, Esch, Self-assembly approaches for the construction of cell architecture mimics, *Soft Matter*, 2009, **5**, 1320–1327.
- 4 R. G. Weiss, The past, present, and future of molecular gels. What is the status of the field, and where is it going?, *J. Am. Chem. Soc.*, 2014, **136**, 7519–7530.
- 5 A. Heeres, C. Van Der Pol, M. Stuart, A. Friggeri, B. L. Feringa and J. V. Esch, Orthogonal Self-Assembly of Low Molecular Weight Hydrogelators and Surfactants, *J. Am. Chem. Soc.*, 2003, **125**, 14252–14253.
- 6 A. Brizard, M. Stuart, K. Van Bommel, A. Friggeri, M. De Jong and J. V. Esch, Preparation of nanostructures by orthogonal self-assembly of hydrogelators and surfactants, *Angew. Chem., Int. Ed.*, 2008, **47**, 2063–2066.
- 7 T. Kato, Y. Hirai, S. Nakaso and M. Moriyama, Liquid-crystalline physical gels, *Chem. Soc. Rev.*, 2007, **36**, 1857–1867.
- 8 S. Koitani, S. Dieterich, N. Preisig, K. Aramaki and C. Stubenrauch, Gelling Lamellar Phases of the Binary System Water–Didodecyldimethylammonium Bromide with an Organogelator, *Langmuir*, 2017, **33**, 12171–12179.
- 9 K. Steck, S. Dieterich, C. Stubenrauch and F. Giesselmann, Surfactant-based lyotropic liquid crystal gels – the interplay between anisotropic order and gel formation, *J. Mater. Chem. C*, 2020, 5335–5348.
- 10 S. Dieterich, S. Prévost, C. Dargel, T. Sottmann and F. Giesselmann, Synergistic structures in lyotropic lamellar gels, *Soft Matter*, 2020, **16**, 10268–10279.
- 11 S. Dieterich, F. Stemmler, N. Preisig and F. Giesselmann, Micellar Lyotropic Nematic Gels, *Adv. Mater.*, 2021, **33**, 2007340.
- 12 M. Laupheimer, K. Jovic, F. E. Antunes and M. da Graça, Martins Miguel and C. Stubenrauch, Studying orthogonal self-assembled systems: phase behaviour and rheology of gelled microemulsions, *Soft Matter*, 2013, **9**, 3661.
- 13 M. Laupheimer, T. Sottmann, R. Schweins and C. Stubenrauch, Studying orthogonal self-assembled systems: microstructure of gelled bicontinuous microemulsions, *Soft Matter*, 2014, **10**, 8744–8757.
- 14 R. Strey, Microemulsion microstructure and interfacial curvature, *Colloid Polym. Sci.*, 1994, **272**, 1005–1019.
- 15 J. Carlfors, I. Blute and V. Schmidt, Lidocaine in microemulsion – a dermal delivery system, *J. Dispersion Sci. Technol.*, 1991, **12**, 467–482.
- 16 M. A. Bolzinger, T. C. Carduner and M. C. Poelman, Bicontinuous sucrose ester microemulsion: A new vehicle for topical delivery of niflumic acid, *Int. J. Pharm.*, 1998, **176**, 39–45.
- 17 M. J. Lawrence and G. D. Rees, Microemulsion-based media as novel drug delivery systems, *Adv. Drug Delivery Rev.*, 2012, **64**, 175–193.
- 18 K. Peng, T. Sottmann and C. Stubenrauch, Gelled non-toxic microemulsions: Phase behavior & rheology, *Soft Matter*, 2019, **15**, 8361–8371.

- 19 D. Nickel, C. Nitsch, P. Kurzendörfer and W. Von Rybinski, Interfacial properties of surfactant mixtures with alkyl polyglycosides, *Trends Colloid Interface Sci.*, 1992, vol. 252, pp. 249–252.
- 20 M. M. Fiume, B. Heldreth, W. F. Bergfeld, D. V. Belsito, R. A. Hill, C. D. Klaassen, D. Liebler, J. G. Marks, R. C. Shank, T. J. Slaga, P. W. Snyder and F. A. Andersen, Safety Assessment of Decyl Glucoside and Other Alkyl Glucosides as Used in Cosmetics, *Int. J. Toxicol.*, 2013, **32**, 22S–48S.
- 21 A. Kogan and N. Garti, Microemulsions as transdermal drug delivery vehicles, *Adv. Colloid Interface Sci.*, 2006, **123**, 369–385.
- 22 B. O. Okesola, V. M. P. Vieira, D. J. Cornwell, N. K. Whitelaw and D. K. Smith, 1,3:2,4-Dibenzylidene-D-sorbitol (DBS) and its derivatives – efficient, versatile and industrially-relevant low-molecular-weight gelators with over 100 years of history and a bright future, *Soft Matter*, 2015, **11**, 4768–4787.
- 23 K. Peng, T. Sottmann and C. Stubenrauch, Gelled non-toxic bicontinuous microemulsions as promising transdermal drug carriers, *Mol. Phys.*, 2021, e1886363.
- 24 W. Jahn and R. Strey, Microstructure of microemulsions by freeze fracture electron microscopy, *J. Phys. Chem.*, 1988, **92**, 2294–2301.
- 25 S. Burauer, L. Belkoura, C. Stubenrauch and R. Strey, Bicontinuous microemulsions revisited: A new approach to freeze fracture electron microscopy (FFEM), *Colloids Surf., A*, 2003, **228**, 159–170.
- 26 B. Lindman, N. Kamenka, T. M. Kathopoulis, B. Brun and P. G. Nilsson, Translational diffusion and solution structure of microemulsions, *J. Phys. Chem.*, 1980, **84**, 2485–2490.
- 27 B. Lindman and U. Olsson, Structure of Microemulsions Studied by NMR, *Ber. Bunsenges. Phys. Chem.*, 1996, **100**, 344–363.
- 28 J. Reimer, O. Söderman, T. Sottmann, K. Kluge and R. Strey, Microstructure of alkyl glucoside microemulsions: Control of curvature by interfacial composition, *Langmuir*, 2003, **19**, 10692–10702.
- 29 T. Sottmann and R. Strey, Evidence of corresponding states in ternary microemulsions of water-alkane, *J. Phys.: Condens. Matter*, 1996, **8**, A39.
- 30 K. Steck, J. H. van Esch, D. K. Smith and C. Stubenrauch, Tuning gelled lyotropic liquid crystals (LLCs) – probing the influence of different low molecular weight gelators on the phase diagram of the system H₂O/NaCl–Genapol LA070, *Soft Matter*, 2019, **15**, 3111–3121.
- 31 K. Steck and C. Stubenrauch, Gelling Lyotropic Liquid Crystals with the Organogelator 1,3:2,4-Dibenzylidene-D-sorbitol Part I: Phase Studies and Sol-Gel Transitions, *Langmuir*, 2019, **35**, 17132–17141.
- 32 C. Stubenrauch, B. Paepflow and G. H. Findenegg, Microemulsions Supported by Octyl Monoglucoside and Geraniol. 1. The Role of the Alcohol in the Interfacial Layer, *Langmuir*, 1997, **13**, 3652–3658.
- 33 T. Sottmann, K. Kluge, R. Strey, J. Reimer and O. Söderman, General patterns of the phase behavior of mixtures of H₂O, alkanes, alkyl glucosides, and cosurfactants, *Langmuir*, 2002, **18**, 3058–3067.
- 34 M. Kahlweit, G. Busse and J. Winkler, Electric conductivity in microemulsions, *J. Chem. Phys.*, 1993, **99**, 5605–5614.
- 35 M. Kahlweit, R. Strey, D. Haase, H. Kunieda, T. Schmeling, B. Faulhaber, M. Borkovec, H. F. Eicke, G. Busse, F. Eggers, T. Funck, H. Richmann, L. Magid, O. Söderman, P. Stilbs, J. Winkler, A. Dittrich and W. Jahn, How to study microemulsions, *J. Colloid Interface Sci.*, 1987, **118**, 436–453.
- 36 K. V. Schubert, R. Strey, S. R. Kline and E. W. Kaler, Small angle neutron scattering near Lifshitz lines: Transition from weakly structured mixtures to microemulsions, *J. Chem. Phys.*, 1994, **101**, 5343–5355.
- 37 S. Burauer, T. Sachert, T. Sottmann and R. Strey, On microemulsion phase behavior and the monomeric solubility of surfactant, *Phys. Chem. Chem. Phys.*, 1999, **1**, 4299–4306.
- 38 M. Kahlweit, R. Strey, R. Schomäcker and D. Haase, General patterns of the phase behavior of mixtures of water, non-polar solvents, amphiphiles, and electrolytes. 2, *Langmuir*, 1989, **5**, 305–315.
- 39 T. Sottmann and R. Strey, in *Fundamentals of Interface and Colloid Science*, ed. J. Lyklema, Microemulsions, Academic Press, London, 1st edn, 2005, vol. 5, pp. 5.1–5.96.
- 40 S. A. Safran, in *Structure and Dynamics of Strongly Interacting Colloids and Supramolecular Aggregates in Solution*, ed. S.-H. Chen, J. S. Huang and P. Tartaglia, Springer, Netherlands, Dordrecht, 1992, pp. 237–263.
- 41 M. Penders and R. Strey, Phase behavior of the quaternary system H₂O/*n*-octane/C₈E₅/*n*-octanol: role of the alcohol in microemulsions, *J. Phys. Chem.*, 1995, **99**, 10313–10318.
- 42 F. M. Menger and K. L. Caran, Anatomy of a gel. Amino acid derivatives that rigidify water at submillimolar concentrations, *J. Am. Chem. Soc.*, 2000, **122**, 11679–11691.
- 43 M. Laupheimer, N. Preisig and C. Stubenrauch, The molecular organogel *n*-decane/12-hydroxyoctadecanoic acid: Sol-gel transition, rheology, and microstructure, *Colloids Surf., A*, 2015, **469**, 315–325.
- 44 A. L. Fameau and M. A. Rogers, The curious case of 12-hydroxystearic acid—the Dr Jekyll & Mr Hyde of molecular gelators, *Curr. Opin. Colloid Interface Sci.*, 2020, **45**, 68–82.
- 45 D. J. Cornwell, B. O. Okesola and D. K. Smith, Hybrid polymer and low molecular weight gels—dynamic two-component soft materials with both responsive and robust nanoscale networks, *Soft Matter*, 2013, **9**, 8730–8736.
- 46 B. O. Okesola and D. K. Smith, Versatile supramolecular pH-tolerant hydrogels which demonstrate pH-dependent selective adsorption of dyes from aqueous solution, *Chem. Commun.*, 2013, **49**, 11164–11166.
- 47 K. Nishinari, Some thoughts on the definition of a gel, *Prog. Colloid Polym. Sci.*, 2009, **136**, 87–94.
- 48 E. R. Draper and D. J. Adams, Low-Molecular-Weight Gels: The State of the Art, *Chem*, 2017, **3**, 390–410.
- 49 J. E. Eldridge and J. D. Ferry, Studies of the cross-linking process in gelatin gels. III. Dependence of melting point on concentration and molecular weight, *J. Phys. Chem.*, 1954, **58**, 992–995.

- 50 M. Raynal and L. Bouteiller, Organogel formation rationalized by Hansen solubility parameters, *Chem. Commun.*, 2011, **47**, 8271–8273.
- 51 J. Gao, S. Wu and M. A. Rogers, Harnessing Hansen solubility parameters to predict organogel formation, *J. Mater. Chem.*, 2012, **22**, 12651–12658.
- 52 K. K. Diehn, H. Oh, R. Hashemipour, R. G. Weiss and S. R. Raghavan, Insights into organogelation and its kinetics from Hansen solubility parameters. Toward a priori predictions of molecular gelation, *Soft Matter*, 2014, **10**, 2632–2640.
- 53 C. M. Hansen, *Hansen Solubility Parameters: A User's Handbook*, CRC Press, Boca Raton, 2nd edn, 2007, pp. 1–26.
- 54 H. Yamamoto, Hansen Solubility Parameters(HSP) Application Notes, <https://pirika.com/NewHP/PirikaE2/Gallstone.html>, accessed 21 May 2021.
- 55 K. Peng, N. Preisig, T. Sottmann and C. Stubenrauch, Formulation of Gelled Non-toxic Bicontinuous Microemulsions Stabilized by Highly Efficient Alkanoyl Methylglucamides, *Langmuir*, 2020, **36**, 12692–12701.
- 56 K. Steck, N. Preisig and C. Stubenrauch, Gelling Lyotropic Liquid Crystals with the Organogelator 1,3:2,4-Dibenzylidene-D-sorbitol Part II: Microstructure, *Langmuir*, 2019, **35**, 17142–17149.

From water-rich to oil-rich gelled non-toxic microemulsions

*Ke Peng, Natalie Preisig, Thomas Sottmann, Cosima Stubenrauch**

Institute of Physical Chemistry, University of Stuttgart, Pfaffenwaldring 55, 70569 Stuttgart,
Germany, *cosima.stubenrauch@ipc.uni-stuttgart.de

Table of Contents

S1.	Phase diagrams at various ϕ -ratios.....	2
S2.	Amplitude sweep of water-rich gelled microemulsions	3
S3.	Hansen solubility parameters (HSPs)	3
S4.	FFEM image of the water-rich non-gelled microemulsion.....	5

S1. Phase diagrams at various ϕ -ratios

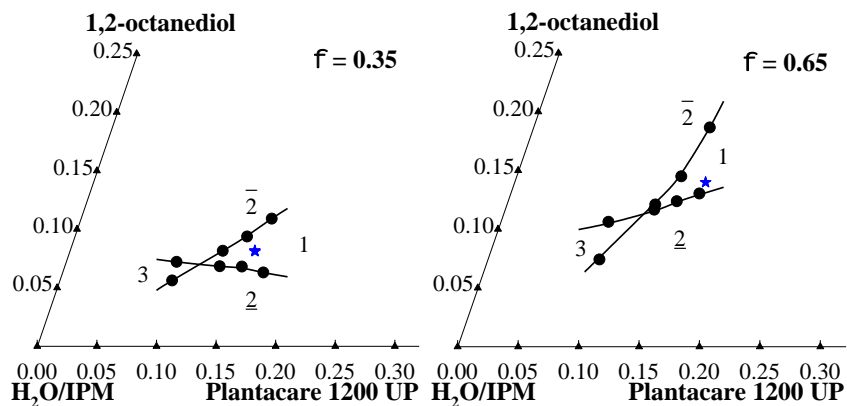


Figure S1. Phase diagrams of the non-toxic system H₂O – isopropyl myristate (IPM) – Plantacare 1200 UP (C₁₂G_{1.4}) – 1,2-octanediol at oil-to-water ratios of $\phi = 0.35$ and 0.65 at $T = 25$ °C. The sample compositions of gelled microemulsions for the rheological measurements are marked in blue star.

The phase diagrams of the microemulsions were measured at a fixed oil-to-water ratio ϕ with two variables, namely the surfactant mass fraction γ_C and the co-surfactant mass fraction γ_D . Since the phase inversion is induced by the addition of the co-surfactant,¹⁻³ the phase diagrams at all ϕ -ratios (Figure S1) have the same trend: along with the addition of 1,2-octanediol, the phase transition has a sequence of $\underline{2} - 3 - \bar{2}$ on the left side of the \tilde{X} point, and $\underline{2} - 1 - \bar{2}$ on the right side of the \tilde{X} point.

S2. Amplitude sweep of water-rich gelled microemulsions

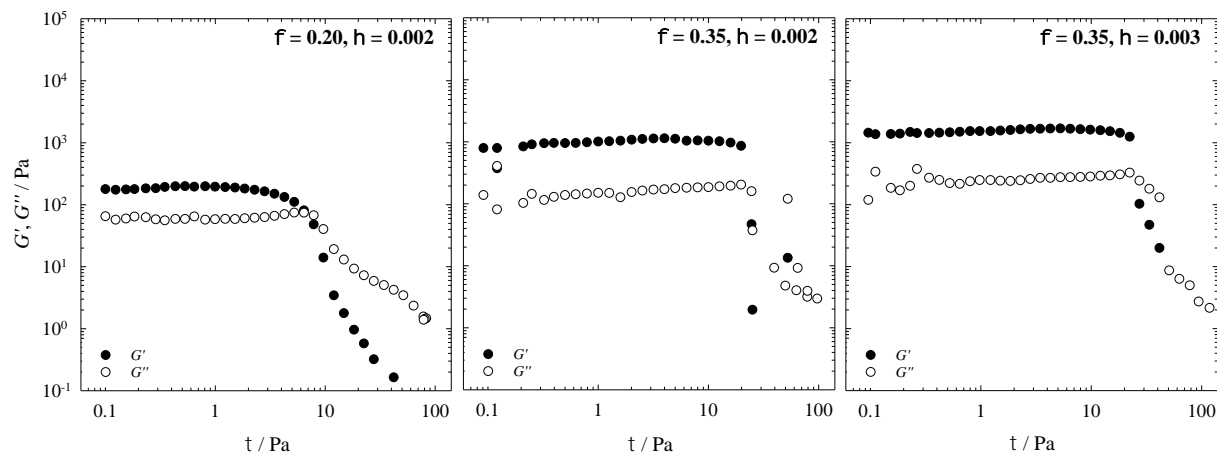


Figure S2. Storage modulus G' (filled symbols) and loss modulus G'' (open symbols) of the gelled microemulsion $\text{H}_2\text{O} - \text{IPM} - \text{Plantacare 1200 UP} (\text{C}_{12}\text{G}_{1.4}) - 1,2\text{-octanediol}$ in the presence of DBS at $T = 25\text{ }^\circ\text{C}$, $\omega = 10\text{ s}^{-1}$ as a function of the shear stress τ with (left) $\phi = 0.20$, $\eta = 0.002$; (middle) $\phi = 0.35$, $\eta = 0.002$; (right) $\phi = 0.35$, $\eta = 0.003$. See Table 2 for sample composition.

Amplitude sweeps with a controlled shear stress were carried out to determine the limit of the linear viscoelastic region (LVE region, Figure S2). The limit shear stress for the sample with $\phi = 0.20$, $\eta = 0.002$ was determined to be $\tau = 2\text{ Pa}$, for the sample with $\phi = 0.35$, $\eta = 0.002$ to be $\tau = 12\text{ Pa}$, for the sample with $\phi = 0.35$, $\eta = 0.003$ to be $\tau = 14\text{ Pa}$. One can already see that the sample with $\phi = 0.20$, $\eta = 0.002$ is a much weaker gel than the two samples with $\phi = 0.35$. The sample with $\phi = 0.35$, $\eta = 0.003$ is slightly stronger than the sample with $\phi = 0.35$, $\eta = 0.002$ due to the higher gelator concentration.

S3. Hansen solubility parameters (HSPs)

We tested the gelation of the organogelator 1,3:2,4-dibenzylidene-D-sorbitol (DBS) in the individual components of the non-toxic microemulsion (Table S1), namely water, the oil IPM, the co-surfactant 1,2-octanediol, and the oil & co-surfactant mixture (4:1 mass ratio), which has a

similar composition with that in our microemulsion. The gel strengths were quickly checked by shaking the test tubes: if the gel was destroyed by the stirring bar with a gentle shake, it is defined as “weak”; if the gel remained still with a hard hit, it is defined as “strong”. DBS is insoluble in water at $\eta = 0.001$. DBS forms an instant gel in IPM. However, with $\eta = 0.003$ as the gelator concentration used in the gelled microemulsion, this binary gel is very weak. With an increase to $\eta = 0.005$, DBS forms a strong gel in IPM. The gel is very strong with $\eta = 0.010$. Up to $\eta = 0.006$, DBS is soluble in the co-surfactant 1,2-octanediol. With $\eta = 0.010$, DBS forms a slow but strong gel in 1,2-octanediol. The addition of 20% 1,2-octanediol in IPM weakens the gel strengths and only forms a strong gel at $\eta = 0.010$.

Table S1. The gelation results of DBS in the individual components of the non-toxic microemulsion.

DBS in	H ₂ O		IPM		1,2-octanediol		IPM & 1,2-octanediol (4:1 mass ratio)	
η	0.001	insoluble	0.003	instant gelation (very weak and transparent gel)	0.003	soluble	0.004	slow gelation (very weak and transparent gel)
	0.003	insoluble	0.005	instant gelation (strong and transparent gel)	0.006	soluble	0.006	slow gelation (very weak and transparent gel)
			0.010	instant gelation (very strong and transparent gel)	0.010	slow gelation (strong and translucent gel)	0.010	slow gelation (strong and transparent gel)

Our microemulsions with varied oil-to-water ratios contain similar amounts of surfactant and co-surfactant, but the amount of water and oil differs. Plotting the gelation results of 1 wt.% DBS in water and IPM on the 3D Hansen space (containing the datasets from ⁴), one sees water and IPM on different sides of the sphere.

continuous water domain. The droplet size ranges from 5 to 20nm, the length of cylindrical droplets expands to 30 nm.

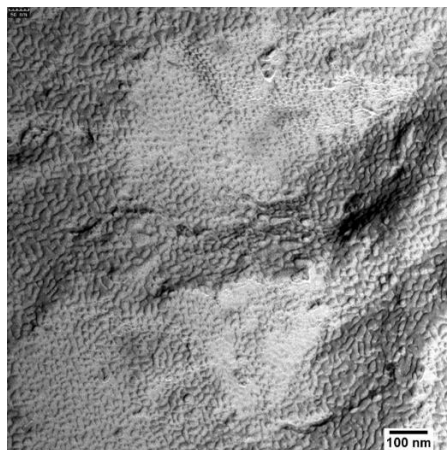


Figure S4. FFEM image of the non-gelled microemulsion H₂O – IPM – Plantacare 1200 UP (C₁₂G_{1.4}) – 1,2-octanediol at oil-to-water ratio $\phi = 0.20$.

References

- 1 H. Kunieda and K. Shinoda, Evaluation of the hydrophile-lipophile balance (HLB) of nonionic surfactants. I. Multisurfactant systems, *J. Colloid Interface Sci.*, 1985, **107**, 107–121.
- 2 C. Stubenrauch, B. Paepflow and G. H. Findenegg, Microemulsions Supported by Octyl Monoglucoside and Geraniol. 1. The Role of the Alcohol in the Interfacial Layer, *Langmuir*, 1997, **13**, 3652–3658.
- 3 T. Sottmann, K. Kluge, R. Strey, J. Reimer and O. Söderman, General patterns of the phase behavior of mixtures of H₂O, alkanes, alkyl glucosides, and cosurfactants, *Langmuir*, 2002, **18**, 3058–3067.
- 4 K. K. Diehn, H. Oh, R. Hashemipour, R. G. Weiss and S. R. Raghavan, Insights into organogelation and its kinetics from Hansen solubility parameters. Toward a priori predictions of molecular gelation, *Soft Matter*, 2014, **10**, 2632–2640.
- 5 C. M. Hansen, in *Hansen Solubility Parameters: A User's Handbook*, CRC Press, Boca Raton, 2nd edn., 2007, pp. 1–26.
- 6 H. Yamamoto, Hansen Solubility Parameters(HSP) Application Notes, <https://pirika.com/NewHP/PirikaE2/Gallstone.html>, (accessed 21 May 2021).

Erklärung über die Eigenständigkeit der Dissertation

Ich versichere, dass ich die vorliegende Arbeit selbständig verfasst und keine anderen als die angegebenen Quellen und Hilfsmittel benutzt habe; aus fremden Quellen entnommene Passagen und Gedanken sind als solche kenntlich gemacht.

Declaration of Authorship

I hereby certify that this dissertation is entirely my own work except where otherwise indicated. Passages and ideas from other sources have been clearly indicated.

Stuttgart, den 19.08.2021

Ke Peng
Ke Peng